General Disclaimer

One or more of the Following Statements may affect this Document

- This document has been reproduced from the best copy furnished by the organizational source. It is being released in the interest of making available as much information as possible.

- This document may contain data, which exceeds the sheet parameters. It was furnished in this condition by the organizational source and is the best copy available.

- This document may contain tone-on-tone or color graphs, charts and/or pictures, which have been reproduced in black and white.

- This document is paginated as submitted by the original source.

- Portions of this document are not fully legible due to the historical nature of some of the material. However, it is the best reproduction available from the original submission.

Produced by the NASA Center for Aerospace Information (CASI)

NASA TECHNICAL MEMORANDUM

NASA TM-75911

GIRL - GERMAN INFRARED LABORATORY
FINAL REPORT OF THE TELESCOPE STUDY, PHASE B

Dr. R. Schlegelmilch et al.

(NASA-TM-75911) GIRL: GERMAN INFRARED LABORATORY. TELESCOPE STUDY, PHASE B Final Report (National Aeronautics and Space Administration) 175 p HC A08/MF A01 CSCL 20F G3/74

N81-20866

Unclas 41849

Translation of "GIRL - German Infrared Laboratory; Schlussbericht der Teleskopstudie Phase B", Messerschmidt-Bölkow-Blohm GmbH, Ottobrunn and Carl Zeiss, Oberkochen, MBB No. R 3600/0170 R, 1980, 197 pages.

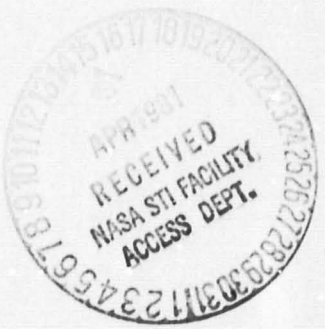

NATIONAL AERONAUTICS AND SPACE ADMINISTRATION
WASHINGTON, D.C. 20546 JANUARY 1981

Preface

The aim of the present study is supplementing and detailing the results gained in phase A for designing the telescope system while taking into consideration the enlargement of the main mirror which has been carried out in the meantime.

After the decision on material obtained from phase A in favor of cerodur, the mounting systems of both mirrors were developed and one model each of the mounted main mirror was produced for thermal and shake tests. The studies were again supplemented by comprehensive calculations on rigidity, natural frequencies, cooling times and temperature gradients; measurements of heat transition in metal/cerodur combinations carried out by the Linde Company supplied important data on the material. The measurements planned for scattered light and reflectivity at low temperatures could not be carried out in the period set aside for the study.

The present final report is divided according to the description of tasks for reasons of continuity; figures have been numbered separately in the individual work packages.

Participants in the study were

Dr. R. Schlegelmilch	Study management
E. D. Knohl, Engineer	Elastomechanical calculations, construction supervision
H. J. Meier, Engineer	Thermal calculations
Dr. P. Henneberg	Optical calculations
H. Weber, B. Bohnert, W. Hafner	Construction
R. Grohmann	Manufacture of the optics
H. Friedow	Manufacturing the mechanical parts, assembly
J. Schmidt	Business supervisor

Time for the study - December 1, 1979 to August 15, 1980

Table of Contents

		Page
AP 3010	Optical studies with polished cerodur samples	1
AP 3011	Measurement methods	1
AP 3012 and 3013	Measurements, aids	1
AP 3020	Geometry, support rings and preparation of the main mirror	5
AP 3021	Optimization of the mirror support ring and the formation	5
AP 3022	Preparation of mirror	9
AP 3030	Construction and tests of the main mirror mount	15
AP 3031	Mounting concepts	15
AP 3032	Calculation of critical tensions and deformations	31
AP 3033	Natural frequencies and concept selection	31
AP 3034	Optimization and construction of the membrane support	35

AP 3035	Shake model and test results	40
AP 3040	Thermal behavior of the main mirror	47
AP 3041	Calculation of the temperature differences of the stationary case	47
AP 3042	Cooling of main mirror	63
AP 3043	Measure of thermal conduction	71
AP 3044	Strength of the thermal contacts	78
AP 3045	Construction of the thermal conductors	78
AP 3050	Collection mirror and support	80
AP 3051	Concept of the support	80
AP 3052	Thermal balance of the collection mirror and chopper	88
AP 3053	Cool-down time for the mirror	98
AP 3054	Natural frequency of the second mirror	102
AP 3055	Deformation of the second mirror during chopping	105
AP 3056	Construction of the mirror mount	106
AP 3060	Three-legged tubular structure	110
AP 3061	Natural frequency calculations	110
AP 3062	Optimizing the heat conductors	120
AP 3063	Three-legged construction, adjustment, focusing	121
AP 3070	The preparation of thermal model	127
AP 3090	Optical testing of the telescope and its components	133
AP 3091	Measurement methods for wave front and stray light at the cooled main mirror	133
AP 3092	Measurement of aberration at the second mirror	145
AP 3093	Tests of a complete telescope system	147
AP 3100	Clean handling	149

Appendix 1 Remarks on the error budget 153

Appendix 2 Thermal calculations on a heat conductor contact 157

Summary 158

FINAL REPORT OF THE TELESCOPE STUDY PHASE B: DEVELOPMENT, CONSTRUCTION AND TEST OF THE COOLED INFRARED TELESCOPE GIRL

Dr. K. Schlegelmilch, et al.

Messerschmidt-Bölkow-Blohm GmbH, Ottobrunn and
Carl Zeiss, Oberkochen

AP 3010
Optical Studies with Polished Zerodur Samples

/1*

AP 3011 Measurement Methods

The helium cryostat of the university in Wuppertal was employed for the measurements of scattered light properties and reflection degree with the mirror samples. Figure 3010/1 shows the principle of the measurement setup for the scattered light measurements.

The cryostat is equipped with two concentric radiation shields, of which the outer shield is cooled with liquid nitrogen and the inner with helium. For this purpose, the shields are covered with evaporation pipes. The helium consumption for one cooling amounts to approx. 100 liters and the cooling time approx. 1 day.

A laser beam (e.g. a CO_2 laser for 10.6 micro m) is collected at an aperture in order to constrict the beam and is then separated from undesirable stray light with a further lens through the entry aperture of the cryostat at a second aperture inside the cryostat. Only a central surface element of the test sample is illuminated in order to exclude with certainty stray portions of the edge. The reflected or the defined stray light is then collected in an disengagement system equipped with a third aperture and fed to the detector. This consists in a Golay cell followed by a watt meter. The disengagement system is mounted on an arm moveable from the outside for varying the stray angle, permitting motion on the incidence plane of the sample.

A separate detector must be employed for reflection measurements. For the relative measurements, this is pivoted over the aperture in the cryostat and also in the image of the aperture reflected by the test sample.

AP 3012 and 3013 Measurements, Aids

/3

In order to reduce the number of cooling cycles, an alternating revolver was developed and prepared by Zeiss, permitting four mirror samples to be mounted and to be exchanged externally. The setup of

*Numbers in the margin indicate pagination in the foreign text.

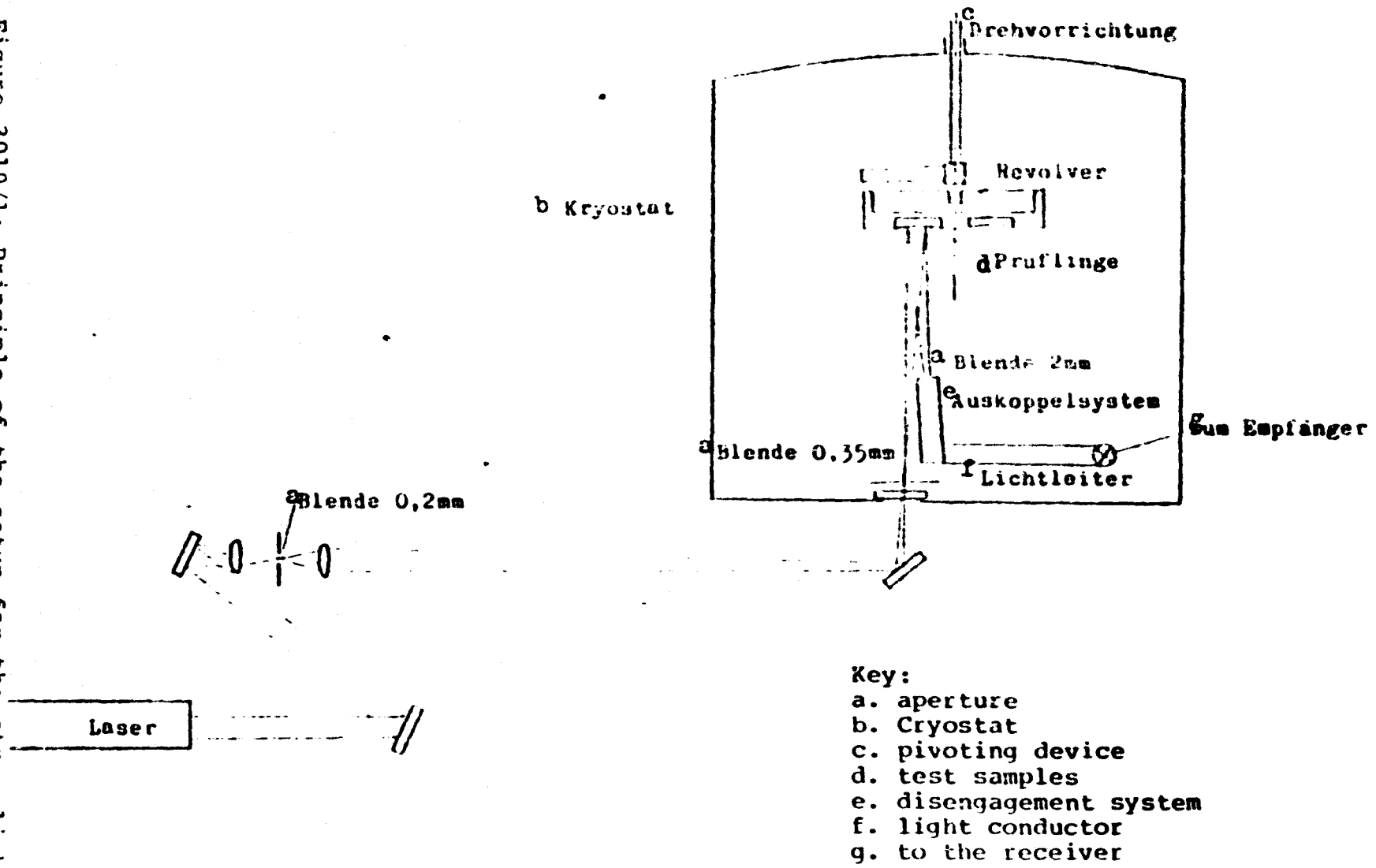

Figure 3010/1: Principle of the setup for the stray light measurements (according to the data of the GHW)

Key:
a. aperture
b. Cryostat
c. pivoting device
d. test samples
e. disengagement system
f. light conductor
g. to the receiver

ORIGINAL PAGE IS
OF POOR QUALITY

the revolver can be seen from Figure 3010/2. For this purpose there is a rotary guide in the cover of the cryostat (compare Figure 3010/1) through which a rotary device can be lowered and set into a slot at the edge of the revolver. The barrel and base plate of the revolver have concentric and opposing grooves, in which steel pellets provide support. Two symmetrically opposite stops define the four basic positions of the barrel. All four mirror samples are situated in mounting rings, supported on three adjustment screws each.

Four cerodur mirrors with a diameter of 75 mm were prepared for the measurements. They received the best possible polish and were coated in a high vacuum with pure aluminum of the following layer thicknesses:

Mirror sample no. 1	50.5 nm
Mirror sample no. 2	100.3 nm
Mirror sample no. 3	200.6 nm
Mirror sample no. 4	400.4 nm

The measurement of thickness was carried out by a frequency measurement with a vibrating quartz positioned next to the sample of the same coating. The spherical surfaces of the samples have a curvature radius of 550 nm adjusted to the geometrical relationships in the cryostat. They were protected during transport from dust and contamination by metallic protective caps (compare AP 3011).

Due to technical difficulties and deadlines, the measurements were not completed during the period of the studies. Visual observation in a dark field with closely bundled light beam (hammer lamp), already produced the clear result that the scattering intensity increases with greater layer thickness. Preliminary orientation measurements with the GHW provided the result that the reflectivity increases by 5% ± 3% in each case at room temperature and with a wavelength of 163 µm with increasing layer thickness between the samples 1 to 3.

In the cooling tests in Wuppertal, it was determined that both the heat conductors and the temperature measurement sensors, attached to the rear surfaces of the mirrors with PRC adhesive, had separated before reaching the helium temperature. A report is presented in AP 3044 and AP 3074 on the results of the corresponding strength tests with adhesive connections between metal and cerodur, subsequently iniated at Zeiss. It was further reported by the GHW that 20 hours were required to achieve approx. 100 K already in the preliminary cooling with liquid nitrogen. /5

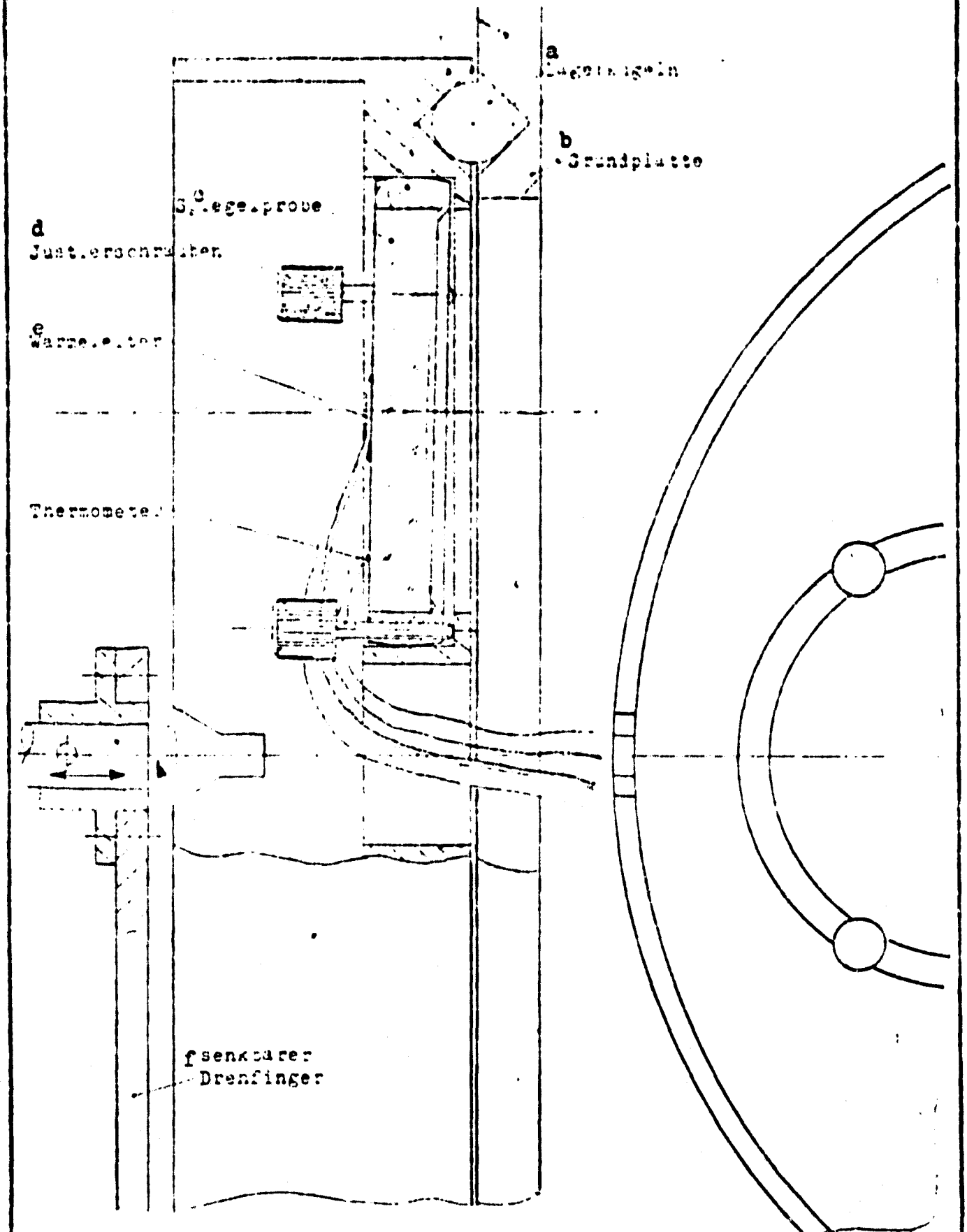

Figure 3010/2: Alternating revolver for 4 mirror samples to be installed in the test cryostat of the GHW (university in Wuppertal).

(Please see Key on following page.)

Key:
a. bearings
b. base plate
c. mirror sample
d. adjustment screws
e. heat conductor
f. rotary finger which can be lowered

AP 3020
Geometry, Support Ring and Preparation of the Main Mirror /6

AP 3021 Optimizing the Support Ring and Deformations

A simple mirror model with smooth rear surface, cylindrical outer edge and cylindrical hole was employed for the first calculations. The study was first limited to a radial section with a single concentric, continuous support ring. The calculation results for the support ring radii 70, 156 and 230 mm are presented together in Figure 3020/1 for a 50 cm mirror with 100 mm hole diameter. The diagram demonstrates how a support near the edge or hole produces maximum deformations on the order of magnitude of several hundred nm, as expected. The support ring with r = 156 nm, on the other hand, very closely approximates the optimal case. It causes a radial remainder deformation of only 66 nm, corresponding to a tenth wavelength in the customary assessment of quality. Through interpolation of these results, the optimal support ring for the simplified model was determined at

$$r_{optimal} = 166.5mm$$

On the basis of this result, a refined model with finite elements was employed for the subsequent calculations. Calculations were carried out with two concentric homogeneous support rings in each knot of this model, adjacent to the optimized support ring radius, i.e. knots no. 28 and 29. The results are those diagrams in Figures 3020/2 and 3 plotted by the computer. In the case of the deflections of the mirror cross-sections represented on a scale of 1:1, 1 nm = 0.02 m when the mirror is subjected to a 10 g load. When an interpolation is carried out from the two total bendings of the surface to the support ring diameter for the smallest bending, the value results in good agreement with the results of the simplified model

$$r_{optimal} = 165.8mm.$$

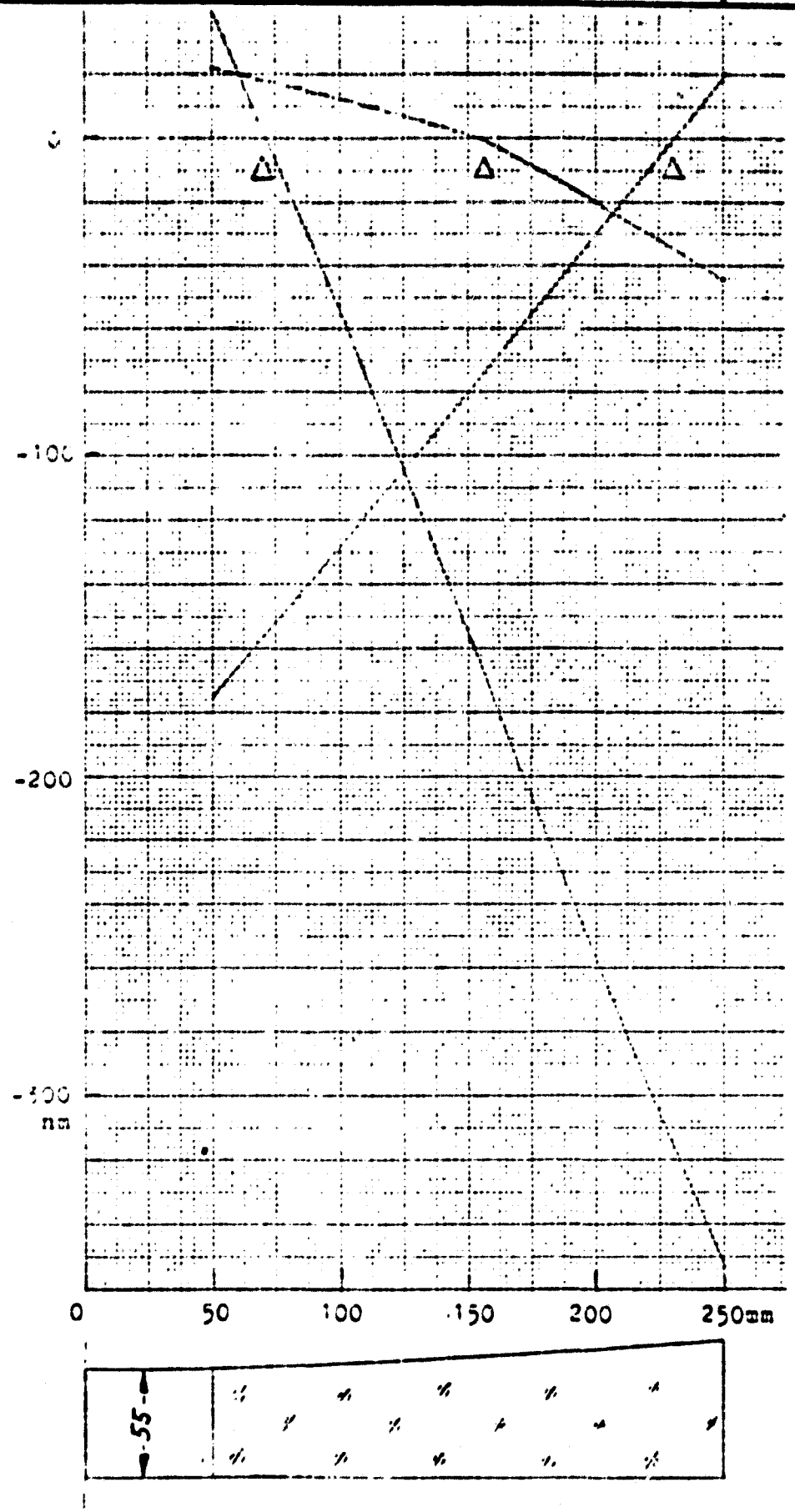

ORIGINAL PAGE IS
OF POOR QUALITY

Figure 3020/1: Bending of a cylindrical mirror model in the radial plane with variation of a rotation-symmetrical support ring

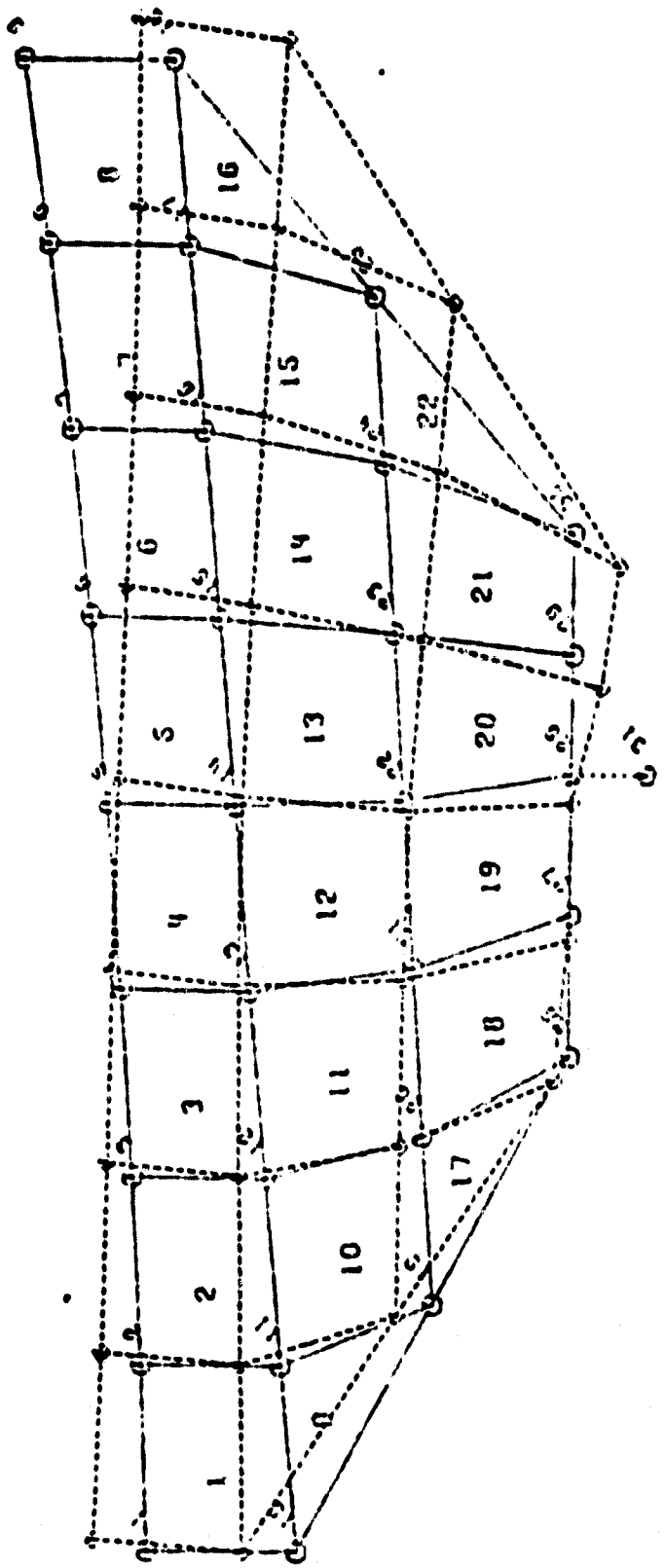

Figure 3020/2: Shaping in the radial section of the mirror with a load of 10 g. 1 mm bending = 0.02 µ. Support ring radius 155 mm.

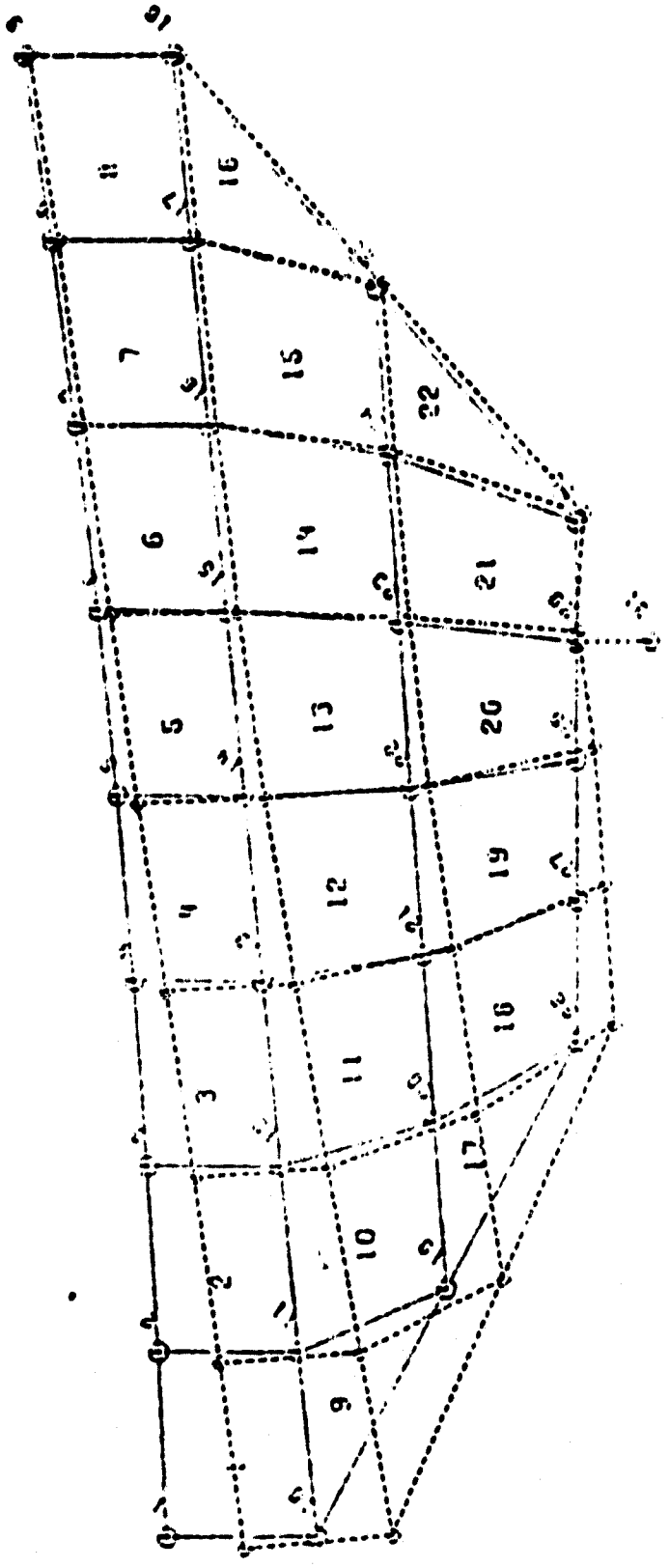

Figure 3020/3: Shaping in the radial section of the mirror with a 10 g load. 1 mm bending = 0.02 μ, support ring radius 171 mm.

Bending along various azimuths of the mirror surface were calculated with the optimized support ring in the simplified model of a largely bevelled cylinder. Figure 3020/4 shows the bending at the whole edge, at the outer edge and over the support ring of the mirror in an azimuth range from the support point up to the azimuth angle 60^{o}, the angle of greatest bending, at the three-point support. The maximum bending occurs at the outer edge and amounts there to 85 nm. It is therefore greater by a multiple than the radial bending. The RMS value over the entire mirror surface amounts to approx. 20 nm. For the present purpose, this is still certainly permissible. /10

The weight of the mirror would amount to approx. 26 kp in the case of a cross-section of the mirror according to Figure 3020/3, when the mirror is prepared from cerodur.

AP 3022 Preparation of the Mirror

Several problems were anticipated in preparing a mirror of the cross-section according to Figure 3020/3. Normally, telescope mirrors have smooth rear surfaces, on which they can be placed during processing when taking into consideration certain measures for load reduction. In the present mirror concept it is no longer possible to reduce the load with simple means. If the mirror is to be polished with already milled rear surface, it must be secured in a bed, providing it with a smooth rear surface. Tensions, however, are ordinarily built between bed and mirror during this securing, leading to deformation of the mirror when the mirror is once again released. This procedure is therefore not preferred. It was therefore planned for the GIRL mirror to apply the deep facets on the rear surface only after conclusion of the polishing. This required a preliminary test for proving the trueness of shape of such a greatly cut mirror, since there was no sufficient information available on this subject. /12

A main mirror reduced to half the size was prepared for the cutting test. The blank was first provided cylindrically with a hole and with a spherical surface of high quality. The remaining wave front aberration can be seen in the two upper interferograms in Figures 3020/5 and 6. In the case of the same position of the mirror, the wave fronts between the blank and comparative normal are tipped in this case by a vertical or a horizontal axis to one another. The remainder error is smaller than one-third wavelength. Now the outer most facet was applied to the mirror and this was tested again in the interferometer under identical conditions. The result, provided in the lower portions of Figures 3020/5 and 6, shows no alteration. In a further procedural step, the inner facet was now also applied to the rear surface of the mirror. This procedural step had a noticeable effect on the wave front of the mirror. As can be seen in Figure 3020/7, the whole edge of the mirror was deformed by approx. 0.4 wavelengths.

In a further test it was now possible to prove that the tensions leading to shaping of the mirror were not latently present in the material, but rather were generated by the surface effect of the cutting

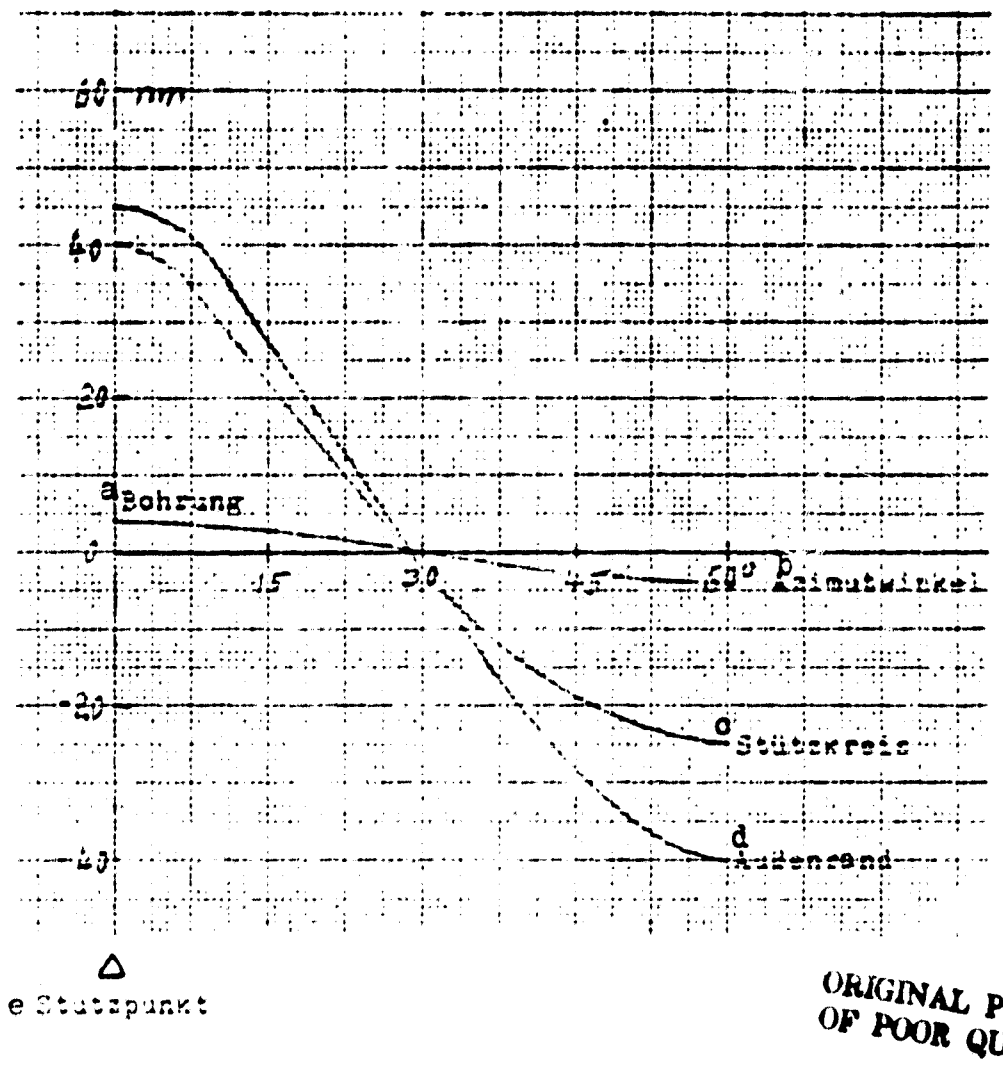

ORIGINAL PAGE IS
OF POOR QUALITY

Figure 3020/4: Bending of the main mirror along concentric circles around the axis in the case of three-point support in a support ring radius of 166.3 mm.

Key:
a. hole
b. azimuth angle
c. support ring
d. outer edge
e. support point

process. Etching the rear surface of the mirror with hydrofluoric acid then caused the disappearance of the deformation. The wave front, as was present after etching, is shown in Figure 3020/8.

The test shows that cutting the GIRL main mirror after polishing should not noticeably influence the wave front. If a small remainder error should occur on the basis of the double size of the original, local manual retouching of the surface would also be possible.

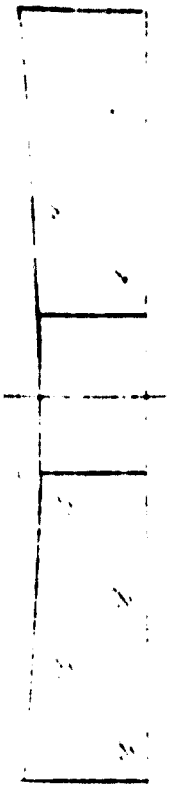

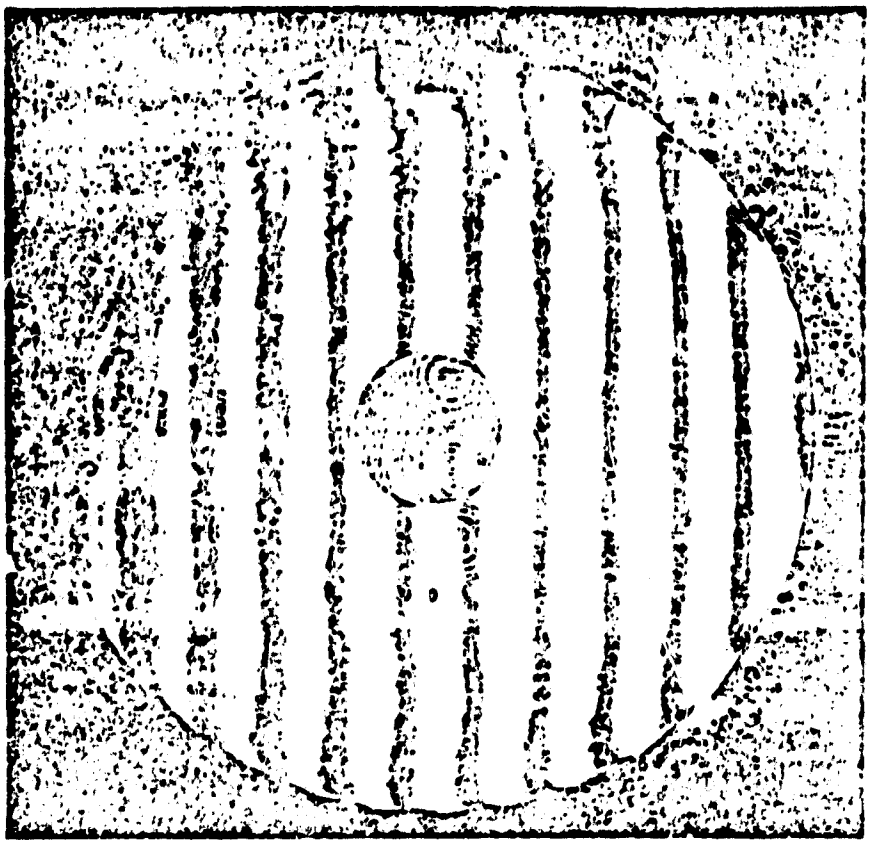

Wave front before cutting.

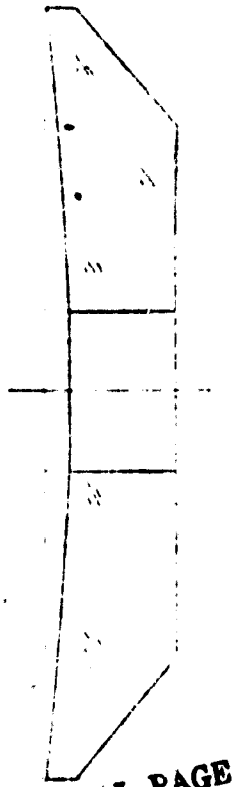

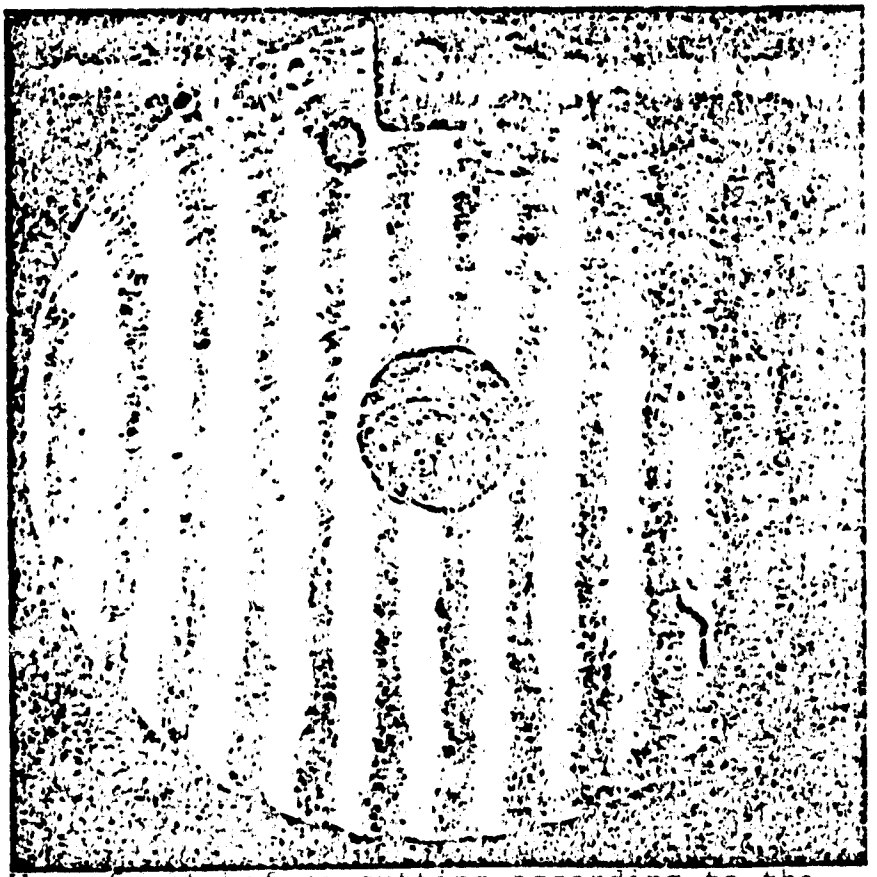

Wave front before cutting according to the adjacent cross-section.

ORIGINAL PAGE IS
OF POOR QUALITY

Figure 3020/5: Result of the preliminary test on the manufacturing technology of the S1.

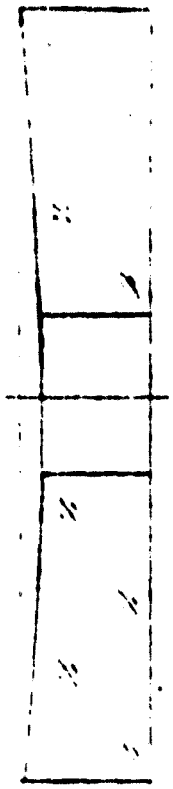

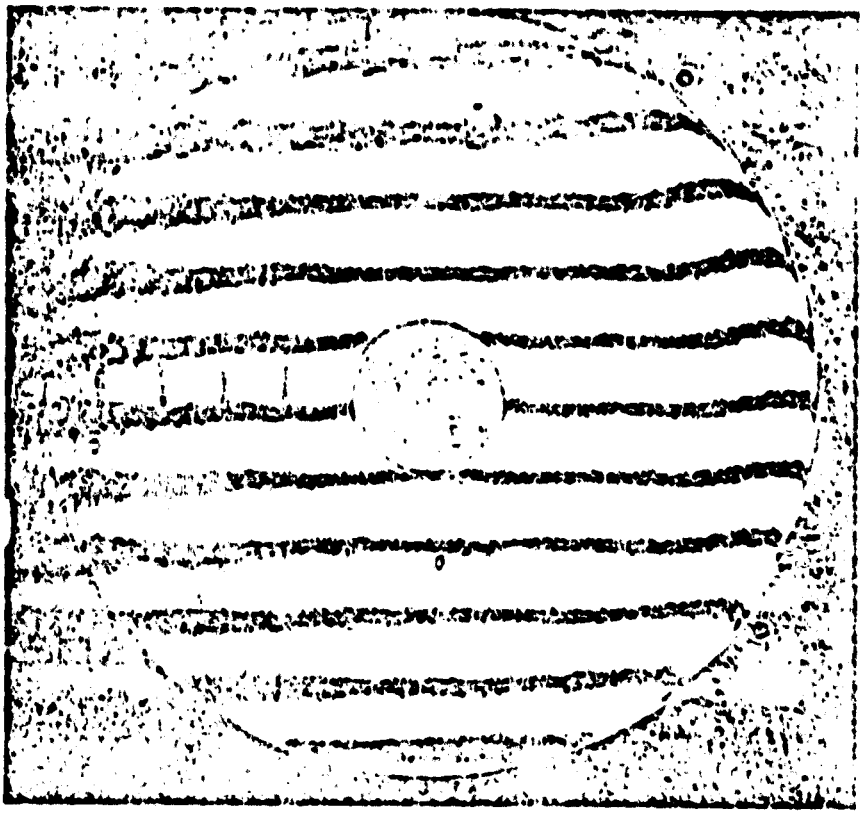

Wave front before cutting.

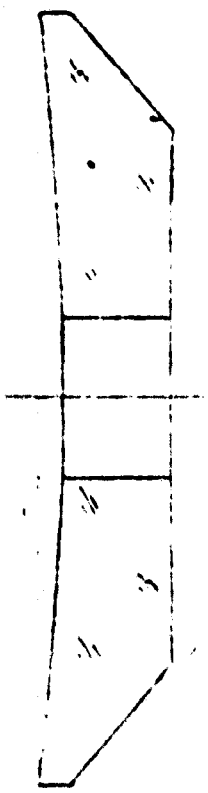

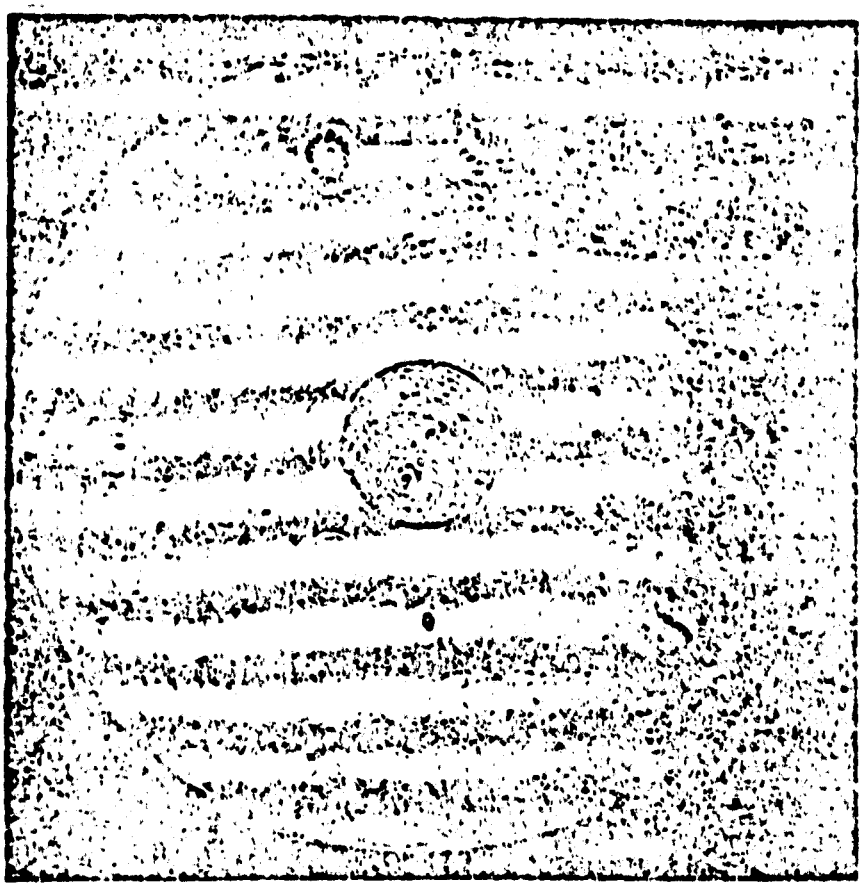

Wave front after cutting according to the adjacent cross-section.

Figure 3020/6: Result of the preliminary test on the manufacturing technology of the S1.

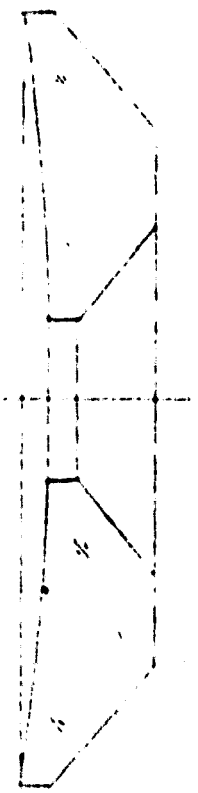

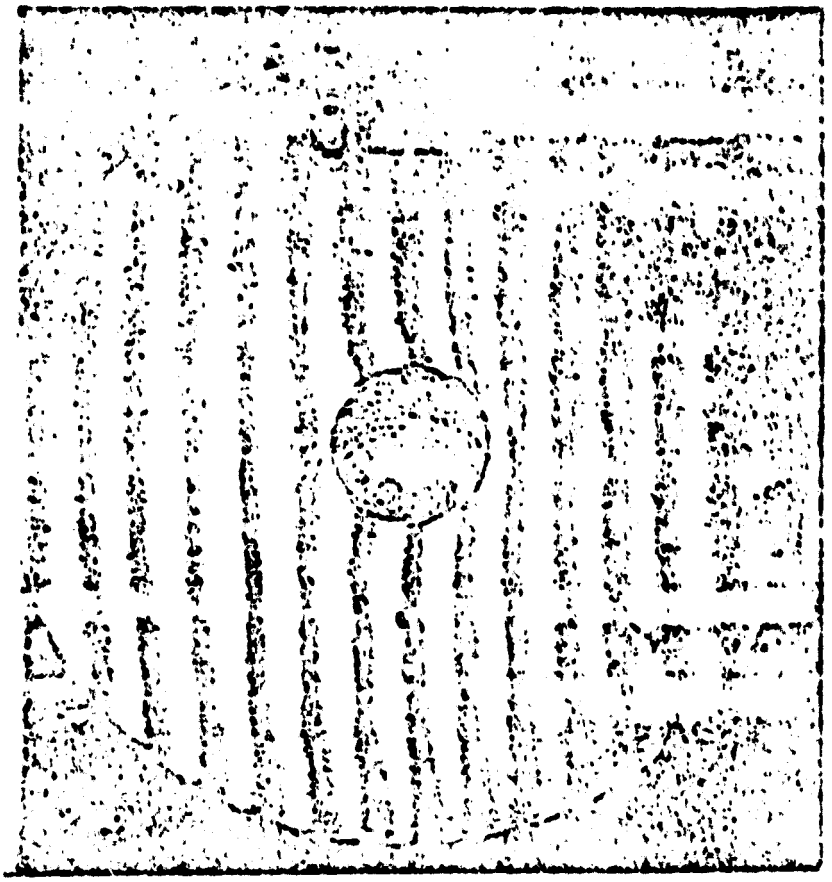

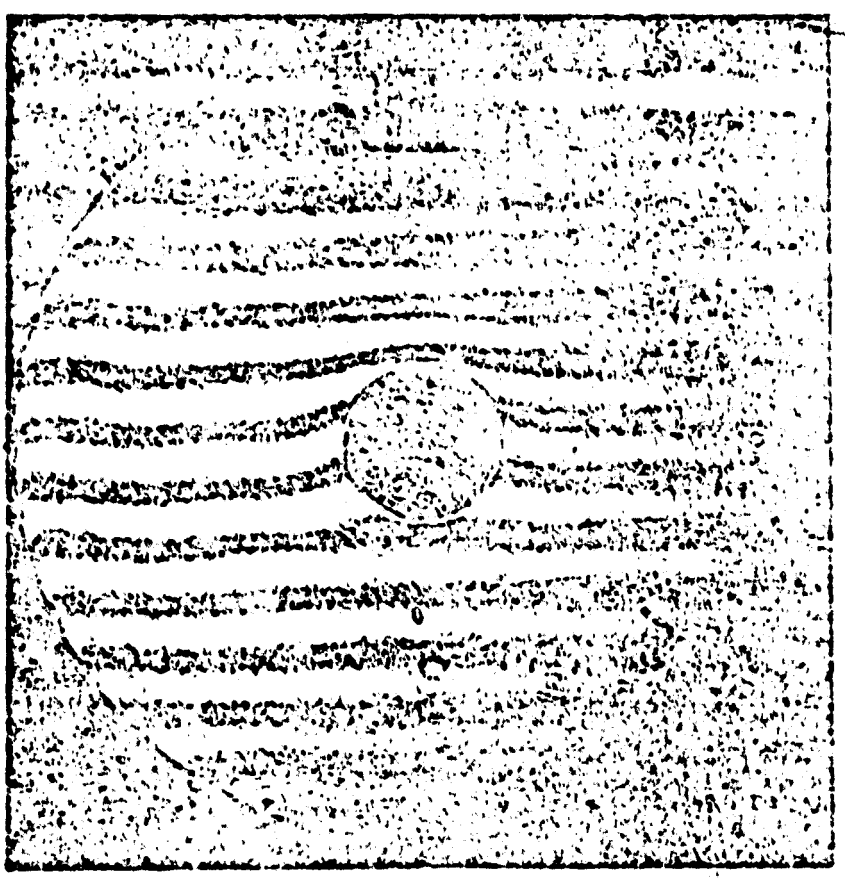

Figure 3020/7: Result of the preliminary test on the manufacturing technology of the S1; wave front after cutting of the inner cone (final state).

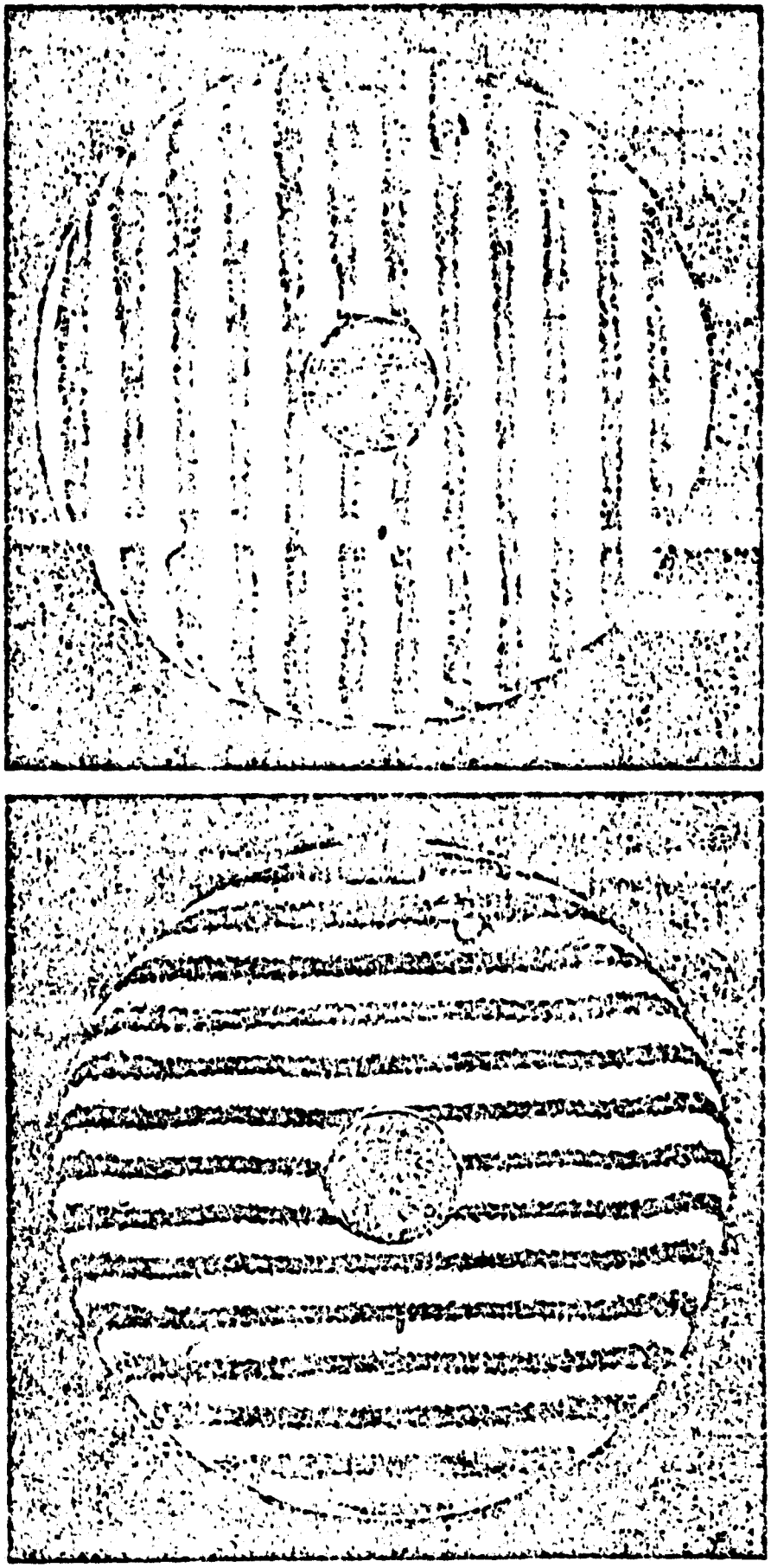

Figure 3020/8: Wave front of the finished cut mirror after one etching.

AP 3030
Construction and Testing of the Main Mirror Mount /17

AP 3031 Mounting Concepts

In mounting the GIRL main mirror, the essential condition consists in the fact that the glass body of the mirror cannot be subjected to any mechanical forces both in the laboratory tests in a heated condition and after cooling, leading to a deformation of the wave front beyond the permissible limit. Furthermore, the mirror mounting must be dimensioned in such a manner that no damaging shaping occurs irreversibly due to starting and cooling. Four drafts were prepared in the effort centered on an optimal mounting concept, explained in the following. In the interest of language continuity, the following designations will always be applied:

a) tension rod mount
b) six-point mount
c) three-point mount
d) membrane mount

a) Tension Rod Mount, Principle and Design

When the thermal expansion of the mirror material and the tension rods is first neglected in the mount principle represented in Figure 3030/1, there is a complete expansion compensation, independent of basis material when

$$r = \frac{R}{2}$$

In reality, however, the zerodur mirror expands during cooling from 293 K to 10 K by 6 µm/100 mm, while the rods are shortened during the same cooling by 38 µm/100 mm (Invar alloy LR 35). As will be explained /19 further below, the geometry can then be altered in such a manner that the effects of the large contraction of the basis ring (radius r) cause an extension of R, equal and opposite in value to the sum of the thermal expansions of cerodur and invar.

A possible construction principle of the tension rod mounting is shown in Figure 3030/2. The radial reduction in load on the mirror by means of the 6 invar rods is combined with an independent axial support through three adjustable, bendable pressure screws. The invar support claws of the mounting are pressed on the tips of the screws with 2 tension springs each. In the case of 20 g initial tension, these must accommodate 40 g total load in the maximum case. An arrangement of screw tips and tension rods in the same plane prevent the transmission of momentum from the mounting to the glass object. The construction aims at an introduction of force as close as possible to the centroidal plane of the mirror.

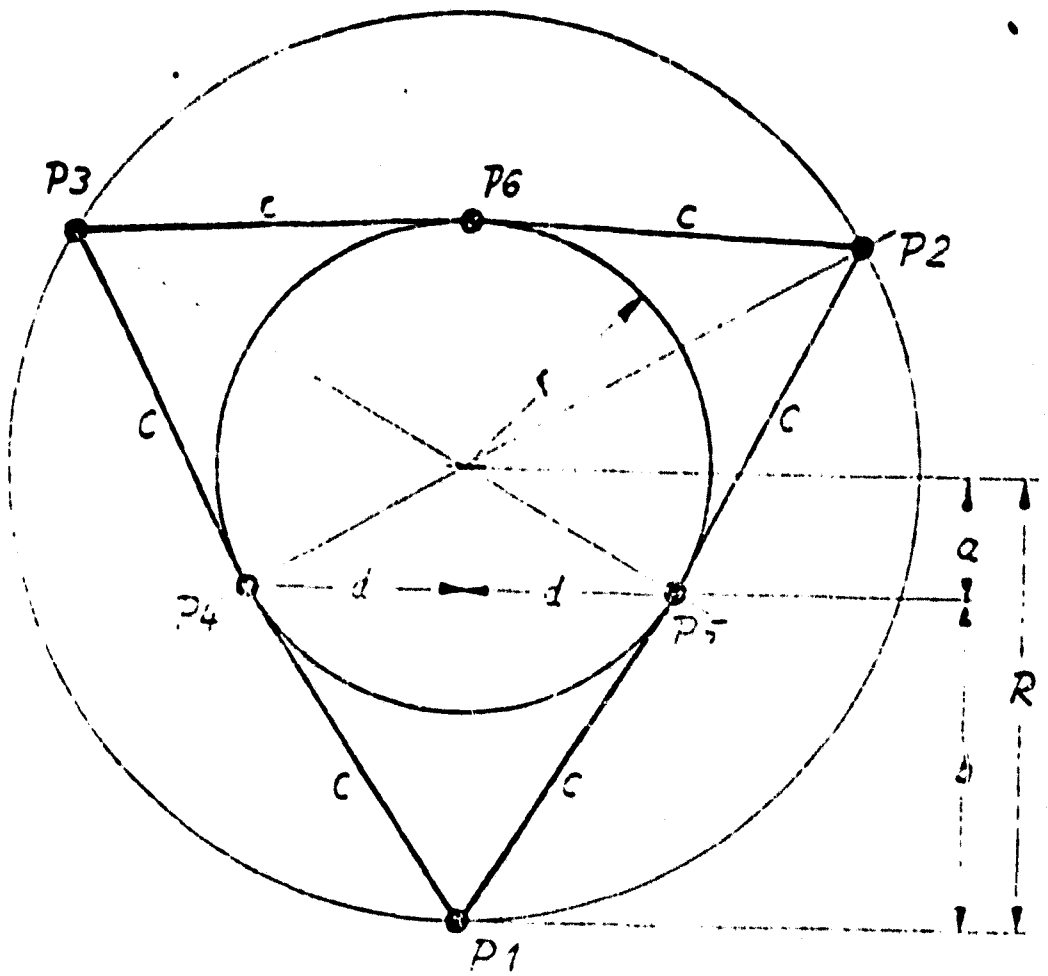

Figure 3030/1: Principle of the tension rod mounting of the main mirror.

P1 - P3 Mounting points on the mirror body
P4 - P6 Mounting points on the basis structure
c Tension rods of invar

According to the principle in Figure 3030/1, the path a is contracted during cooling according to the thermal contraction of the basis material. The simultaneous contraction of d, on the other hand, acts as an expansion of b (increasing proportional to the ratio d/b). For a total expansion resulting from these two components during cooling,

$$r > \frac{R}{2}$$

must be met. R = 170 mm according to Figure 3030/2. When the basis consists in an aluminum malleable alloy, the dependence of r presented in Figure 3030/3 results for the total expansion $\Delta a + \Delta b$ of the mounting (without the portion of expansion of the invar rods). In an actual case, however, an additional $\Delta R = +10$ µm (see above) can be expected in the case of cerodur and an additional $\Delta b = 45$ µm in the case of invar on the basis of the finite expansions. The components from the expansion of the basis material must therefore result in

$$\Delta a + \Delta b = +55 \text{ µm}$$

This amount is obtained according to Figure 3030/3 at r = 102 mm (the result of an approximation, not yet taken into consideration in Figure 3030/2). /21

Disadvantages of the Tension Rod Mount

The theoretical expansion compensation produces a rod length of

$$\ell = \sqrt{(r \cdot \cos 30^\circ)^2 + (R - r/2)^2} \approx 1.6 \text{ mm}$$

After subtracting the support claws, an actual rod length of approx. 93 mm remains.

When an erroneous compensation of r is undertaken without knowledge of the precise expansion coefficients, so that an erroneous length of the tension rods results after cooling, a considerable radial force on the mirror is produced. In the direction of the rod it is

$$F_c = \frac{\Delta c}{c} E \cdot q$$

In the case of $E = 1.37 \times 10^4$ kp/mm^2, the result for a rod diameter of 5 mm and an erroneous compensation of $\Delta c = 10$ µm is

$$F_c = 29 \text{ kp.}$$

The resulting force F in the direction R is then

$$F = 2 F_c \cos 36^\circ = 47 \text{ kp}$$

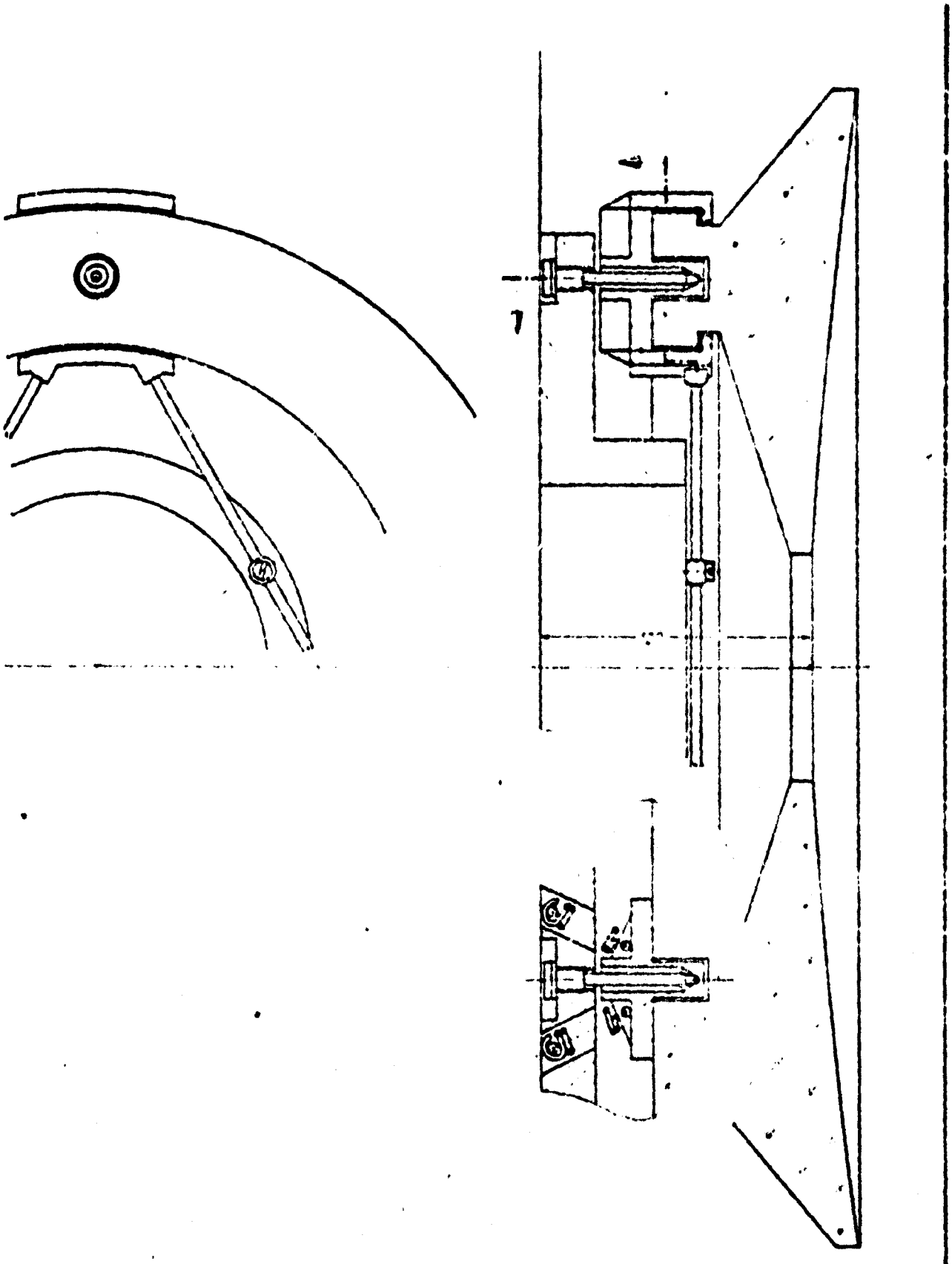

Figure 3030/2: Technical and constructive realization of the tension rod mount.

A force of this amount would be entirely impermissible. The compensation of rod lengths would have to be carried out with an accuracy of at least ±1.5 μ. Since a compensation at low temperature is probably not possible, a iteration process would become necessary. This is the sole large disadvantage of the system. An additional Δc of 1 μ during cooling requires a Δr according to the increase in the curve in Figure 3030/3. /23

$$\Delta r = 256\ \Delta R \cdot \cos 36^{\circ} = 207\ \mu m$$

The axial support screws (Figure 3030/2) are deflected toward the outside during cooling by f = 0.7 due to the high expansion differences between the basis (aluminum) and mirror. In this case a radial force is produced of

$$F_R = \frac{f \cdot 3E \cdot d^4}{2l^3} = 0,4\ kp$$

(l = length of screw = 52 mm, d = diameter of screw = 5 mm)
This is a completely safe value. Moreover, there is a portion from the microwelding at the screw tip, which can be reduced in size, however, by suitable coating.

Initial Load on the Mounting Elements

With a maximum acceleration of 20 g in the radial direction in the case of a 27 kg mirror weight, there is a force of maximum

$$F_c = \frac{20 \cdot 27}{2} \cos 30^{\circ} = 218\ kp$$

in 2 tension rods. When the four other rods would be missing, this would result in a rod extension of

$$\Delta c = \frac{F_c \cdot c}{E \cdot q} = 76\ \mu m$$

as well as a tension of 11 kp/mm^2. The 0.2% expansion limit of invar, however, amounts to 119 kp/mm^2 at 10 K, amounting to a multiple of almost 11 in certainty.

At 20 g in an axial direction of the mirror, 360 kp are exerted on each supporting screw. The bending load F_K results in the case of E = 13,700 kp/mm^2 (invar at 10 K) at /24

$$F_K = \pi^2 Ed^4/10l^2 = 3125 \text{ kp}$$

The certainty is therefore almost a multiple of 9.

b) Six-point Mount, Principle and Design

The six-point principle was created by replacing the three flat springs with three two-arm rockers in the case of the principle of the flat spring mounting (final report, phase A, Figure 27). Through this means, doubling the 3 mounting points at the mirror was possible in favor of a desired slighter initial load on the individual mounting point and a reduced deformation of the glass under natural load.

Figure 3030/4 shows the principle of the six-point mounting. The spring joints at the ends of the rockers are countersunk in the mirror base. A third joint is located under the center of each rocker. The rockers are adjusted to the thermal expansion of the zerodur by compensation members.

The function of the system is based on the fact that the rockers are only fixed in the axial direction of their joints, i.e. no shift between the mirror and assembly basis occurs in the direction of the joint longitudinal axis. With differing thermal expansion of the mirror and basis, the rockers are tipped on the longitudinal axis and the centering of the mirror is maintained.

Figure 3030/5 demonstrates a possibility of the practical application of the six-point mounting. Invar sockets in eight sections are sunk into the mirror base, prestressing the hole edge with a slight axial force (in the direction of the mirror axis). The axial expansion differences are undercompensated by aluminum rings (theoretically) in such a manner that a radial play in the sockets arising at 10 K of +5 µm is eliminated by sliding on the conical surfaces.

Inside each socket there is a spring joint BF 2, to which the rocker is mounted. For expansion compensation, the rockers are provided with aluminum connection pieces, introducing large forces in the mirror, however, with a completely fixed rocker and a small error compensation. For this reason, the "right-hand" end of the rocker is provided with a flat spring BF 3, accommodating the remainder forces. In Figure 3030/6, the dependence of temperature is presented for the expansion difference of aluminum + invar compared to cerodur in addition to other compensation examples. In the case of a precise compensation for 293 K and $T < 10$ K, an expansion difference of max. 18 µm occurs (at 180 K). With the planned spring cross-section of $Q = 1.5 \times 15$ mm^2 and an effective spring length of $l = 12$ mm, a remainder force then results, for example,

/27

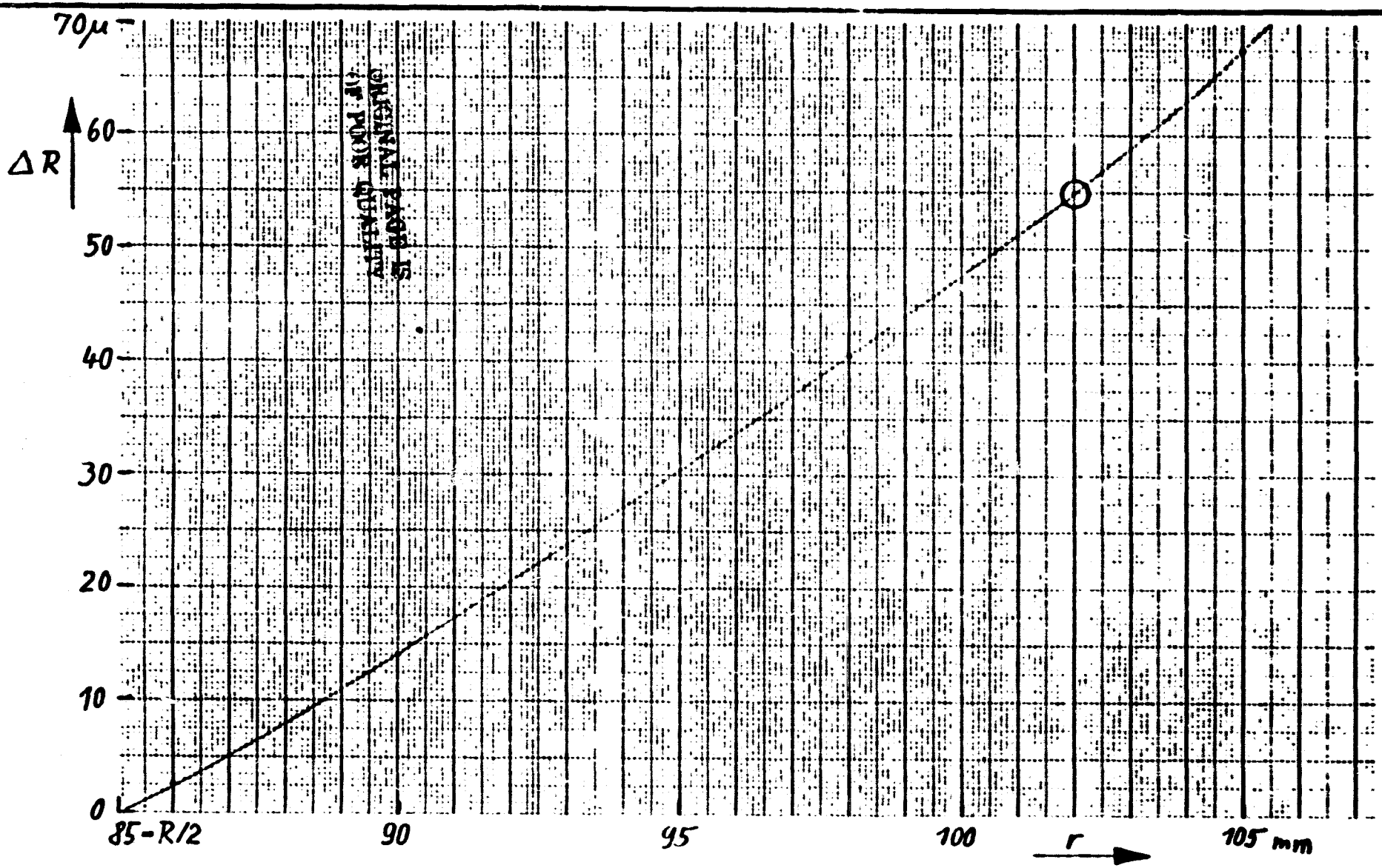

Fig. 3030/3: Total expansion of the tension rod mounting $\Delta l = 0$ $R = a + b = 170$ mm

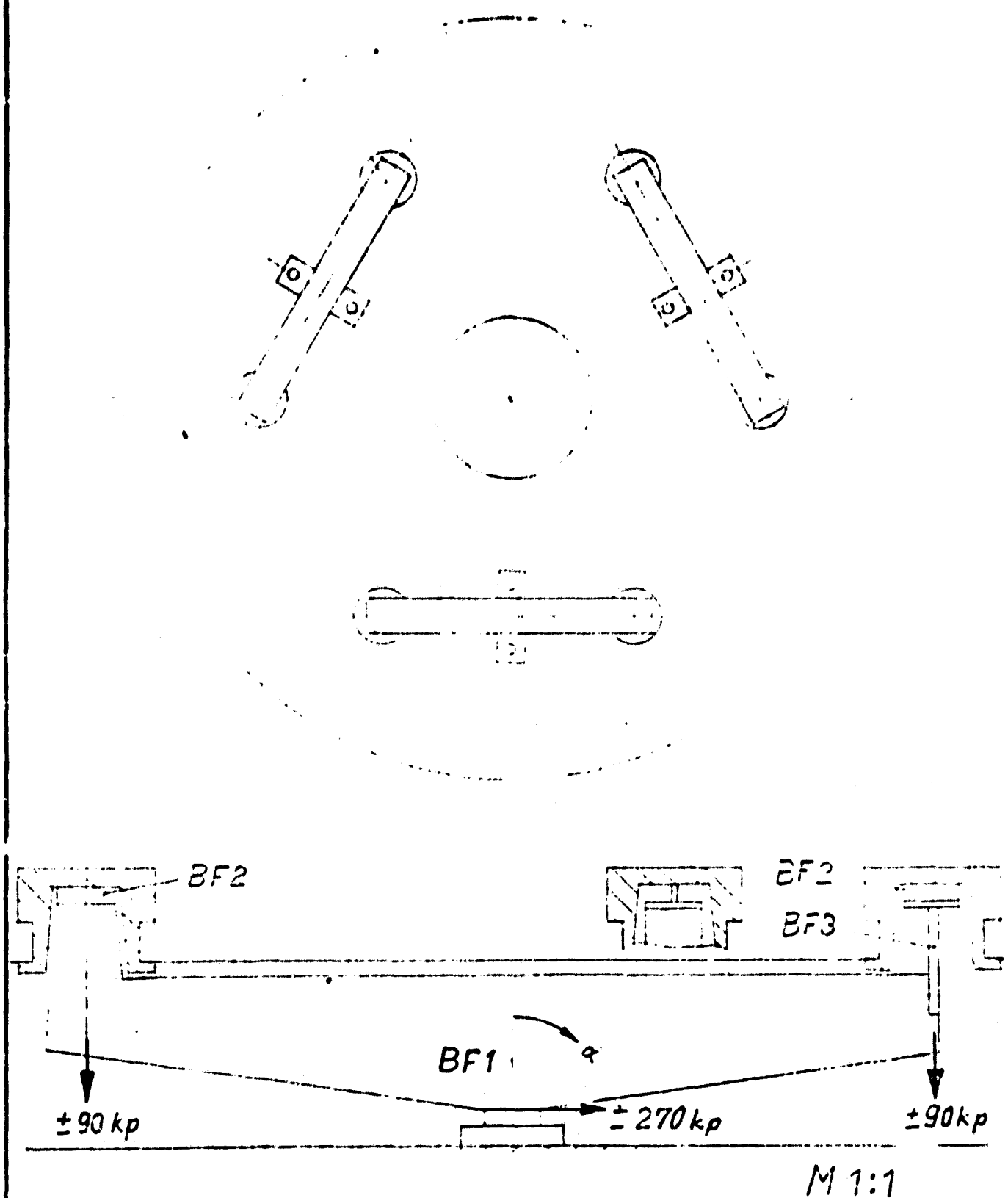

Figure 3030/4: Principle of the six-point mount (without expansion compensation in the longitudinal direction of the rockers).

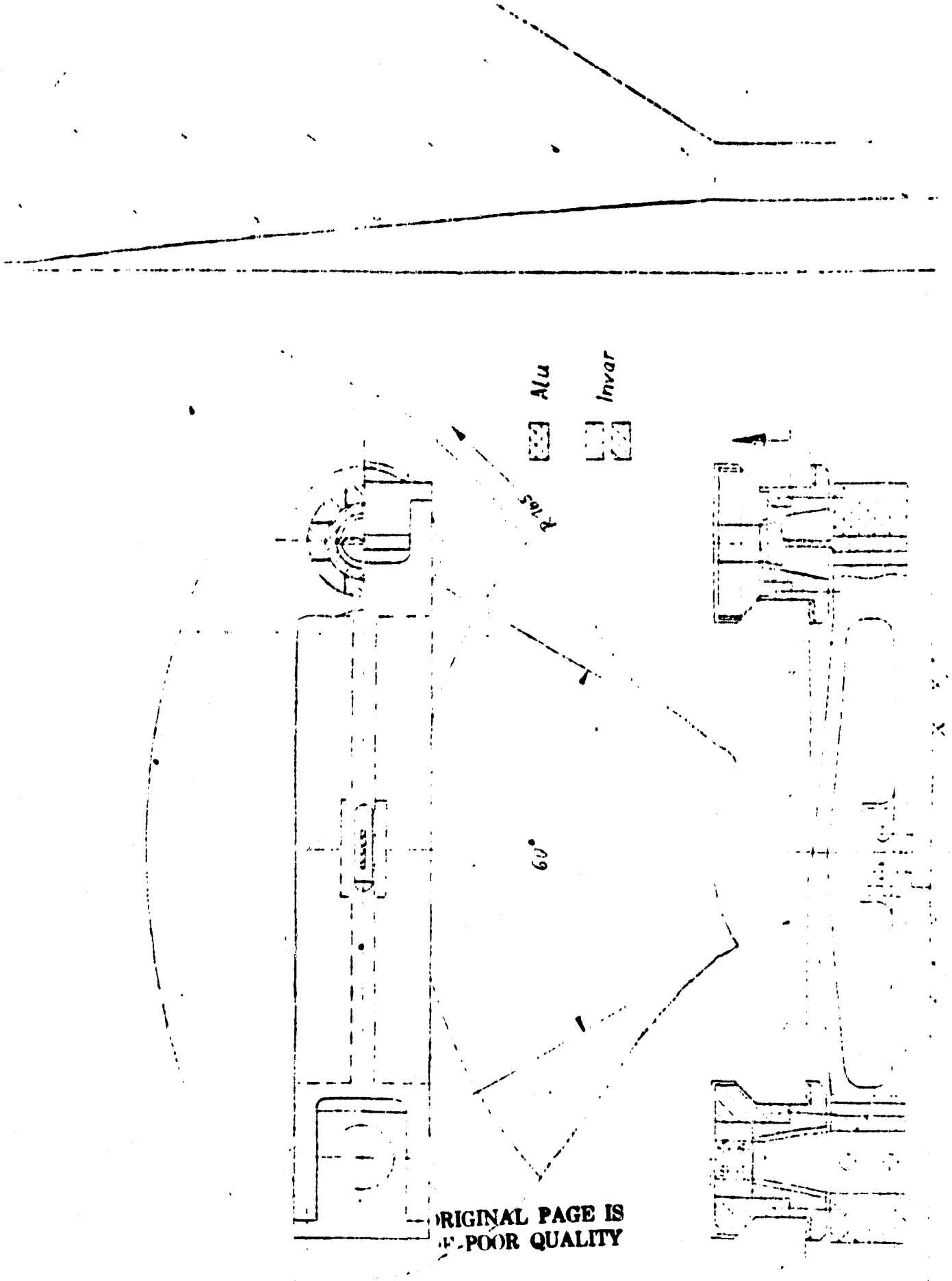

ORIGINAL PAGE IS
OF POOR QUALITY

Figure 3030/5: Construction draft of the six-point mounting.

$$F = \frac{f \cdot E \cdot bd^3}{l^3} = 7{,}2 \text{ kp}$$

An error compensation of 10 µm at 10 K would then still be approximately permissible.

Beneath the center of each rocker there is a spring joint BF 1, rigidly mounted to the base plate. A slight expansion of the rocker in the coordinate α (Figure 3030/4), necessary if the base plate bends, is possible due to the remainder elasticity of the bearing in this coordinate.

The expansion difference between the aluminum basis and the zerodur mirror in the support ring radius amounts to 0.54 mm in the present draft in the case of cooling to 10 K. This effects a tipping of the rocker by 0.78°, resulting in a radial force of 2.6 kp per rocker through the joint BF 1 with the dimensions d = 1, b = 10 and l = 3 mm. Additional forces are produced due to the bending of BF 2. They have the dimensions 0.8 x 10 x 3 mm and therefore exert half the force on the mirror in each case. The sum of the forces at each mirror supporting element is then also 2.6 kp.

Initial Load /28

When an acceleration of 20 g acts in the direction of the rocker axis, a force of F = 270 kp is produced in the case of a mirror weighing 27 kg. The ends of BF 1 then experience a parallel off-set f of

$$f = \frac{F \cdot l^3}{d\, b^3\, E} = 0{,}53 \text{ µm},$$

where E is again the elasticity modulus of invar at 10 K.

Only the "left" spring of the BF 2 springs is loaded in the direction of the rocker longitudinal axis. It is bent 0.67 µm at 270 kp. The lateral natural frequency of the system would be situated at approx. 750 Hz, when a total deflection of 2 µm is assumed.

With an axial acceleration, BF 1 is most greatly endangered. The tension occurring in this case is

$$\sigma_z = \frac{180}{10} = 18 \text{ kp/mm}^2$$

This is, however, one-seventh of the tensile strength of invar at 10 K.

In the case of no bending, the buckling load of BF 1 in the most disadvantageous case of the Euler buckling is

$$F_K = \frac{\pi^2 \cdot E \cdot b \cdot d^3}{48\, l^2} = 3130 \text{ kp}$$

The buckling stress would then be situated at 313 kp/mm^2, i.e. higher than the tensile strength δ, prohibiting the application of the Euler formula. With the tensile strength of invar, δ = 119 kp/mm^2, a buckling load of

$$F_K = 1200 \text{ kp}$$

would be achieved, again corresponding to a multiple of 6.7 of the maximum actually occurring load.

The buckling load of BF 3 is not at all critical because of dividing the force in half and the clamping introduced on both sides. /30

Disadvantage

The critical load on the glass is produced in the six-point model by bending the rockers under the axial initial load. The maximum force of 180 kp acting at the center of the rockers would cause a bending of the rocker by 43 µm in the case of the double T rocker cross-section chosen in Figure 3030/5. This amount would initiate an impermissible high moment in the mirror at the transition of rocker end and cerodur. A maximum achievable rocker cross-section would permit a reduction in bending to 10 µm, but this amount is still critical.

c) Three-point Mount

The concept of a three-point mount comprises a system, fixating three flat springs mounted tangentially on the support ring to the mirror in accordance with Figure 27 in the final report of phase A. On the mirror side, the three flat springs are mounted at invar sockets, engaged in three holes on the mirror rear surface. On the structure side, compensators are connected during assembly so that the relative expansion between structure (aluminum) and cerodur can be precisely removed theoretically, at least at 293 K and at the operating temperature of the telescope. To avoid base plate bending around an axis perpendicular to the flat spring, an additional elastic joint is planned, connected "in series" with the flat spring. While the actual flat spring is deflected in a radial direction of the mirror, i.e. permitting translations of the mirror in this direction, the perpendicular joint cannot permit any translation of the mirror in the flat spring direction. Flat spring and joint are designed for the axial buckling loads of the mirror during starting. The system is also capable of avoiding anisotropic expansion of the mirror basis structure. /31

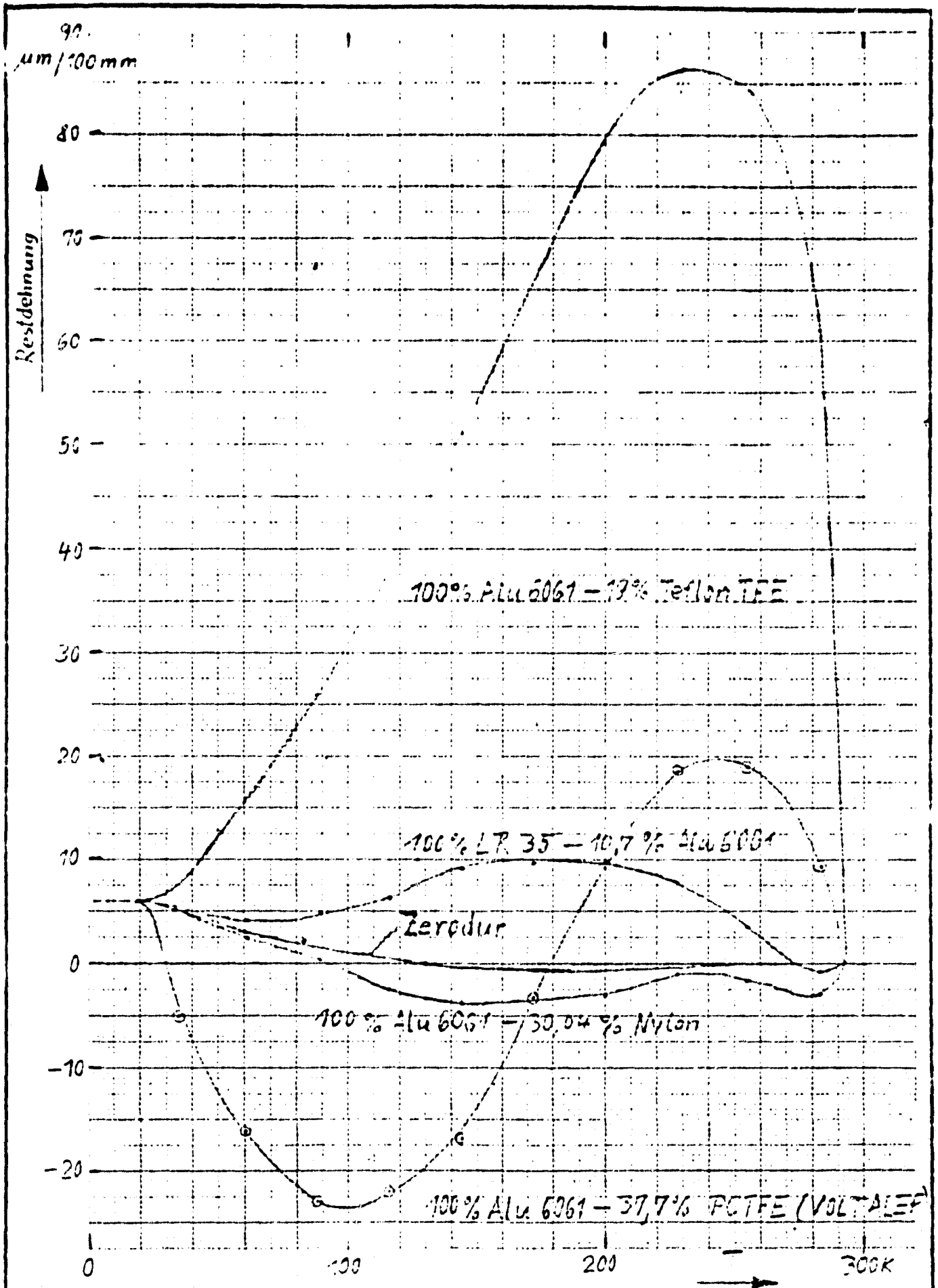

Figure 3030/6: Thermal expansion compensation compared to zerodur.

The calculations provide the result that the alteration in the distance of two support points from one another results in a translation of the mirror parallel to the connection line of the two affected supporting points and amounting to 55% of the alteration in distance.

In the conception of the three-point model, difficulties were encountered because the compensator extending in the mirror radius first required a rotary connection, in which play could not be completely eliminated. The mirror support would therefore obtain a softness of concern. In the search for a better solution, the so-called membrane model was finally favored, a further development of the three-point model to a certain extent. Both models are identical in principle, so that the explanation of the technical design can be limited here to the membrane model.

d) Membrane Mount, Principle and Design

The construction principle of a mounting group of the membrane model is presented in Figure 3030/7. In the lower portion of the figure, the group cut at a tangent to the support ring in a radial direction can be seen, in the upper portion of the figure, the section is carried out radially. The two important flat springs BF 1 are arranged symmetrically to both sides of the compensator. A further spring BF 2 extends in a radial direction of the mirror, preventing the bending of the mirror base plate as in the six-point model. The flat springs BF 1 are located with the ends on the mount side at the two brackets of the invar sleeve, suspended between the two circular membranes. The axial degree of freedom of this sleeve is controlled by the compensator extending into the sleeve. It is connected at the free end via an annular groove with the 33
sleeve, and at the other end via an invar nut with the stationary bearing pedestal. The effective length of the compensator can be altered, for example, by turning the nut in the bearing pedestal outward in the case of a compensator length which is too small, resulting in the sleeve of the compensator moving out with the same thread slope in relation to its core. The axial load of the mirror is therefore carried in a system of three flat springs behind one another, eliminating forces from the compensator.

The teflon-type material polychlortrifluorethylene (PCTFE) was employed for the compensators under the trade name Voltalef 300 of the DuPont Company. Compared to teflon, it does have a lower expansion coefficient, but a larger compression strength, so that it has a lower tendency to flow. According to reports of MBB, Voltalef 300 is planned for space projects such as the project HAD (Jupiter interferometer in the Galileo Project) and has passed the contamination and fumigation tests required there. Several thermal properties of this synthetic material are contained in the Figures 3030/8, 9, and 10. In Figure 3030/9, the modulus of elasticity for invar is also plotted, of great significance for estimating the rigidity.

The largest possible value for the rigidity of the two membranes was selected in the interest of a high stability of the mirror. This is, however, only possible up to that membrane thickness at which the

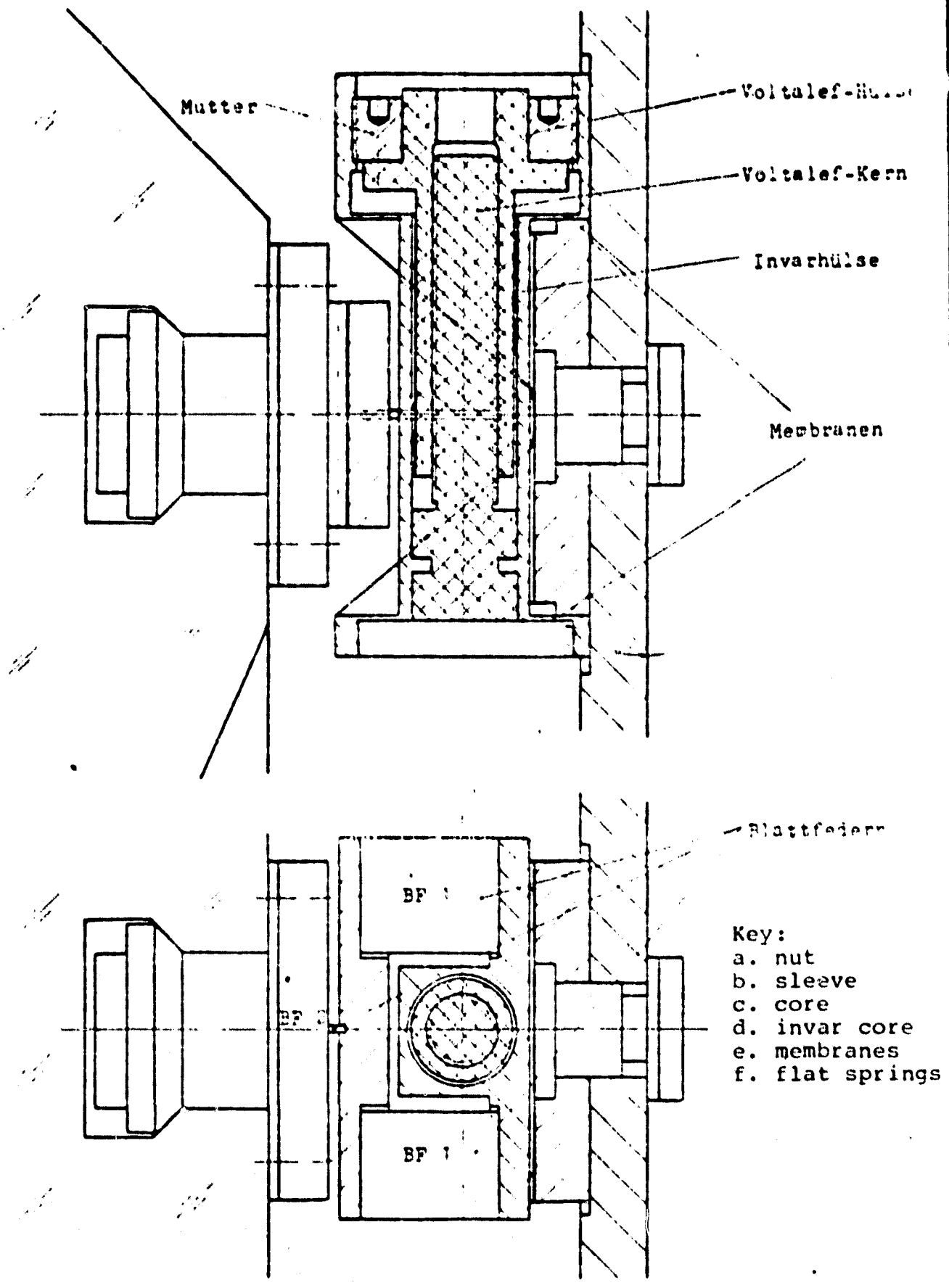

Figure 3030/7: Principle of construction for one of the three mount groups of the membrane model.

elastic shaping of the compensators is still small compared to the thermal contraction. Otherwise, the necessary compensator length would exceed the amount defined purely by thermal conditions at an impermissible level. A force of approx. 100 kp would be required, for example, to bend a 0.5 mm thick membrane by the amount of expansion difference between aluminum and cerodur.

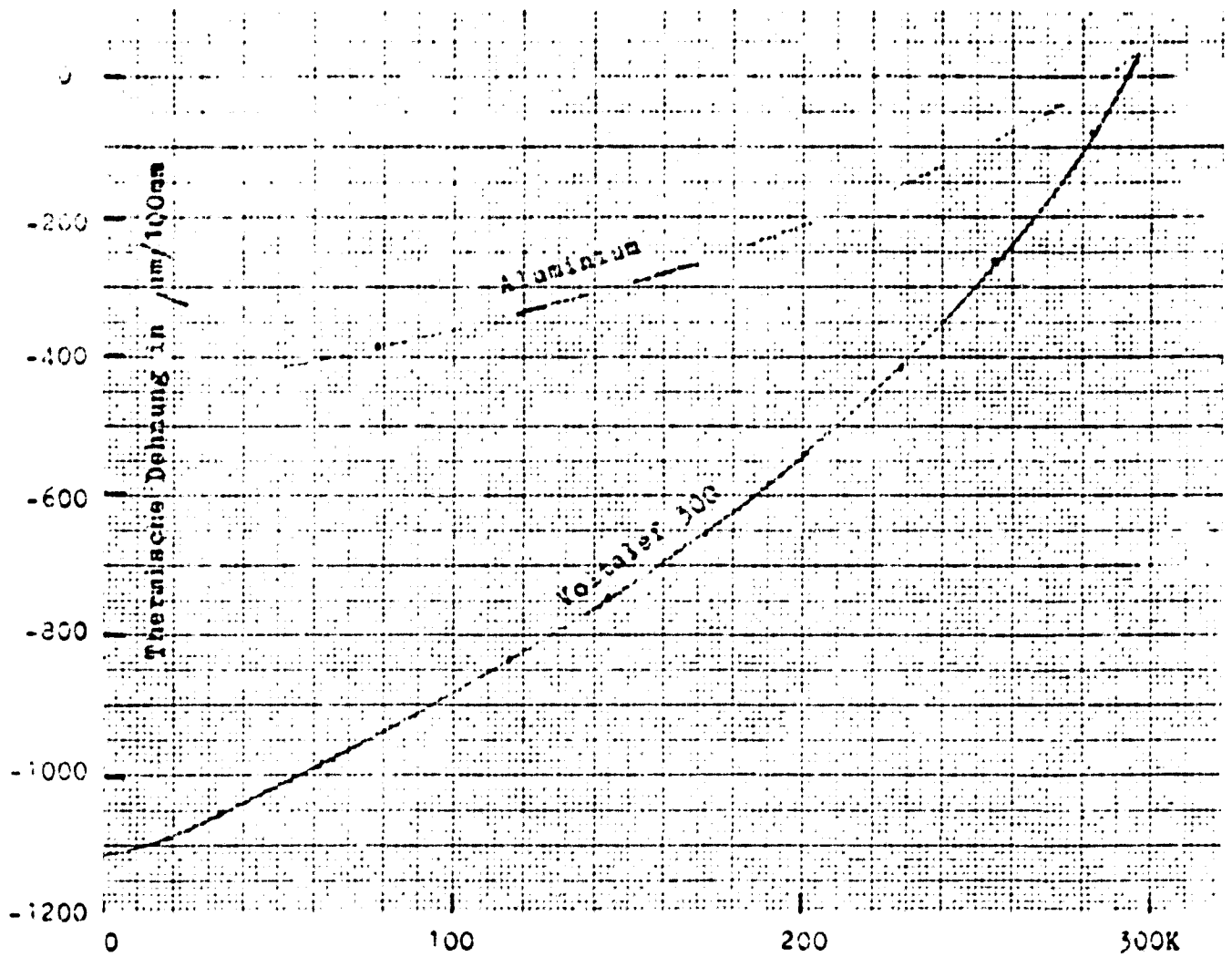

Figure 3030/8: Total thermal expansion of Voltalef during cooling.

Key:
a. thermal expansion

ORIGINAL PAGE IS
OF POOR QUALITY

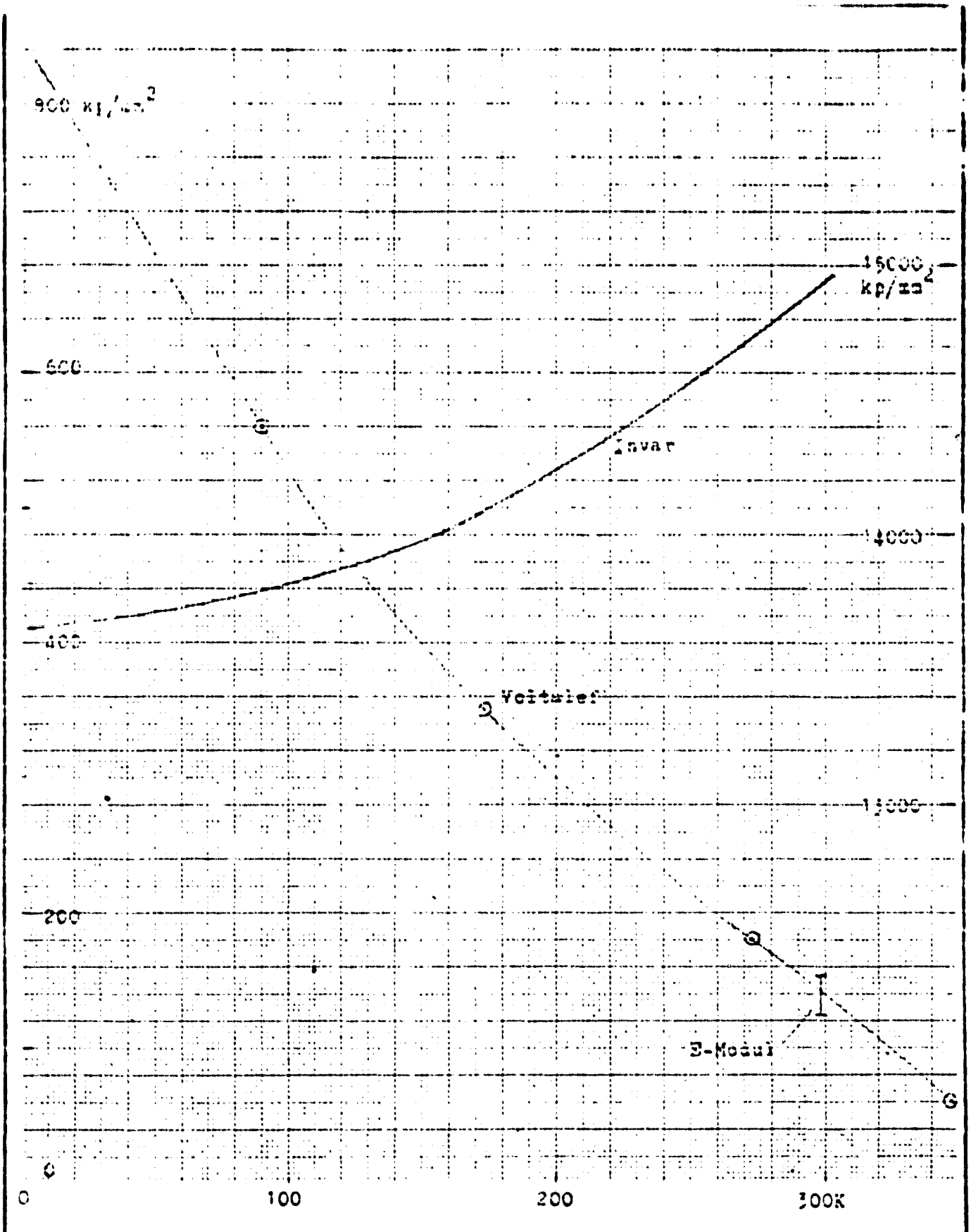

Figure 3030/9: The dependence on temperature of the torsion modulus of Voltalef and of the elasticity modulus of invar.

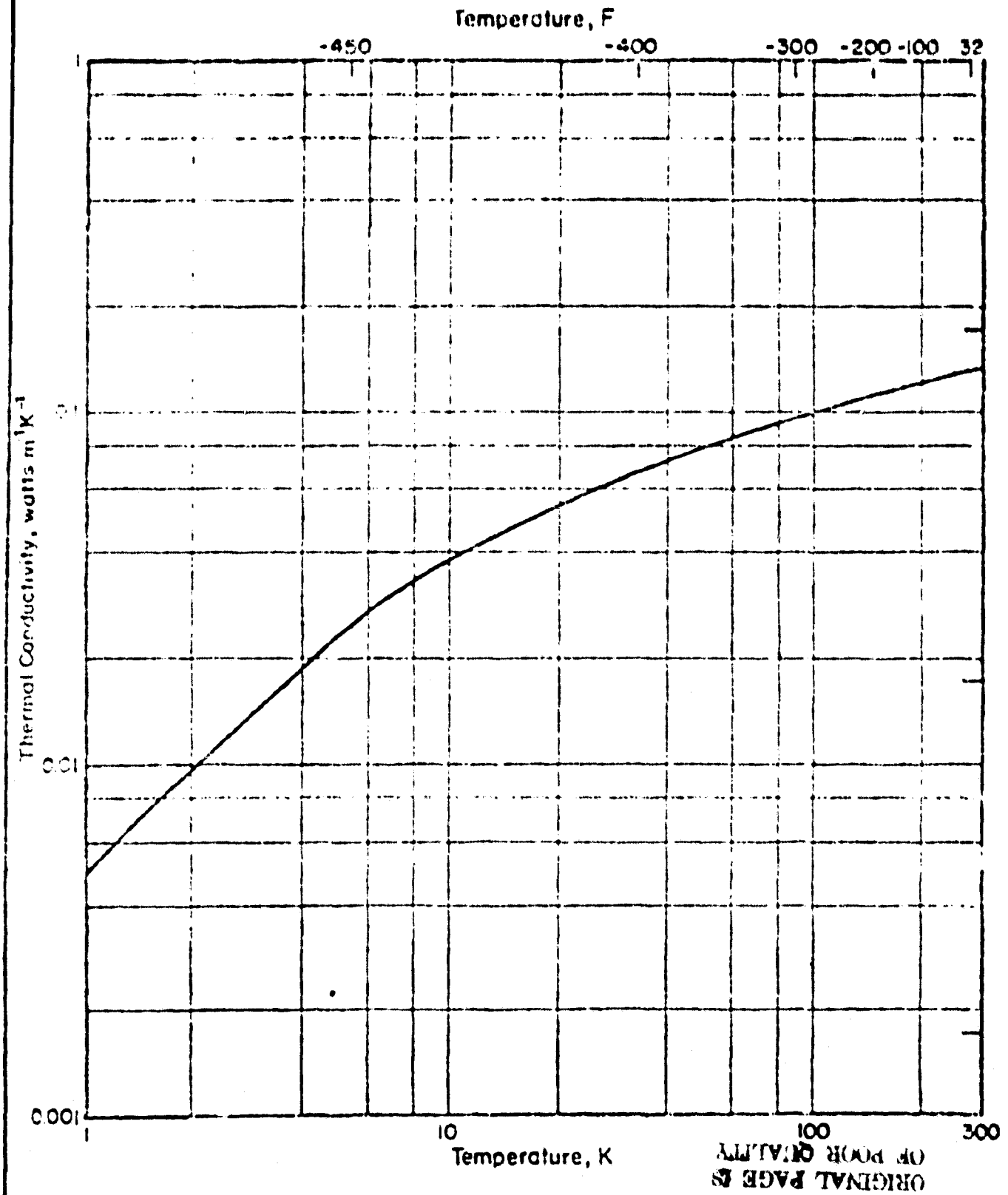

ORIGINAL PAGE IS
OF POOR QUALITY

Figure 3030/10: Thermal conductivity versus temperature for polychlorotrifluoroethylene (KEL-F)

AP 3032 Calculation of Critical Tensions and Deformations /37

In order to complete the elastic and mechanical calculations, more exact studies with a complicated knot model were carried out with finite elements. These studies were concentrated on surroundings of the mounting points in the mirror material. In order to keep the work within justifiable limits, a model was selected, surrounding the metallic mounting member concentrically. The shaping in a sectional plane of the model was made visible in a diagram. The effect of a radial force of one-third of the mirror weight at an acceleration of 20 g is given in Figure 3030/11. It was assumed in this model that the metallic mounting member exerts an initial tension of 0.2 kp/mm^2 in all radial directions on the cerodur. The total force at the hole was is then exactly compensated on that side from which the force acts, but doubled on the opposite side. The maximum deflection of the mirror material at the hole wall, seen in the diagram, amounts to approx. 0.1 µm.

The effective deformation of an axial load amounting to 20 times the mirror weight with even distribution to the three support points is given in Figure 3030/12. Both in the transverse and in the axial load case, the maximum tensions occurring achieve values of approx. 0.25 kp/mm^2. They are therefore situated in a safe range at room temperature for the cerodur material. As was already reported in the final report of phase A, the conclusions on the strength of glass and low temperatures deviate so greatly from one another that at the present time a more or less constant strength must be assumed. The empirical values for the tensile strength of cerodur at room temperature is situated at approx. 2 kp/mm^2.

A further form of initial load is the bending of the mirror object between the support points in the case of an axial load on the mirror. For the most precise determination possible of the maximum tension occurring in the glass, a model with finite elements was again employed. This model is presented in perspective in Figure 3030/13. The three support points are connected in a straight line with the most adjacent /41
intersections of the mirror body. Between the support points, the thickness of the knots was reduced for reasons of a more simplified calculation. The calculations produce the result that a maximum tension of 0.08 kp/mm^2 occurs in the case of an axial initial load of 20 g. The result demonstrates that this value is still approximately four times smaller than that in the surroundings of the mounting elements, as was established in the two preceeding diagrams.

AP 3033 Natural Frequencies and Concept Selection

A precise calculation of the natural frequencies in the system mirror + mounting elements was not possible in the stage of development work at that time, since completed construction drawings would have been required. It was therefore only possible to make a rough estimation of the natural frequencies. These are determined by the softest element in each case in the drafts of the four mounting principles studied. All estimations were carried out with the coefficient of

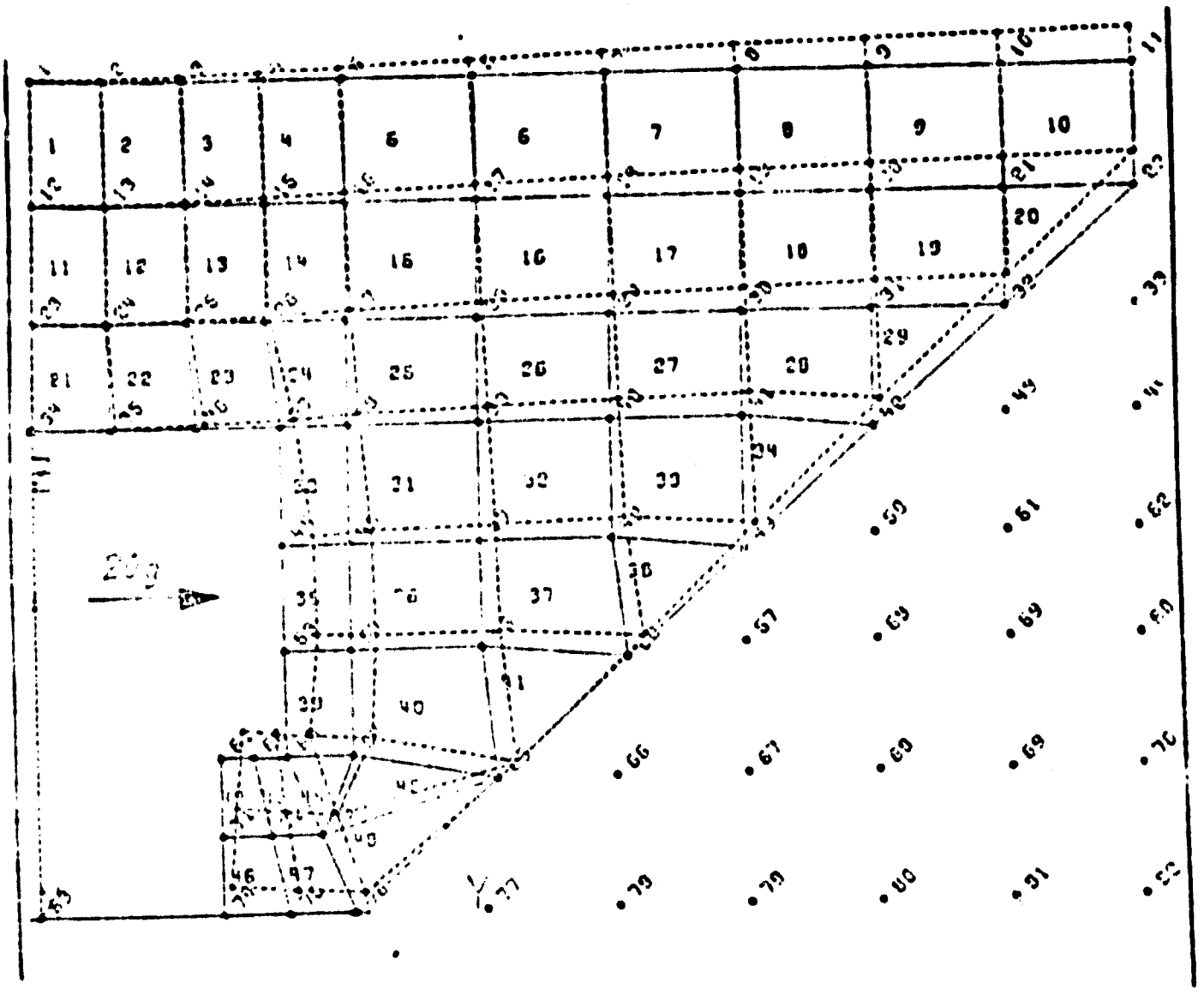

Figure 3030/11: Deforming effect of a transverse load of 20 g on the surrounding of a main mirror support point (concentric model).

elasticity of invar at 10 K, presented in Figure 3030/9.

The results of the frequency estimation are contained in an evaluation matrix (Figure 3030/14), intended to facilitate the most comprehensive comparison possible for the four mounting principles. The columns 1 - 3 as well as 1 - 12 of the matrix merely contain relative comparison values. The values in the remaining columns based on dimensions, however, also have more comparative than absolute significance.

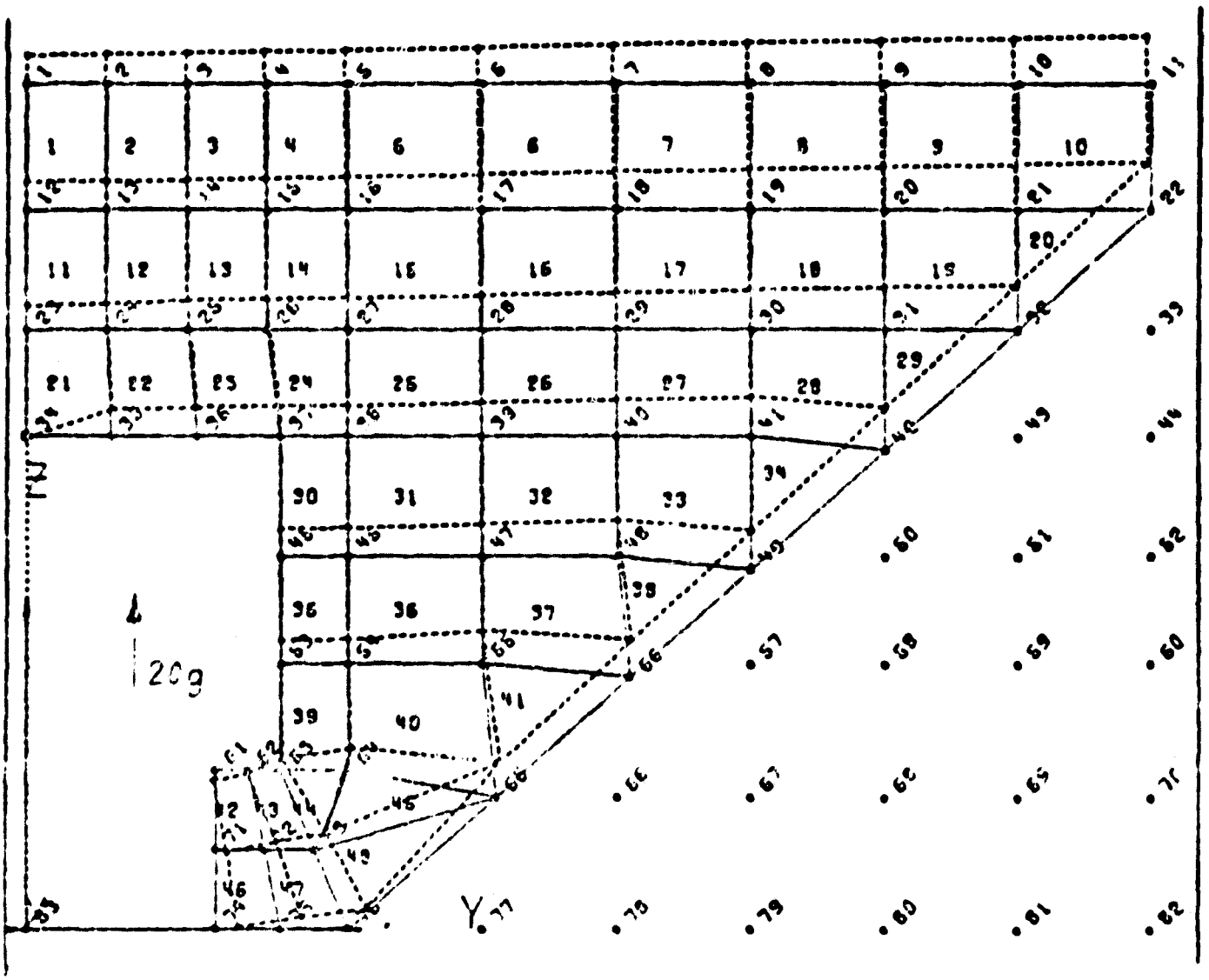

Figure 3030/12: Deforming effect of an axial load of 20 g on the surrounding of a main mirror support point (concentric model)

In the evaluation, the six-point mounting was first put aside, since it comprises an increased load on the glass material in spite of increased preparation work due to the effective moment explained above. The advantage lies solely in the smaller axial bending of the mirror under natural load, not necessary in the present case in this high quality. Furthermore, when it is considered that the three-point mount was a precursor of the membrane mount requiring improvement, then only

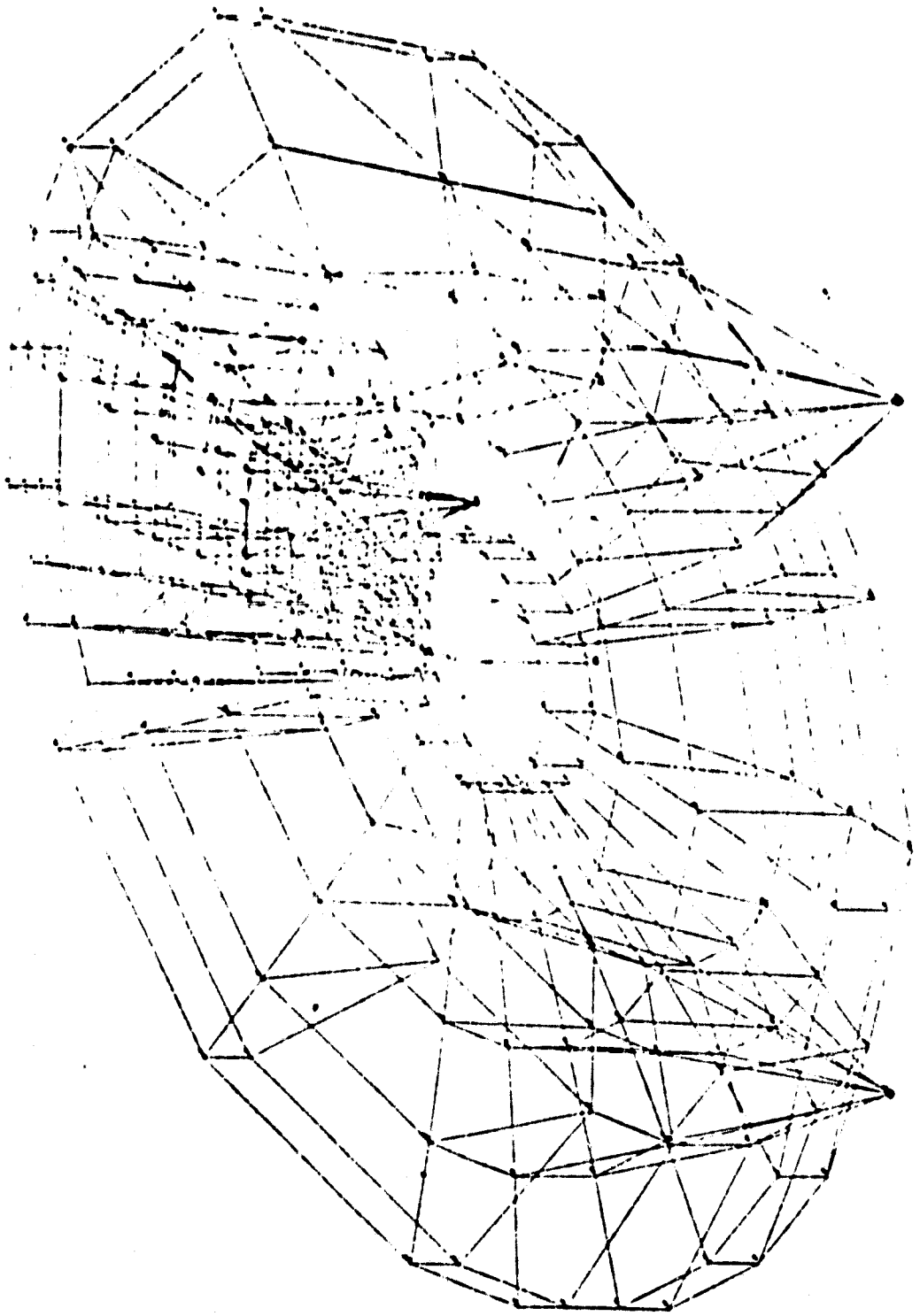

Figure 3030/13: Model for studying the elastic and mechanical behavior of Sl under the action of a three-point mount.

ORIGINAL PAGE IS
OF POOR QUALITY

the tension rod mount and the membrane mount can be included in the final selection. Although the tension rod mount makes the problem of the above-explained rod compensation at low temperatures necessary, it would still be desirable to compare both principles parallel to one another. There are, however, no available means for this purpose. The membrane mount, with only very slight advantages, was therefore favored. Its construction details are examined in the following section.

AP 3034 Optimization and Construction of the Membrane Support

The principle of the membrane support has already been presented in Figure 3030/7. It corresponds essentially to the constructive design. The entire unit is constructed of invar, with the exception of a compensation disc for the axial thermal expansion compensation of the sockets mounted in the glass and an aluminum mounting screw at the base of the unit. The flat spring BF 2 for avoiding bends in the base plate of the mirror was positioned as close as possible to the mirror in order to minimize additional initiation of moments. The radial play of the invar sockets in the mirror is dimensioned in such a manner that even at the extreme value positions of the summated expansion curve (Figure 3030/6) no pressure forces can be transmitted to the mirror. The conical surface of the socket is provided with a thin compensating coating to ensure a close fit on the glass all the way around. All flat springs are welded in their mountings by means of an electron beam procedure, tested in several preliminary trials with the material. The Figures 3030/15 and 16 show illustrations of the completed support units.

In addition to the two membranes with three slits, the welded seam for mounting the flat spring BF 2 on the mirror side can be seen on the round portion of the unit. The compensator with the metallic nut is screwed into the circular opening of the group (Figure 3030/16). /46

The complete main mirror support can be seen in the top view in Figure 3030/17 with the mirror removed. A ribbed aluminum welded construction was selected, complicated by the fact that the support points of the three-legged construction for the collector mirror assembly are not situated above the mounting feet of the instrument platform. They are shifted, as can be seen in the drawing, by 22.5° in relation to the middle of each mounting foot, i.e. in relation to the mounting element of the main mirror. The mounting points of the three-legged construction overhanging in this manner are supported by a system of pipes and flat ribs. A central pipe may serve later for assembling the main mirror baffle, the design of which is not yet final.

	a Startkräfte im Glas (relativ)			b Startdeformation der Metallstrukt.		c Eigenfrequenz des Systems		d Radiale Restkraft auf Spiegel bei 1 g Umlage	e Axiale Verbieg. des Spiegels bei 1g	f Herstell-kosten (relat.) Glas	h Strukt.	i Montage-empfindl.	
	axial 1	radial 2	Moment 3	axial 4	radial 5	axial (Hz) 6	lateral (Hz) 7			11	12	axial	radial
[illegible]-bung	1	1	mehr klein	33/u	33/u	200	200	50kp	20nm RMS	1,5	13 (incl. Abgl.	1	1
[illegible]pkt.-[illegible]	1,5 (incl. Mom.)	0,8	o mittel (ax.)	15/u	2/u	300	150	2kp	5nm RMS	2,5	10	2	2
[illegible]pkt.-[illegible] [illegible].	1,2	1,2	p klein (rad.)	12/u	12/u	300	300	2kp	20nm RMS	2	7	2	-
[illegible]pkt.-[illegible] [illegible] [illegible]embranen	1,2 1	1,2	klein (rad.)	17/u	5/u (?)	300	500	5kp	20nm RMS	2	10	2	2

Figure 3030/14: Evaluation matrix of the four various mount principles for the mirror.
(For Key please see following page.)

Key:
a. initial forces in the glass (relative)
b. initial deformation of the metal structure
c. natural frequency of the system
d. radial remainder force on mirror at 10 μ error compensation
e. axial bending of the mirror at 1 g
f. manufacturing costs (relative)
g. glass
h. structure
i. centering sensitivity
j. tension rod mount
k. six-point mount
l. three-point mount with hole
m. three-point mount with membranes
n. very small
o. medium
p. small

/44

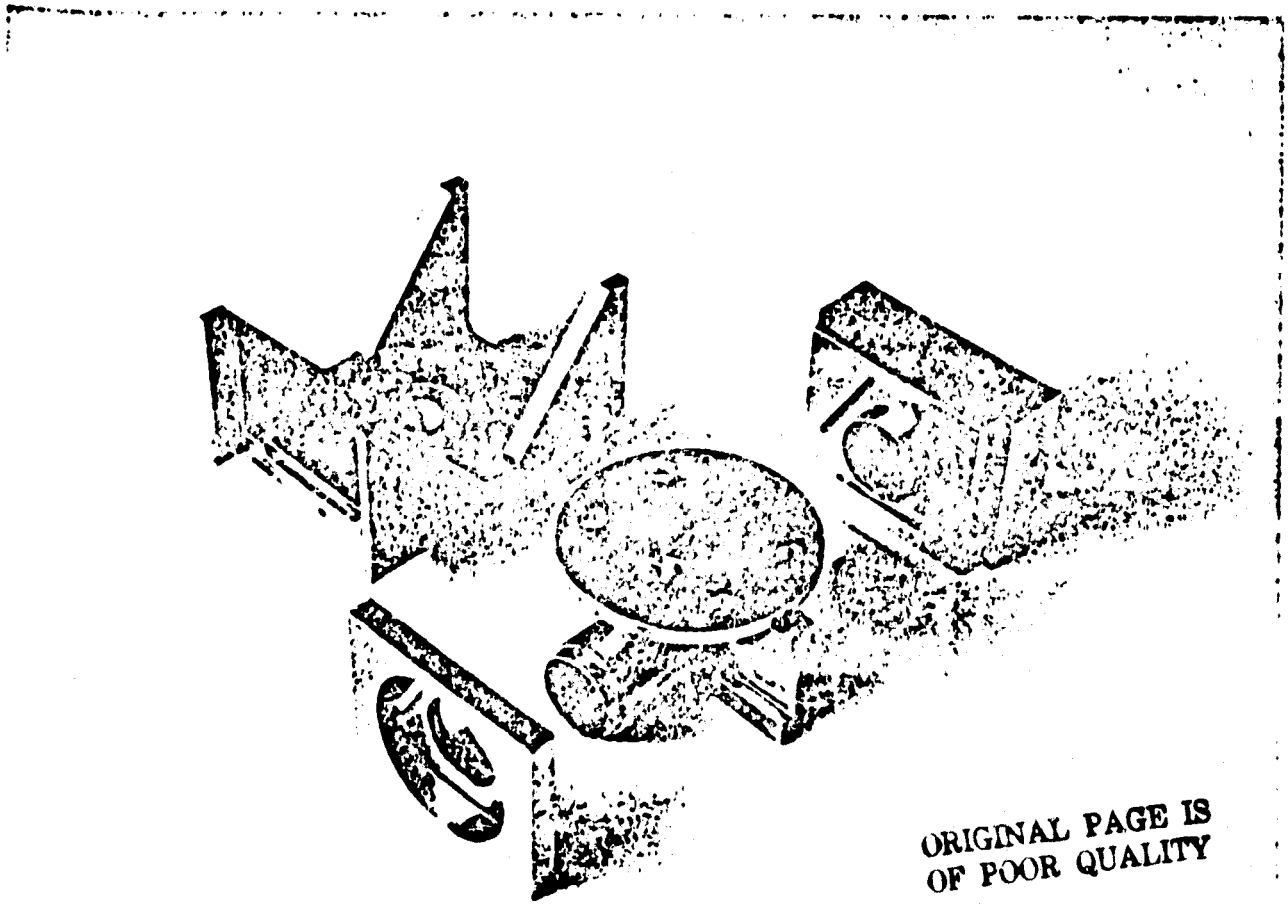

ORIGINAL PAGE IS
OF POOR QUALITY

Figure 3030/15: Support unit for the shake and thermal model of the main mirror in partially assembled state.

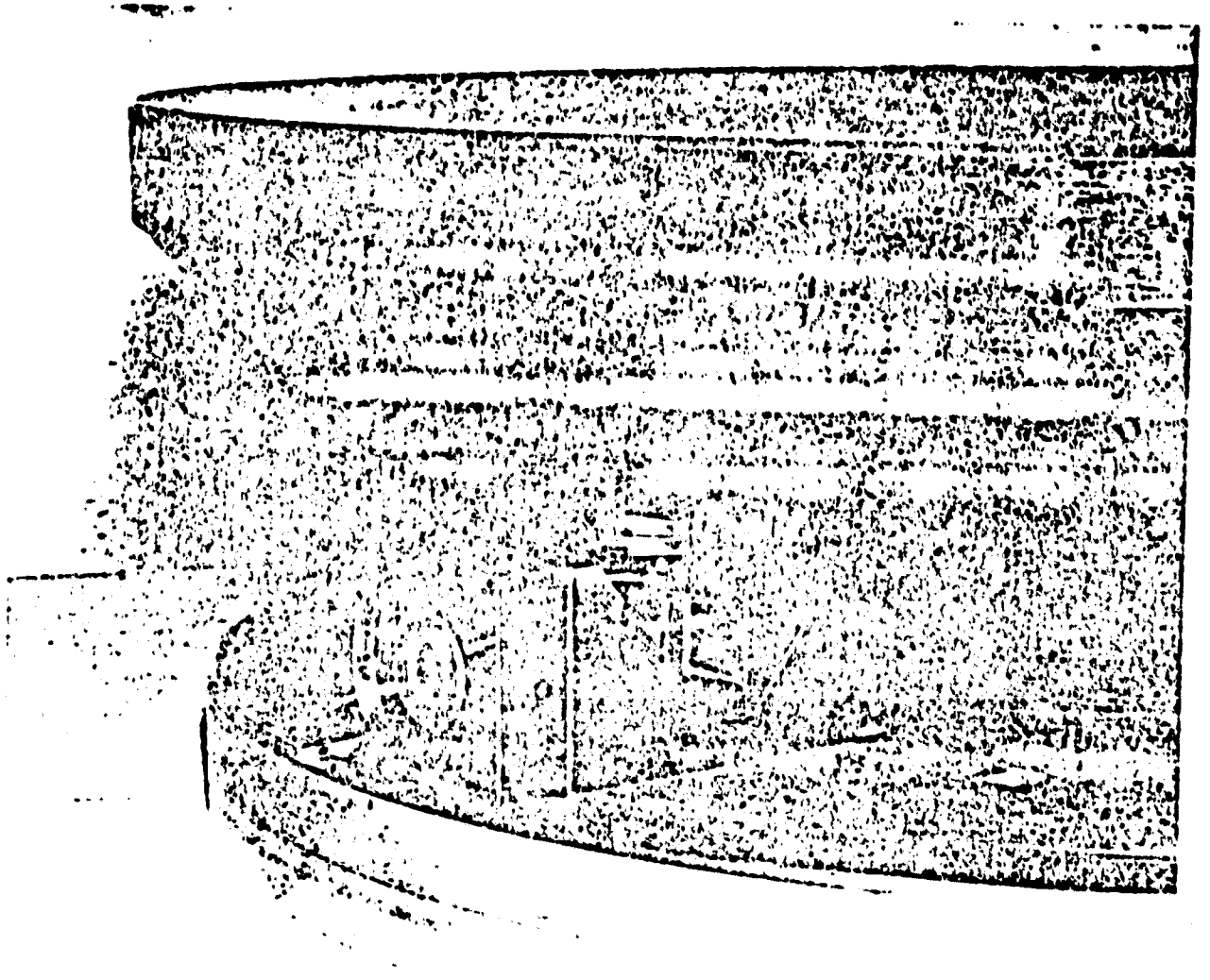

Figure 3030/16: Completely assembled support unit of the main mirror (simplified base plate of the shake model).

Weights

The weight of the main mirror body alone determined on scales amounts to 25.0 kp, while the weight of a support unit of invar, also determined on scales, amounts to 1.4 kp. The weight of the welded support construction of aluminum was first estimated; the result is 7.8 kp. The total resulting weight for the supported main mirror is therefore 37 kp. This does not yet include the main mirror baffle and the system of thermal conductors and collector lines.

ORIGINAL PAGE IS
OF POOR QUALITY

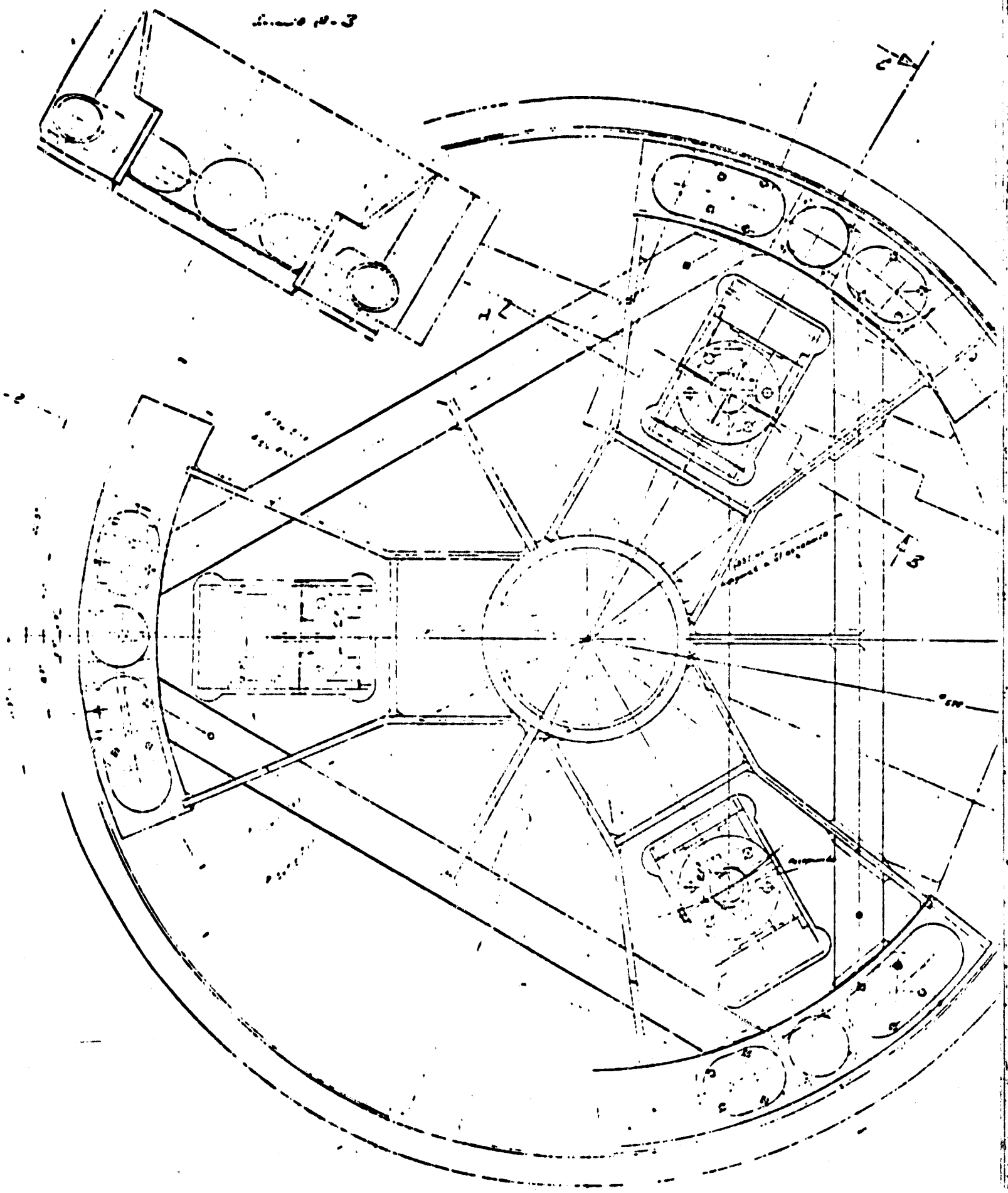

Figure 3030/17: Complete main mirror support.

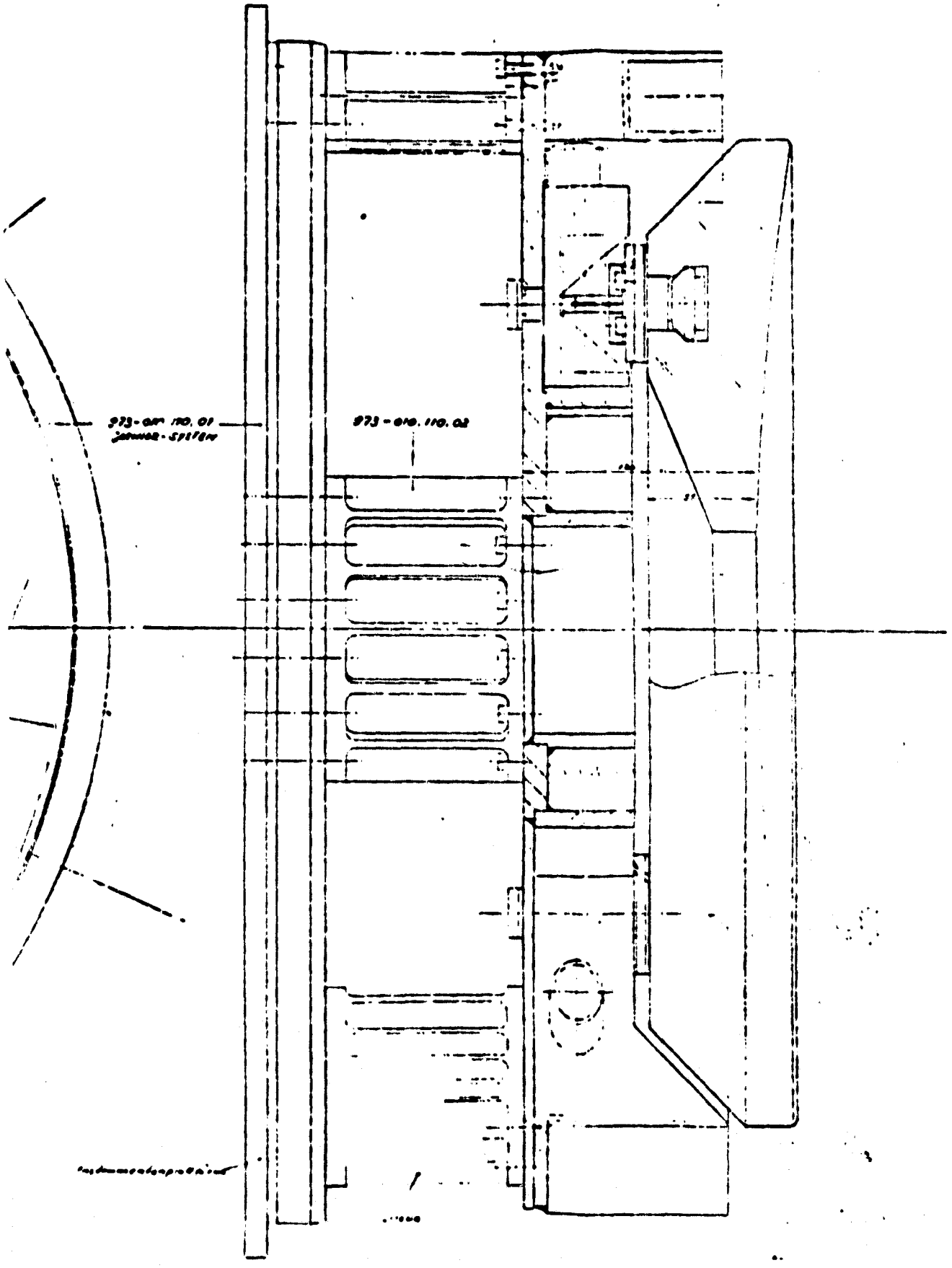
973-010.110.01
973-010.110.02

AP 3035 Shake Model and Test Results /48

A shake model for vibration and shock tests was prepared with a cut main mirror in the original dimensions. In order to remove surface cracks, the completely cut mirror was subjected to etching with a mixture of fluoric acid and sulfuric acid. The depth of material removed was between 0.3 and 0.5 mm. The mirror was assembled with the same support groups, as were prepared for the thermal model (Figure 3030/16). They were screwed onto a 40 mm thick annealed aluminum plate free of tension. The heat conductors were not mounted at the mirror. Figure 3030/18 shows the complete shake model.

Two acceleration pick-ups were cemented on the mirror surface for these tests in order to achieve quantitative measured results. Figure 3030/19 shows the coordinate system employed. On the lower side of the mirror a plane mirror was cemented, closely opposite to a second mounted on the aluminum plate, so that both mirror surfaces could be aimed at simultaneously with a collimator of high resolution. The directions of the individual coordinates for the acceleration pick-ups were switched in such a manner that in the X direction the phases were in step, while they were out of step in Y and Z. Torsion and slope vibrations could also be ascertained in this manner. In the plane of focus in the collimator, the coordinates parallel to the optical axis of the test sample are designated with u, the perpendicular ones with v.

First, measurements were carried out in the case of axial sine vibration of the test sample. The constant acceleration of excitation amounted to 0.5 q in this case. The consequence of the tests and the intermediate control of grid images in the collimator is presented in Table 3030/1. The torsion and tipping of the mirror measured between the individual vibration tests are in relation to the value zero in each case before beginning the test. The first test series, ending at 100 Hz, did not show any resonance point. The torsion was less than 1 arc second, and tipping the mirror was determined at approx. 3 arc seconds after this test series. This corresponds to an alteration in height at one of the three support points by 0.7 µm. In the second test series of 10-500 Hz, a resonance point was found /52 at 160 Hz. The amplitude of the mirror was so great in this case, that it required two further test series (no. 3 and 4), until the amplitude of the mirror could be clearly read off. The third resonant series (test series no. 4) is given in Figure 3030/20. The 6 tracks of the recorder correspond to the three coordinates of the two acceleration pick-ups. The illustration shows that the mirror achieved an amplitude of ±18 q in the axial direction. A considerable radial motion was also combined with this, as the deflections in z_1 and z_2 demonstrate.

As the time scale in the diagram shows, the individual deflections of the recorder do not correspond to the actual vibration in the mirror. The actual vibrations are rather extended with the aid of a sampling procedure in such a way that they supply a local frequency of identical size on the recording strip at all frequencies. The conversion is carried out, of course, true to amplitude and speed. In the

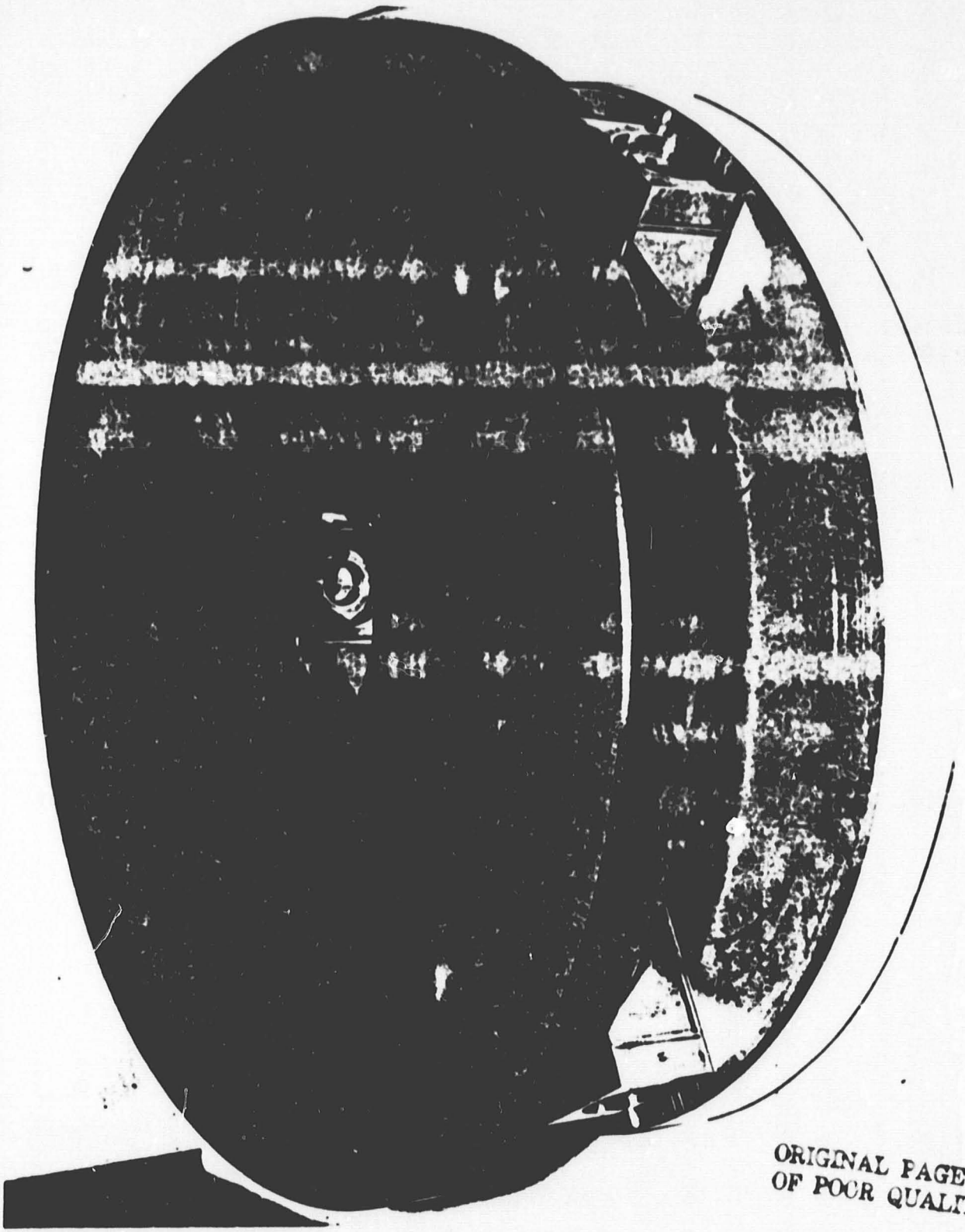

ORIGINAL PAGE IS
OF POOR QUALITY

Figure 3030/18: Shake model of the main mirror.

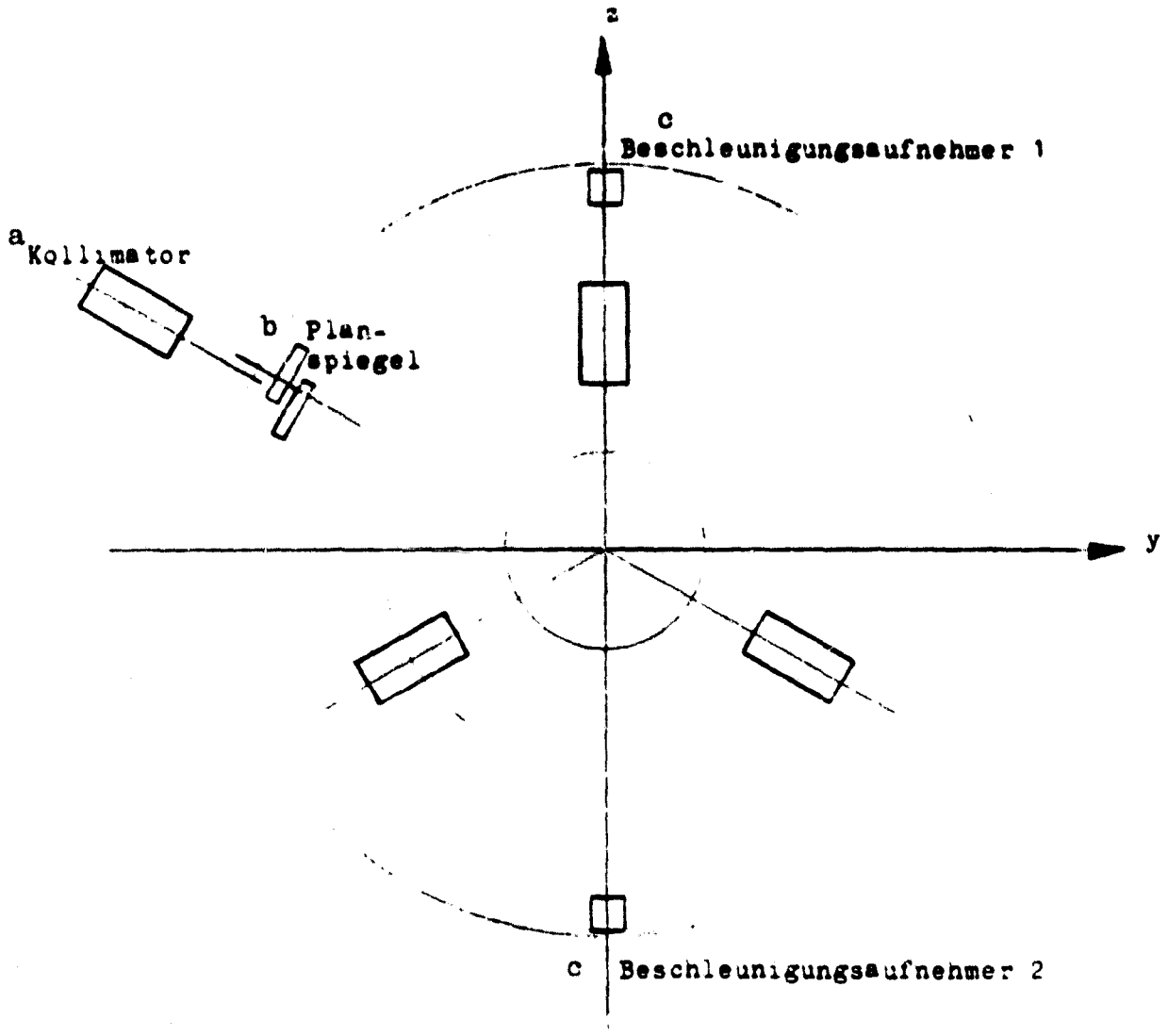

Figure 3030/19: Coordinate system for the measurements of acceleration in the shake model. X coordinate = optical axis.

Key:
a. collimator
b. plane mirror
c. acceleration pick-up

a Test Nr.	b Frequenz-Bereich in Hz	c Frequenz-änderung Okt./min	d Resonanz bei Hz	e Torsion u gegen Grundpl.	f Kippung v gegen Grundpl.
1	5 - 100	1			
				0	3"
2	10 - 500	3	160		
				27"	24"
3	10 - 500	3	160		
				57"	43"
4	10 - 500	3	160		
				170"	32"
5	10 - 1000	3	160		
				172"	38"

Table 3030/1: Test series with axial sine vibration

(Please see following page for Key.)

Key:
a. test number
b. frequency range
c. frequency alteration octave/minute
d. resonance at Hz
e. torsion u against the base plate
f. tipping v against the base plate

recording duration of the resonance process of approx. 5 sec., the mirror was subjected to approx. 800 individual vibrations.

In the test series 5, a determination was to be made whether further resonance points can be found at higher frequencies. While the resonance point at 160 Hz must be attributed to the flat springs BF 2 (Figure 3030/7), the resonance behavior of the springs BF 1 as well as the membranes was expected at higher frequencies. The resonance points, ascertained in the test series no. 5 are presented in Figure 3030/21. The scale in the two axes of the diagram are identical to those in the previous figure. The result shows that in addition to the resonance point at 160 Hz there is a further one at 640 Hz. It cannot be stated with certainty whether this is the second overwave of the base vibration, since it exhibits exactly a multiple of four, or whether this resonance was caused by another of the participating flat springs. Moreover, the result shows that the resonance behavior at 160 Hz is greatly disrupted in contrast to the recordings up to now. The amplitude of x_2 is greatly reduced, pointing to a beginning decoupling of the mirror. The other curves are overlapped by effects of higher frequency, also pointing to the initiation of mirror support destruction. The amplitude of x_1 is over-controlled in between, so that no maximum value can be read off in this case. As the values of torsion and tipping (Table 3030/1), measured with the collimator, show, the destruction of the mirror support must have begun in test no. 2. After test no. 3, the measured deformation is increased to a double value, after test no. 4 the torsion has a substantially higher value. /55

In spite of beginning destruction of the mirror mounting, an attempt was still made in another assembly of the mirror on the shake table to determine the resonance point in the case of radial sine excitation. The low-frequency excitation up to 100 Hz at the beginning with a constant maximum value of 0.5 g already led to the fracture of one of the springs BF 2. The tests had to be subsequently discontinued.

The result clearly points to the fact that the springs BF 2 must be strengthened. Moreover, this elastic member must be designed in such a manner that the torsion motions of the mirror are substantially limited; i.e. no translation may occur involving both mounting points of the spring BF 2 in relation to one another. A reconstruction of the mounting groups and a repetition of the vibration test, as would have been desirable, was not possible with the means in phase B.

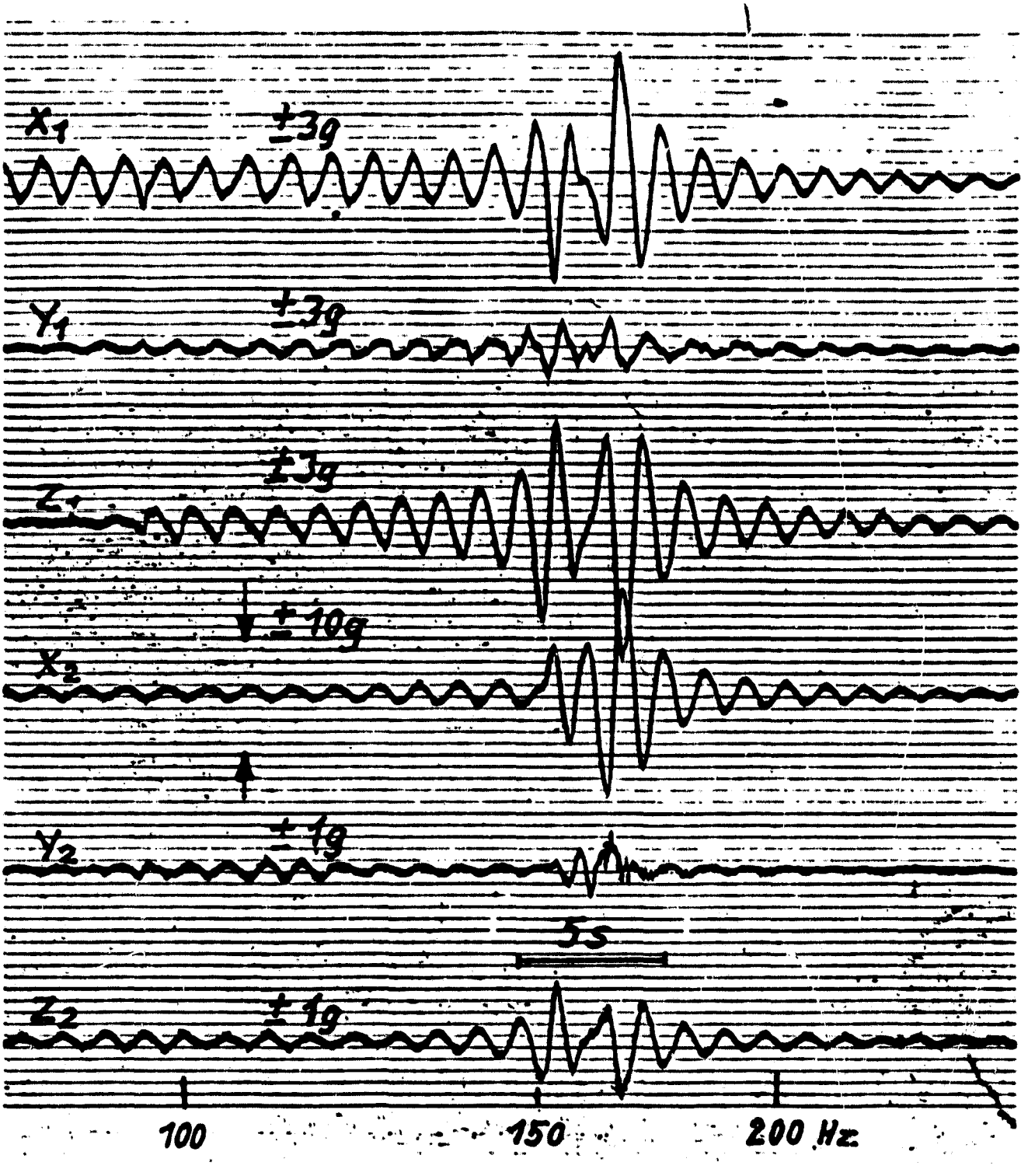

Figure 3030/20: Resonance behavior of the main mirror in the case of axial sine excitation registered in the sampling procedure at 0.5 g (test no. 4).

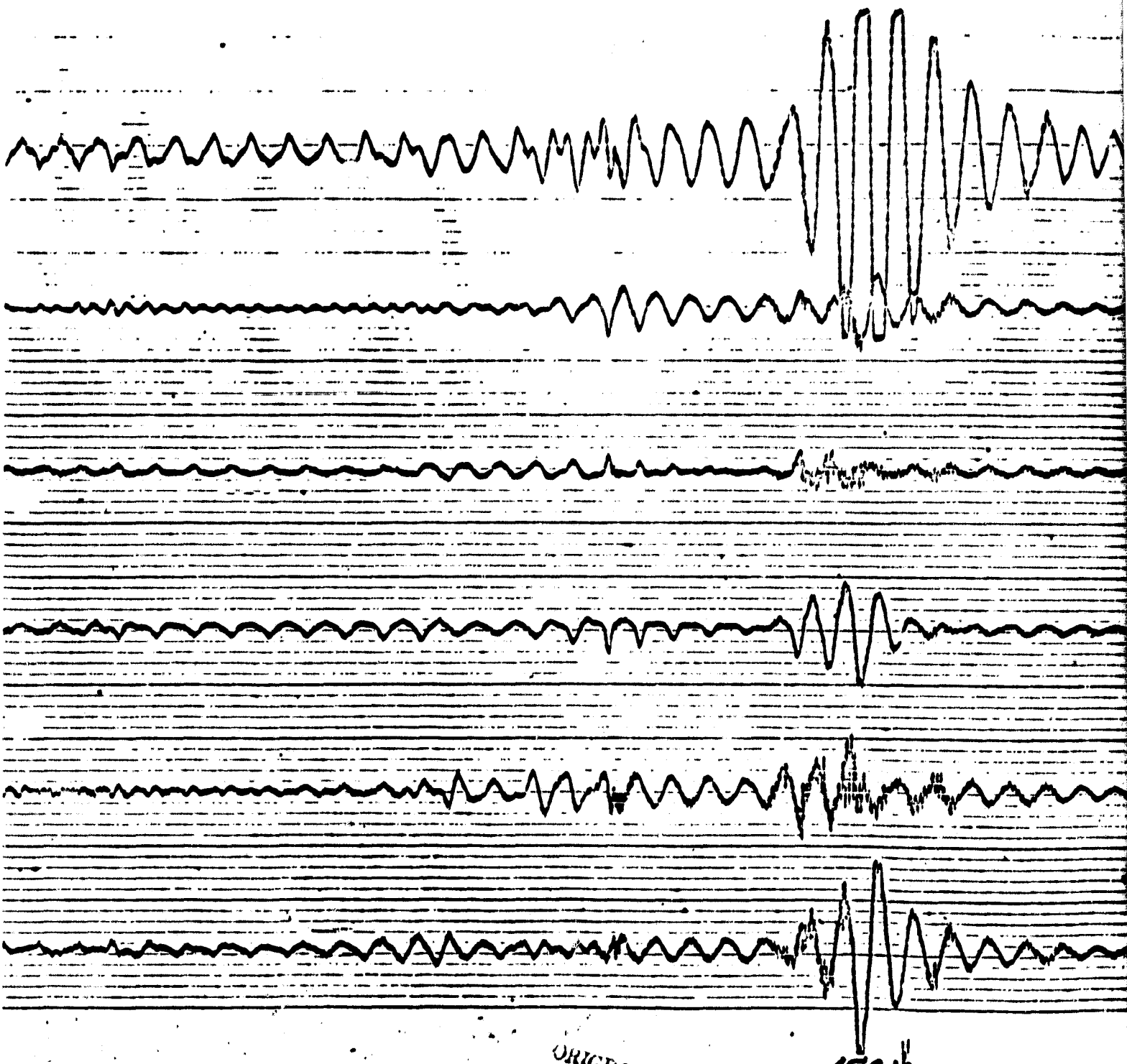

FOLDOUT FRAME

ORIGINAL PAGE IS
OF POOR QUALITY

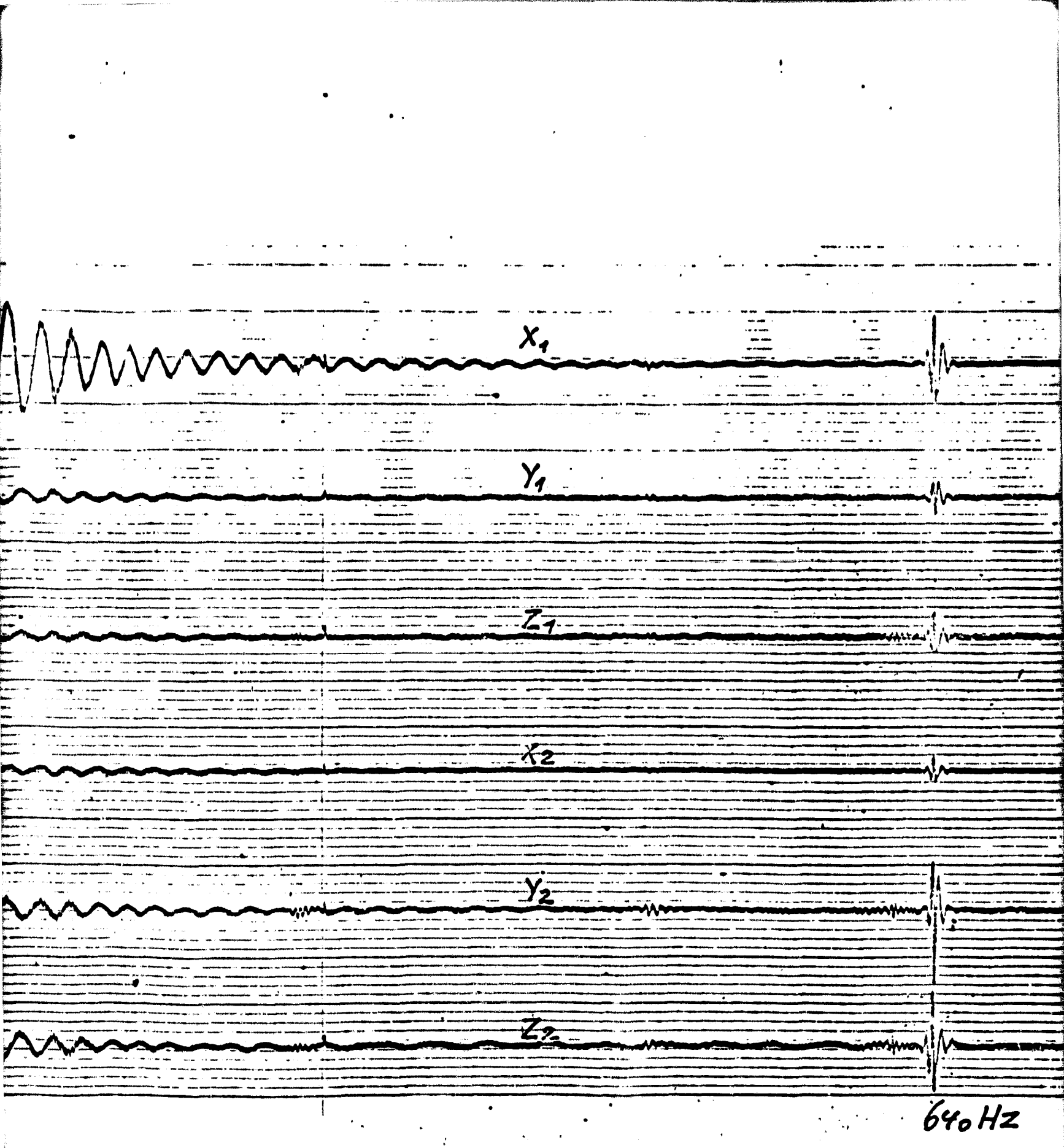

FOLDOUT FRAME

Figure 3030/21: Resonance behavior of the main mirror with axial sine excitation at 0.5 g (test no. 5).

Supplementary Remarks

All natural frequencies were determined in a later stage, using the thermal model of the main mirror in such a manner that the mirror was not subjected to any dangerous excitation, but was merely excited by a light blow with a rubber hammer. The following frequencies were recorded:

transverse, perpendicular to a flat spring	48 Hz
transverse, parallel to a flat spring	77 Hz
axial	125 Hz
torsion	78 Hz

AP 3040 Thermal Behavior of the Main Mirror /56

AP 3041 Calculation of the Temperature Differences of the Stationary Case

An nodal model was selected for the thermal calculations in the main mirror with nodal numbers in a radial cross-section of the mirror to be found in Figure 3040/1. Each intersection represents a ring around the axis of the mirror, having multiple values with respect to the azimuthal angle. An angle resolution along the nodal rings is only relevant in the case of an asymmetrical radiation load on the mirror or in the subsequent calculation stage in the case of a study on the thermal effect of the head conductors with azimuthal discreet distribution.

The first computation on stationary temperature distribution in the mirror surface was carried out under the assumption of two concentric rings of heat conductors on the lower side of the mirror with the radii 150 and 206 mm. The discreet distribution of the heat contacts was not first taken into consideration in the calculation model, but instead an enclosed heat conductor cylinder was assumed, in which only axial heat conduction was permitted. The heat conductivity of the cylinder was selected at a value corresponding to 18 individual sensors in the external circle of the total heat conduction with characteristics taken from the first measurement results of the Linde Company. This result, later proving to be defective, contains values situated exactly one order of magnitude above the realistic values. The base points of the heat conduction cylinder were placed at a temperature of 1.6 K. The calculation results for the cases of homogenous and inhomogenous radiation, as well as an explanation of radiation distribution in the asymmetrical case can be seen in Figure 3040/2. The radiation was assumed within the useful surface of the mirror of 400 mm diameter. The total capacity absorbed by the mirror amounted to 15 mW for this and all subsequent calculations.

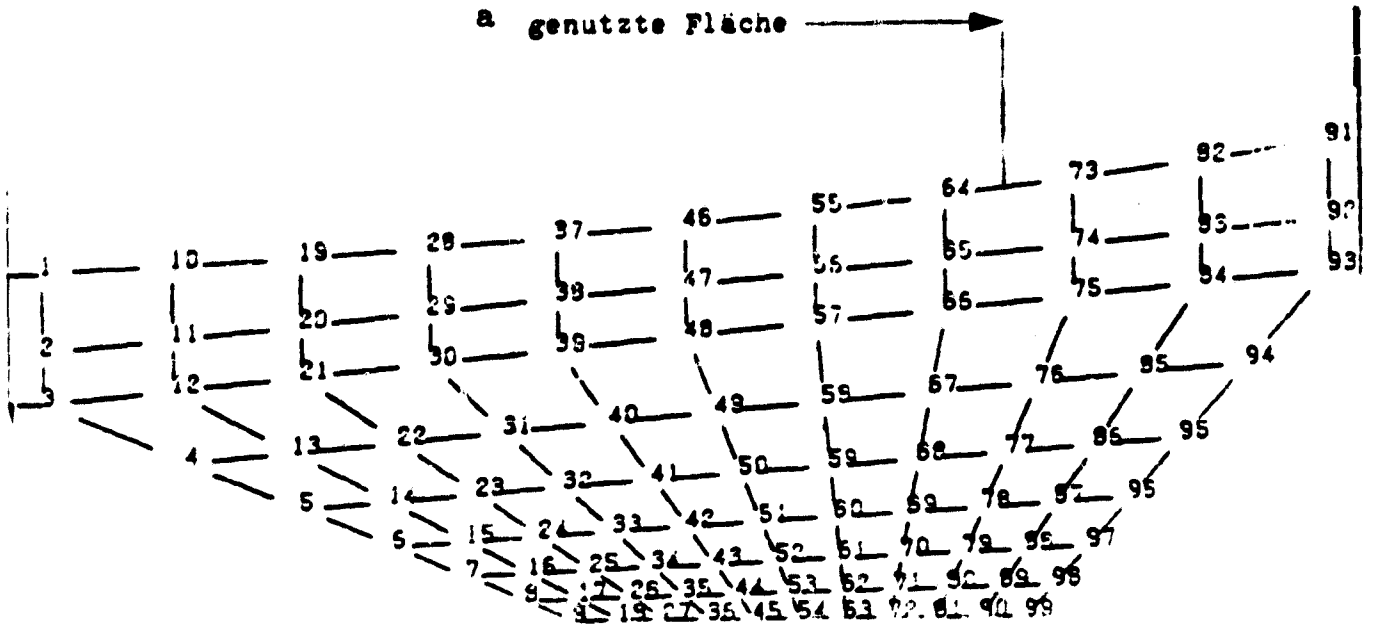

Figure 3040/1: Intersection model for the thermal calculations in the main mirror. In the half section presented, each intersection represents a concentric ring around the mirror axis.

Key:
a. utilized area

The inhomogenous or asymmetrical case of radiation was simulated by the reduction in radiation capacity from the azimuth angle 0° to the azimuth angle 180° in the form of a cosine distribution (compare Figure 3040/2). The radiation densities are constant along each radius in this case. /59

In the case of homogeneous radiation, the coldest point in the mirror surface is situated at the node 91, as expected. The warmest point, i.e. the point of poorest heat dissipation, is found in the nodal circle 1 at the hole edge. A monotone drop in temperature dominates from there up to node 64. The greatest temperature difference in the utilized mirror surface amounts to 0.109 K. In the case of asymmetrical radiation, the area around the azimuth angle 180° is the coldest point, as expected; it achieves almost the temperature of the heat conductor cylinder base points. While the temperature difference in the individual radii is less than in the case of homogeneous radiation, the temperature difference between the azimuths 0° and 180° is substantially greater and is situated at 0.43 K.

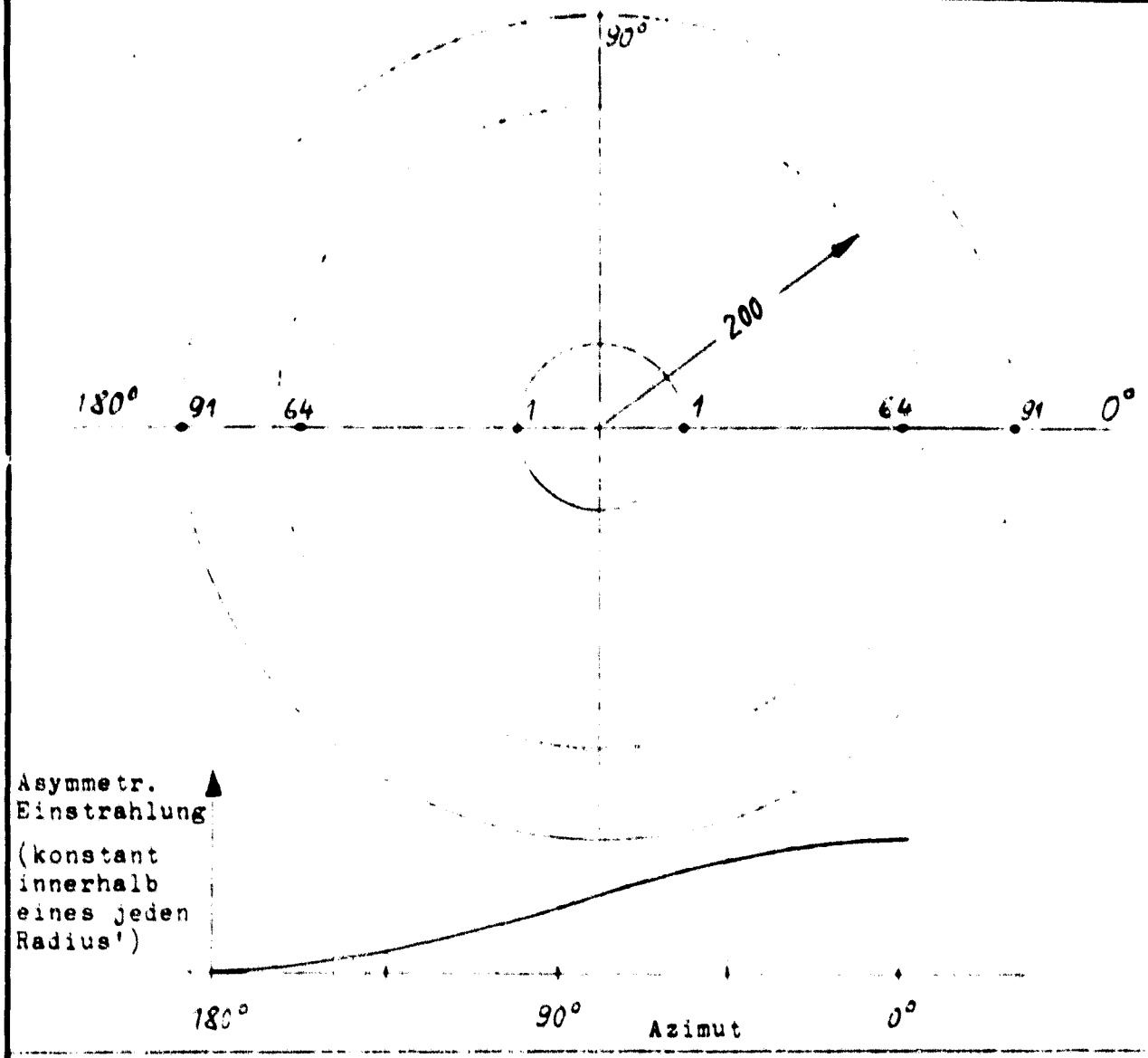

c Temperaturen der Spiegeloberfläche in K bei einer homogenen Temperatur der Instrumentenplatform von 1,600K.

d Knoten Nr.	91	64	1	1	64	91	e größte Temp. differenz
f bei homogener Einstr.	1,982	2,051	2,160	2,160	2,051	1,982	0,109
g bei asymm. Einstr.		1,645	1,684	2,077	2,006	1,929	0,432

Figure 3040/2: Mirror temperatures in the stationary case with a radiation of 15 mW in total.

Key:
a. asymmetrical radiation
b. (constant within each individual radius)
c. temperatures of the mirror surface in K at an homogeneous temperature of the instrument platform of 1,600 K.
d. intersection number
e. greatest temperature difference
f. in the case of homogeneous radiation
g. in the case of asymmetrical radiation

Both heat conductor cylinders were shifted to smaller radii in the second calculations. The calculations were now carried out with the realistic measurement results of the Linde Company (Table 3040/2). The conductivity of cerodur gained in the measurements conducted by Linde were also included in the calculations. In the expectation of a substantially poorer calculation result in this respect, the heat conductor values of the copper litz wires were arbitrarily increased to a multiple of 7 for the value measured by Linde. Figure 3040/3 presents the radii of the heat conductor cylinder, a cross-section of the mirror model and the graph of the calculation results in the case of homogeneous radiation. The distribution curve exhibits a considerable heat bulge, approximately in the middle between the heat conductor cylinders in the mirror surface. Since the temperature differences amount to more than 0.5 K in the case of homogeneous radiation, the case of a symmetrical radiation was not calculated.

In a further computation, the number of heat conductor cylinders was increased to 3. In the meantime, the calculations carried out by the Dornier system on temperature distribution in the instrument platform were available. They justified an increase in base point temperature of the conductor cylinder to 3 K. By this means, the studies extended into a substantially more favorable area of heat conductivity of the materials involved. The heat conductivity in the conductor cylinders, however, was again reduced to a realizable measure. Two calculations with different numbers of copper litz wires were carried out in the three concentric rings. The distribution of the conductors, as well as the graph of the calculation result are presented in Figure 3040/4. Curve 1, in which only half of the heat conductor litz wires were assumed in the individual partial circles in comparison to curve 2, demonstrates no appreciable increase in temperature difference within the irradiated mirror surface. It is merely raised parallel to curve 2. On the basis of this result it appeared permissible to further reduce the number of heat conductors. /61

In the final calculations, 9 copper litz wires were provided for the innermost circle of heat conductors, 15 for the middle circle and 18 for the outermost circle. The base temperatures of the litz wires were again assumed at 3 K and the conductivities of litz and cerodur taken from the Figures 3040/18 and 19. Now several cross-sections of the mirror were plotted from these calculations results, visibly containing isotherms. Figure 3040/5 first shows a temperature distribution in the mirror body in the case of homogeneous radiation, i.e. in the case of absorption of 15 mW within a circle of 400 mm diameter. It can be seen from the diagram that in this area of radiation not even two isotherms are present, i.e. that the temperature difference is less than 0.15 K.

The Figures 3040/6-10 show the temperature distribution in the mirror in the case of asymmetrical irradiation. Beginning with the azimuth angle 0°, where full radiation density dominates, a similar picture is shown to that in homogeneous radiation, only with the difference that the temperatures are shifted somewhat to lower values. With less radiation, i.e. in the transition to an azimuth angle of

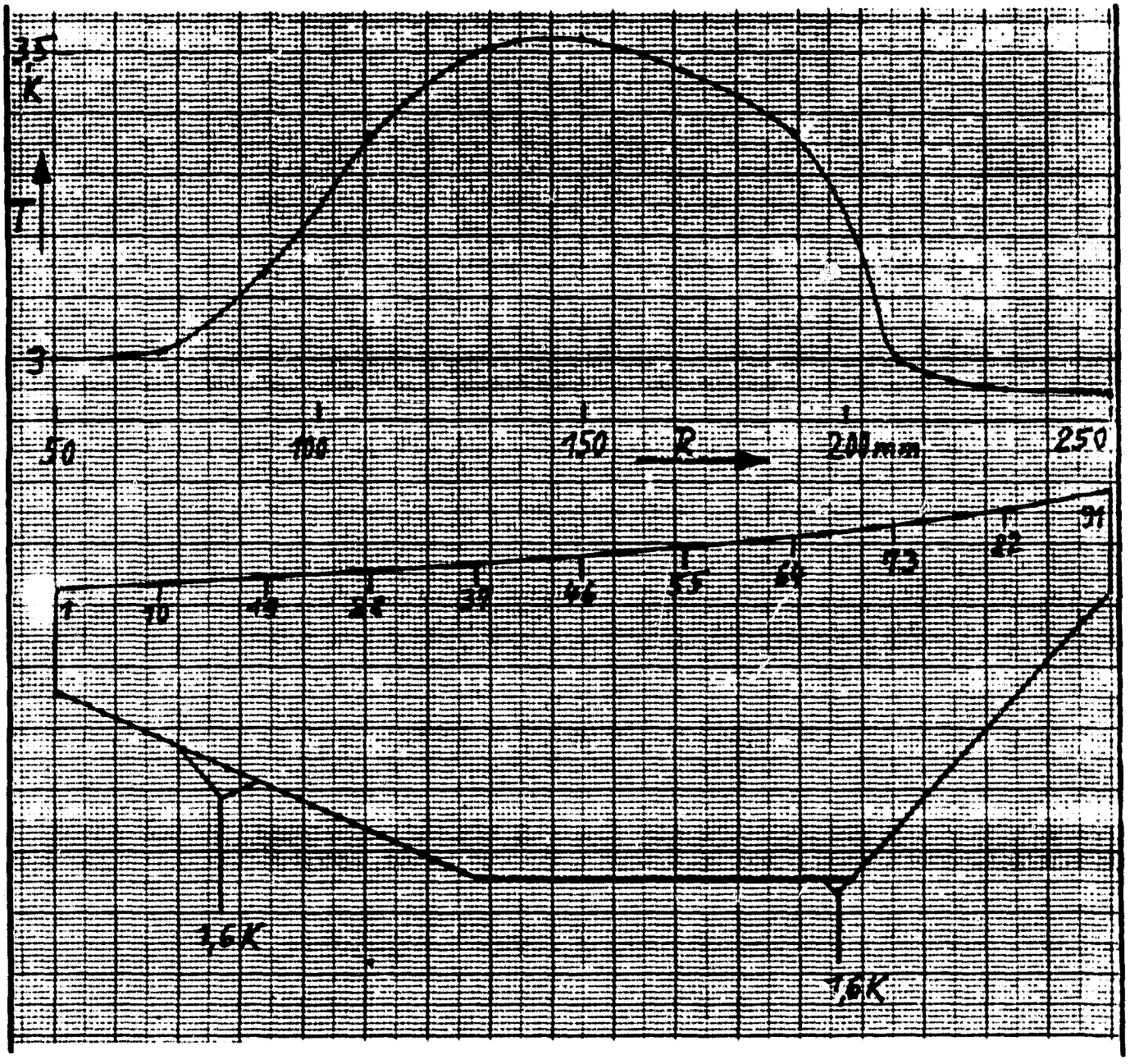

Figure 3040/3: Course of temperature on the S 1 surface in the case of homogeneous radiation and cooling through conductor rings between the intersections 10 and 19 or 64 and 73.

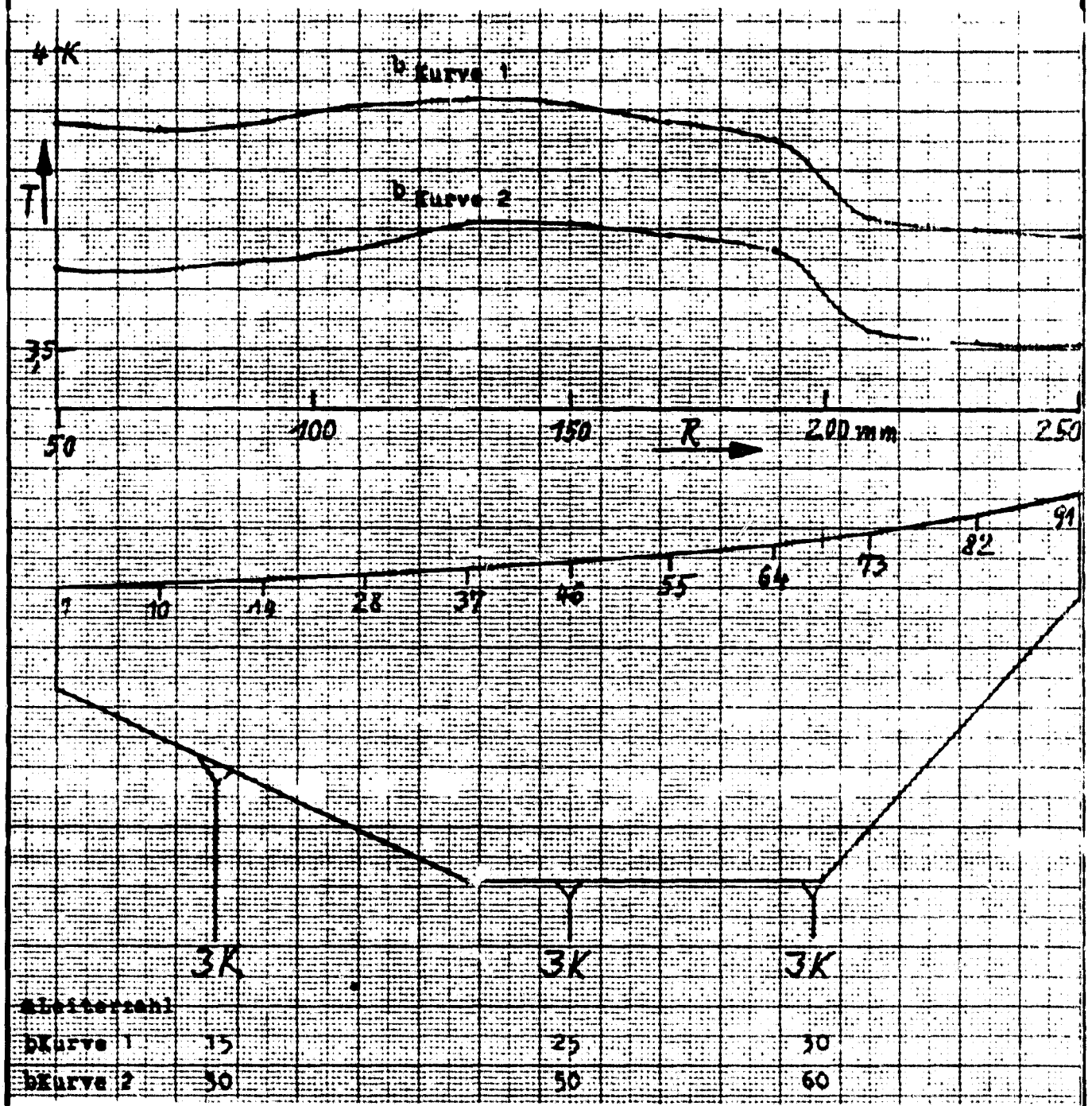

Figure 3040/4: Course of temperature on the Sl surface in the case of homogeneous radiation and cooling through 3 conductor rings.

Key:
a. number of conductors b. curve

180°, the temperature differences in the mirror section become increasingly smaller. Finally, they are so small at 180°, that no isotherms of the selected temperature difference 0.15 K are visible any longer. Between the maximum temperature at the azimuth angle 0° and the minimum temperature at the azimuth angle 180°, a difference of approx. 0.7 K prevails. According to a communication of the GHW of April 23, 1980 to the MPIA in Heidelberg, the temperature difference /69 within the mirror surface may amount to 1 K.

In a further calculation, the concentric heat conductor cylinders were now replaced by discrete heat conductor litz wires in the calculated model. Figure 3040/11 shows the triple beam, symmetrical distribution on the back surface of the mirror. The three larger circles offset by 120° to one another, signify the position of the mounting component groups. The calculated results of the stationary temperature distribution in the case of homogeneous radiation now demonstrates very dramatically how the temperature differences between the conductors on the back side are still reduced considerably, while on the front surface of the mirror to a minimum. The temperature distribution along some representative nodal zones or nodal rings is presented in the diagrams of Figure 3040/12. In the nodal zone with the number 99 and in which the outer circle of heat conductors is contacted, a temperature difference of 0.33 K prevails between the contact point and the coldest positions of the zone. The greatest difference in the mirror upper surface exists in the nodal zone 19 (compare Figure 3040/1). The temperature difference at this point amounts to 0.01 K. At node no. 46, it has finally become unmeasurably small. When the radial and the azimuthal distance of the heat conductors are compared, this result is amazing. While these distances differentiate only insubstantially from one another, the radial temperature difference in the mirror surface is approx. 15 times greater than the azimuthal.

In Table 3040/1, the radial and azimuthal temperature differences in the mirror surface in the case of homogeneous radiation are compiled again. Just as in Figure 3040/12, the data is limited to 1/3 of the mirror surface. The given distribution is identical with that of the other two sectors. The maximum values of temperature are in the nodal zone 37 at 3.916 K, the minimum values in the nodal zone 64 of the mirror at 3.853 K.

Since placing a preference on soldered heat conductor contacts /73 was not yet fully justified at the time of the study conclusion, stationary temperature calculations were also conducted with cemented contacts. The measurement results no. 4 of Linde in Table 3040/2 served for this purpose. The distribution of contacts was the same as in the last calculations with soldered contacts (Figure 3040/13). These were also first replaced by concentric, homogeneous conductor cylinders in order to simplify calculations.

The results of the calculations with cemented contacts are compiled in the Tables 3040/2 and 3. In the case of homogeneous radiation of a total of 15 mW, an average temperature of $\overline{T}$ = 5.028 K was reached in the mirror surface. The difference between the result with concentric

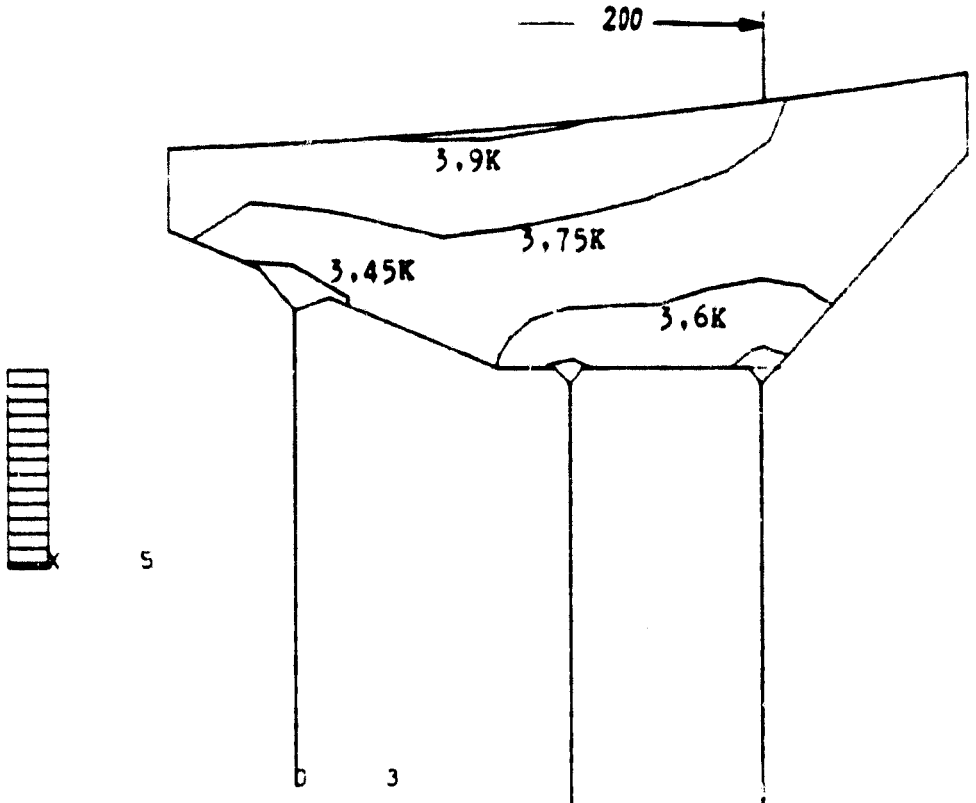

Figure 3040/5: Temperature distribution in the main mirror with completely homogeneous radiation. T_{max} = 3.915 K, T_{min} = 3.853 K.

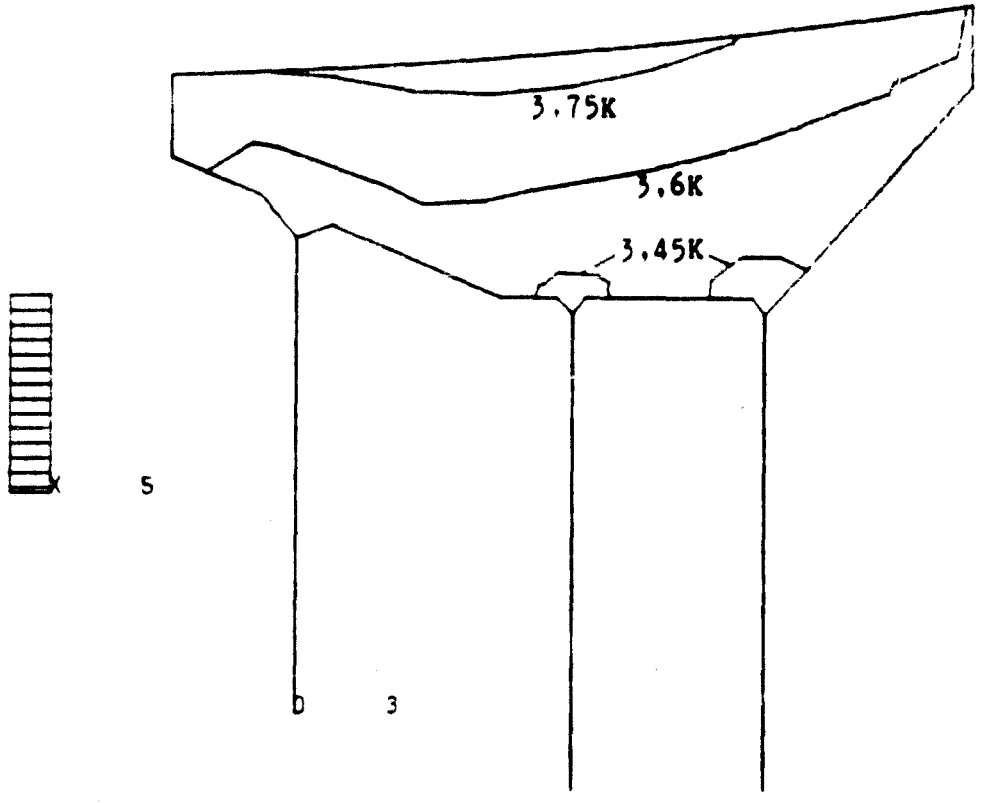

Figure 3040/6: Temperature distribution in the main mirror in the case of an azimuth angle of 0° (complete radiation density). T_{max} = 3.805 K, T_{min} = 3.743 K.

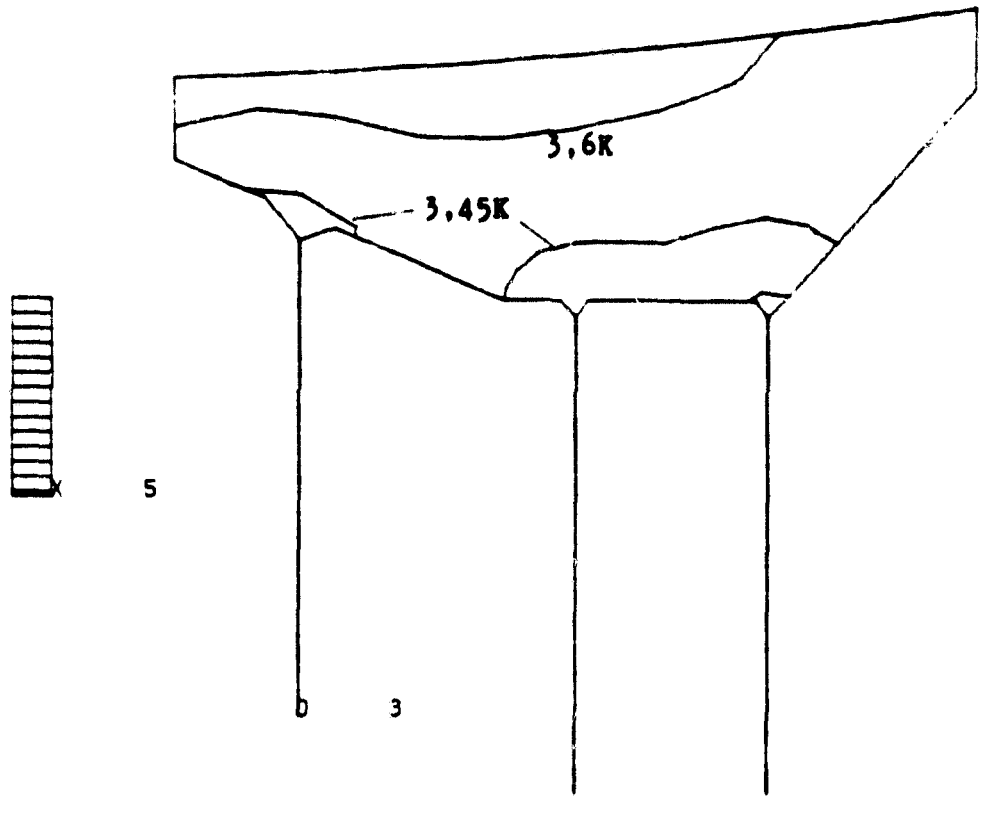

Figure 3040/7: Temperature distribution in the main mirror at an azimuth angle of 45° (85% of the total radiation). T_{max} = 3.706 K, T_{min} = 3.654 K.

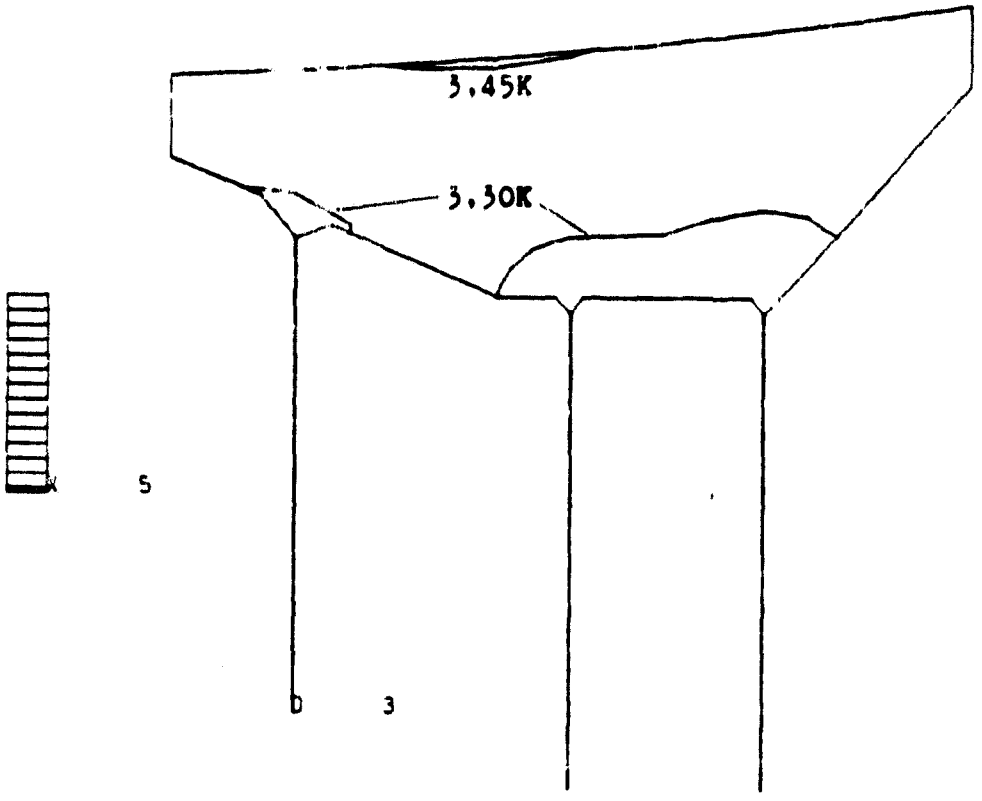

Figure 3040/8: Temperature distribution in the main mirror at an azimuth angle of 90° (50% of the total radiation). T_{max} = 3.458 K, T_{min} = 3.427 K.

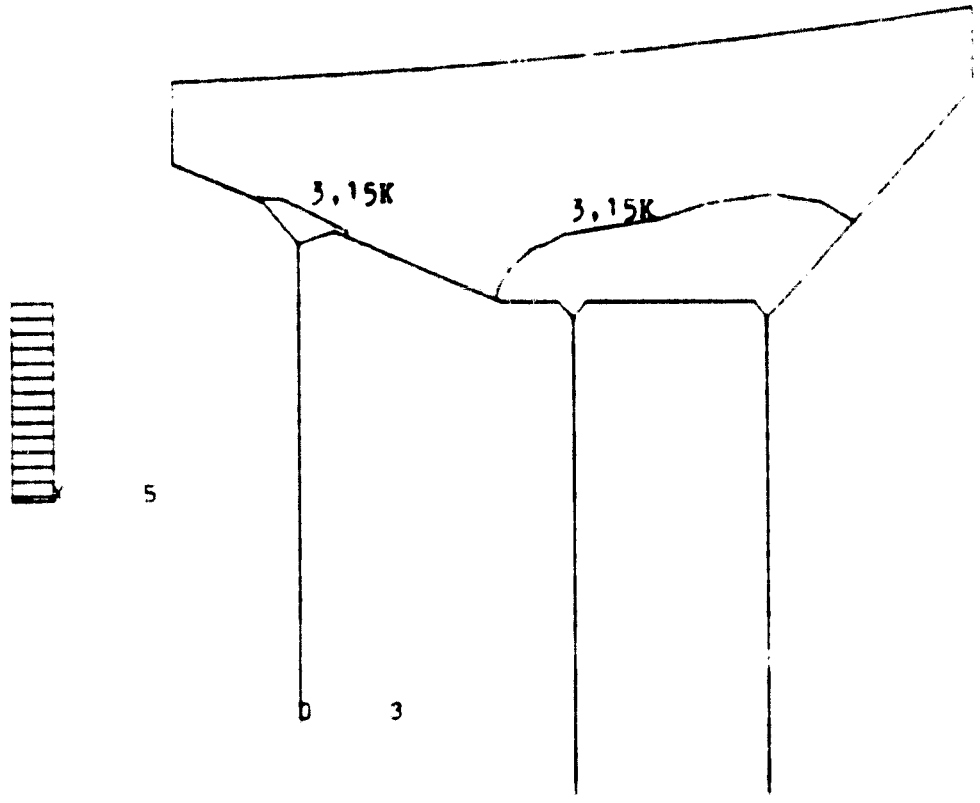

Figure 3040/9: Temperature distribution in the main mirror at an azimuth angle of 135° (15% of the total radiation). T_{max} = 3.223 K, T_{min} = 3.190 K.

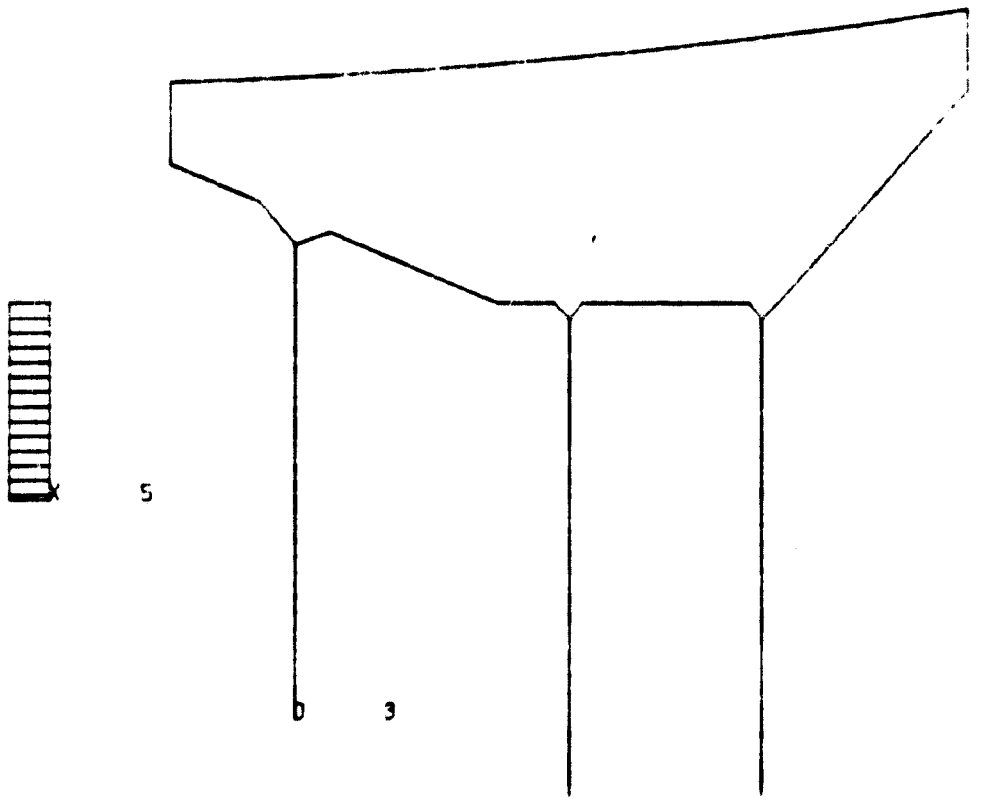

Figure 3040/10: Temperature distribution in the main mirror at an azimuth angle of 180° (radiation of 0). T_{max} = 3.134 K, T_{min} = 3.093 K.

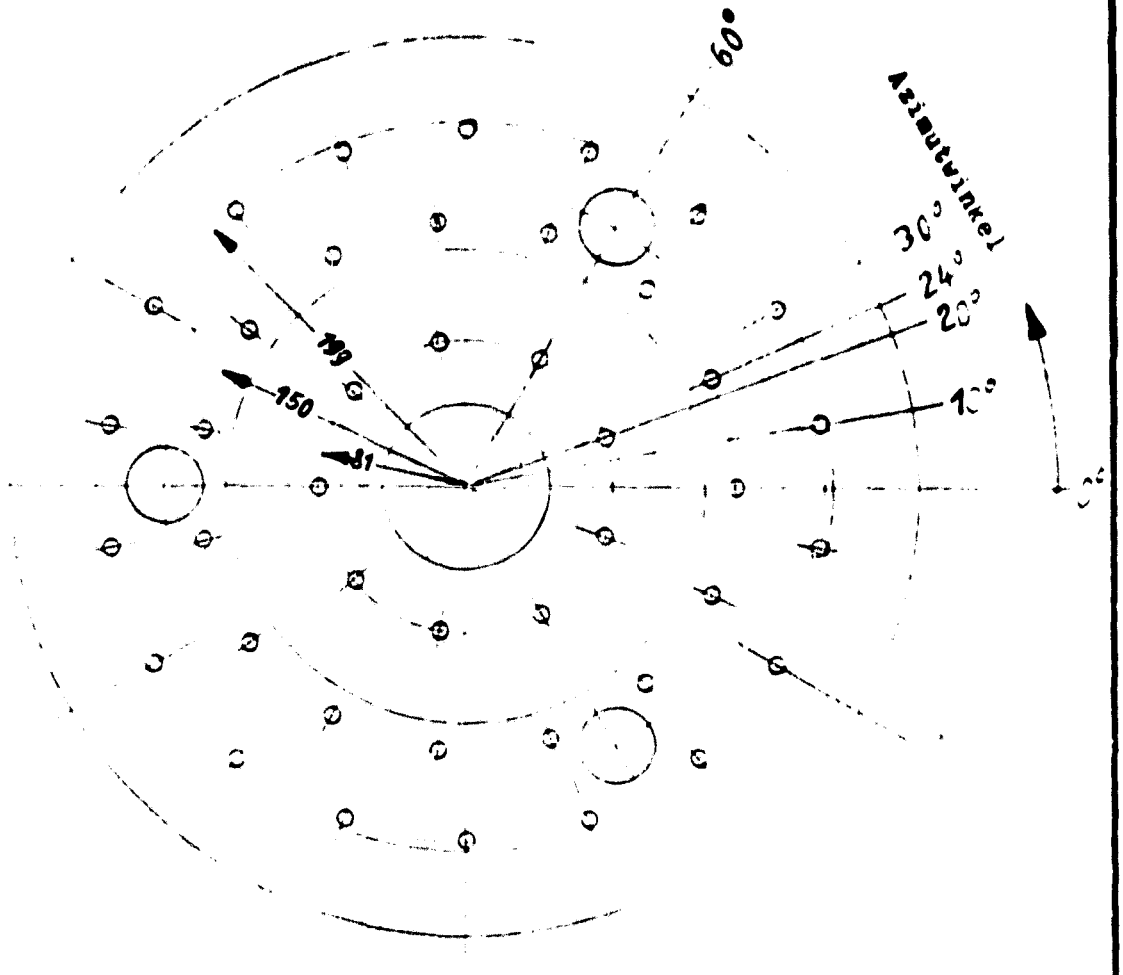

Figure 3040/11: Distribution of heat conductors on the rear side of the main mirror in three concentric rings. The outermost ring has 18 conductors, the middle ring 15 conductors, and the inner ring 9 conductors.

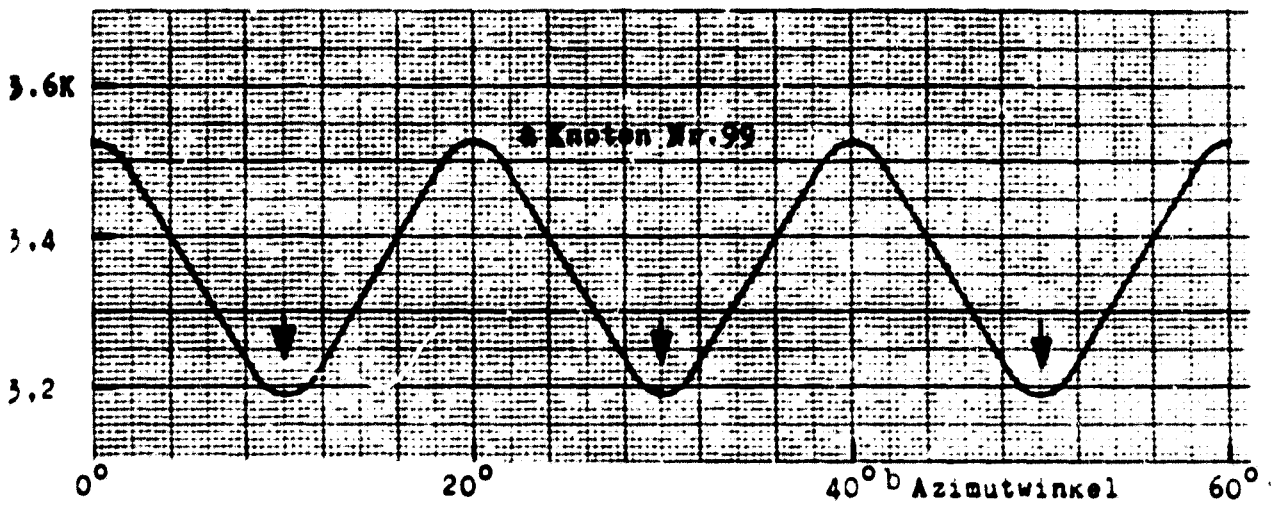

c Kontaktkreis der äußeren Wärmeleiter

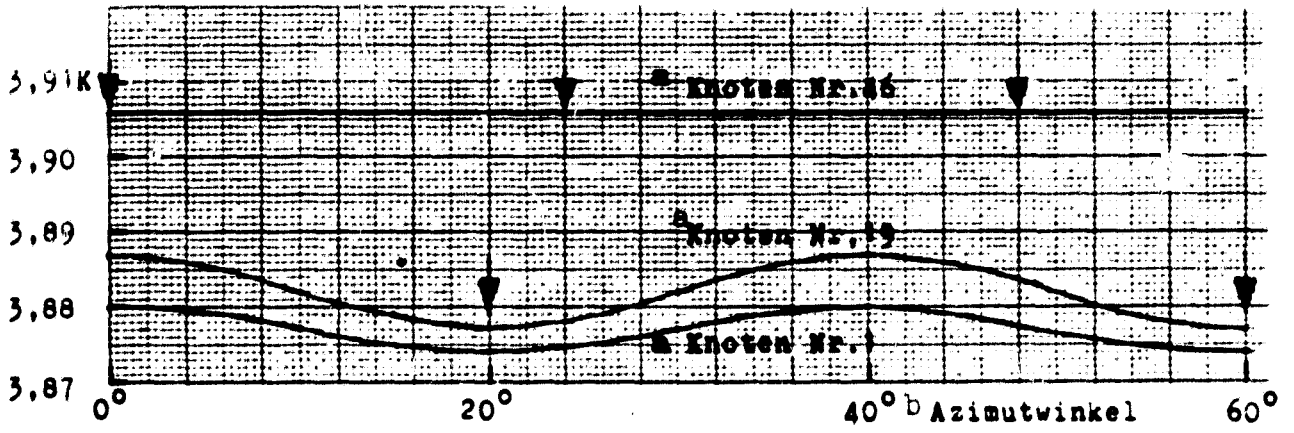

d Knotenzonen in der Spiegeloberfläche

Figure 3040/12: Azimuthal temperature distribution in the main mirror in the case of homogeneous radiation within r = 200 mm. The arrows designate the position of the most adjacent heat contacts.

Key:
a. node
b. azimuth angle
c. contact circle of the outer heat conductors
d. nodal zones in the mirror surface

a Knoten Nr. / b Azimutwinkel	1	10	19	28	37	46	55	64	73	99
0°	-0,005	-0,009	0,002	0,025	0,031	0,021	-0,001	-0,032	-0,17	-0,360
± 10°	-0,008	-0,013	-0,003	0,022	0,030	0,021	-0,001	-0,032	-0,17	-0,694
± 15°	-0,010	-0,016	-0,006	0,021	0,030	0,021	-0,001	-0,032	-0,17	-0,526
± 30°	-0,008	-0,013	-0,003	0,022	0,030	0,021	-0,001	-0,032	-0,17	-0,694
± 40°	-0,005	-0,009	0,002	0,025	0,031	0,021	0	-0,031	-0,17	-0,359
± 49°	-0,008	-0,012	-0,002	0,023	0,030	0,021	-0,001	-0,032	-0,17	-0,686
± 60°	-0,011	-0,017	-0,008	0,020	0,030	0,021	-0,001	-0,031	-0,17	-0,359

Tab. 3040/1

Azimutale und radiale Temperaturverteilung in der Hauptspiegeloberfläche bei homogener Einstrahlung innerhalb r = 200 mm, bezogen auf $\bar{T}$ = 3,885K.

Table 3040/1: Azimuthal and radial temperature distribution in the surface of main mirror in the case of homogeneous radiation within r = 200 mm related to $\bar{T}$ = 3.885 K

Key:
a. node no.
b. azimuth angle

conductor cylinders and that with discrete conductor litz wires are insignificant; they are less than 3 mK. $\bar{T}$, however, is 1.14 K greater than in the case of soldered contacts. In contrast, the temperature varies in the utilized surface in the case of cement contacts only by 28 mK, while it varies by 31 mK in the case of soldered contacts (Table 3040/1). The greater effect of the soldered contacts with substantially better conducting capacity therefore produces better cooling of the surface, but also more greatly emphasizes the conductor distribution in the surface.

The temperature distribution given in Table 3040/3 in the case of inhomogeneous radiation shows a variation of ± 0.321 K at an average temperature of $\bar{T} = 4.012$ K. This is therefore approximately as great as in the case of soldered heat conductor.

The calculations show that the cemented contacts also satisfy the presently known thermal requirements. They only have the disadvantage of producing an average surface temperature approx. 1 K higher in the case of absorbing earth radiation on the mirror.

AP 3042 Cooling of Main Mirror /76

Calculating the cooling time is carried out with almost the same node model as presented in Figure 3040/1. Only the node numbering of the heat conductor connections was slightly supplemented. The tips of the triangular cerodur rings theoretically intended for the rear of the mirror are divided into two nodes with a distance equal to the diameter of the soldering points. The model modified in this manner is shown in Figure 3040/13. The base points of the conductors are on the temperature 3 K.

The calculations were based on the course of temperature of the instrument platform presented in Figure 3040/14. In this case, six hours of cooling with liquid nitrogen, subsequently another six hours of cooling with helium and then three hours of pumping off the helium are provided. In the course of calculations, it is discovered that this total of 15 hours is definitely not sufficient to bring the mirror even close to the final temperature.

Originally, an extrapolation of the final result was intended for limiting the calculation costs. Several alterations in the computer program employed in phase A, however, made calculations possible almost up to the balanced state of the mirror.

Figure 3040/14 shows the essential temperature functions in relation to time in a summarized form. The black curve is the already-mentioned course of temperature of the instrument platform, the red curve is the course of the warmest mirror node, the blue curve is the course of the coldest, the green curve is that of the difference between the warmest and coldest point in the mirror multiplied by ten, and the red dotted curve is the thermal expansion coefficient of cerodur. The zero line of the latter-mentioned curve is situated at 200 K; 100 K of their ordinate correspond to 5×10^{-7} K^{-1} of expansion. The course is plotted indirectly over the average mirror temperature.

c Knoten-Nr.	1	10	19	28	37	46	55	64	73	82	91
Δ T	0,027	0,023	0,021	0,021	0,015	0,004	-0,01	-0,027	-0,086	-0,094	-0,096

a) Temperaturdifferenzen bei drei konzentrischen Wärmeleitzylindern gemäß Abb. 3040/13, bezogen auf $\bar{T}$ = 5,028K (Mittelwert im bestrahlten Bereich).

c Knoten Nr. / d Azimutwinkel	1	10	19	28	37	46	55	64	73	82	91
0°	0,028	0,024	0,022	0,022	0,015	0,004	-0,010	-0,027	-0,086	-0,094	-0,096
± 10°	0,027	0,023	0,021	0,021	0,015	0,004	-0,010	-0,027	-0,086	-0,094	-0,097
± 15°	0,026	0,022	0,019	0,021	0,015	0,004	-0,010	-0,027	-0,086	-0,094	-0,096
± 30°	0,027	0,023	0,021	0,021	0,015	0,004	-0,011	-0,027	-0,086	-0,094	-0,097
± 40°	0,028	0,024	0,022	0,022	0,015	0,004	-0,010	-0,027	-0,086	-0,094	-0,096
± 49°	0,027	0,023	0,021	0,021	0,015	0,004	-0,011	-0,027	-0,086	-0,094	-0,097
± 60°	0,026	0,021	0,019	0,020	0,015	0,004	-0,010	-0,027	-0,086	-0,094	-0,096

b) Temperaturdifferenzen bei insgesamt 42 diskreten Leitern gemäß Abb. 3040/13, bezogen auf $\bar{T}$ = 5,028K (Mittelwert im bestrahlten Bereich).

Table 3040/2: Temperature distribution in the mirror surface in the case of homogeneous radiation and cemented heat conductors.

(Please see the following page below the table for Key.)

c Knoten Nr. / d Azimutwinkel	1	10	19	28	37	46	55	64	73	82	91
0	0,292	0,297	0,306	0,317	0,321	0,319	0,311	0,298	0,240	0,232	0,229
45°	0,211	0,214	0,220	0,228	0,229	0,227	0,219	0,208	0,158	0,151	0,149
90°	0,015	0,013	0,012	0,013	0,010	0,004	-0,003	-0,011	-0,041	-0,045	-0,046
135°	-0,181	-0,187	-0,196	-0,202	-0,210	-0,219	-0,225	-0,230	-0,240	-0,241	-0,241
180°	-0,262	-0,271	-0,282	-0,291	-0,301	-0,311	-0,318	-0,321	-0,322		-0,322

Table 3040/3: Temperature differences in the mirror surface in the case of inhomogeneous radiation according to Figure 3040/2 and cemented heat conductors (3 concentric cylinders) in relation to $\overline{T}$ = 4.012 K in a diameter of 400 mm.

Key:
a) Temperature differences in the case of 3 concentric heat conductor cylinders according to Figure 3040/13 related to $\overline{T}$ = 5.028 K (average value in the irradiated area).
b) Temperature differences in a total of 42 discrete conductors according to Figure 3040/13 related to $\overline{T}$ = 5.028 K (average value in the irradiated area).
c. node number
d. azimuth angle

PRECEDING PAGE BLANK NOT FILMED

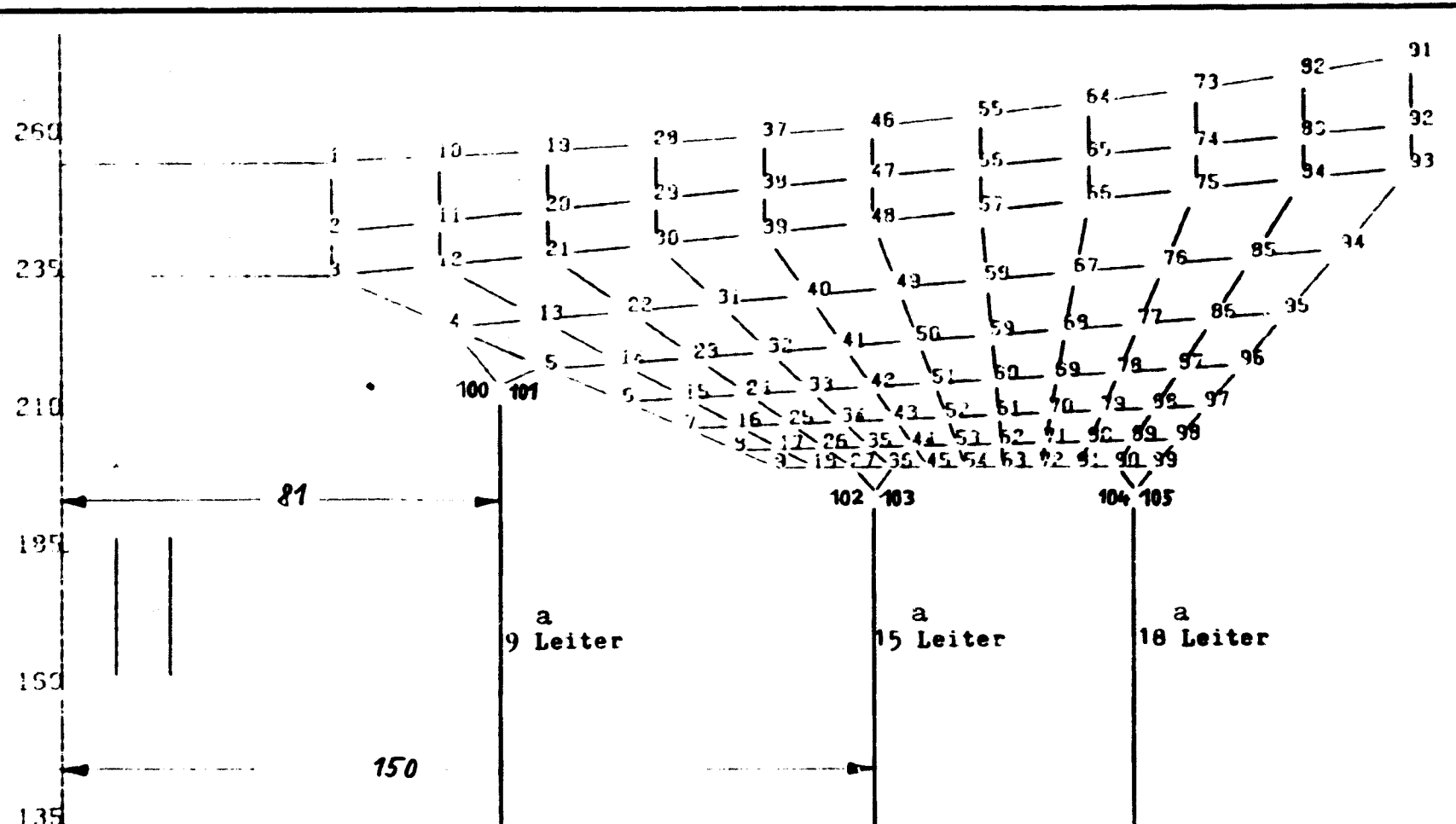

Abb.3040/13 Knotenmodell für die Berechnung der Abkühlzeit des Hauptspiegels

Figure 3040/13: Node model for calculating the cooling time of the main mirror.

Key: a. conductors

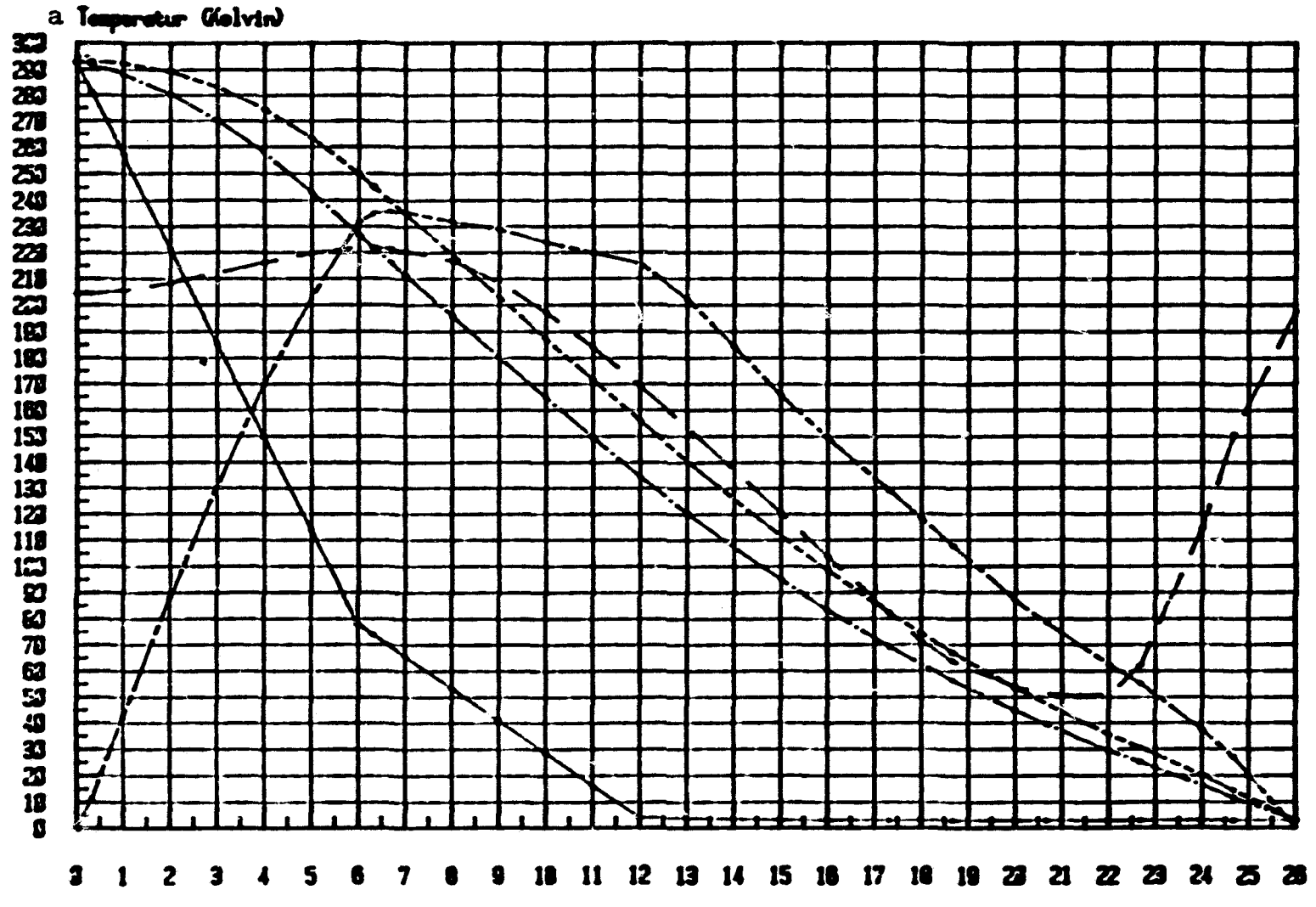

Figure 3040/14: Courses of temperature and coefficients of expansion for cerodur as a function of cooling time of the main mirror.

Key:
a. temperature
b. cryostat temperature
c. black
d. coldest mirror point
e. blue
f. warmest mirror point
g. red
h. ten times the maximum difference
i. green
j. linear expansion
k. times (hours)

ZEISS
Tritt

The curves demonstrate that the mirror is cooled to only 95 K after the 15 hours given. Eleven hours more are required until the mirror reaches the 3 K of the base point and the internal temperature difference (green curve) runs to the zero point. Table 3040/4 shows the temperatures of the extremely tempered nodes no. 36 and 91, respectively, in the last stage of cooling. /79

a Zeitpunkt nach Abkühlbeginn in Stunden	b Temperatur des wärmsten Knotens Nr. 91	c Temperatur des kältesten Knotens Nr. 36
20,00	53,434 K	44,748 K
20,67	47,214	39,383
21,33	41,299	34,312
22,00	35,649	29,396
22,67	30,608	25,079
23,33	25,284	20,615
24,00	20,006	16,274
24,67	14,433	11,729
25,33	8,156	6,745
26,00	3,016	3,008

Table 3040/4: Extreme temperatures in the main mirror approaching the end of cooling time.

Key:
a. time after start of cooling in hours
b. temperature of warmest node no. 91
c. temperature of coolest node no. 36

More clearly than the curves, the table shows how the last half hour of cooling brings the decisive step to the desired temperature. The remaining difference between the base of the mirror and mirror surface has been reduced to 0.008 K; the differences below the surface are even smaller by one order of magnitude.

Tension in the Cerodur

The mechanical tension in the cerodur caused by the inhomogeneous temperatures was determined at several points in the course of cooling. Impermissibly high tension occurred in those triangles in this case, introduced in the calculation model as coupling points for the heat conductors. This area was then studied separately in a locally limited model concentrically around the axis of heat conductors. The /81

results are found in the appendix of this report. When these triangles are excluded here, the three largest tensions are obtained near the triangles. They are presented in Table 3040/5 for six different stages in cooling. The greatest tensions occur after 22 hours at an average mirror temperature of 33 K. At 0.12 kp/mm^2, this value is still sufficiently below the critical value.

/80

a Zeitpunkt nach Abkühlbeginn	b F im Spiegel	σ max kp/mm^2	c zwischen den Knoten Nr.			
6,67 h	227 K	0,0102	5	6	15	14
		0,00802	4	5	14	13
		0,00762	1	2	11	10
7,67 h	212 K	0,0222	35	26	27	36
		0,0127	4	5	14	13
		0,00814	89	90	99	98
11,0 h	160 K	0,0672	35	26	27	36
		0,0616	4	5	14	13
		0,0561	1	2	11	10
12,0 h	145 K	0,0903	35	26	27	36
		0,0896	4	5	14	13
		0,0853	1	2	11	10
19,3 h	56 K	0,0643	1	2	11	10
		0,0613	2	3	12	11
		0,0590	3	4	13	12
22 h	33 K	0,121	35	26	27	36
		0,0807	4	5	14	13
		0,0440	44	35	36	45

Table 3040/5: The three individual, largest tensions in the main mirror at six different stages in cooling (disregarding contact triangles of the node model).

Key:
a. time after start of cooling
b. temperature in the mirror
c. between the node numbers

AP 3043 Measure of Thermoconduction /82

The determination of heat transition resistance between cerodur and a metallic contact proved to be one of the substantial problems in the study, caused by an underestimation of the mounting technology.

Within the framework of the AP, the exclusive study of soldered contacts was first intended, after this type of connection appeared useable in preliminary tests. These preliminary tests were conducted with a round cerodur disc, with baking silver baked into the finely ground surface at 500° C for one-half hour. In a separate test, the permanence of a very precise plane surface was proven after the heat treatment. Figure 3040/16 shows the interferogram of this surface before and after tempering. The treatment causes no visible alterations in the interferon picture.

The contacts all consisted in the invar nipples presented in Figure 3040/17, into which the copper litz wires had been solidly soldered. These were varied insofar as the nipples were first drilled, but later only provided with sack holes. Soldered copper nipples dropped off with partial cooling without application of force. The first invar nipple soldered onto the test disc with special soft solder and special flux and with a hole was quenched three times in liquid nitrogen and then demonstrated a tensile strength of more than 20 kp. Encouraged by this result, the samples for the measurements of the Linde Company were also treated in this manner, but with the difference that they were etched with fluoric acid before soldering to ensure freedom from cracks. It could then be assumed that etching or the insufficient utilization were the cause for this solder defect. Subsequently, only half of the circular test disc was etched, neutralized for ten minutes in cold Na_2CO_3 solution and 16 hours in warm water. The soldered conductor cracked on this etched surface after quenching in nitrogen at F = 5.5 kp, on the unetched, ground surface at 7.5 kp. The "etched nipple" cracked without glass damage with silver and solder, the unetched nipple when three-fourths of the glass surface was broken. /84
Although the strengths did not differ substantially, etching does appear to have a negative effect on the connection.

In a further preliminary test, the nipple was now provided with sack holes, so that the copper litz wires with their greater thermal contraction could not transmit any direct forces on the cerodur. The nipples were soldered onto unetched surfaces. After a single quenching in liquid nitrogen, one conductor ripped at 30 kp (!) with a large amount of glass breaking off, the other, however, already at 5 kp without glass breakage. Unfortunately, this result permits no systematic conclusions. Passing the copper through the solder layer, however, does not appear to be disadvantageous so that the model for the heat transmission measurements were provided with holes passing through the invar.

The measurement set up agreed upon with Linde is shown in Figure 3040/17. The cerodur sample consists in a column with quadratic cross-section with a constantan layer as heat conductor vaporized onto

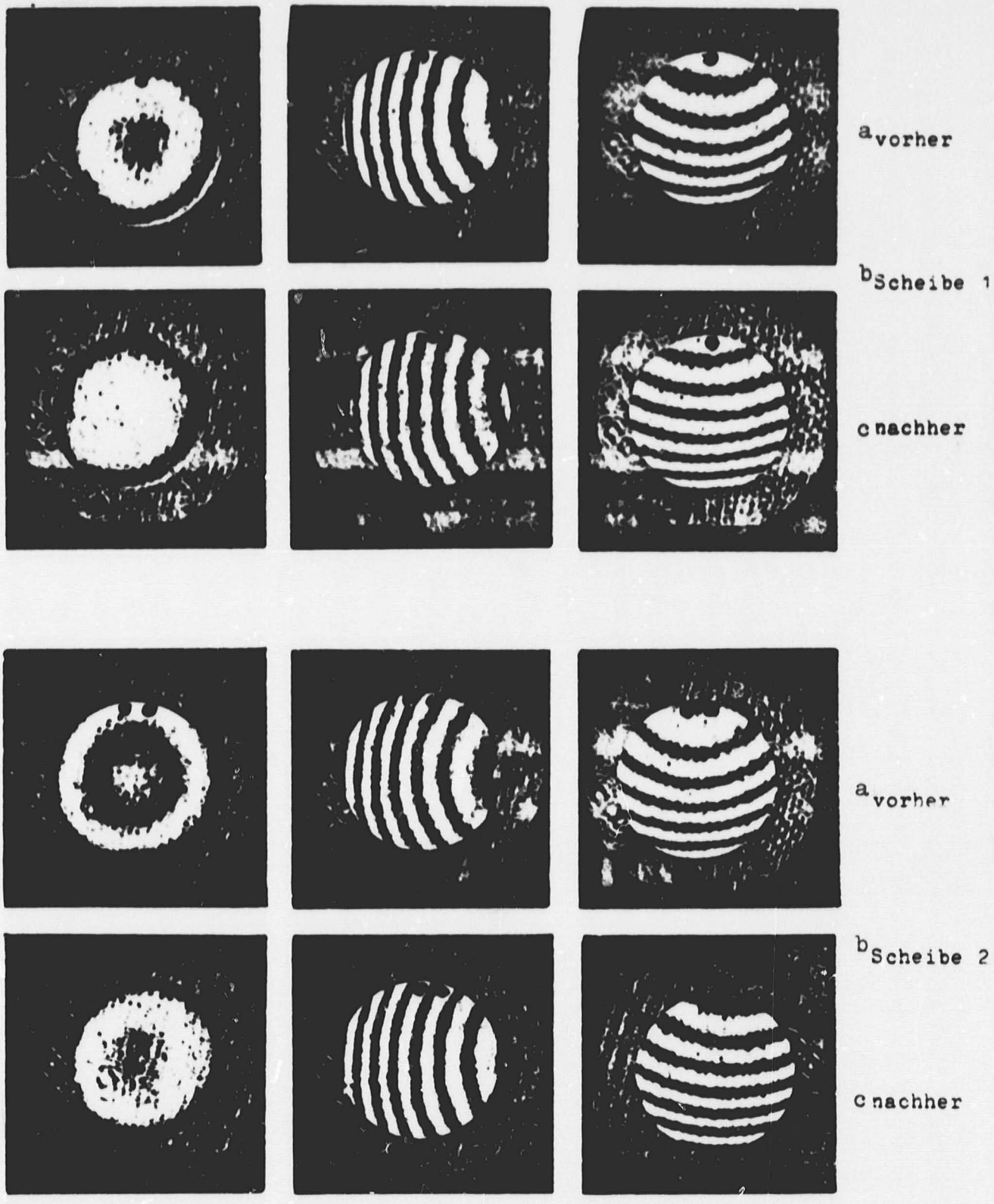

Figure 3040/16: Wave front aberration of a cerodur disc before and after baking of a silver layer for the solder connection with a heat conductor. Baking temperature 500° C, duration one-half hour.

Key:
a. before
b. disc
c. after

ORIGINAL PAGE IS
OF POOR QUALITY

the surface. The heat conductor is soldered onto the lower side of the column and bent to a circle on which a support spring pulls. In order to replace the sample, the conductor ends in a small piece of copper screwed to the base plate. Near the contact and in the middle of the cerodur column are temperature measurement sensors in holes, also in the copper piece and in the base plate. The four supports of the measurement table consist in steel of low heat conductivity in order to minimize the thermal shunt to the conductor.

The shape of the sample additionally makes a measurement of heat conductivity of the cerodur possible, not known in literature. In a stationary balance, the heat capacity supplied generates a defined temperature drop between the individual sensors, two of which are situated in homogeneous glass. The cerodur conductivity measured in this manner also serves for correcting the heat transition conductivity result, since it is unavoidable that this includes a cerodur path between sensor and contact.

The results of the measurements conducted by Linde are compiled in Table 3040/6. A total of three samples were measured, of which the first were measured twice, i.e. with various types of measurement sensor contacts. The measurements were carried out in each case with two temperatures in a range below 7 K. In addition to both heat transition resistors R_{zer} and R''_{kon2}, the specific heat conduction of cerodur and the resistance of the heat conductor corrected by the cerodur path are contained in the table. R''_{kon2} is composed of the resistance series cerodur/soft solder/copper/hard solder/copper/copper. The 12 cm long copper litz wire with a 2.3 mm^2 cross-section is in the third position; the last transition corresponds to that transition R_{kon1} discussed in AP 3052, contributing only 3.5 KW^{-1} at 4 K. It is first surprising that the conductivity of cerodur is approximately five times less than the conductivity of quartz known from literature. When the measurement results are plotted in a diagram, it appears that the plateau of conductivity characteristic for quartz glass at 5 to 20 K (Figure 3040/18) does not occur in the case of cerodur. On the other hand, the conductivities at high temperatures are in complete agreement with those of quartz. /86

The transition resistors of the soldered contacts corrected by the measured cerodur path are plotted in Figure 3050/19. In measurement one, the insufficient contact of the sensor becomes apparent in the form of a greatly deviating course. Measurement 2 produces an exact inverted temperature law, while measurement 3 contains a power of t difficult to explain. It is also not understandable that the inverted temperature result pointing to conductance of electrons supplies the higher resistances. The more arbitrary than systematic results are a challenge to further activity in this area.

The cemented contact is so far below the values of the soldered contact in conductivity, that it was not plotted in Figure 3050/19 and would probably hardly be employed.

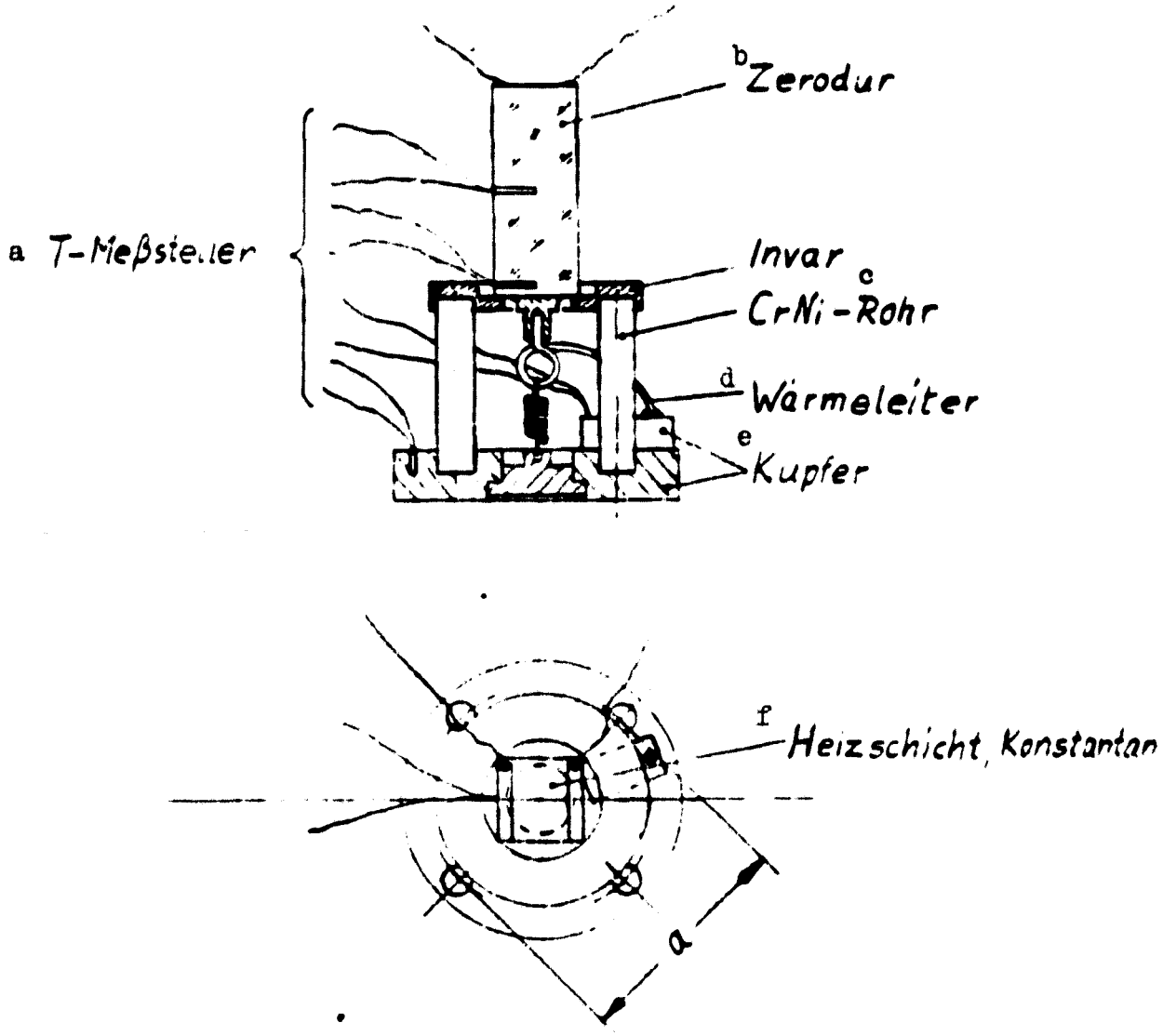

Figure 3040/17: Measurement device for determining the heat transition resistance R_{kon2} between cerodur and copper and the thermal conductivity of cerodur.

Key:
a. temperature measurement points
b. cerodur
c. pipe
d. heat conductor
e. copper
f. heating layer, constantan

[a] Messg. Nr.	T_{Zer} K	R_{Zer} K/W	R''_{kon2} K/W	λ_{Zer} W/cmK	R'_{kon2} K/W	b Probenart
1	4.5	4540	1580	2×10^{-4}	741	[c] 1.Zerodurprobe; Thermometer nicht geklebt, Nippel gelötet
	2.8	7120	2200	1.3×10^{-4}	885	
2	4.5	4550	2000	2.10^{-4}	1160	[d] 1. Zerodurprobe Thermometer geklebt, Nippel gelötet
	2.3	8000	3750	1.1×10^{-4}	2270	
3	4.4	3000	1350	3×10^{-4}	800	[d] 2. Zerodurprobe Thermometer geklebt, Nippel gelötet
	1.9	7140	4170	1.3×10^{-4}	2850	
4	6.3	3580	5850	2.5×10^{-4}	5190	[e] 1. Zerodurprobe Thermometer geklebt, Nippel geklebt
	3.5	5630	10000	1.6×10^{-4}	8960	

Table 3040/6: Compilation of the results of heat resistance measurements with cerodur/copper contacts conducted by the Linde Company.

Key:
a. measurement number
b. type of sample
c. cerodur sample; thermometer not cemented, nipple soldered
d. cerodur sample; thermometer cemented, nipple soldered
e. cerodur sample; thermometer cemented, nipple cemented

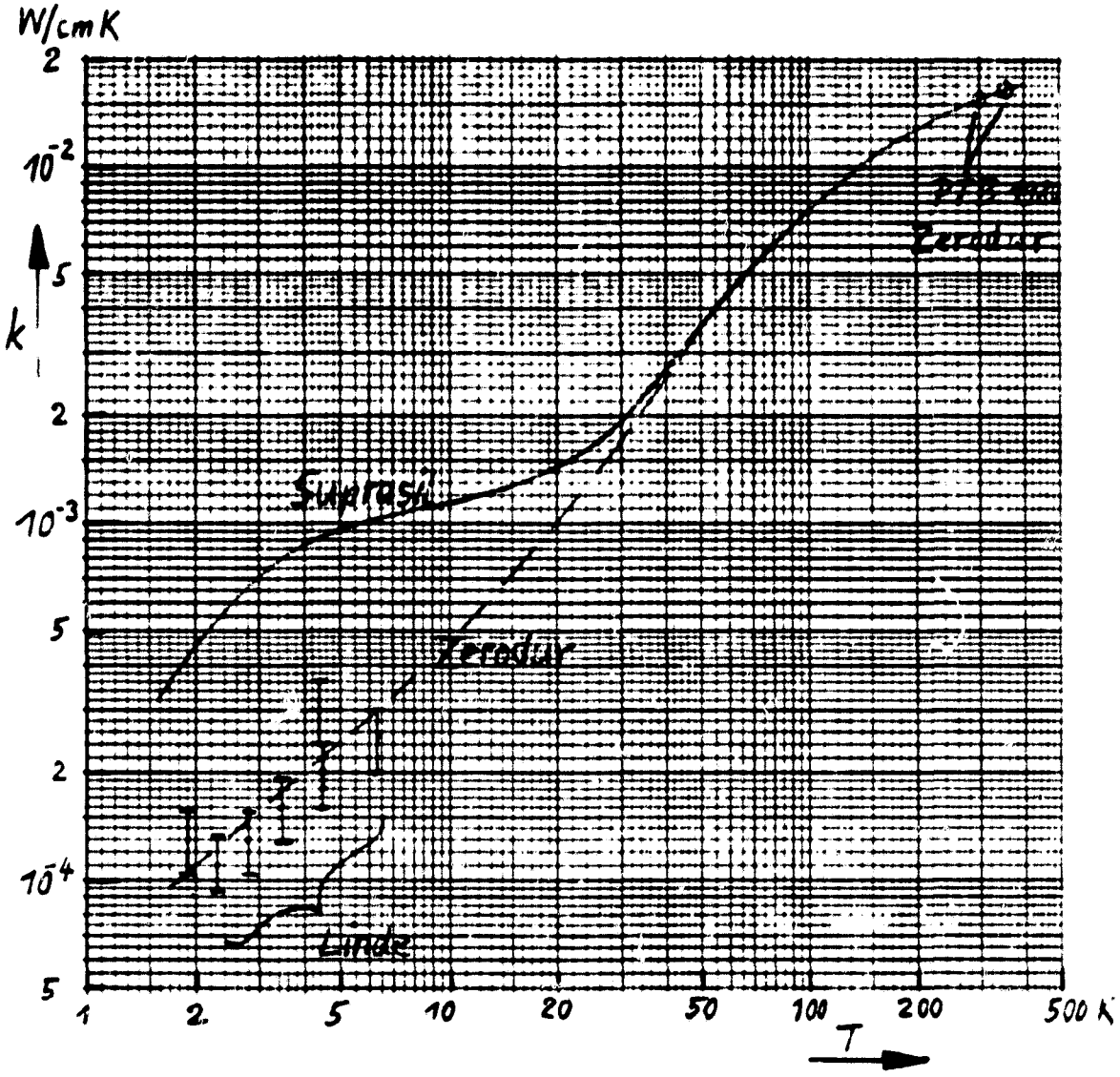

Figure 3040/18: Dependence of temperature on heat conductivity of cerodur according to various measurement results of Linde.

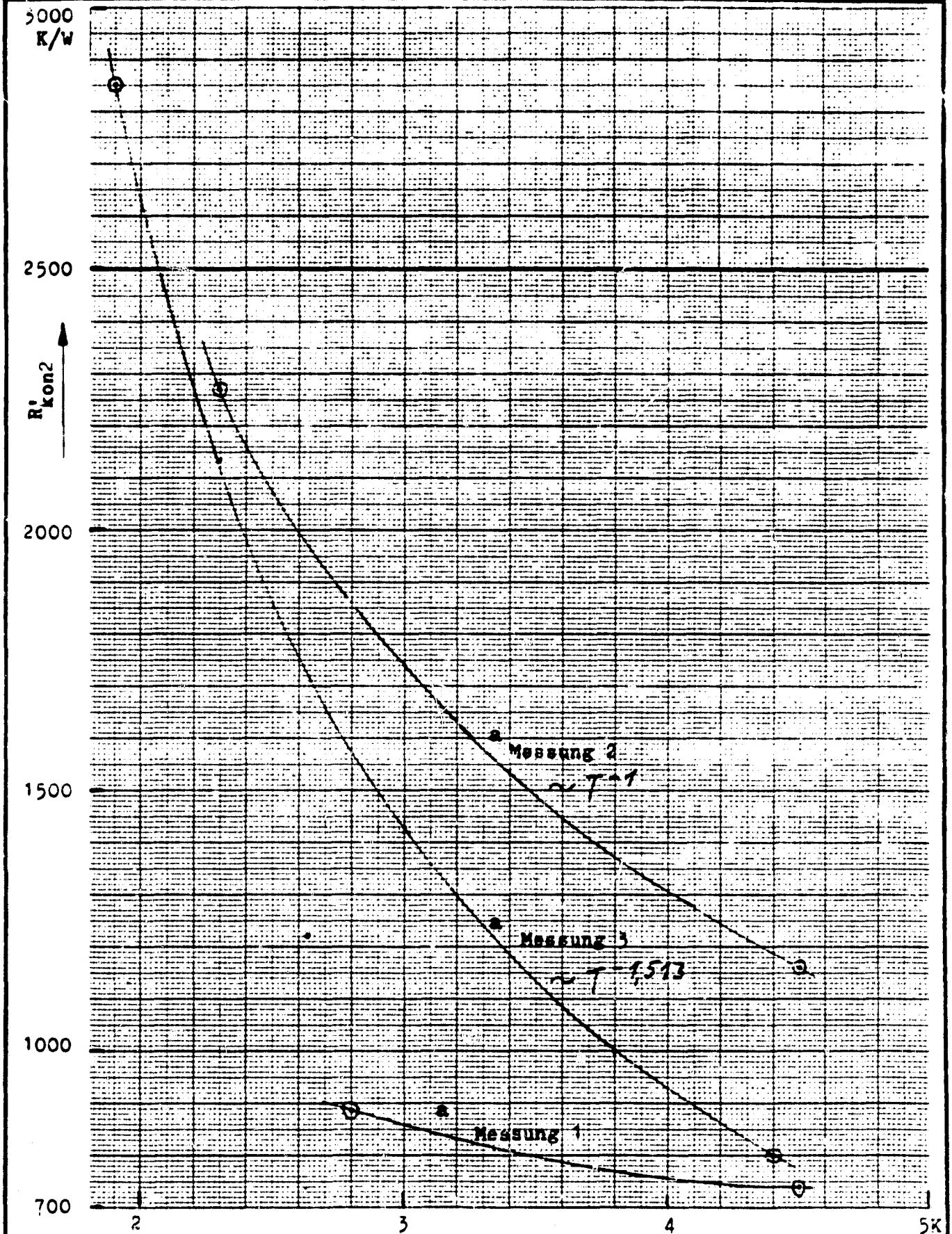

Figure 3050/19: Heat transition resistance of soldered cerodur/copper contacts as a function of temperature according to measurement results undertaken by Linde

Key: a. measurement

AP 3044 Strength of the Thermal Contacts /90

A report was presented in the preceding AP on preliminary tests on the tensile strength of cerodur and metal combinations. No system can be recognized, as was mentioned there. The only thing which is not subject to doubt is that a defect in the contact occurring in the cooling process is not cured during reheating and therefore remains accessible to a measurement when heated.

In the preliminary tests it still remained open whether additional cooling from the temperature of liquid nitrogen to that of liquid helium causes substantial alterations in strength. The following tensile strengths were ascertained in the samples measured by Linde and cooled to approx. 2 K after reheating (numbering according to Table 3040/2):

Tensile strength of the first sample according to measurement no. 2 (soldered)	< 0.2 kp
Tensile strength of the second sample according to measurement no. 3 (soldered)	> 18 kp
Tensile strength of the first sample according to measurement no. 4 (cemented)	1.5 kp

A relationship to the measured heat resistances exists only insofar as the soldered sample of less strength exhibits the higher resistance. A greater difference in resistance, however, would be expected from the large differences in strength. A substantially greater strength was expected from the cemented sample, after results of other cemented connections (see AP 3074) had favorable results. The cemented connection had to be rejected, not only because of the poor conductivity but also due to the lack in strength, although proven only in one case. A decision was subsequently made to solder all heat conductors with continuous copper litz wires.

AP 3045 Construction of the Heat Conductors /91

On the basis of knowledge in the last two AP's, the heat conductors are now designed in the form presented in Figure 3040/20. The copper litz wire is soldered in the invar nipple with a hard solder of high heat conductivity, so that it first projects on the subsequent soft solder side. After hard soldering, this side is faced and tin-plated with phosphoric acid as flux. The entire contact must then be cleansed from the remaining flux through extraction. Only then can the nipple be soldered onto the baking silver of the cerodur with an extremely mild flux. In this case, even light overheating already appears to be damaging to the durability of the soldering point.

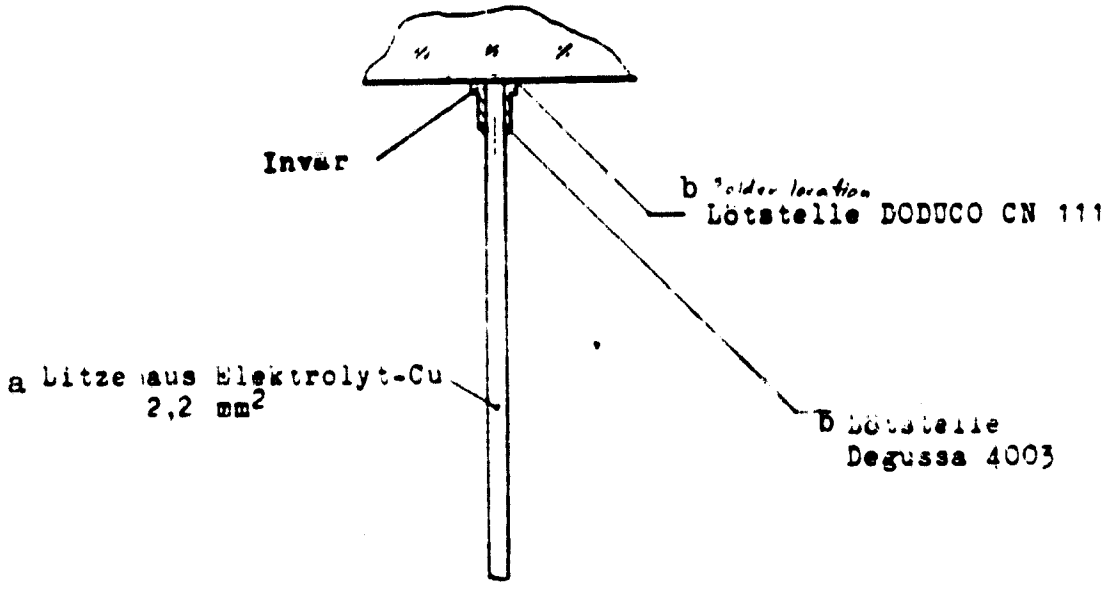

Figure 3040/20: The type of cerodur/copper contact employed in the GIRL

Key:
a. litz of electrolyte copper
b. solder point

For the systematic study of soldered connection strength yet to be undertaken, the study of the effect of the following parameters is recommended: baking temperature of the silver, type of dewaxing of the cerodur, type of cerodur surface, solder temperature and type of neutralization of the flux.

Thick copper discs are connected to the litz wires with hard solder in order to connect the copper litz wires with the copper strip functioning as busbar. They are screwed to the strips in a special manner. For reasons of simplicity, a single hole mounting is employed for this purpose. An invar disc is inserted so that commercially available steel screws can be employed (see Figure 3040/21), with a thickness determined according to the following equation so that the total contraction of the screw is identical to that of the elements to be screwed during cooling. /92

$$l_{invar} = \frac{l_{Cu}\,(\alpha_{Cu} - \alpha_{St})}{\alpha_{St} - \alpha_{invar}}$$

l = Länge
α = Dehnungskoeffizient

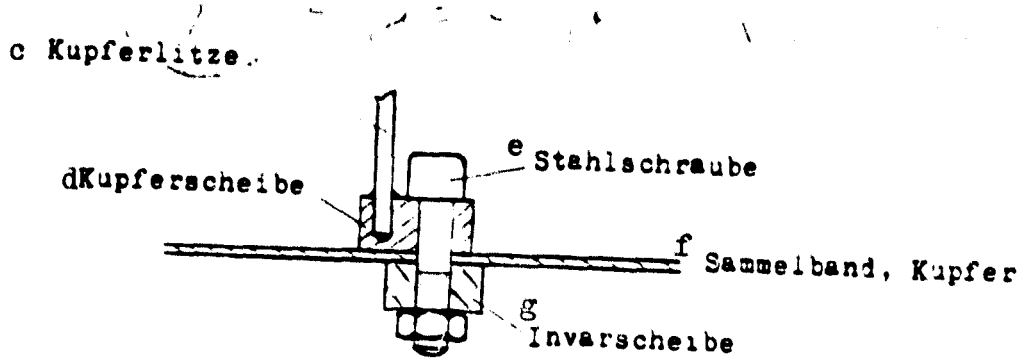

Figure 3040/21: Connection of the contact litz wires coming from the mirror with the busbar for the connection to the instrument platform.

Key:
a. length
b. coefficient of expansion
c. copper litz wire
d. copper disc
e. steel screw
f. busbar, copper
g. invar disc

AP 3050 /93
Collection Mirror and Support

AP 3051 Concept of the Support

After the durability of the solder connections between invar and cerodur had been proven in principle, as described in AP 3044, such a connection was provided between the mirror and mounting in the first concept of the collection mirror supports. This concept was first based on preliminary data of the MPI for astronomy in Heidelberg, outdated in the meantime. The data assumed two cylindrical iron cores opposite to one another, alternating pull by the electromagnetic coils of the chopper. The mounting concept which would have made an assembly of the iron cores at the mirror possible is presented in Figure 3050/1. A decisive condition for this and the following concepts is that the axis of rotation of the chopped mirror is centered in the plane of gravity of all moveable parts. All concepts are to be designed in such a way that no additional balance weights are required to satisfy this

condition. This had the consequence for the first draft that the pivot had to be shifted into the mirror. When it is considered that the central area of the collection mirror within a diameter of 24 mm is shaded by the shading effect in the incident parallel bundle, this area can be well utilized for a recess to accommodate the pivot. Deformation of the mirror, caused by the reduced wall thickness of the central area is then not critical. Complete penetration, however, is not permissible for reasons of light scattering.

An important component element of the first mounting draft is a six-pointed star of invar, supporting flat springs on three arms connected to invar discs which are soldered in cylindrical indentations of the mirror base. The two magnetic iron cores are located on the opposite side of the star. Two further arms of the star serve merely to provide the configuration with symmetry. Two brackets /95
extend from the star into the depressions of the mirror (in Figure 3050/1 below), on which 2 universal spring joints are mounted. The fixed ends of the universal spring joints are mounted in a socket extending into the central hole of the six-pointed star.

In the presentation of the concept of the collection mirror support, an expansion compensation between the six-pointed star and the cerodur mirror was first disregarded. The dimensions were chosen in such a manner that the deformation of the 3 flat springs would be almost identical at room temperature and at 10 K, leading to a radial expansion difference of approx. 20 μ at both temperatures. When the calculations or an experiment demonstrate that this load on the mirror body is impermissible, it would be relatively simple to design the points of the star in such a manner that compensation elements of aluminum can be inserted.

The result of weight estimation of the moving parts in the first mounting draft at the intended weight limit of 200 g cannot be maintained. The mirror body had already been subjected to a reduction in weight and has a weight of approx. 240 g in this form in addition to 60 g of the metallic parts. The further studies on collection mirror mounting were oriented toward an improved model of the chopper. In this model, the cylindrical iron cores are replaced by beam-shaped core yokes. The center of gravity of the moving system is shifted substantially to the rear by their larger weight. In the meantime, the necessity for a larger mirror thickness compared to that in the first draft of the assumed mounting had been recognized from AP 3055 (compare the text there). Although the mirror no longer has any larger depression in the center, the thickness still had to be increased to 15 mm.

A survey of the second mounting draft is shown in Figure 3050/2. It is supplemented by two views in the figures 3050/3 and 4. Since the final dimensions of the collection mirror baffle was not yet available at the time of these studies, a diameter of the chopper housing projecting beyond the collection mirror was considered permissible with respect to a standard baffle. The consequences of automatic focusing, as is explained in more detail in AP 3063, are already included in the draft. Figure 3050/4 shows the arrangement

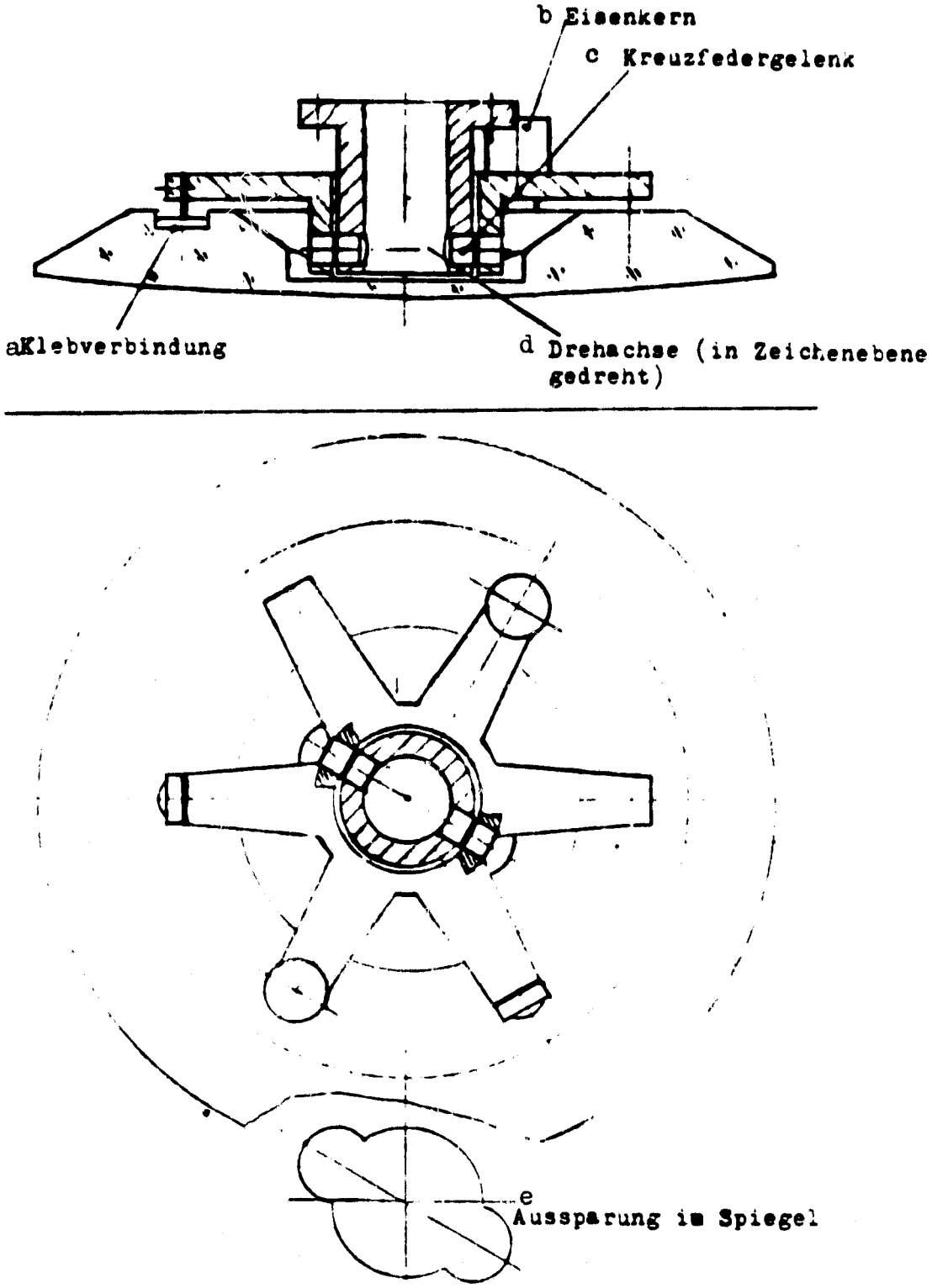

Figure 3050/1: First draft of the collection mirror support (scale 1:1)

Key:

a. cemented connection
b. iron core
c. universal spring joint
d. axis of rotation (turned in the plane of the drawing)
e. depression in the mirror

of the magnetic coils and the iron cores of the chopper. In the remaining space between the coils acting alternately, an assembly bridge is provided mounted on 4 synthetic material compensators. These compensators are the essential members for automatic focusing. Their length was optimized in AP 3063. The chopper housing and the bridge consist of invar. The two supports for the fixed ends of the universal spring joint are attached to the bridge. Calculations on the center of gravity produced the result that the axis of rotation must be situated approximately in the rear surface of the mirror. /99

The cage can be seen in Figure 3050/3, in the depressions of which first the 3 aluminum compensators are situated for the assembly of the support springs for the collection mirror and on which the magnetic yokes are mounted on the one side and the moveable ends of the universal springs joints are mounted on the other side. This cage also consists of invar.

In the attempt to create a form-fitting design for the support of the collection mirror, the type of mounting selected for the main mirror could not be considered. The finishing method of the back cut sack holes in the rear surface of the mirror could not be applied to the small dimensions of these holes. In the third draft for the collection mirror support, the mirror was therefore provided with a circular bar unto which 3 support claws engage from the outside. These are of a weak elastic design and are screwed to the invar cage in a similar manner to the flat springs in the second draft via aluminum compensation elements. A schematic cross-section through the third mounting draft is shown in Figure 3050/5. With the exception of the mounting of the mirror, the entire concept is similar to the second one. The diameter of the chopper housing was reduced so that the housing is situated in the shadow of the collection mirror. Due to the stiffening effect of the circular bar on the rear side of the mirror, the mirror could be provided with a central rear depression, similar to the one in the first draft but this time for reasons of weight. The stiffness of this mirror cross-section was selected with the aid of rough estimations in such a manner that it corresponds to the massive mirror in the second mounting draft. In the left edge of Figure 3050/5, a small portion of the counterbalance weight is still visible, vibrating in the phase opposite to the mirror for the purpose of compensating the mirror moment during the oscillation. This will probably consist of an aluminum plate, held with universal spring joints and as the mirror. This plate is excited with the same magnetic yokes as are mounted on the cage of the mirror support. /101

A sketch of the heat conductor system is presented in Figure 3050/6, as it is intended on the rear side of the collection mirror. Four invar nipples are soldered on the smooth ring zone near the edge of the mirror, not with copper litz wires as in the main mirror, but with short copper rods soldered in the holes, connected directly to an annular bar of copper sheet. The nipples therefore serve simultaneously for supporting this bar. Two further nipples serve for cooling the middle of the mirror. They are located on the smooth base surface of the central depression of the mirror rear surface.

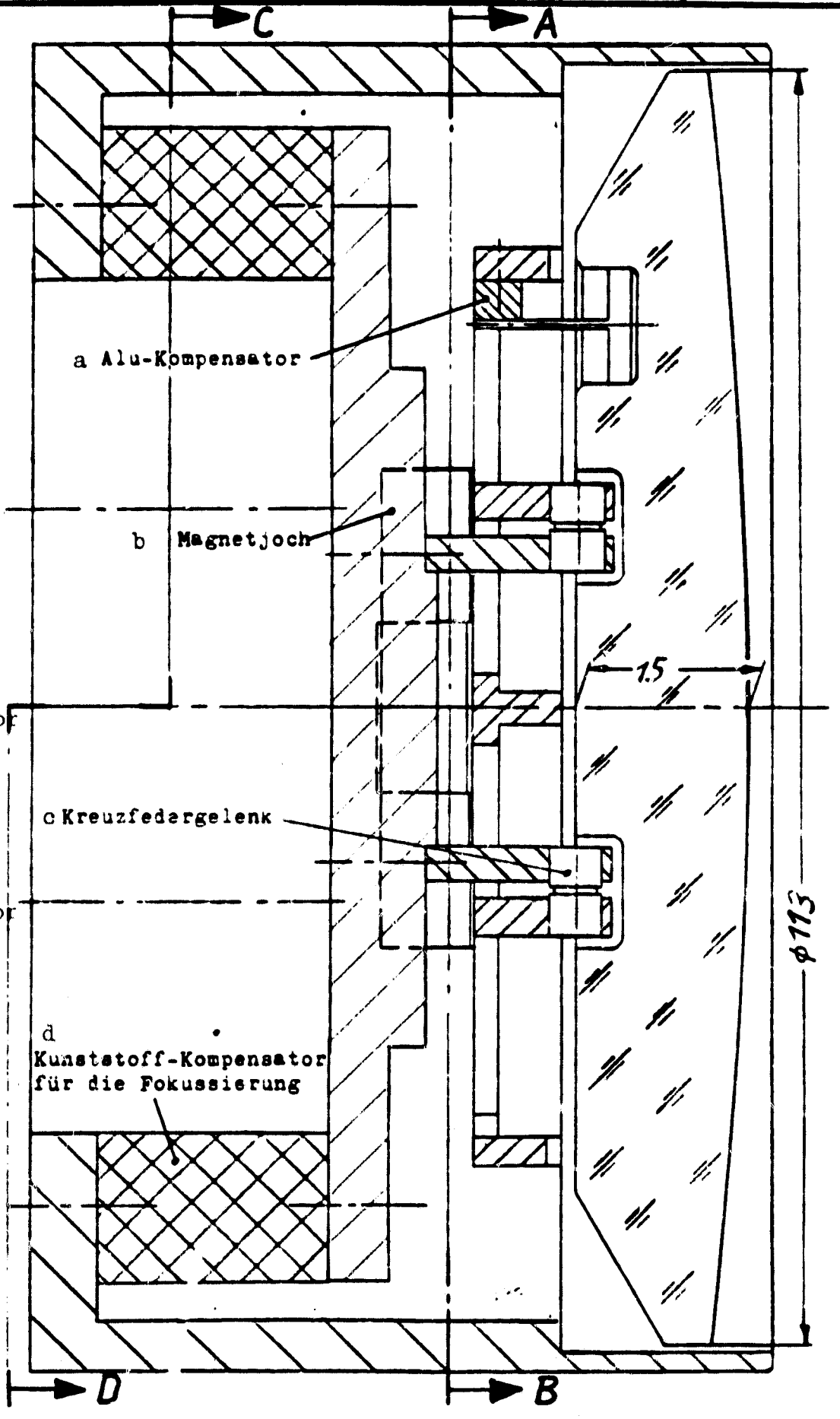

Key:
a. aluminum compensator
b. magnetic yoke
c. universal spring joint
d. synthetic material compensator for focusing

84 Figure 3050/2: Second draft of the collection mirror support (scale 2:1)

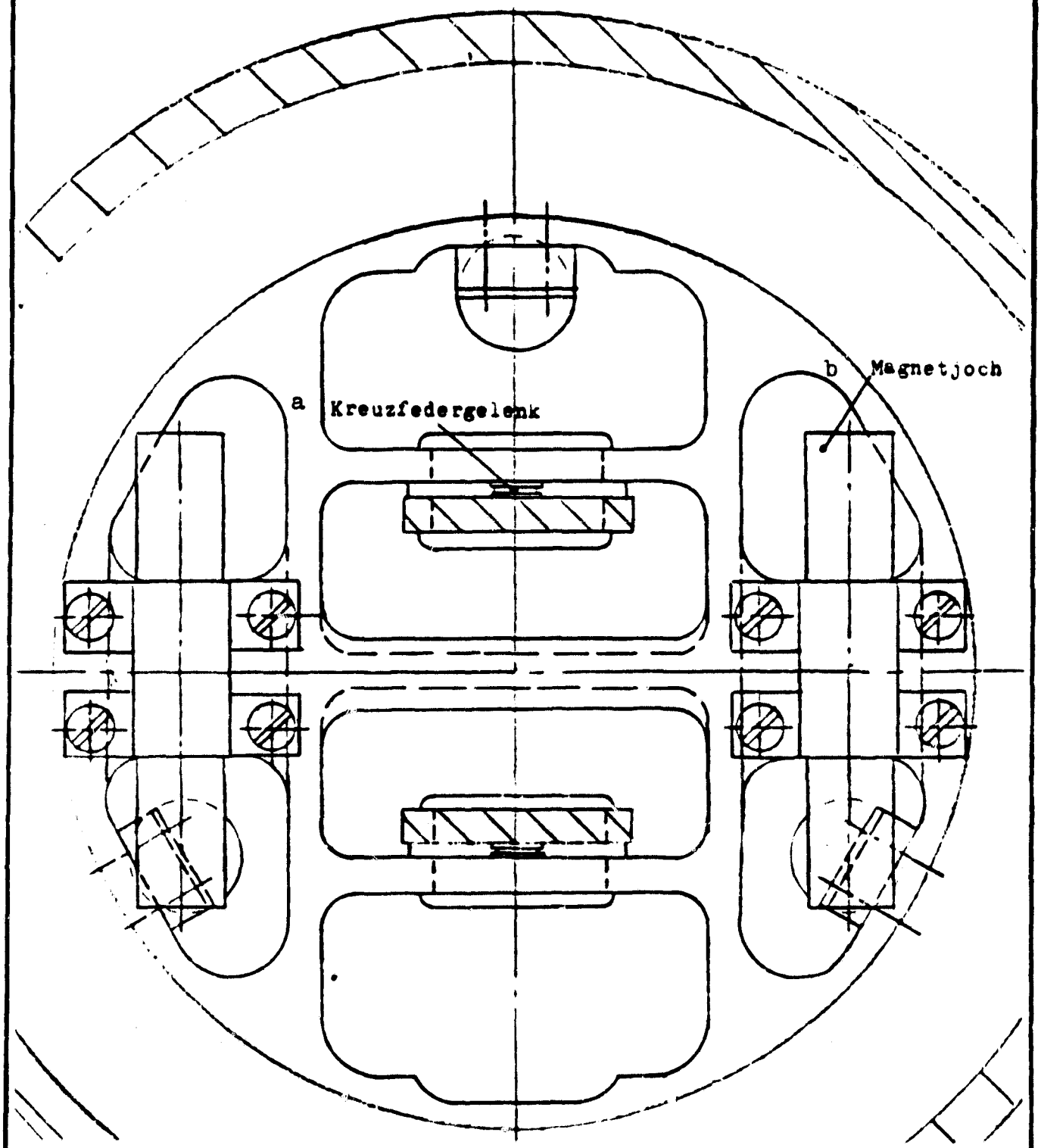

Figure 3050/3: Second draft of the collection mirror support. View A-B (compare Figure 3050/2)

Key:
a. universal spring joint b. magnetic yoke

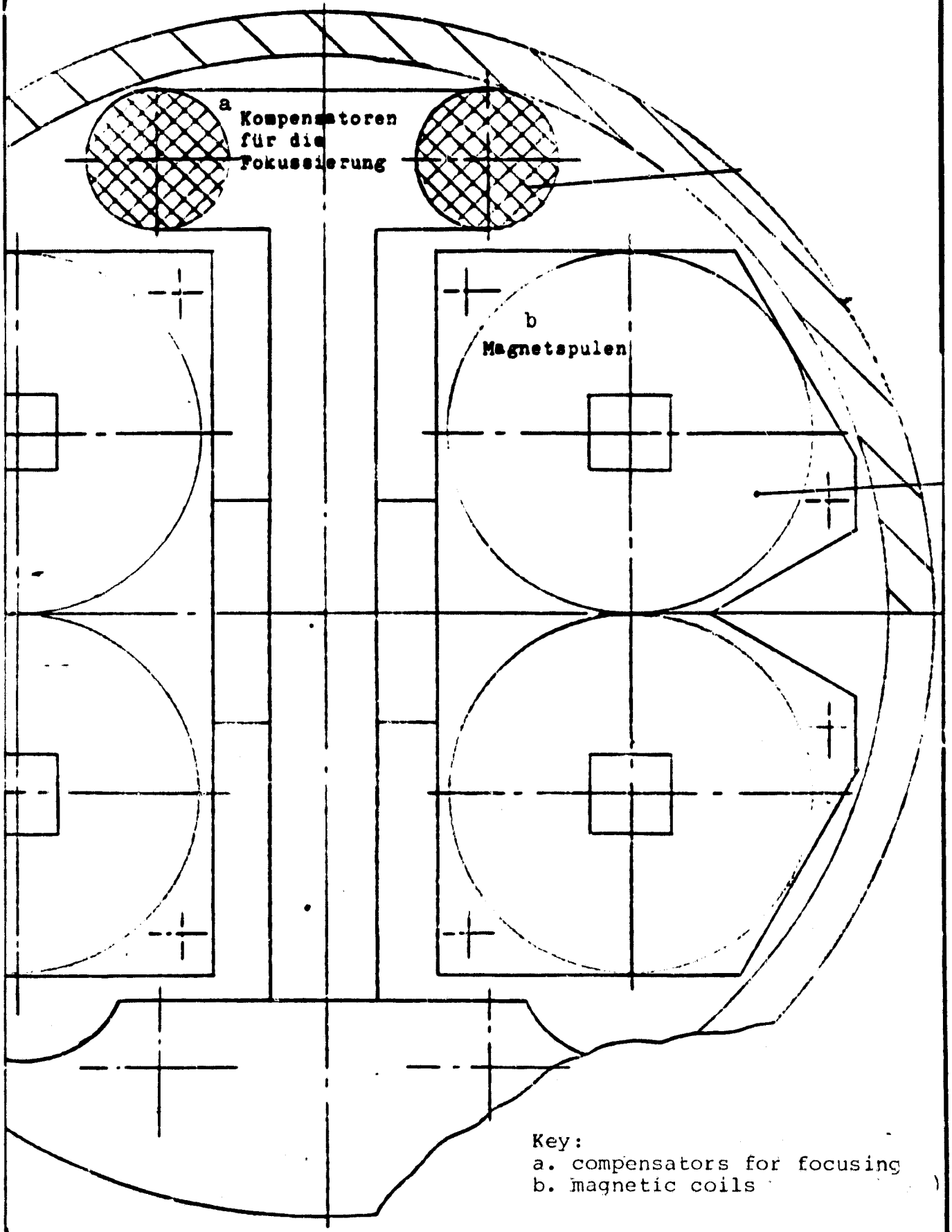

Figure 3050/4: Second draft of the collection mirror support, section C-D (compare Figure 3050/2)

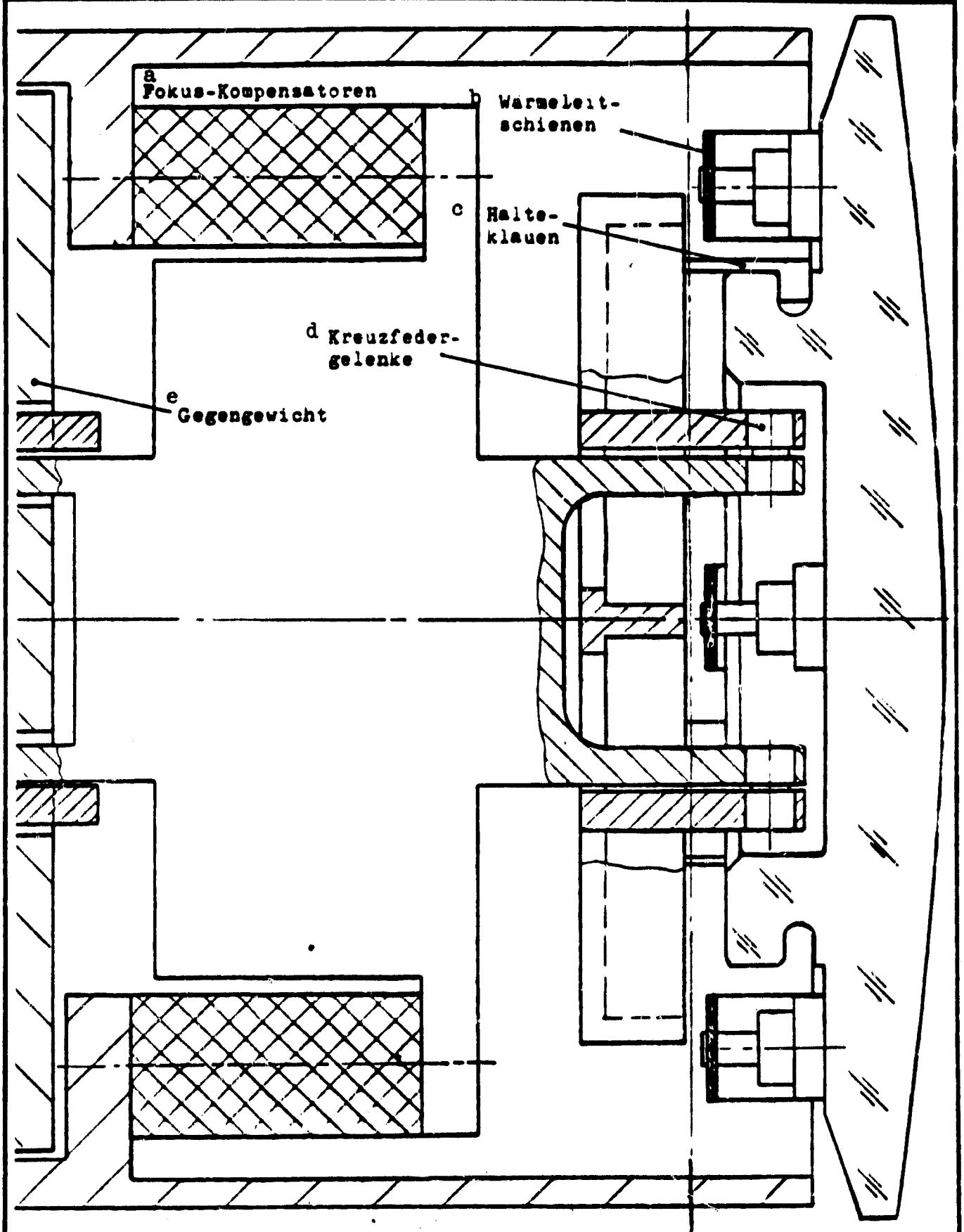

Figure 3050/5: Third draft of the collectio mirror support (scale of 2:1)

Key:
a. focus compensators
b. heat conductor bars
c. support claws
d. universal spring joint
e. counterbalance weight

They are also soldered to strips via copper rods, leading to the outer copper ring. At the top and bottom of the figure the guide strips of the annular busbar are visible, situated in the axis of rotation of the mirror. They are then led further into the hollow spaces of the tripod. Since these leads are situated in the axis of location, they are merely subjected to slight torsion when the mirror vibrates. The force of torsion and therefore the cross-section of the copper strip depend on the conductivity of the copper quality employed. It is only mentioned here on the constructive design of this conductor system that the circular bar is bent at right angles twice at both sides of the nipple, so that the differences in expansion between copper and cerodur is compensated in the case of light exersion of force. More details on this subject follow in AP 3056.

Weights

The weights for the individual component groups listed in Table 3050/1 result from the data of the MPI for astronomy as well as from the estimations using the third draft of the collection mirror support. In the case of the weight of the counterbalance weight vibrating in the phase opposite to the mirror, it was first assumed that this has a similar distribution of mass as the collection mirror. A reduction could be undertaken when the counterbalance weight would be optimized to the maximum moment of inertia and minimum total mass. The sum of the weights from Table 3050/1 amounts to approx. 2.3 kp and is therefore higher by 15% than indicated by MPI.

Table 3050/1: Weights of the component groups in the third draft of the collection mirror support. /103

Mirror body	285 g
Invar cage	160 g
2 magnetic yokes	37 g
Heat conductor system, complete	80 g
Magnetic coils including cores	700 g
Chopper housing including focus compensators and assembly bridge	450 g
Counterbalance weight, complete	562 g
Total weight of chopper and collection mirror	2,274 g

AP 3052 Thermal Balance of the Collection Mirror and Chopper /104

The power losses of the individual component groups were taken from a computer print-out of the MPI for astronomy in Heidelberg for the smallest and largest given frequency and compiled in Table 3050/2. At the maximum amplitude of 10 arc minutes, 29 mW power loss occurs

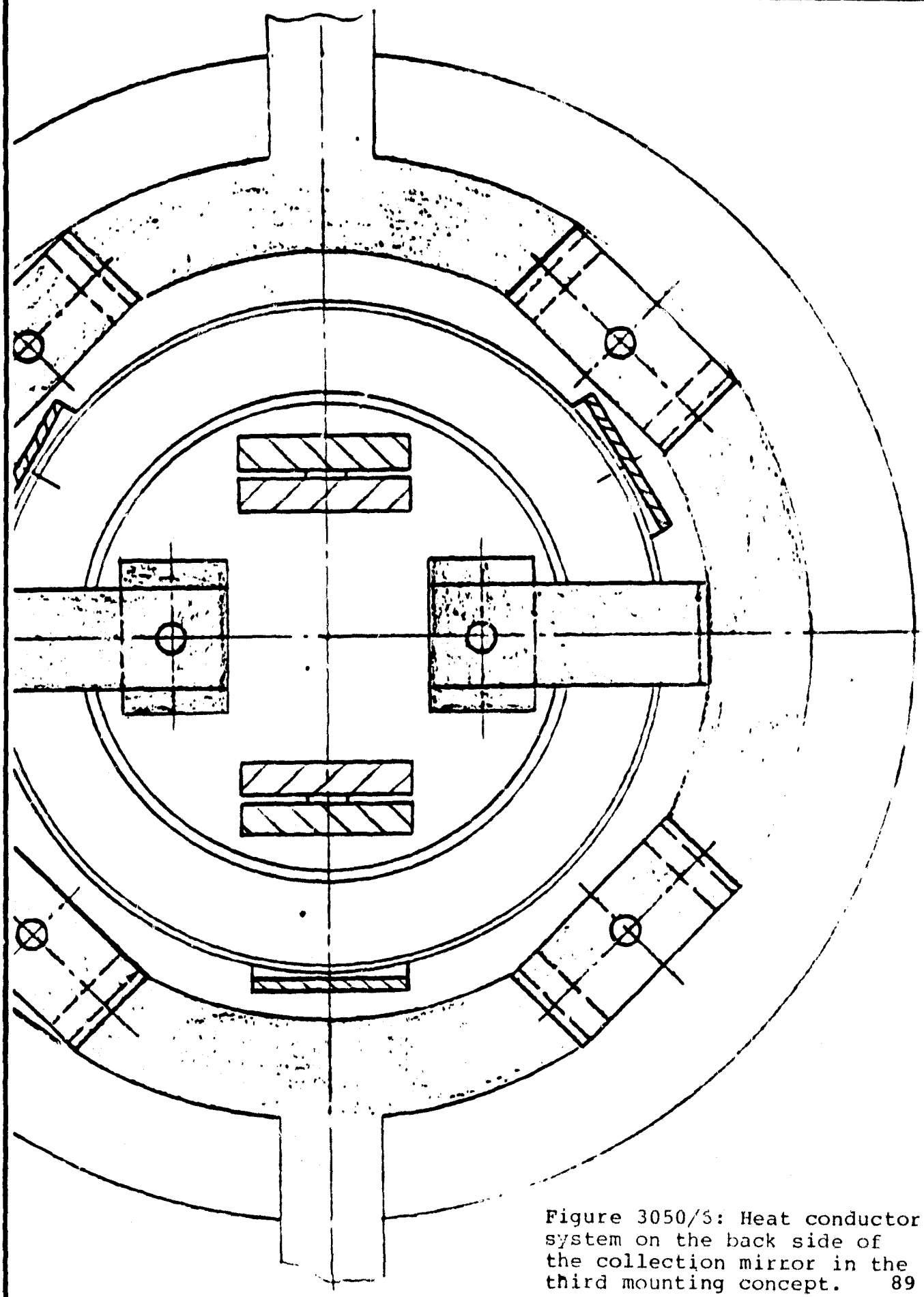

Figure 3050/5: Heat conductor system on the back side of the collection mirror in the third mounting concept.

in the chopper with a certainty factor of 5, when 25% of the power loss are added to the chopper. A power loss of 4.4 mW in the form of hysteresis and turbulence occurs in both core yokes in the mirror, i.e. in the moveable mounting part, also with a certainty factor of 5. While the maximum power loss in the chopper occurs at the operating frequency of 10 Hz, it is produced in the mirror at 50 Hz. Still another 5 mW must be added for the copper, dropped at the switch relay, path pick-up and capacitor. In aeronomy operations, approximately the same radiation is absorbed additionally by the collection mirror and by the main mirror. The minimum off-axis angle of 1° provides no substantial reduction.

The thermal relationship at the collection mirror and chopper are presented in Figure 3050/7 and the maximum power losses are plotted where they occurred. The heat dissipation system W1 is provided for the heat source of chopper + counterbalance weight + electronics; the system W2 is provided for the heat source of mirror + yoke A maximum of 34 mW can be dissipated by W1, and 13 mW by w 2, since the chopper is not in operation in the aeronomy case of radiation load.

Heat Transition Resistors

Within the framework of the third intermediate presentation (MBB handout of April 16, 1980), measurement results on the transition resistors in metal-metal transitions were presented by the Linde and Dornier companies. The results provided by Linde show that the smoothly turned surface, of three surface types studied, provides the highest heat conductivity, while an electropolished sample is 4 times poorer and a gold-plated sample 20 times poorer in conducting heat. /107
The advantage of the turned sample is apparently in the remainder roughness, suitable for penetrating the oxide layer at many points, therefore making it possible to conduct electrons. The latter is is confirmed by the measured T proportionality. In the case of the electropolished surface, the surface pressure is apparently not sufficient for breaking open the oxide layer, so that chiefly are conducted, reflected in a measured T proportionality of 2:3. Since a nickel layer had to be applied in the case of the gold-plated sample for reasons of adhesion, a total of 5 metal-metal transitions participate, having a substantially more negative effect than slight oxide layers.

The pressure of a metal-metal combination exerts a great effect on the transition resistance in the low temperature range. The results provided by Linde show an over proportional relationship in the case of the turned surface, and a more proportional relationship in the two other types. Figure 3050/8 shows the dependency measured by Linde of the contact conductivity between two turned aluminum surfaces with a raw depth of 1 m on temperature and amount of tightening of the connection screw.

	a Arbeitsfrequenz	10 Hz	50 Hz
Amplitude 10 arc min	b Hystereseverluste in allen 8 Kernelementen	0,027	0,134
	c Wirbelstromverluste in den fixen Kernen und den Jochen des Gegengewichts	0,42	1,96
	d Wirbelstromverluste in den Jochen des Spiegels	0,18	0,84
	e Ohmsche Verluste in den 4 Spulen	2,1	1,3
	f Ohmsche Verluste in Zuleitungen	13,1	8,2
Amplitude 1 arc min	b Hystereseverluste in allen 8 Kernelementen	0,003	0,013
	c Wirbelstromverluste in den fixen Kernen und den Jochen des Gegengewichts	0,07	0,21
	d Wirbelstromverluste in den Jochen des Spiegels	0,03	0,09
	e Ohmsche Verluste in den 4 Spulen	0,3	0,2
	f Ohmsche Verluste in Zuleitungen	2,0	1,3

Figure 3050/2: Guide values of thermal power losses during chopper operation (in accordance with an informal notification of the MPIA of June 18, 1980, for a collection mirror weight of 200 g).

(See Key on following page.)

C-2

Key:
a. operating frequency
b. hysteresis losses in all 8 core elements
c. turbulence losses in the fixed cores and the yokes of the counterbalance weight
d. turbulence losses in the yokes of the mirror
e. ohmic losses in the 4 coils
f. ohmic losses in feed lines

/106

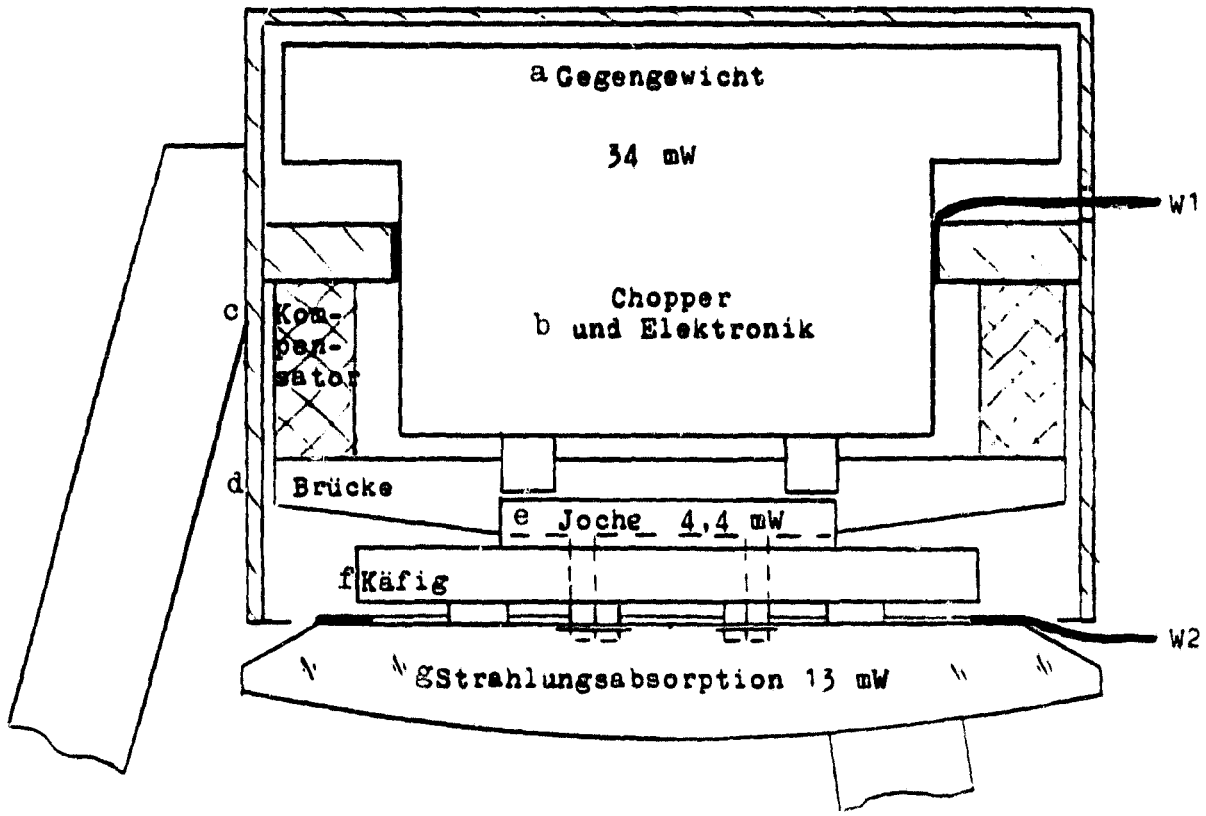

Figure 3050/7: Schematic thermal model of collection mirror and chopper with heat sources and lines for heat dissipation.

Key:
a. counterbalance weight
b. and electronics
c. compensator
d. bridge
e. yoke
f. cage
g. radiation absorption

Measurements were carried out by the Dornier system, corresponding even better to the transitions provided at the collection mirror. A strip of Cu 99.999% with a cross-section of 25 x 0.25 mm^2 was pressed onto a surface of AlMgSi 0.5 - 1/3.3214 with an M8 screw. The contact surface amounted to 16 x 25 = 400 mm^2, the torque moment of the screw 19 Nm. The result of three different measurements is shown in Figure 3050/9.

When the result attained by Linde is converted to the unit of the contact surface, it is then 2.2 times better than the corresponding Dornier system result. In the following estimations on heat dissipation, the calculations are carried out with an average value of

$$0.1 \text{ W cm}^{-2} \text{ K}^{-1} \text{ with } T = 4\text{K}$$

for all screw connections. In the case of a contact surface of 12 x 12 mm^2, the contact resistance at 4 K would then be $R_{kon1} = 3,5 \text{ KW}^{-1}$

In addition to the transition conductivity of the metallic screw connections, the conductivity of the homogeneous conductor material is of significance. The specific conductivities of some highly pure qualities of copper were taken from the literature and are presented in Figure 3050/10 (curves 1-4). In addition, measurements were undertaken by Dornier system with copper and aluminum strips, added to the diagram as curves 5 and 6. The measurement result for Cu 99.999% deviates by more than the factor 3 from the value in literature for the pure, tempered material. For reasons of certainty, the lower of the two values is inserted in the following estimations on the collection mirror. /111

When strips with a cross-section of 20 x 0.5 mm^2 are employed for dissipating heat, the strip resistance in the case of a strip length of 80 cm and a temperature of 4 K is

$$R_{\underset{a}{band}} = \frac{1}{\lambda \cdot q} = \frac{80}{22 \cdot 0,1} = 36,4 \text{ KW}^{-1}$$

Key: a. strip

For the cerodur/metal transition, the pessimistic value at 4 K is produced from the results in AP 3043

$$R_{kon2} = 1240 \text{ KW}^{-1},$$

when the portion of the electrolytic copper litz wire (160 KW^{-1} at 4 K) is subtracted from the Linde measurement result.

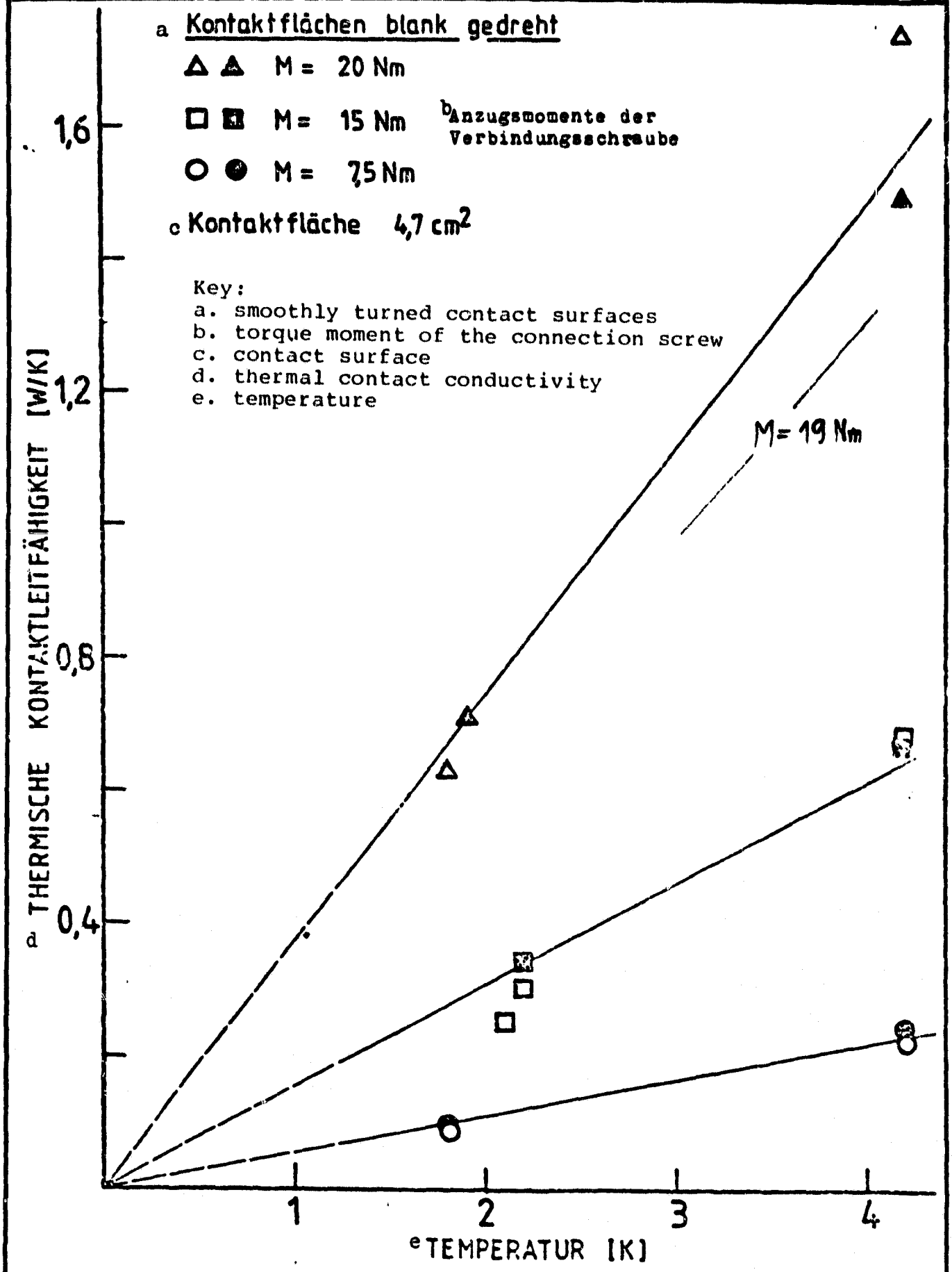

Figure 3050/8: Heat conductivity of an aluminum-aluminum screw connection according to Linde

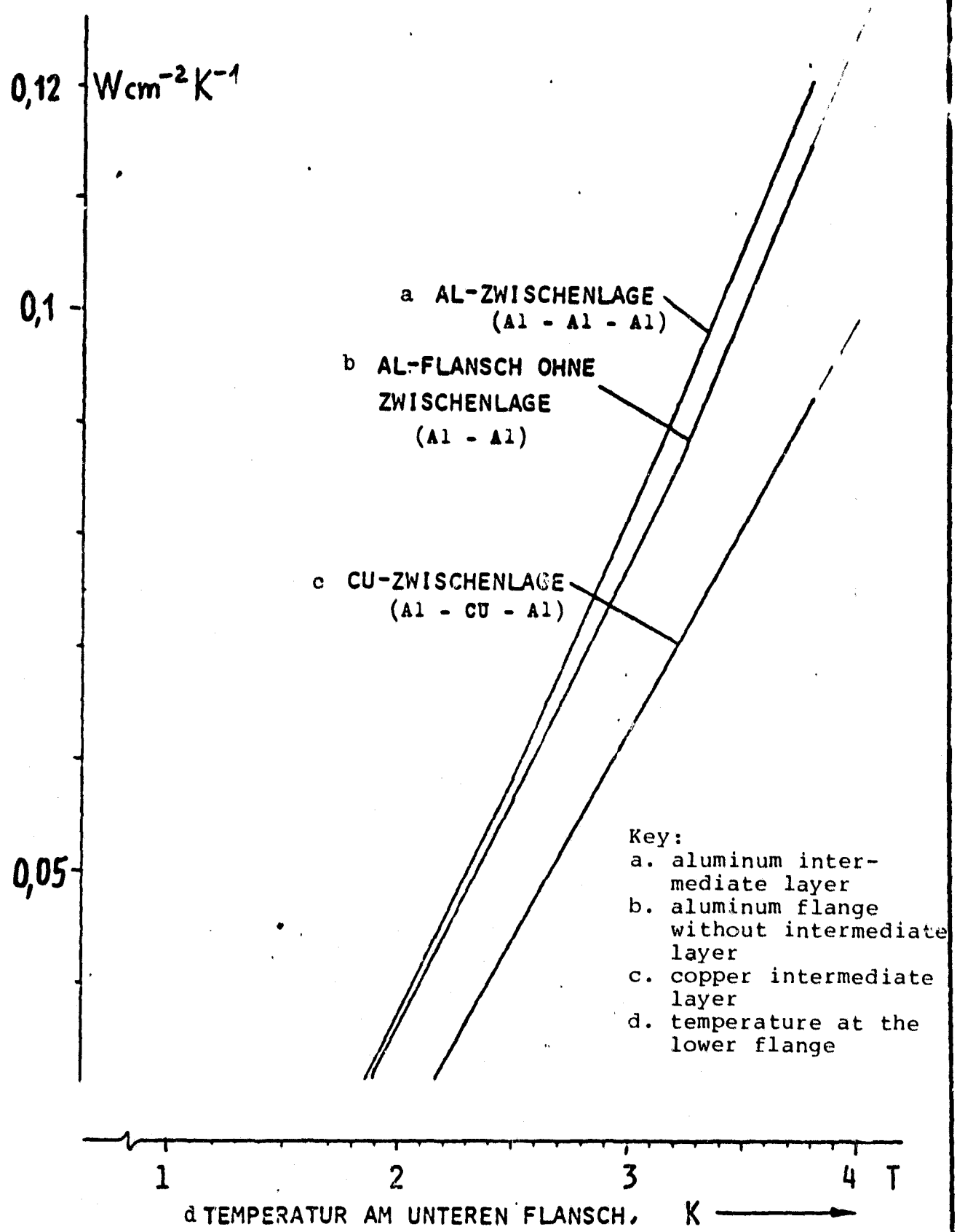

Figure 3050/9: Specific conductivity of metal screw connections according to the Dornier system.

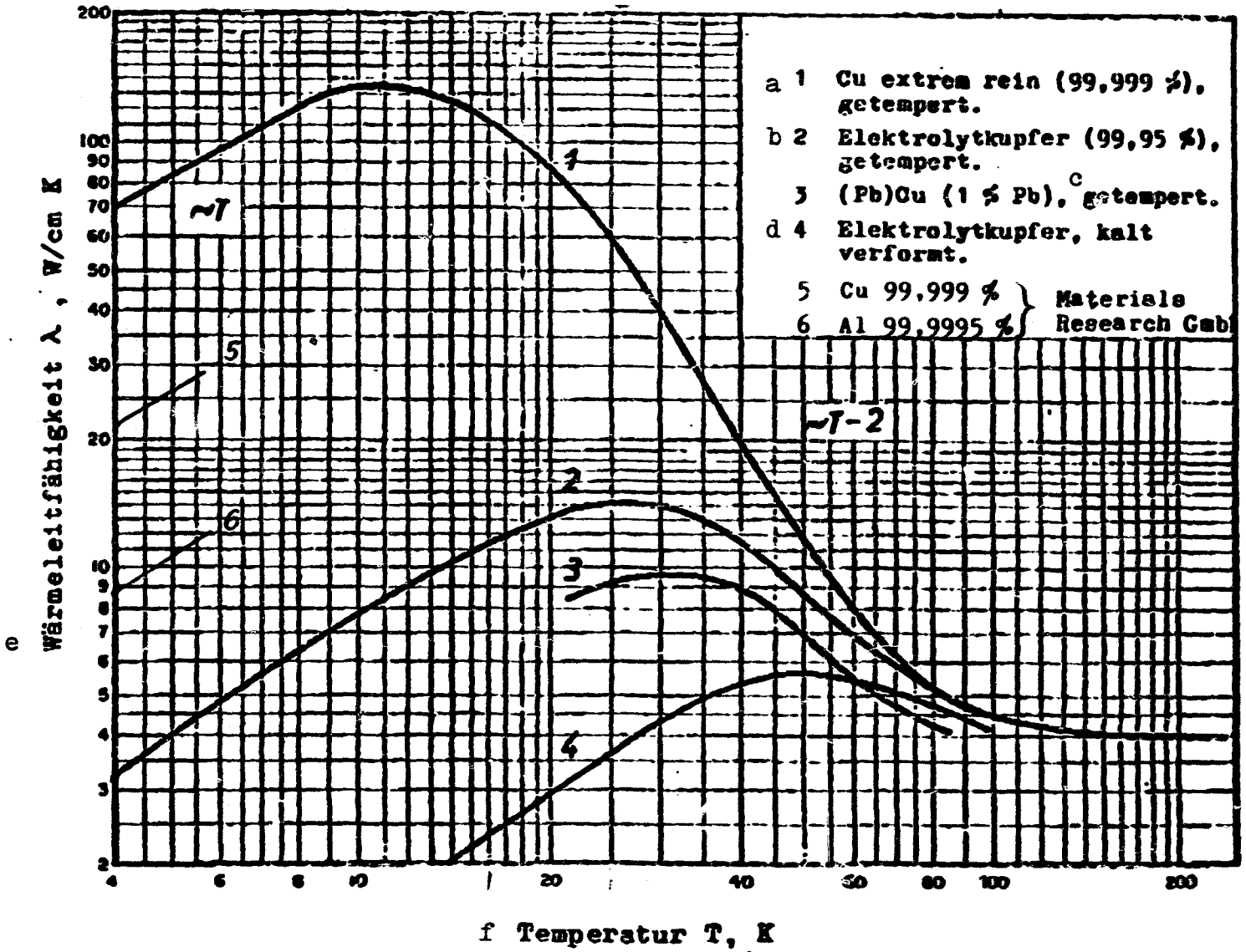

Figure 3050/10: Heat conductivity of highly pure metals at low temperature

Key:
a. Cu, extremely pure, tempered
b. electrolytic copper, tempered
c. tempered
d. electrolytic copper, cold shaped
e. heat conductivity
f. temperature

Heat Dissipation /112

When the heat dissipation line W1 from the chopper (Figure 3050/7) is first examined, a series of four screw connections can be realistically expected here in the heat conduction system, in addition to the conduction strip of 20 x 0.5 mm^2 Cu 99.999%, already assumed at a realistic length of 80 cm. This results in a total resistance of

$$R_{ges}^{a} = 4 \cdot R_{kon1} + R_{band}^{b} = 50{,}4\ KW^{-1}$$

Key: a. total
b. strip

at 4 K. Since the capacity leading away, however, only amounts to 34 mW, a temperature drop of only 1.7 K is achieved over the entire dissipation system. This is completely sufficient, since on the one hand the temperature of the instrument platform can be assumed at 3 K < T < 4 K and on the other hand, the chopper may achieve a maximem temperature of 10 K. Since the heat resistances become smaller with increasing T at least in an inverse proportional relationship, R_{kon1} and R_{band} can still be doubled without exceeding the range limit of 10 K.

Care must be taken that the heat is taken up by the heat conduction system before reaching the chopper housing by establishing a clever contact of the chopper, the counterbalance weight and the other fixed heat sources, as is indicated in Figure 3050/7. Moreover, it was assumed in the previous considerations that the surface of the housing facing the sky is mirrored optimally so that in the case of radiation reaching the earth there is no substantial absorption to be dissipated additionally. In the case of mirroring the absorption with 12 cm diameter is approx. 1.2 mW.

The heat loss of the core yoke is first directed into the cage. Heat is built up at the three flat springs connecting cage and mirror, on the same order of magnitude as the buildup at the universal spring joints between cage and bridge. The "yoke heat" /113
is dissipated accordingly in approximately equal portions over the dissipation systems W1 and W2. Since they must flow over the compensators in the case of W1 and over the mirror in the case of W2, a direct thermal contact of the yoke would also be practical here. Compared to the results above, dissipation of the 4.4 mW is completely without problems and could be carried out over W2.

The contact resistances R_{kon2} between cerodur and copper are determining factors for the dissipation of radiation. In the case of the 6 contacts planned, $R_{kon2} = 1240/4 = 310\ KW^{-1}$. The resulting temperature jump at 13 mW and 4 K would then be 4 K. This contact number therefore appears to form the lower limit. More precise estimations on this problem follow in the next AP.

AP 3053 Cool-down Time of the Mirror

The calculation of the cool-down time was combined with the determination of the tensions in the cerodur occurring during the cooling process as a result of inhomogenous course of the temperature. As in the case of the main mirror, a model of finite elements was selected for the calculations, the structure of which can be seen in Figure 3050/11. The model is simplified insofar as all heat conductors on the rear side of the mirror as in the case of the main mirror are collected to a concentric, homogeneous ring with a heat conductivity permitted only in the y direction. The cylinder has a total cross-section of 18 mm^2 of a material, equivalent to the heat resistance of the measured cerodur/copper combination. The cylinder therefore corresponds to exactly 7.8 pieces of the measured connections (individual cross-section 2.3 mm^2). This is 30% more than intended according to Figure 3050/6. /115

The calculations were carried out with the temperature relationships of the thermal expansion of cerodur from the final report of phase A (p. 16) and the heat capacity in accordance with the following average values from data in literature for various qualities of quartz:

a			a		
bei 2K	$1,5 \times 10^{-5}$	Ws/gK	bei 50K	0,10	Ws/gK
4K	$1,4 \times 10^{-4}$	"	100K	0,26	"
10K	3×10^{-3}	"	200K	0,55	"
20K	$1,8 \times 10^{-2}$	"	293K	0,73	"

Key: a. at

The values of heat conduction were taken again from the Figures 3040/18 and 19.

Since the collection mirror must only be cooled to less than 10 K, the third phase of cooling from 4 K to 3 K, as appeared justified in the case of the main mirror, was disregarded in the calculations. The course of temperature of the base therefore extends in the case of the collection mirror only up to 4 K over a total of 12 hours in accordance with Figure 3040/14.

The results of the cool-down calculation is presented in Figure 3050/12 by a computer printout. In addition to the curves of temperatures for the base (cryostat), as well as the coldest and hottest points in the mirror, the difference between the coldest and hottest points of the mirror multiplied by ten is presented. This first increases to a plateau of $\Delta T = 8.5$ K converting to a lower plateau of $\Delta T = 2$ K after six hours with a slowing of the increase in base temperature. One hour before attaining the final temperature, T drops to less than 1 K, and at the final point all temperature differences have disappeared, as far as the diagram shows. The remaining differences, however, are greater than zero, as expected, and can be seen in precise form from Table 3050/3.

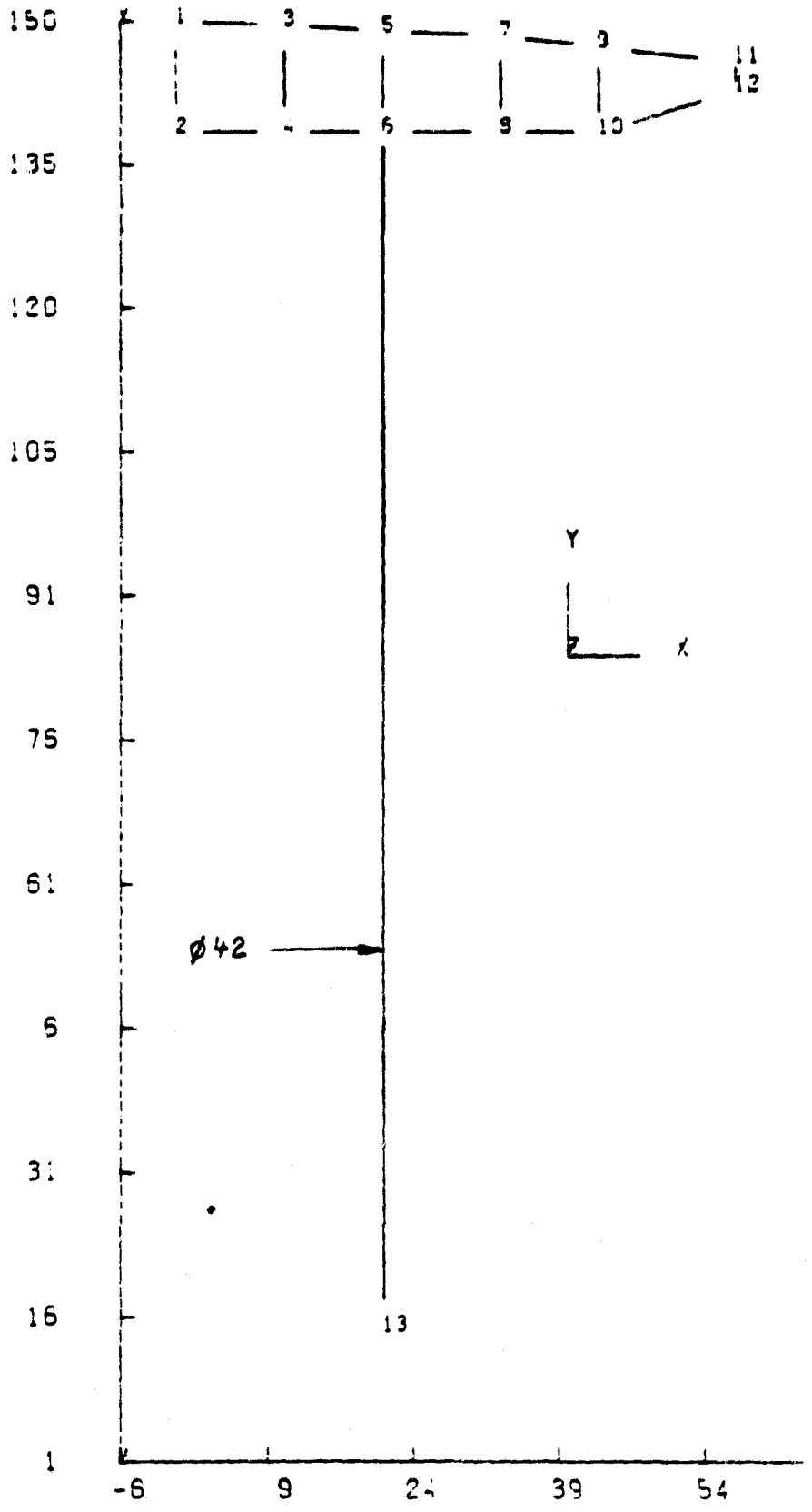

3050/11: Collection mirror model for the cool-down calcu- - lations. 1---2 optical axis, 6---13 heat conductor cylinder. Mirror diameter 113 mm, thickness 11.5 mm.

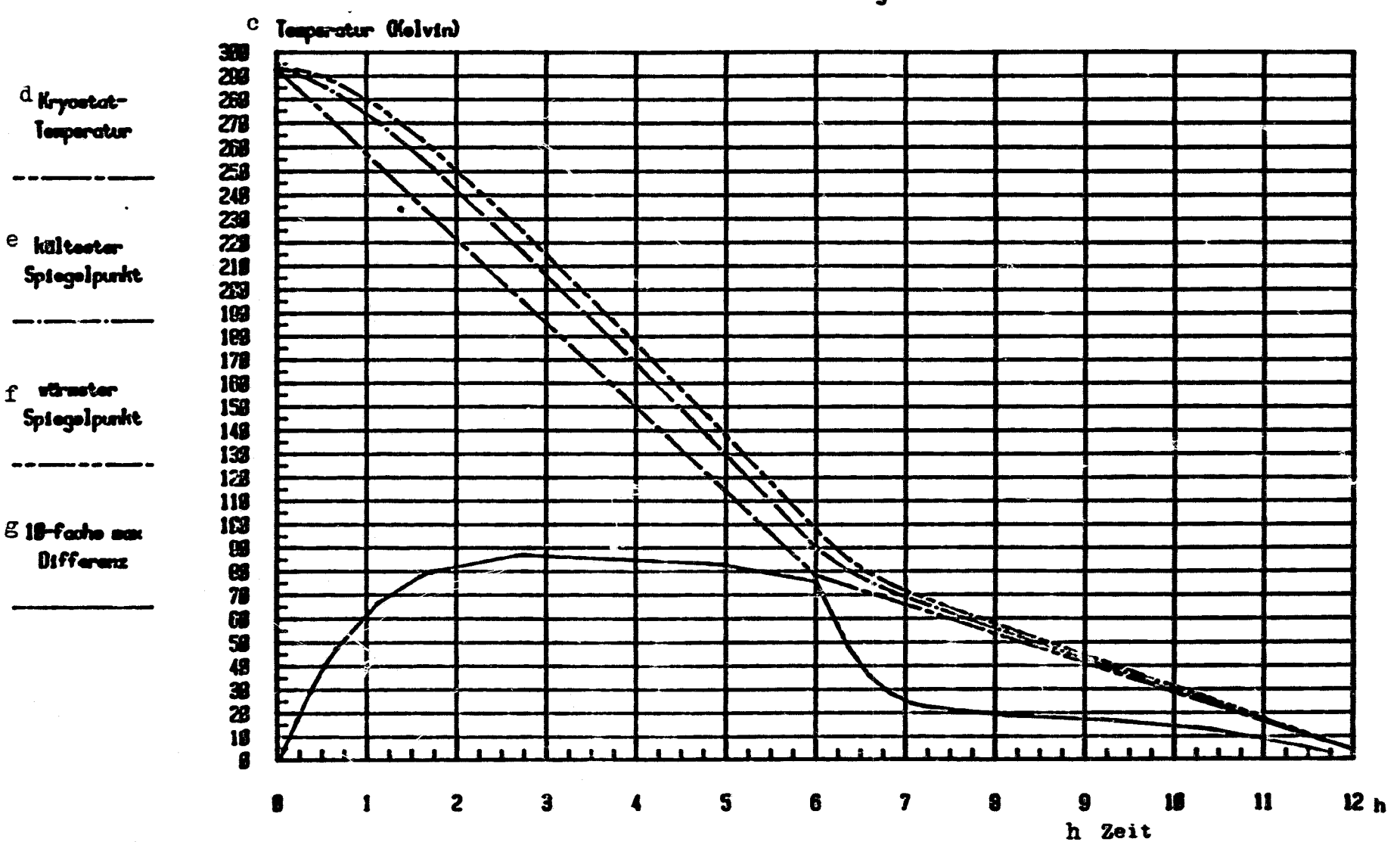

Figure 3050/12: Calculated result of the cool-down for the collection mirror
(Please see following page for Key)

Key:
a. collection mirror
b. cool-down calculations
c. temperature
d. cryostat temperature
e. coldest point in the mirror
f. hottest point in the mirror
g. maximum difference times 10
h. time

***** TEMPERATURE SOLUTION ***** TIME = 43200.

NODE	TEMP	NODE	TEMP	NODE	TEMP
1	4.0359	2	4.0351	3	4.0325
6	4.0176	7	4.0519	8	4.0551
11	4.0686	12	4.0686	13	4.0000

LOAD STEP= 12 ITERATION= 3 CUM. ITER.= 42

NODE	TEMP	NODE	TEMP
4	4.0350	5	4.0396
9	4.0639	10	4.0635

Table 3050/3: Final temperatures according to 43200 s = 12 hours cooling down of the collection mirror corresponding to 42 calculation iterations.

It can be seen from the table that the greatest temperature /117
difference in the mirror surface occurs between nodes 3 and 11 at 0.0361 K and a difference of 0.0176 K remains over the heat conductor. With a better distribution of heat conductors, as is provided according to Figure 3050/6, the differences in the mirror surface are still smaller.

The maximum stresses in the cerodur were now determined from the course of temperature. The computer print-out in Table 3050/4 shows the normal tension SX and SY in the plane of the drawing from Figure 3050/11 of the rotation-symmetrical model. In addition, the shearing stresses TXY and the maximum values SMX, the minimum values SMN as well as the maximum shearing stresses TMX are given. The greatest value occurring is 0.24 kp/mm^2. The table shows that the greatest stresses occur after 2.8 hours, when the temperature difference also passes through a maximum. The calculated stresses are completely/119
uncritical so that a cool-down time of 12 hours would also be

permissible under this aspect. This model does not include stresses near contacts.

The results of the cool-down calculations were so positive that it appears completely permissible to apply the heat conduction system presented in Figure 3050/6 to the collection mirror. Further optimizing is therefore superfluous, at least in heat technology. The technical details are explained in AP 3056.

AP 3054 Natural Frequency of the Second Mirror

As in the case of the main mirror, the critical natural frequencies are also determined in the collection mirror by the weakest member of the mirror mounting. According to Figures 3050/2 and 5, the rigidity of the flat springs attached to the mirror, of the cage and the universal springs joints are to be studied in any case comparatively in this respect.

Flat springs for mounting the mirror are provided with a cross-section b x d = 10 x 0.7 mm^2 and a length l = 8 mm. During cool-down, they are deflected in accordance with Figure 3030/6, by 4 m, when the compensation of the invar cage in relation to the cerodur mirror is carried out with aluminum and the support ring diameter amounts to 68 mm. A force of 0.4 kp is initiated temporarily in the mirror through this deflection. It completely without danger.

The axial rigidity of the three flat springs results directly from the Hook law and is with the coordinates of Figure 3050/11:

$$F/\Delta y = \frac{b \cdot d \cdot E}{l} = 11900 \text{ kp/mm}$$

E is the modulus of elasticity of invar at 10 K (13600 kp/mm^2). /120
The axial natural frequency f is then, in the case of a mirror weight of G = 0.34 kp including heat conductors

$$f = \frac{1}{2\pi}\sqrt{\frac{F \cdot g}{\Delta y \cdot G/3}} = 5{,}1 \text{ kHz}$$

This frequency is reduced to 3478 Hz, when the natural rigidity of the mirror body is included in the estimation. The following transversal and torsion frequencies are also obtained from the rigidity of the flat springs by including the mirror rigidity:

a
Zustand nach
2,8 Stunden

NODE	SX	SY	TXY	SMX	SMN	TMX
1	-.14	-.23	.00	-.14	-.23	.04
2	.13	.24	-.00	.24	.13	.05
3	.01	-.02	.00	.01	-.02	.02
4	-.03	.02	-.00	.02	-.03	.02
5	.01	-.02	.00	.01	-.02	.01
6	-.03	.02	-.00	.02	-.03	.02
7	-.00	-.01	-.00	-.00	-.01	.00
8	-.01	.01	.00	.01	-.01	.01
9	.00	-.01	-.00	.00	-.01	.01
10	-.01	.01	.00	.01	-.01	.01
11	.00	-.01	-.00	.00	-.01	.00
12	.00	.00	-.00	.00	.00	.00

b
Zustand nach
3,8 Stunden

NODE	SX	SY	TXY	SMX	SMN	TMX
1	-.08	-.10	.00	-.09	-.10	.01
2	.07	.10	-.00	.10	.07	.01
3	.01	-.01	.00	.01	-.01	.01
4	-.01	.01	-.00	.01	-.01	.01
5	.01	-.01	.00	.01	-.01	.01
6	-.01	.01	-.00	.01	-.01	.01
7	-.00	-.00	.00	-.00	-.00	.00
8	-.00	.00	.00	.00	-.00	.00
9	.00	-.00	-.00	.00	-.00	.00
10	-.00	.00	.00	.00	-.00	.00
11	.00	-.00	-.00	.00	-.00	.00
12	.00	.00	-.00	.00	.00	.00

Table 3050/4: Stresses in the collection mirror body in defined states of cooling down. SX, SY normal stresses, TXY shearing stresses, SMX maximum normal stresses SMN minimum normal stresses, TMX maximum shearing stresses. All values in kp/mm^2.

Key:
a. condition after 2.8 hours b. condition after 3.8 hours

ZEISS
C I R L
116

transversal frequency	in the direction of a spring normal	in the direction of a spring surface
	1584 Hz	1584 Hz

torsion frequency around the optical axis

1929 Hz

The relatively soft universal spring joints supply much lower frequencies. The rigidities of the type provided in the drafts with 3/16" diameter and 7.5° angle of rotation in two-part design can be seen in Table 3050/5.

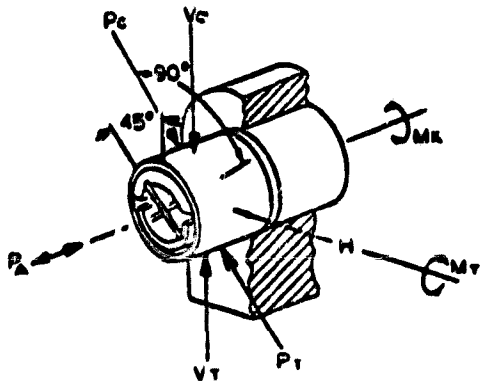

v_c = 9000	pounds/inch	=	161 kp/mm
v_t = 7000	"	=	125 "
p_c = 10500	"	=	188 "
p_t = 8500	"	=	152 "
p_a = 11000	"	=	197 "

Table 3050/5: Rigidities of a universal spring joint 3/16", 7.5°. /121

The smallest axial natural frequency of the collection mirror is given by the rigidity p_t, the joint is installed with a rotation of 45°. G is 0.55 kp.

$$f = \frac{1}{2\pi}\sqrt{\frac{p_t \cdot g}{G/2}} = 371 \text{ Hz}$$

The rigidity in the direction H (Table 3050/5) is just as large as that in the direction v, producing a transversal frequency perpendicular to the support axis which is just as large, since the latter is situated in the plane of gravity of the moving systems. In the axial direction of the support, p_a determined the transversal frequency. With the identical weight of the moving parts, f = 422 Hz is obtained.

In estimating the torsion frequency caused by the universal spring joint, the distance of the joints is a decisive factor. In order to maintain the smallest possible depression in the mirror, a small distance is highly valued. When the calculations are carried out with r_2 = 16 mm in accordance with the drafts Figures 3050/2 and 5, the result is /122

$$f = \frac{1}{2\pi}\sqrt{\frac{2p_t \; 2g \; r_g^2}{G \quad r^2}} = 208 \text{ Hz}$$

This value, however, can only be an approximation, since the inertial moment of the system was set equal to that of a complete cylinder with the diameter of the collection mirror. Accordingly, r_g should not be decreased.

In comparison to the flat springs and the universal spring joints, the rigidity of the cage is so high that the natural frequencies of the system caused by it are certainly higher than those of the joints, so that a complicated calculation of these values can be disregarded here.

AP 3055 Deformation of the Second Mirror during Chopping

In the determination of the deformation, a tested procedure could be reapplied, already employed in another study. The procedure treats the surface deformation of a plate of constant thickness rigid to bending, mounted on several support points and carrying out sine vibrations by one diameter. The RMS value of the total deformation is obtained by means of a finite-element calculation. With the aid of an examination of similarities, the results of a defined case can be converted to another one. The equation applies: /123

$$W_2 = W_1 \left[\frac{G_2}{G_1} \cdot \frac{d_2^2}{d_1^2} \cdot \frac{A_2}{A_1} \cdot \frac{f_2^2}{f_1^2} \cdot \frac{h_1^3}{h_2^3} \cdot \frac{X_2}{X_1} \right]$$

G = weight
d = mirror diameter
A = amplitude
f = frequency
h = mirror thickness
x = support factor

W = RMS value of the surface deformation

The support factors X result from the theory of thin plates. They depend on the number of points and on the geometrical distribution. The mirror thickness is that of a homogeneous, cylindrical disc with the original weight. The maximum values of A_2 and f_2 result from the computer diagram of the MPIA, Heidelberg, in Figure 3050/13. With G_2 = 203 g, d_2 = 112 mm, A_2 = ±10 arc min., f_2 = 50 Hz sine oscillation, h_2 = 8.2 mm and x_2 = 5.49, the result for the surface of the GIRL collection mirror is

$$W_2 = 22 \text{ nm RMS}$$

for the wave front:

$$W_2 = 44 \text{ nm RMS.}$$

This value is somewhat too large and would endanger the picture quality of the telescope to an impermissible limit. On the basis of this knowledge, the average thickness of the mirror at 11.5 mm (draft 1) was increased to 15 mm (draft 2). The new values are then G_2 = 285 g, h_2 = 11.48 mm. The improved value of the wave front abefration is

$$W_2 = 24 \text{ nm RMS}$$

AP 3056 Construction of the Mirror Mount /125

The construction of the mirror mount is closely connected to that of the chopper and is greatly influenced by the requirements of automatic focusing. While the latter can already be comprehended based on the aspect of thermal expansion, the development of the chopper is still in the experimental stage. The work therefore had to be undertaken with preliminary data, which also provided a mounting construction of the collection mirror with only a preliminary value. In addition, the collection mirror diameter is still controversial and will only result from the BASC study on the stray light relationships not yet begun.

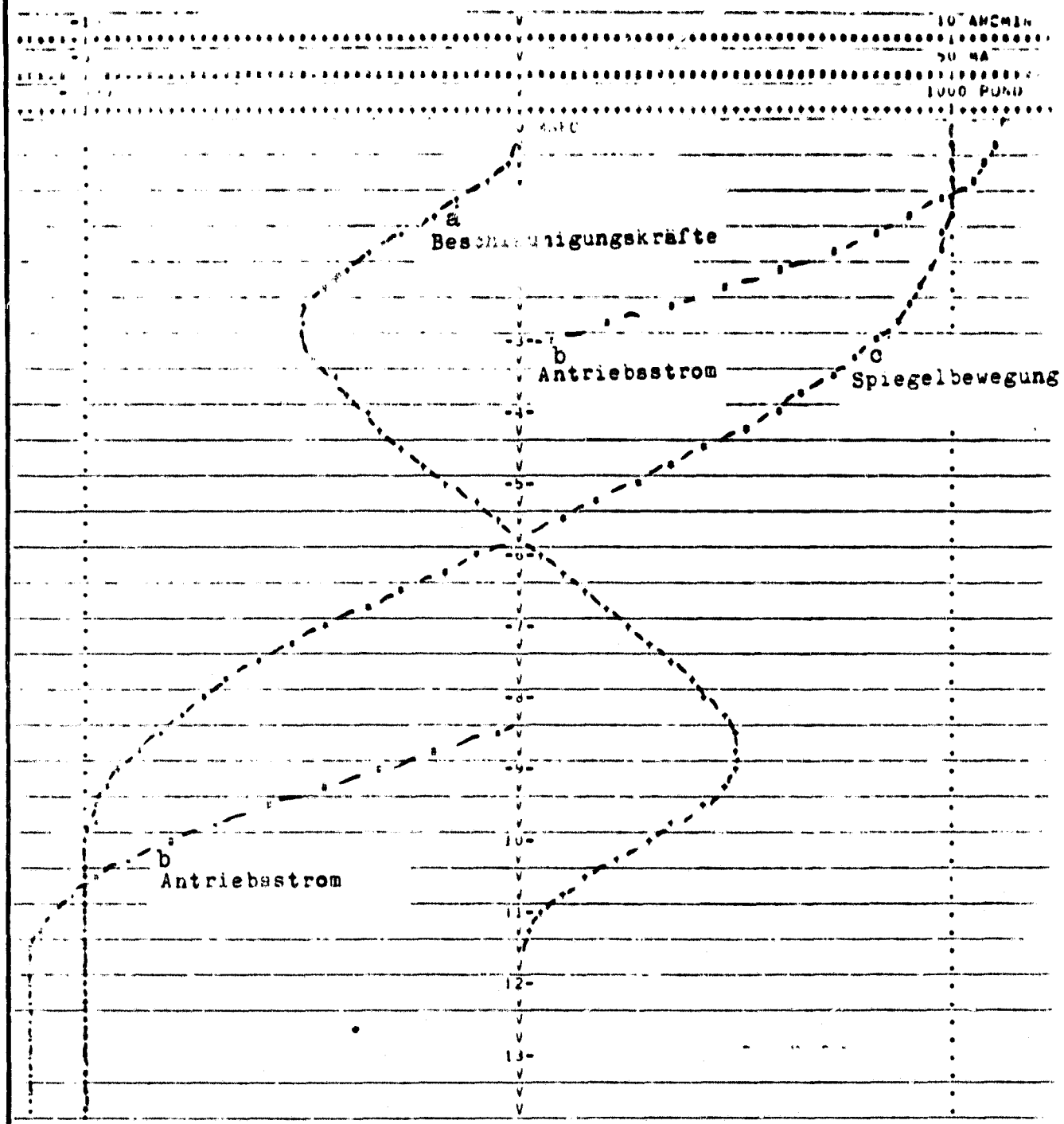

Figure 3050/13: Temporal course of the dynamic quantities in chopping (according to data of the MPI for astronomy in Heidelberg)

Key:
a. acceleration forces
b. driving current
c. mirror motion

The result in the previous work packages have shown that the two last drafts for the mounting satisfy the presently applicable system requirements. The second draft (Figure 3050/2) is the more simple one and would be preferable when the positive connections at cerodur mentioned in AP 3044 were already reliable. Since this cannot be guaranteed before conducting appropriate test series, a decision between draft 2 and 3 is not possible now, unless it was forced by deadlines. Both drafts are therefore being further developed into stages ready for detailing work. The heat conduction system was merely completed in draft 3.

Special constructive consideration is required by the assembly of collection mirror and counterbalance weight. The collection mirror must be assembled through the chopper, since it cannot be drilled. Resetting springs and path pick-ups, however, must still be adjustable after installation. After the assembly of the mirror unit, the chopper housing is completed with the counterbalance weight. This has several holes for assembly.

As can be seen from Figure 3050/14, the heat conductor busbars (compare Figure 3050/6) are positioned in the axis of rotation of the mirror and folded twice for reducing the torsion moment. They are /127
clamped between two insulating synthetic material jaws in guiding then through the leading edge of the chopper housing. While one strip leads to the tripod in a straight line, the other is led along the circumference of the housing at an angle of 60°, until it is led into the tripod. It will depend on the type of heat dissipation of the chopper, whether two legs are available for the mirror. If they are needed for the chopper, the slighter amount of heat of the mirror can also be dissipated in a single leg with the appropriate redesign of the conduction system.

The exact drawings of both collection mirror supports are not contained in this final report; they will be handed out separately if requested.

Open Problems

It can be stated in summary that the following studies must still be carried out in order to reach a decision on the type of collection mirror support:

1. The strength of the glass-metal combination in draft 3050/2.

2. The effect of soldering (or cementing) on the mirror surface.

3. In the case of a negative result of 1 or 2: strength of the circular glass ring in draft 3050/5, finishing technology.

4. Vibration behavior of the surface in a model test with exact mirror geometry in order to supplement the simplifying calculations.

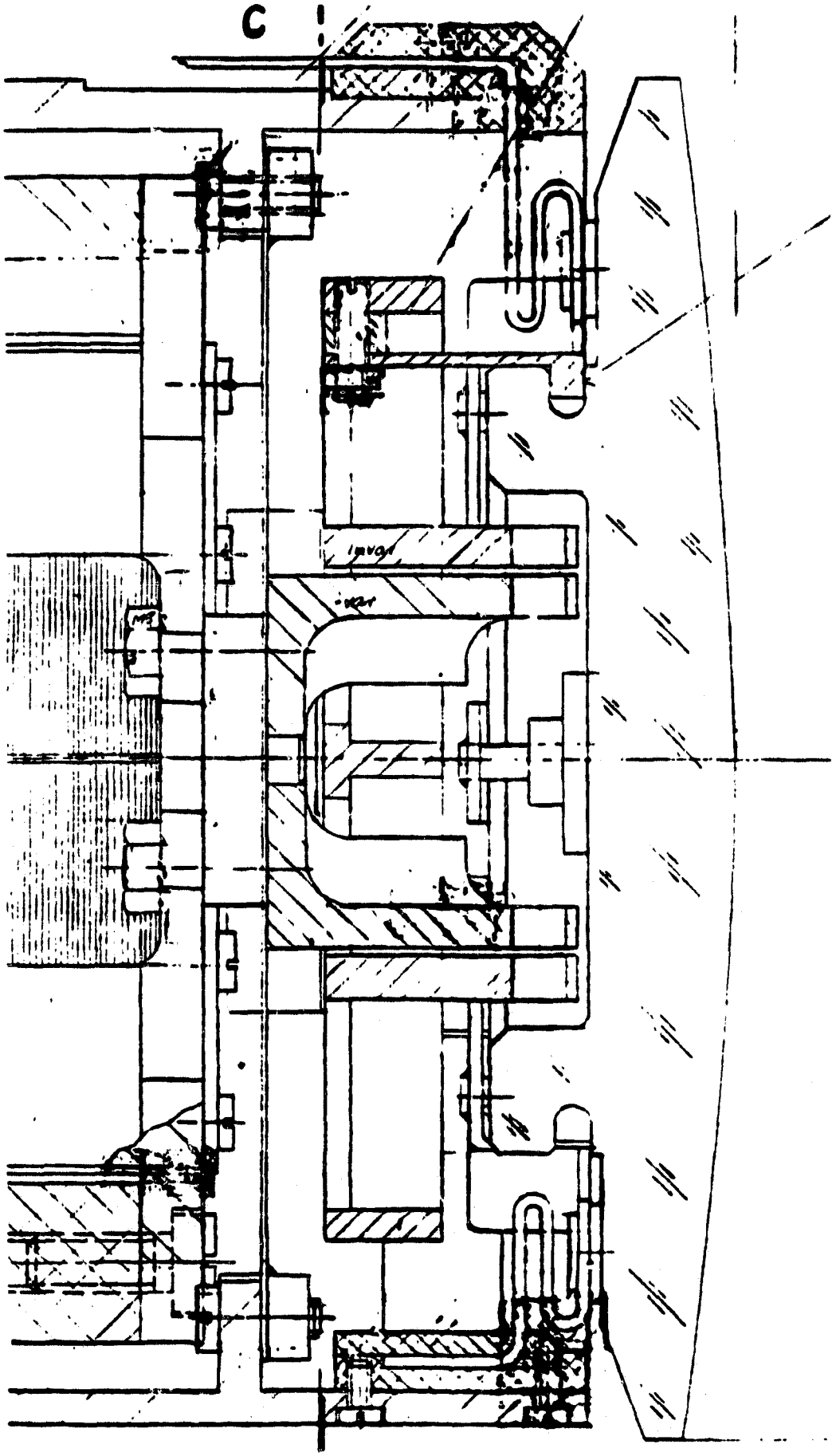

Figure 3050/14: On the construction of the heat conduction system in draft 3.

AP 3060
Three-Legged Tubular Structure /128

AP 3061 Natural Frequency Calculations

In phase A, several cross-sections of the tripod supports were already tested for rigidity and the natural frequencies of the system. In the meantime, new information has been gained on the leg cross-section. On the recommendation of BASC, the cross-section is to be that of an equal-sided triangle with one side facing the optical axis.

The model presented in Figure 3060/1 serves as calculation model. The supports divided into several nodes are connected at the foot points by joints, representing an adjustment device, to bending rods extending in the plane of the base plate and simulating a projection of these beyond the feet of the instrument platform. At the front end, the supports are rigidly connected to the copper housing. Short rods are located at the connection points in the direction to the main mirror, on the points of which the total mass of chopper and collection mirror is concentrated, so that it is situated in the plane of gravity of the system. In the nodal model, the rigid connections are applied in nodes no. 1, 2 and 3 or 19, 23 and 27, and the joints in the nodes no. 4, 9 and 14. The chopper mass is concentrated in the nodes no. 31, 32 and 33. The orientation of the coordinate system is such that the z axis is the optical axis and the x axis points to node no. 4.

The calculations produce the result that the vibrations are not limited to a defined coordinate, but rather that the movements are coupled with one another in several coordinates. The vibration forms also deviate from one another in the individual natural frequencies.

The first calculations were made with a leg cross-section in accordance with Figure 3060/1. Invar was chosen as the material and the modulus of elasticity was inserted in the calculation at 10 K. The sequence of the natural frequencies are listed in Table 3060/1. /130
In spite of the relatively large leg cross-section, the frequencies are still somewhat too low. The cause for this is the mass of copper and mirror including the counterbalance weight, increased in the meantime to 2.3 kp.

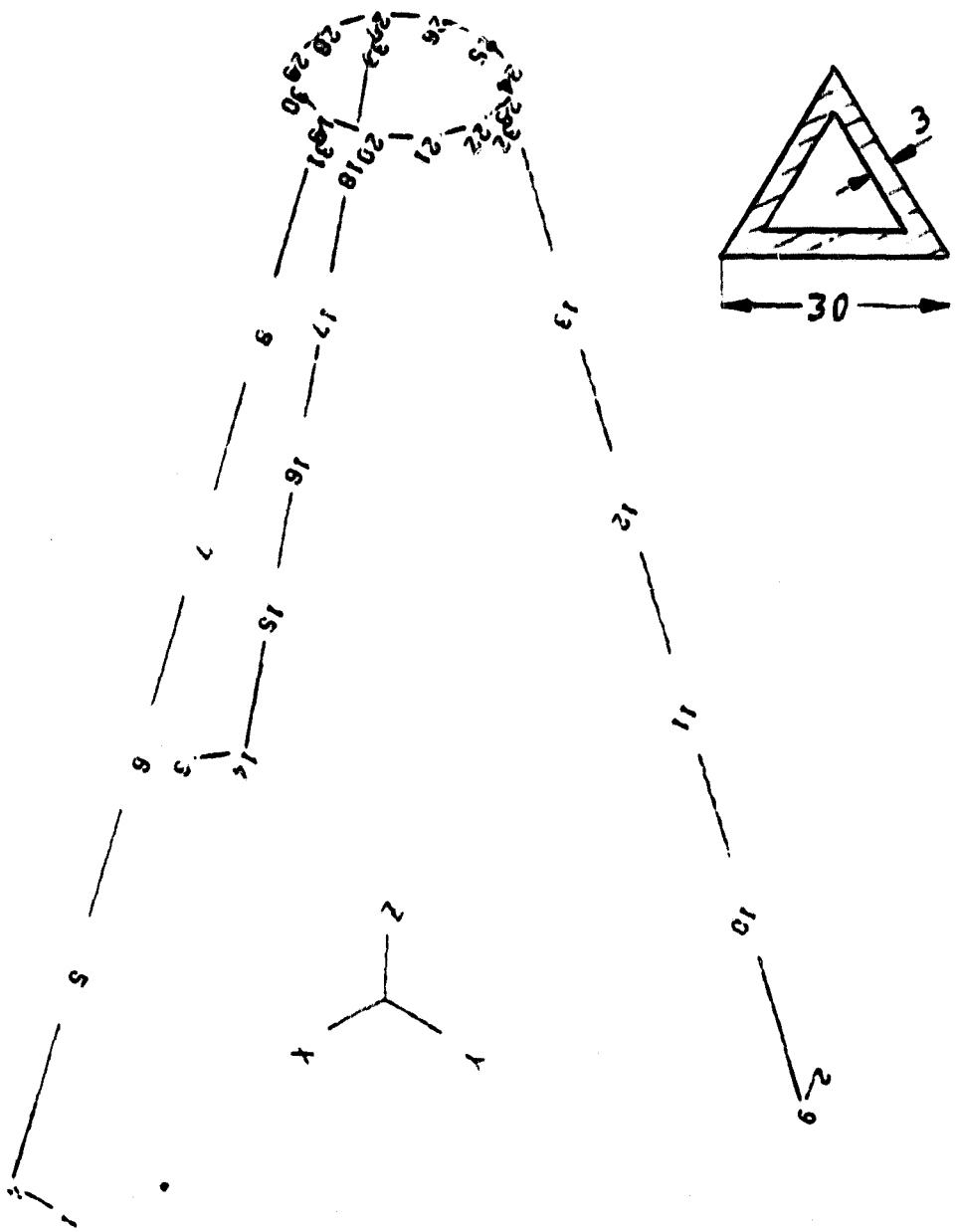

Figure 3060/1: Nodal model in perspective for the vibration calculations of the tripod for the collection mirror support.

***** EIGENVALUE (NATURAL FREQUENCY) SOLUTION

MODE	FREQUENCY (CYCLES/TIME)				
1	64.95545	21	890.5733	41	3021.971
2	64.95546	22	979.0269	42	3021.971
3	83.66511	23	979.0269	43	3311.158
4	154.2979	24	1053.112	44	3519.545
5	154.2980	25	1089.050	45	3519.554
6	160.2976	26	1089.050	46	4144.896
7	211.9139	27	1114.359	47	4144.896
8	211.9139	28	1394.865	48	4237.741
9	239.5610	29	1395.218	49	4299.446
10	365.0885	30	1395.218	50	4595.842
11	365.0886	31	1649.282	51	4797.835
12	452.5617	32	1685.382	52	4912.979
13	483.1053	33	1685.382	53	4912.980
14	483.1053	34	1732.060	54	5329.724
15	561.2592	35	1752.332	55	5445.232
16	573.1311	36	1752.332	56	5445.832
17	573.1312	37	2172.584	57	6008.635
18	732.8875	38	2172.586	58	7448.045
19	834.1587	39	2551.467		
20	834.1590	40	2558.555		

Table 3060/1: Sequence of the natural frequencies of the system collection mirror unit plus tripod.

The Figures 3060/2 show the different vibration pictures in the first seven natural frequencies of Table 3060/1. It can be seen that in the two first, virtually identical frequencies, the amplitudes stand almost perpendicular to one another, but essentially the chopper mass is vibrating. In the next four figures, the motion has passed almost completely to the supports. In Figure 3060/8, the vibration form is finally mixed and can be analyzed only with difficulty. The absolute value of the amplitudes depend on the degree of excitation and are also not comparable between the individual figures. /138

In order to raise the natural frequencies, the leg cross-section was increased for the second calculations. The cross-section was only increased at the foot of the support to 40 mm on a side of the triangle and left at 30 mm at the end of the mirror in order not to increase the mass of the collection mirror unit any more than necessary. Corresponding to the nodal model, the tapering was carried out toward the front in five steps. In practical situations, this would be continuous. The natural frequencies, resulting with this stiffening, are listed in Table 3060/2.

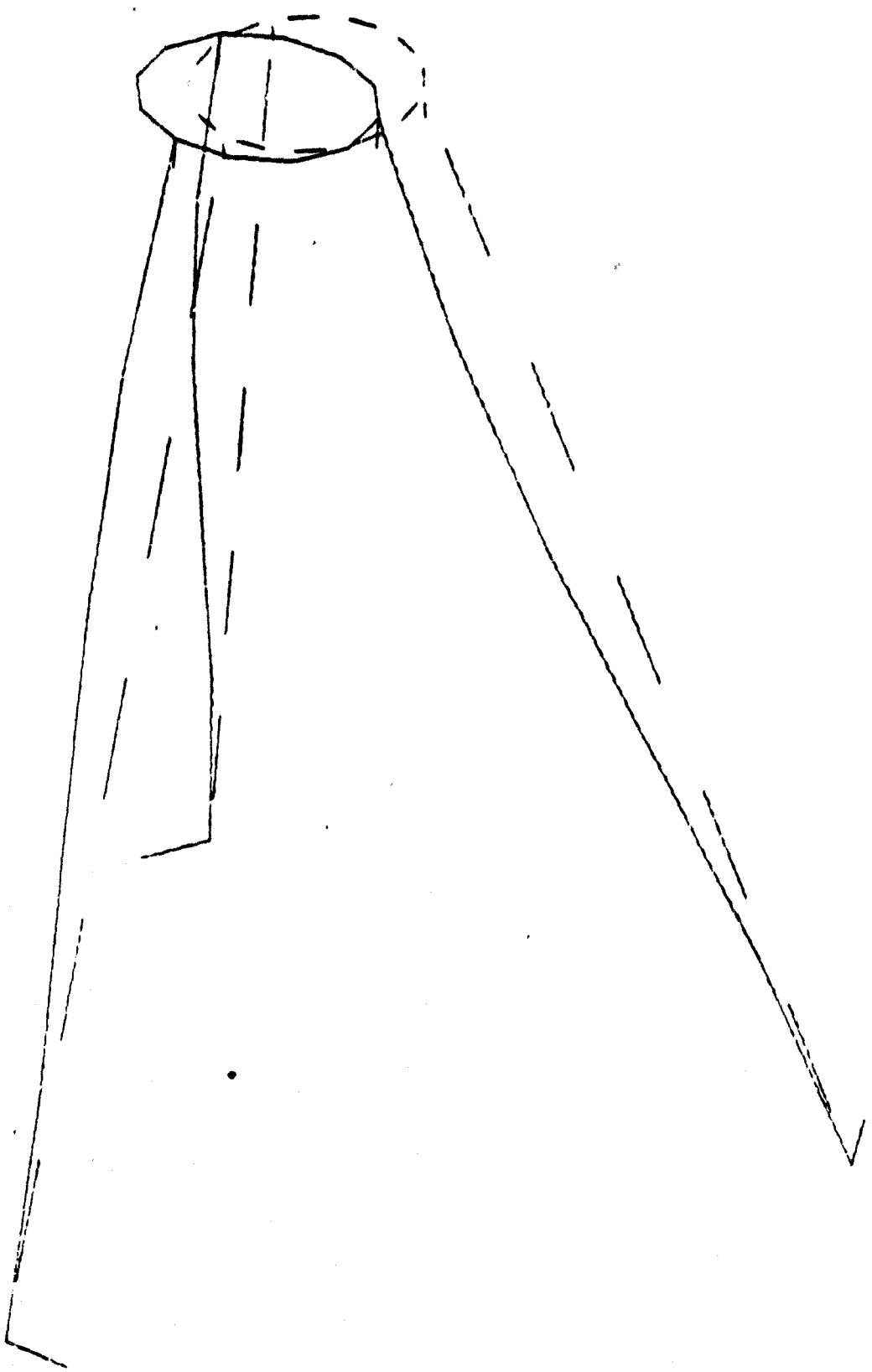

Figure 3060/2: Vibration picture of the tripod in the case of excitation at 64.95545 Hz.

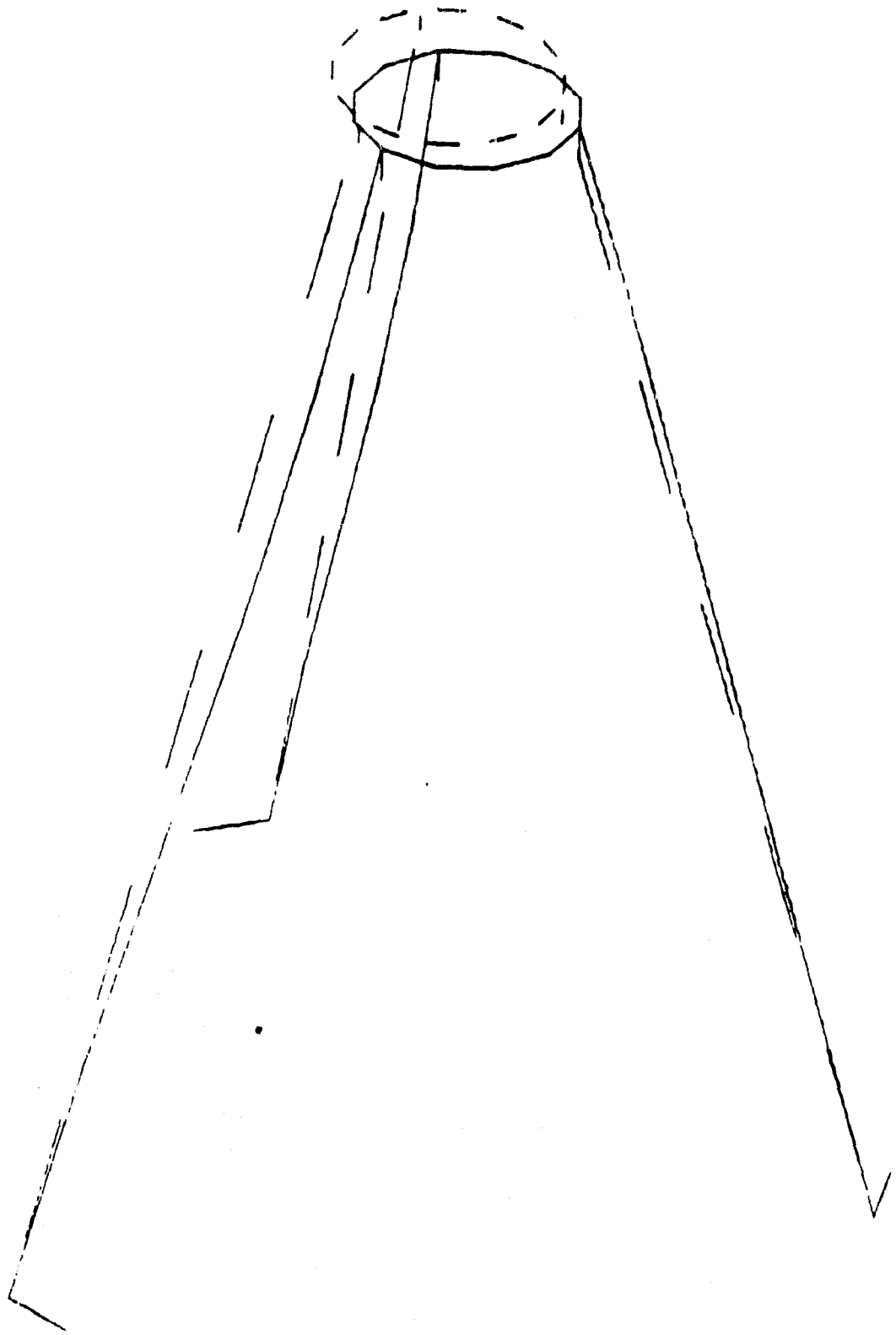

Figure 3060/3: Vibration picture of the tripod in the case of excitation at 64.95546 Hz.

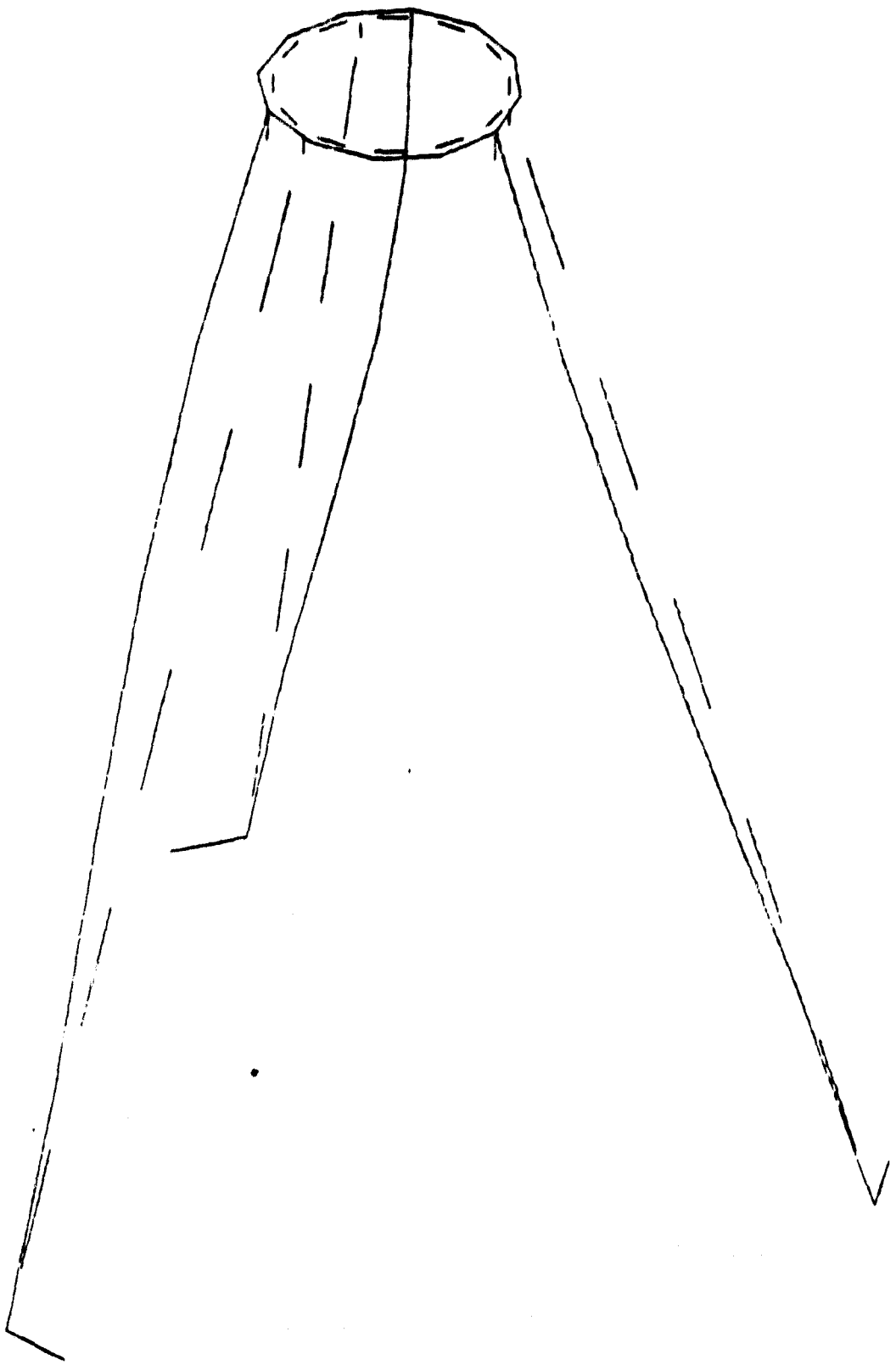

83,66511 Hz

Figure 3060/4: Vibration picture of the tripod in the case of excitation at 83.66511 Hz.

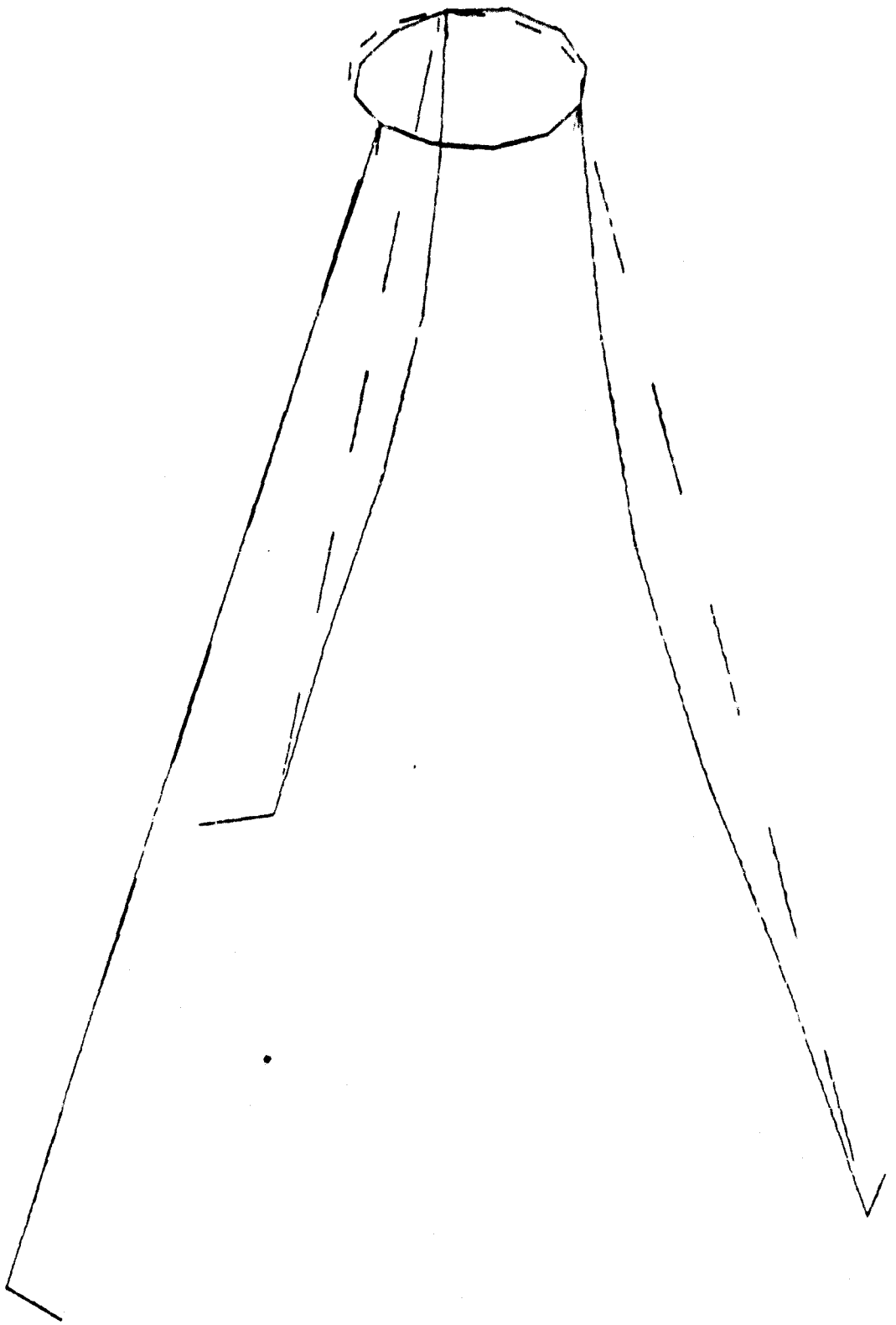

154.2979 Hz

Figure 3060/5: Vibration picture of the tripod in the case of excitation at 154.2979 Hz.

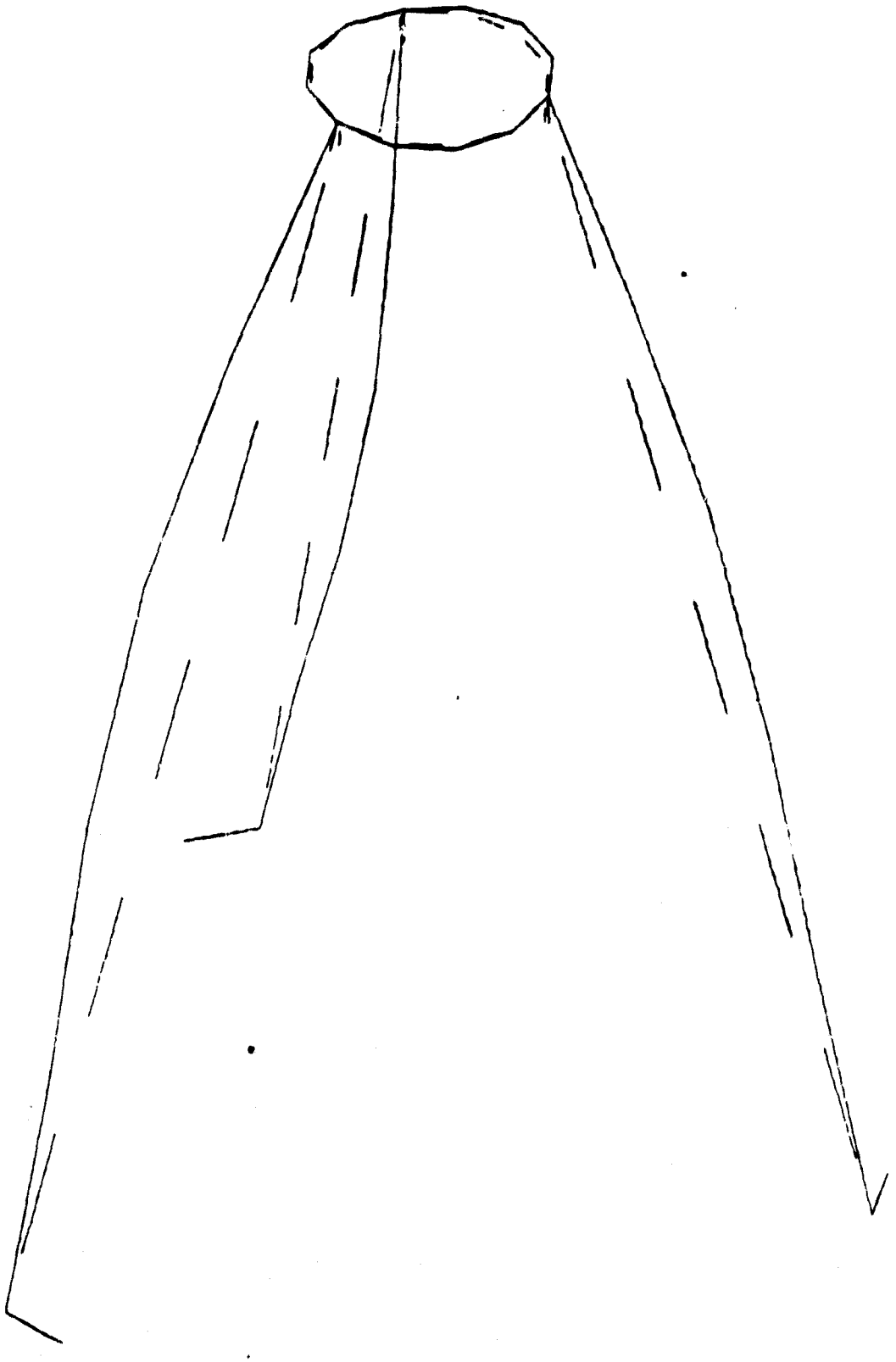

154,2980 Hz

Figure 3060/6: Vibration picture of the tripod in the case of excitation at 154,2980 Hz.

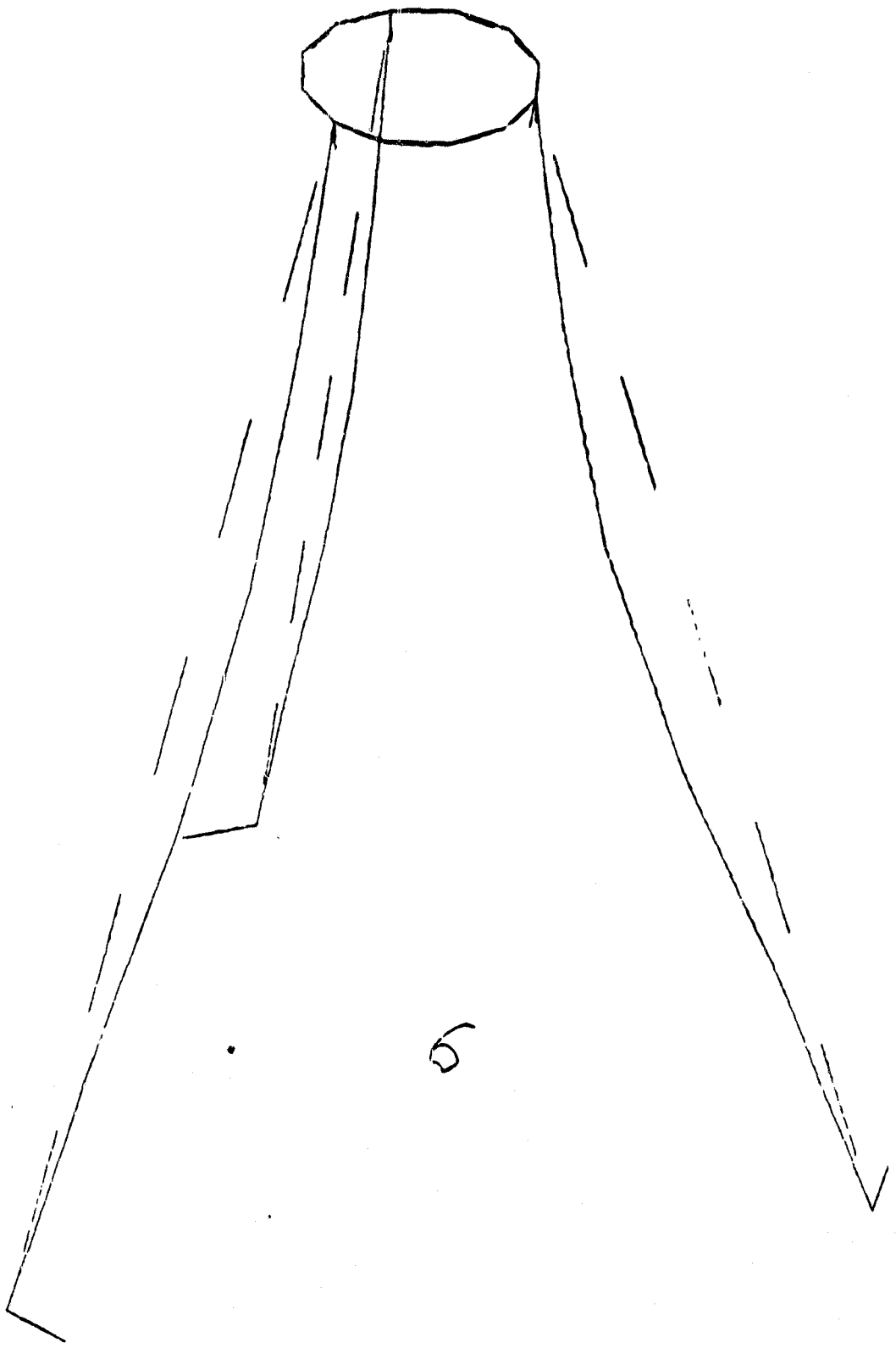

160,2976 Hz

Figure 3060/7: Vibration picture of the tripod in the case of excitation at 160.2976 Hz.

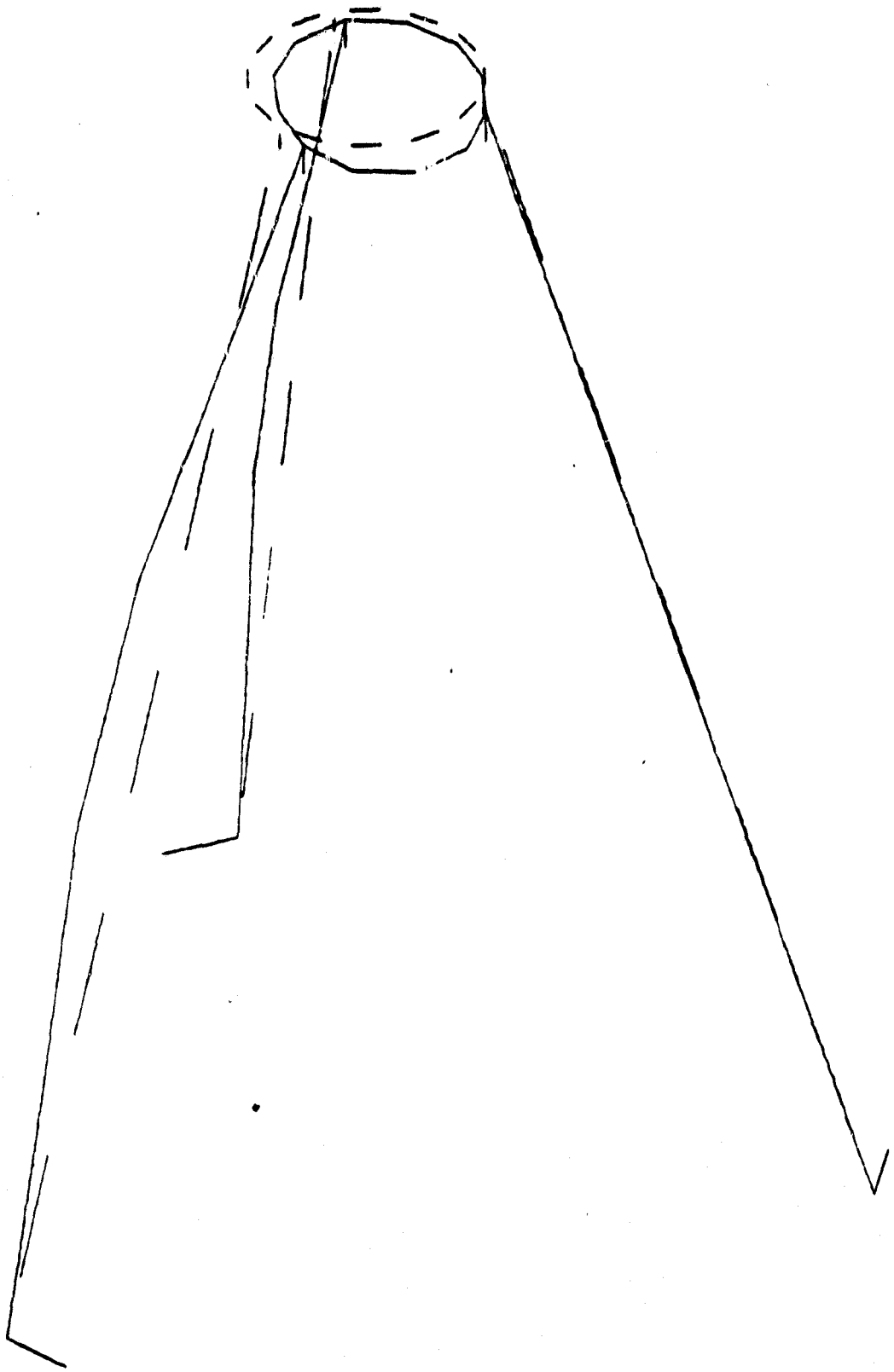

211,9139 Hz

Figure 3060/8: Vibration picture of the tripod in the case of excitation at 211.9139 Hz.

MODE	FREQUENCY (CYCLES/TIME)				
1	76.85141	21	982.2662	41	2973.726
2	76.85142	22	1121.821	42	2973.726
3	101.4233	23	1121.821	43	3274.370
4	186.2001	24	1223.176	44	3567.326
5	186.2001	25	1247.976	45	3567.335
6	193.7134	26	1256.771	46	4145.365
7	249.5642	27	1256.771	47	4145.370
8	249.5642	28	1457.296	48	4244.901
9	280.8551	29	1501.596	49	4606.796
10	395.2548	30	1501.596	50	4606.796
11	395.2548	31	1907.584	51	4622.715
12	527.3196	32	1913.226	52	4851.756
13	568.1340	33	1913.221	53	4851.760
14	568.1340	34	2014.237	54	5273.117
15	663.4794	35	2026.359	55	5724.252
16	664.5738	36	2026.359	56	5724.252
17	664.5738	37	2254.556	57	5940.209
18	783.2576	38	2254.560	58	7546.096
19	914.1714	39	2578.930	59	7546.096
20	914.1715	40	2609.459	60	[illegible]

Table 3060/2: Sequence of the natural frequencies of the tripod after improved cross-section of the supports.

The lowest frequency is already close to the predetermined lower limit value of 80 Hz at 77 Hz. The last fine details of the calculation are to be prepared after the final collection mirror diameter and the final baffle weight are ascertained.

AP 3062 Optimizing the Heat Conductors /139

It was explained in AP 3052 that the decisive transition resistance for the collection mirror cooling is the copper-cerodur contact. It amounts to a multiple of ten of the heat transition resistance of the 120 mm long, 2.5^2 thick litz wire of electrolytic copper. A resistance of 36.4 KW^{-1} resulted for the approx. 800 mm long copper strips, running inside the supports of the tripod, when the strip consists of Cu 99.999% and has a cross-section of 20 x 0.5 mm^2. Even with only one such strip, the total heat loss of 34 mW at a temperature difference of 1.2 K at the strip ends could therefore be dissipated. There are, however, three supports available for accommodating

three strips with a thickness, which could moreover be doubled without difficulty. The necessity of optimizing therefore is not actually present. The strips could be led to the outside by appropriate slits in one of the three walls of the support. While the lower strip surface for screwing would lie directly on the instrument platform, a seam would have to be created between support and collection mirror unit.

AP 3063 Three-legged Construction, Adjustment, Focusing

The connection of the tripod to the base structure of aluminum involves similar problems as the assembly of the main mirror. Because of the large differences in expansion, single hole attachments must be resorted to. It seemed reasonable to employ these for purposes of adjustment and it proved advantageous. The strips to be welded of invar with a triangular cross-section tapering to the front aimed at the bottom in a terminal plate with an adjustable screw connection to a counter plate. In the screwed plate there is a bolt of steel with low heat expansion, simultaneously providing a possibility for vertical adjustments. The two spherical discs at the lower end of /141
the bolt consist of invar for adaptation to the higher heat expansion of the basic aluminum body.

All experiments must be adjustable or the plane mirrors situated in front of them and independent of one another for the adjustment of the telescope with respect to the Cassegrain focusing. If this adjustment was undertaken with the telescope, it could be done for only one of the experiments. The focus of all other experiments would have to correlate with the focus of this one. Since this cannot be expected, an adjustability of the other experiments would be necessary in any case.

The collection mirror can be adjusted with the three adjustment sleeves shown in Figure 3060/9 in distance and angle to the main mirror. In this case, however, an off-set of the axis during tipping is unavoidable. It must be compensated by shifting the entire tripod in the opposite direction. The slip surfaces on the lower terminal plates of the supports serve for this purpose. After conclusion of the adjustments, the slip surfaces are cotter-pinned to one another. In order to facilitate the simultaneous shift of all three supports, an auxiliary ring can be mounted at the feet of the tripod, also fixating the feet to one another by the appropriate rigidity in the release state.

The adjustment possibilities serve the subsequent precise adjustment by means of controlling the defraction image of an artificial star. They can probably be undertaken only under heat. They must be preceeded in any case by a rough adjustment with alignment telescope and collimator, guaranteeing by appropriate adjustment measures that all continuous adjustment devices are initially situated at the center of their adjustment range.

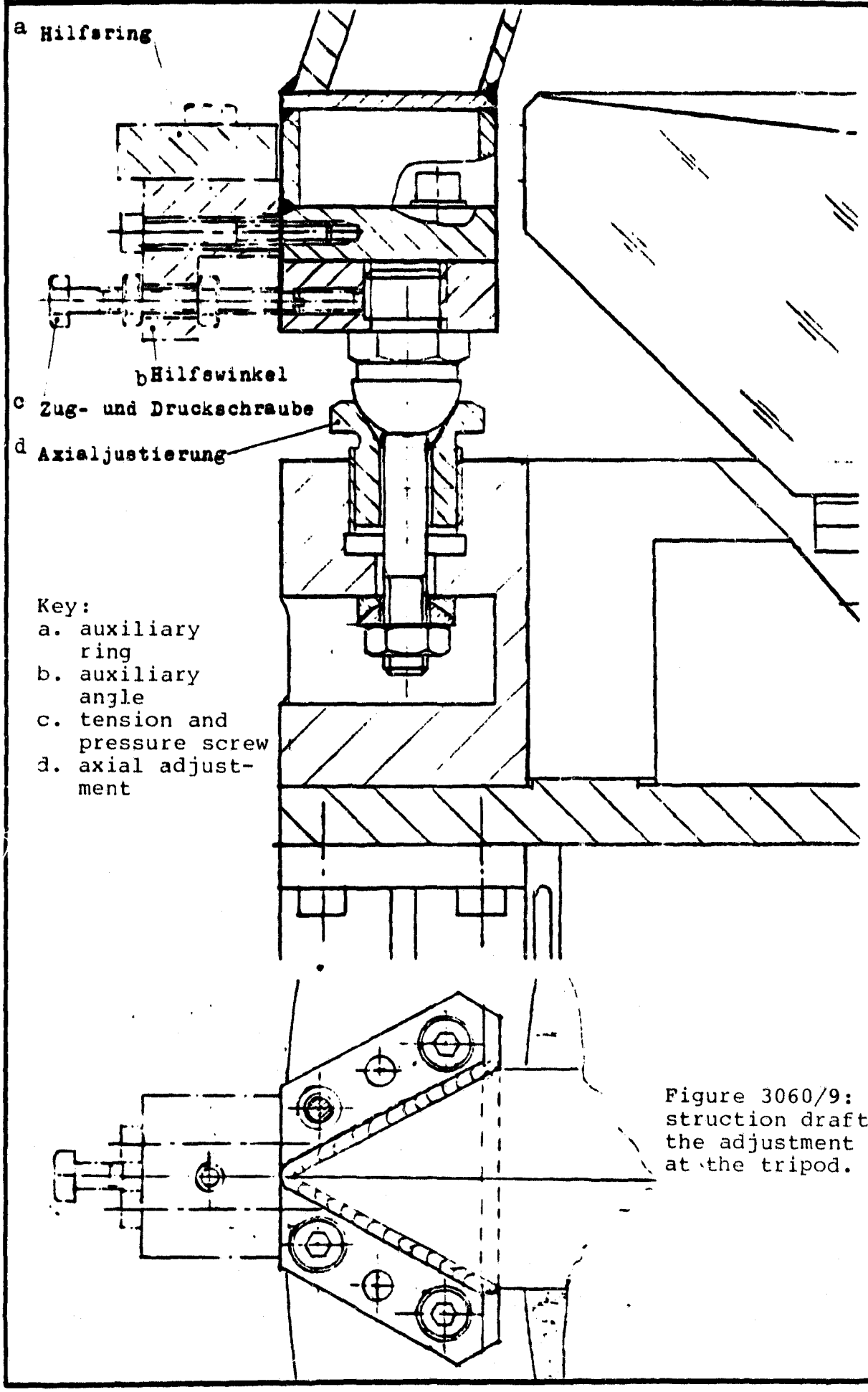

Key:
a. auxiliary ring
b. auxiliary angle
c. tension and pressure screw
d. axial adjustment

Figure 3060/9: Construction draft for the adjustment device at the tripod.

Reference system of each adjustment should be the main mirror axis and the top of the main mirror, after both have been roughly adjusted for the experiment with the least shift possibility. It will still have to be tested in this connection to what degree the main mirror is reversibly fixed to this experiment focus after cooling and start load simulation.

Focusing /142

In order to make focusing after cooling superfluous, the following requirement must be fulfilled in principle:

$$\Delta g = -(m^2-1)\,\Delta e \quad [1]$$

This means that when the focus distance g of the experiment E1 is reduced by Δg from the top of the main mirror (see Figure 3060/10) by contraction of the aluminum structure, the top distance Δe between the mirrors must be increased by 1/24 of Δg (where m = the enlargement factor of the telescope = 5). This requirement can only be fulfilled when the supports of the tripod are manufactured of invar and not of titanium, contrary to the concept up to now. Moreover, it is necessary that it be lowered to the base plate of the main mirror without intermediate aluminum parts. In order to attain the largest possible construction length h for over compensating the invar shrinkage in cooling, the supports should be mounted as far as possible to the front of the chopper housing. An appropriate synthetic material compensator and must still be inserted. The presently known dimensions and their temperature alterations are given in Table 3060/3 in the left-hand portion. In cooling from 293 K to 10 K, the result is

$\alpha_{Alu} = 4{,}12/\mu m/mm$, $\alpha_{Invar} = 0{,}36/\mu m/mm$, $\alpha_{Voltalef} = 11{,}0/\mu m/mm$

$\alpha_{Zerodur} = -0{,}06/\mu m/mm$ $\qquad (\alpha = (l_{293} - l_{10})/l)$

$$\Delta e = 64{,}5/\mu m.$$

---

[1] The alteration in focal length of the mirror, caused by cooling by $\Delta f_1 = 0.49$ µm or $\Delta f_2 = 0.16$ µm is not taken into account here because it is so slight.

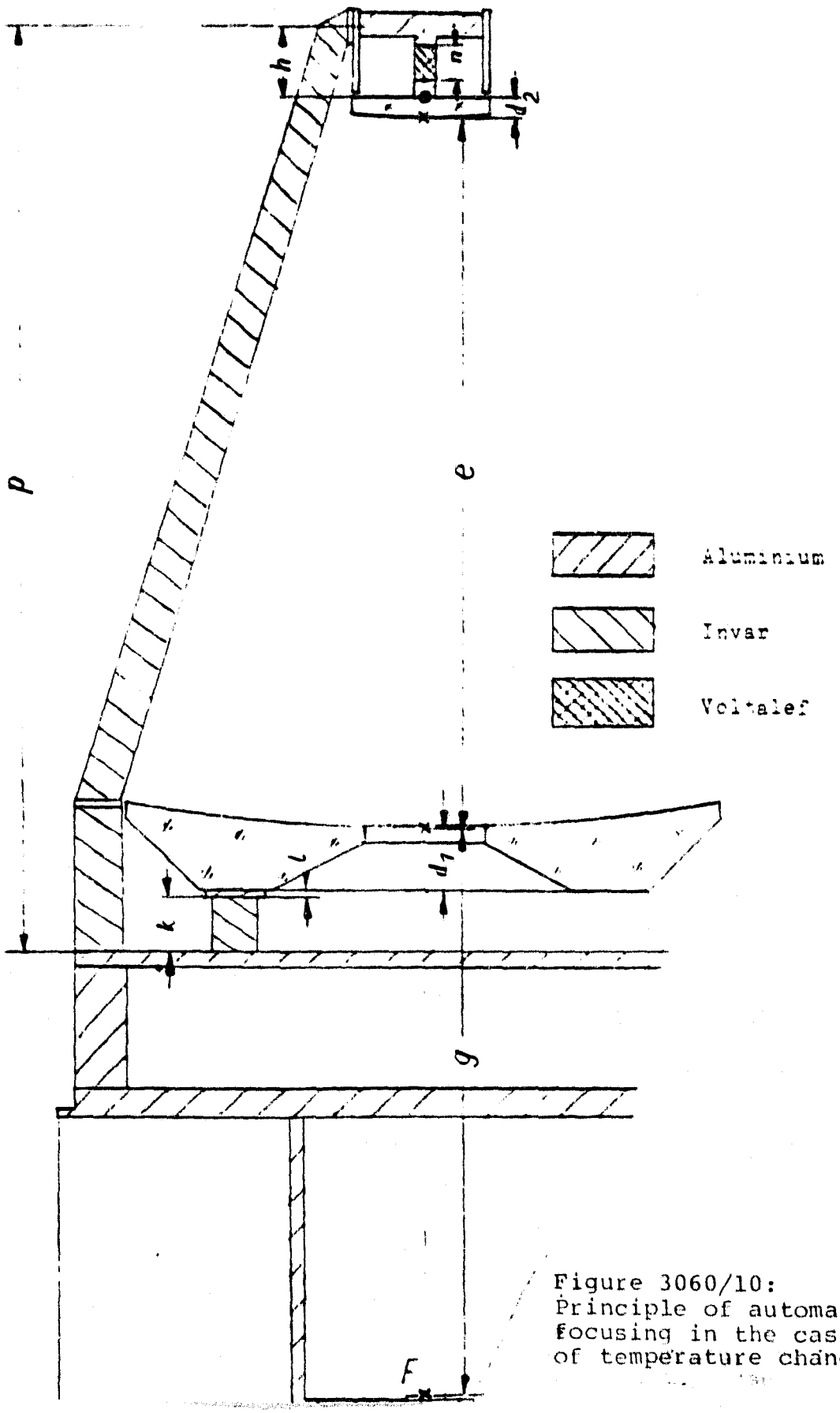

Figure 3060/10:
Principle of automatic focusing in the case of temperature change.

As a condition for the determination of h (and n), it results that: /144

$$h = \frac{\alpha_{Inv}(e+d_1+d_2+l\ ) - \alpha_{Volt}\, n + \alpha_{Alu}(n-l) - \alpha_{Zer}\,(d_1+d_2) + \Delta e}{\alpha_{Alu} - \alpha_{Inv}}$$

When n = 0 is first inserted, the result with the dimensions from Table 3060/3:

$h = 80.3$ mm and $p - k = 746.3$ mm

	d_1	l	k	$g-(\beta_1+l+k)$	g	d_2	n	h-n	p-k
	Material	Zer.	Alu	Inv	Alu		Zer	Vol	Alu	Inv
a	Länge gemäß Konstr.-Stadium vom 25. 5. 80	55	1,5	53	370,5	(480)	11,5	0 10 20	80,3 52,0 23,8	746,3 728,0 709,8
b	Längenänderung bei Abkühlung von 293 auf 10K in /um	+3,3	-6,2	-19,1	-1526,5	-1548,5	+0,7	0	331	268,7

Table 3060/3: Compilation of the data important for automatic focusing.

Key:
a. length according to the stage of construction of May 25, 1980
b. alteration in length during cool-down from 293 to 10 K in µm

When n = 10 or n = 20 mm is arbitrarily assumed, the reductions in structural height of the chopper given in the table are obtained.

Disruption in Focusing /145

When the above-given coefficients of expansion deviate by 2%, the shifts in focus given separately in Table 3060/4 for the telescope space and for the experiment space result. In the most unfavorable case, both amounts may be added to one another. Moreover, an addition of the different material effects is possible. Even assuming this worst case, however, defocusing would amount to only 0.3039 mm.

a Störungsursache	$\Delta\alpha_{Alu}$	$\Delta\alpha_{Inv}$	$\Delta\alpha_{Volt}$	$\Delta\alpha_{Zer}$
b Störung hinter dem S1-Scheitel	29,8	0,4	0	0,1
c Störung vor dem S1-Scheitel, bezogen auf Fokus	45,6	122	105,6	0,4
d Gesamtstörung im ungünstigsten Fall	75,4	122,4	105,6	0,5

Table 3060/4: Defocusing in m in the case of deviation of the coefficients of expansion by 2% of the expected value in the most unfavorable direction in each case.

Key:
a. cause of trouble
b. disturbance behind the S1 vortex
c. disturbance in front of the S1 vortex in relation to focus
d. total disturbance in the most unfavorable case

An increase in temperature of all three legs from 10 K to 50 K produces defocusing of 72 µm with a coefficient of expansion of -8.5×10^{-7} (Dilavar Ni. 36). When voltalef compensator with a length of 20 mm and a temperature of 25 K, is subjected to an alteration temperature of 5 K, the focusing is approx. 60 µm with a coefficient of expansion of 2.5×10^{-5} K^{-1}. Finally, when the aluminum structure in the chopper is heated from 10 K to 50 K, this results in defocusing of only 0.2 µm with $\alpha = 7 \times 10^{-8}$ K^{-1}.

Considering the aspect of thermal expansion, automatic focusing /146
would therefore be possible by suitable dimensioning of the participating structural elements with sufficient accuracy. Even a slight scattering of material data, a certain amount of heating through irradiation or chopper operation would have tolerable effects. It is uncertain, however, how large the possible irreversible portions of initial loads or thermal shaping are. The optical control of the shake model before and after vibration resulted neither in a representative or a positive statement on this question. The behavior of the improved shake model will not be decisive. Similar control measurements as there would also be desirable in the thermal model. In both cases, they would also be an important supplement for the evaluation of the constancy of the adjustment state (compare on this subject appendix 1).

Cassegrain Baffle

In order to gain an idea on the simplest form of a Cassegrain baffle, a standard baffle was calculated with the aid of an optimizing program, providing minimum shading. The dimensions can be seen in Figure 3060/11.

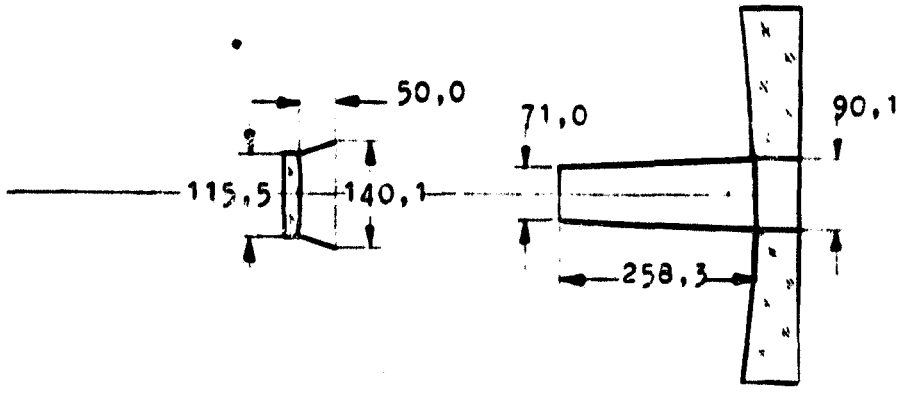

Figure 3060/11: Dimensions of a standard Cassegrain baffle.

AP 3070
The Preparation of the Thermal Model /147

The thermal model of the telescope consists essentially in the mounted main mirror provided with the heat transfer system. The collection mirror is not contained in the model. The supports of the tripodare simulated by short rods with a heat resistor mounted on a copper plate at the front ends. The resistors of the screw-on type DALE, 330 ohm, 5 W, almost independent of temperature, serve to introduce the power loss of the chopper. Between the copper plate and the instrument platform (IP), provided by the Dornier system, the thermal connection is established by a copper strip with a length of 207 mm and a cross-section of 10 x 1 mm^2. This corresponds to the conductivity of the subsequent original strip of 100 mm length and 30 x 1 mm^2 cross-section. All conductor strips consist in 99.99% copper from the production of Carl Schreiber GmbH, Neunkirchen.

The thermal model is mounted on a greatly simplified base plate of AlMg5 with a thickness of 15 mm with a rolling direction positioned parallel to that of the IP in agreement with the Dornier system. The original component groups, according to Figure 3030/16 have been employed for mounting the main mirror. Figure 3070/1 shows the rear view of the mirror with the heat conduction system and 11 temperature sensors, produced by the Linde Company according to Zeiss data. The 42 heat contacts (distribution see Figure 3040/11) were soldered as shown in Figure 3040/20. During handling, however, 7 conductors

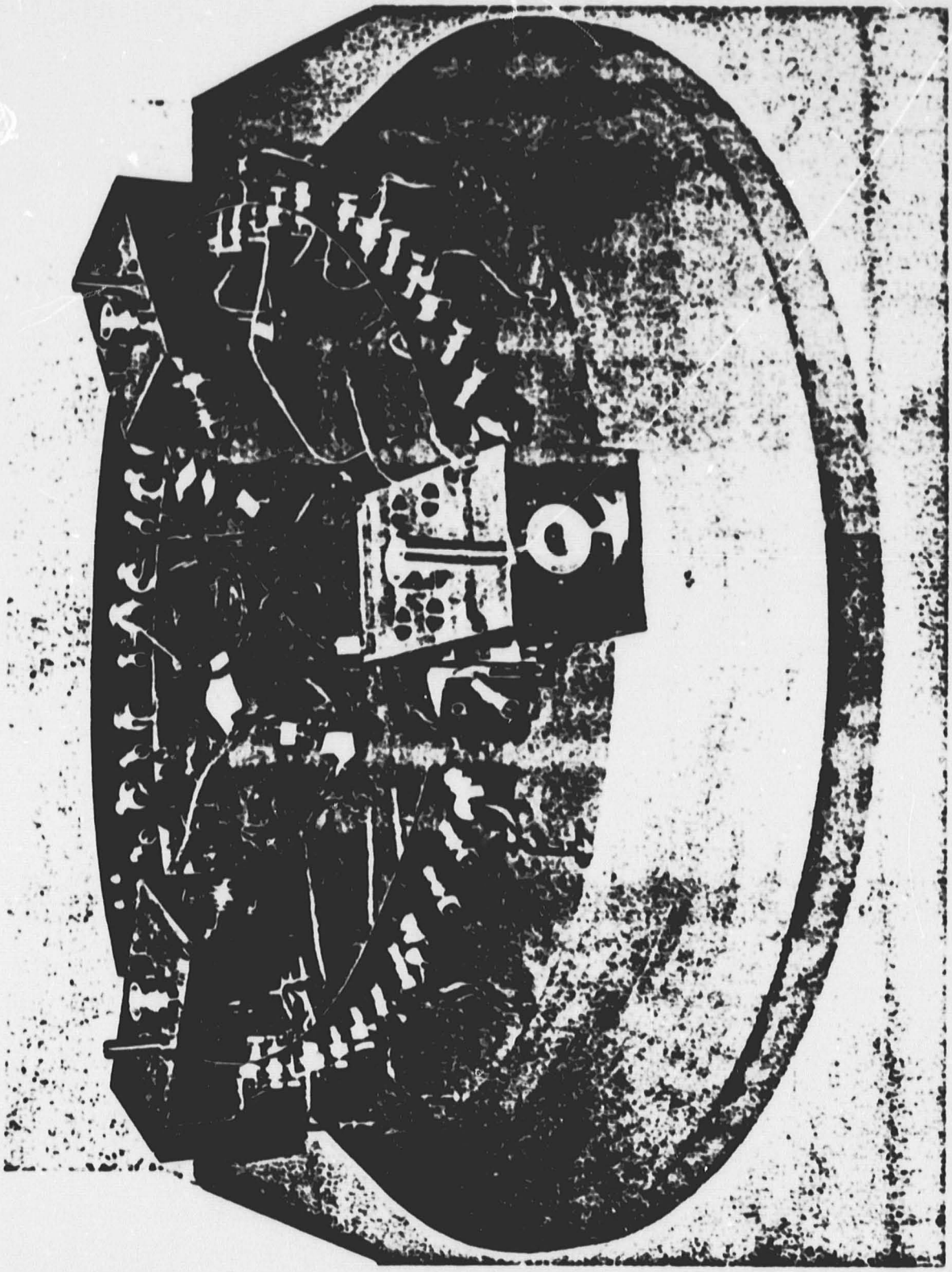

Figure 3070/1: Rear view of the main mirror thermal model.

ORIGINAL PAGE IS
OF POOR QUALITY

a Kleber	b Material, Maße	d Ergebnis
Stycast 1266	Aluminium, 17Ø	e nach 1x Kühlen bei Zugkraft 500g Ausriß großer Zerodur-Scherben
Deltabond 155	Aluminium, 17Ø	f nach 1x Kühlen abgefallen, Kleber zu 100% am Metall
General Electric 7031	Aluminium, 17Ø	g während der 1. Kühlung abgefallen, Kleber auf beide Flächen verteilt
Stycast 1266	c Titan 99,4%, 17Ø	h nach 5x Kühlen (93% der Gesamtkontraktion des Ti) bei Zugkraft 11kp nicht abgerissen, Risse jedoch sichtbar

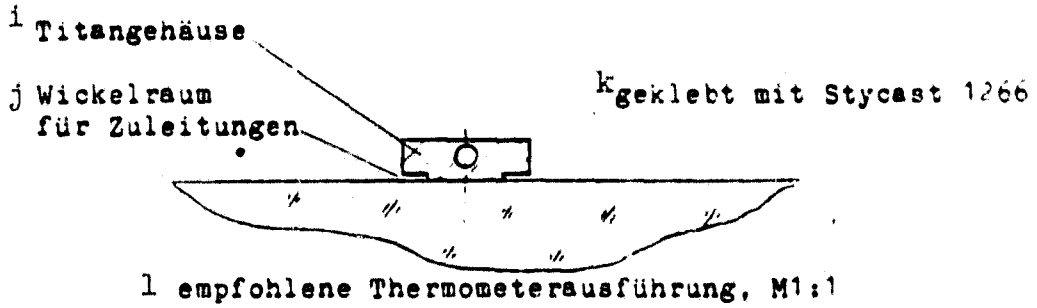

l empfohlene Thermometerausführung, M1:1

Figure 3070/2: Cementing tests of cerodur and metal for attaching the measurement sensors at the thermal model. Cooling with liquid N_2 to 78 K.

(Please see following page for Key.)

separated from the mirror again. Repeated soldering was not possible, since the baking silver had been destroyed. These contacts were cemented. They are not situated in the direct vicinity of the thermometer.

The cement contact of the temperature measurement sensor at cerodur was problematical. The durability was tested in preliminary trials with the adhesives Stycast 1266, Deltabond 155 and General Electric 7031 (see Figure 3070/2). According to these tests, aluminum housing proved unusable, so that titanium housing with reduced cement surfaces was recommended. The free space created in this manner was /150
successfully utilized for accommodating the thermometer lines for the purpose of heat contact with a mirror (see Figure 3070/2). The windings were cemented with low temperature varnish from General Electric 7031.

The arrangement of thermometers and heaters as well as the plug connections for their connection can be seen in Figure 3070/3. The thermometers designated with simple numbers are directly connected to the plugs with 0.2 mm thick manganin wires, as are the heaters H1-H3. The distribution of the connections to the two 25-pole and the 37-pole plugs can be seen in Table 3070/1.

Key for Figure 3070/2:

a. adhesive
b. dimension
c. titanium
d. result
e. after one cool-down with a tensile force of 500 g, tearing away of large pieces of cerodur
f. after one cool-down, fell off, adhesive is completely on metal
g. fell off during the first cool-down, adhesive distributed on both surfaces
h. after cooling 5 times (93% of the total contraction of the TI) not ripped off with a tensile force of 11 kp, but cracks are visible
i. titanium housing
j. winding space for lines
k. cemented with Stycast 1266
l. recommended thermometer design, M1:1

Thermometer Nr.	[a] Kohlewiderstand Nr.	[b] Stecker-Pin Nr.		
T 1201	3221	1 + 2,	20 + 21	
T 1202	3220	3 + 4,	22 + 23	
T 1203	3224	5 + 6,	24 + 25	
T 1204	3222	7 + 8,	26 + 27	St 1
T 1205	3223	9 + 10,	28 + 29	
T 1206	3217	11 + 12,	30 + 31	
T 1207	3216	13 + 14,	32 + 33	
T 1208	3214	7 + 8,	20 + 21	
T 1209	3219	5 + 6,	18 + 19	
T 1210	3218	3 + 4,	16 + 17	St 2
T 1211	3215	1 + 2,	14 + 15	
T 1212	3198	9 + 10,	22 + 23	
T 1213	3199	11 + 12,	24 + 25	

[c] Heizer Nr.			
H 1	1 + 2,	14 + 15	
H 2	3 + 4,	16 + 17	St 3
H 3	5 + 6,	18 + 19	

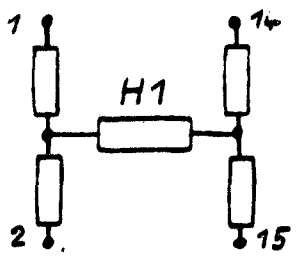

Table 3070/1: Plug wiring at the main mirror thermal model.

Key:
a. carbon resistor no.
b. plug pin no.
c. heater no.

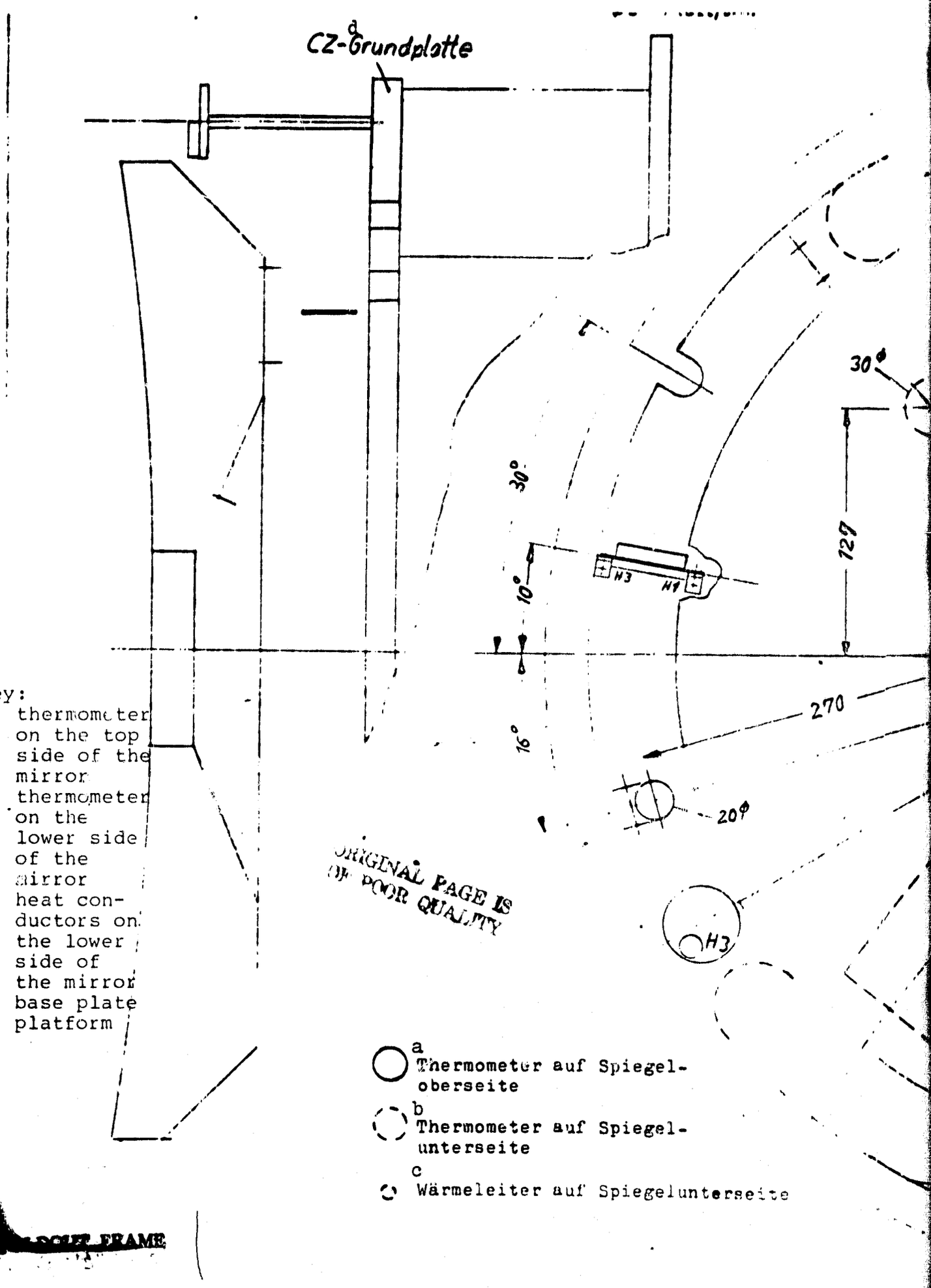

Key:
a. thermometer on the top side of the mirror
b. thermometer on the lower side of the mirror
c. heat conductors on the lower side of the mirror
d. base plate
e. platform

a
Thermometer auf Spiegeloberseite

b
Thermometer auf Spiegelunterseite

c
Wärmeleiter auf Spiegelunterseite

ORIGINAL PAGE IS
OF POOR QUALITY

POOR FRAME

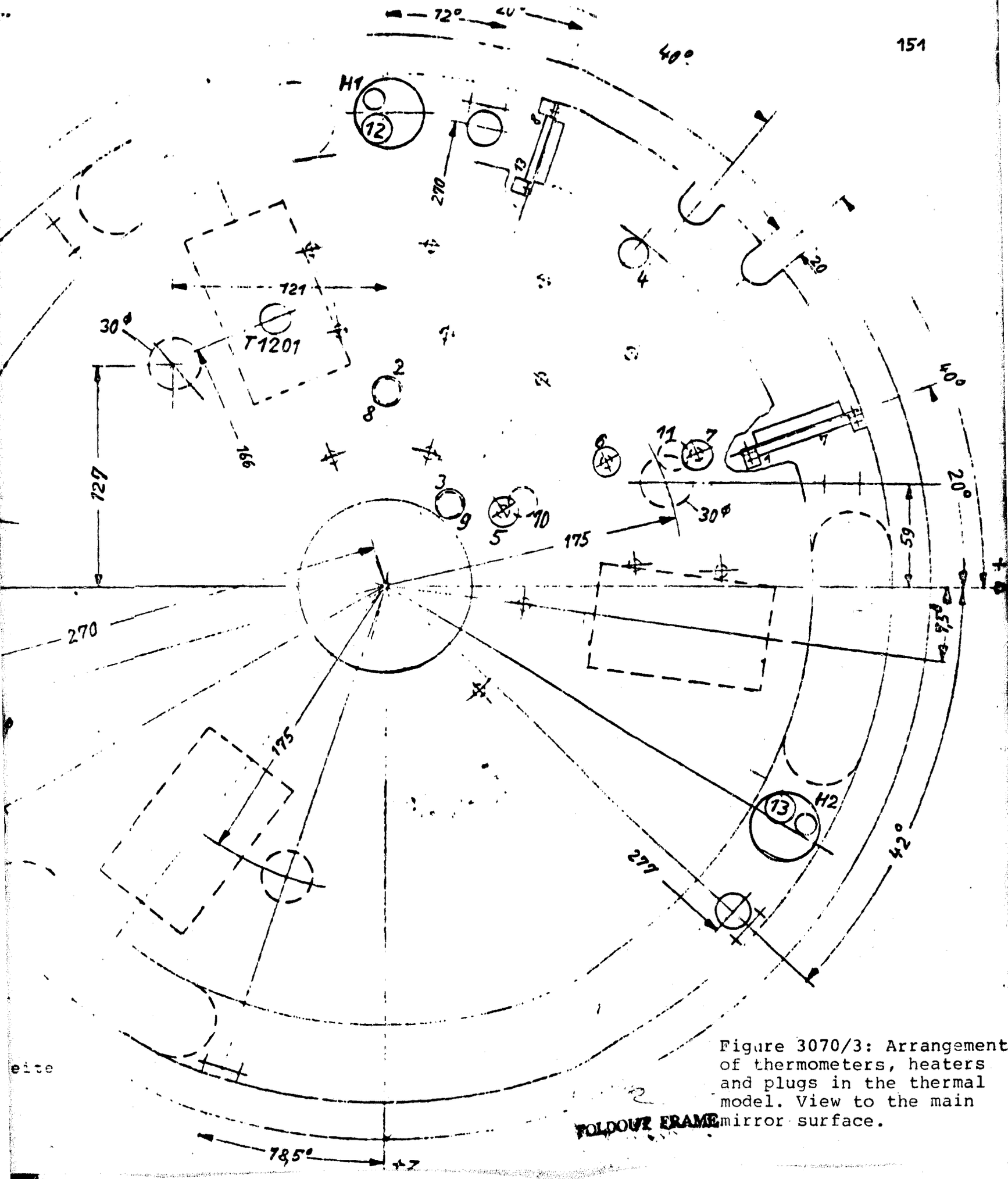

Figure 3070/3: Arrangement of thermometers, heaters and plugs in the thermal model. View to the main mirror surface.

AP 3090
Optical Testing of the Telescope and its Components /152

AP 3091 Measurement Methods for Wave Front and Stray Light at the Cooled Main Mirror

A procedure of laser interferometry has been employed for many years at Karl Zeiss for testing hollow mirrors with the advantage of determining the ascertained defect in the test sample both in amount and direction and also according to the location at which they occur on the test sample. In this testing procedure a Twyman interferometer assists in comparing the test sample with a smooth comparison standard, usually smaller in size. Since the lengths of both radiation passages in the branches of the interferometer are often very different, it is necessary to employ a laser as light source because of its large coherence length.

Figure 3090/1 shows the center of a test interferometer, in principle, for concave mirrors. The laser beam is projected with a microscope objective on a very small aperture. This aperture functions as artificial star. Behind the aperture a second, larger objective is located, again making the beam parallel. Both objectives taken together act as cross-section expanders of the laser beam. The expanded beam is now divided into two components in a beam divider, generally consisting in a partially mirrored plate with optimally demirrored rear surface. The reflected component is mirrored on the comparison standard and reaches the camera through the divider plate. The component passing through is collected by a further objective, usually termed diverger, in the curvature center point of the test sample.

In the simplest case, the test sample consists in a spherical mirror. In the ideal case, all partial beams, originating from the curvature center point then come back into this. They are then made parallel once again by the diverger and now mirrored partially at the divider plates in the camera. There they overlap with the component, /153 coming from the comparison standard. When the interferometer is adjusted for parallelity of both wave fronts, an image completely without structure should be created in the camera. A slight inclination between wave fronts is introduced, however, from the quantitative evaluation of the image, so that in the ideal case, i.e. in a test sample free of defects, a system of equidistant straight strips is created. If these strips are bent at some points, this indicates a remainder defect of the test sample which can be correlated clearly to the location of origin by using the photograph.

When the test sample has an aspherical surface, it cannot be expected that all partial beams reunite in the focus of the diverger. Since this is necessary, however, for comfortable evaluation of the interferogram, a so-called compensation system is introduced, consisting in several highly precise spherical lenses, compensating for the aspherical portion of the test sample. The system test sample + compensation system can therefore be considered in its entirety as a spherical mirror. The compensation system is calculated and produced

individually for each test sample. The quality is tested with a Hartmann test.

A topography of the wave front reflected from the mirror can be gained for evaluating the completed mirror from the photograph of the interferogram. An example for this is shown in Figure 3090/2. The lines of gravity for the interference strips in the Cartesian coordinates must be taken from the interferogram for the evaluation. A computer program calculates not only the lines of identical wave front deviation from these input data, but also the parameter of the Seidel astigmatism according to amount and direction of the astigmatic axis. Furthermore, the program eliminates the tilting and defocusing of the interferometer. Moreover, the RMS value of the wave front deviation is calculated from the entirety of all individual defects.

It is necessary to accommodate the GIRL main mirror in the cooled state within a helium cryostat for the test. The interferometer, however, must be set up outside of the cryostat, because it is /156 not cold-resistant nor does it permit adjustments in the cold. Accordingly, the cryostat must be equipped with a window of very high quality, since all defects in this window are included doubly in the test. The bending of the window due to the outside air pressure is not of concern for the test. As the size of the window increases, the structural length of the cryostat may be decreased. When a 20 cm size window is employed, for example, the structural length of the cryostat must amount to 110 cm in the case of a main mirror focus of 81.4 cm. In the case of a window size of 10 cm, a structural length for the cryostat of 142 cm would be required.

The test of the main mirror at a low temperature fulfills, above all, the purpose of determining possible compulsory forces, transmitted by the mounting parts to the mirror. For this purpose, the test must be carried out with disassembled tripod. Setting up the mounted mirror with the veritcal axis would be greatly advantageous in this case, since the influence of the natural weight would then be reduced to a minimum.

Secondly, the set-up could be employed for acquiring information on the shaping of the unmounted mirror through possible inhomogeneities of the material properties. Such a test would then not be required when the result of the test of the mounted mirror is positive. The test of the unmounted mirror would also have to be conducted with a vertical mirror axis, since the otherwise preferable band suspension cannot be applied at the mirror edge due to the great number of facets of the mirror body. Instead, the mirror could be positioned on 3 balls under the smooth rear surface. The window of the cryostat must then be arranged above the mirror and the mirror is situated in the cryostat in any case. The test beam is then diverted by a 45° deflector mirror from the interferometer, always set up horizontally, into the vertical of the cryostat, a procedure which has already been applied repeatedly.

If it is not possible to use a cryostat with vertical orientation, the mirror could at least be protected partially from the influence

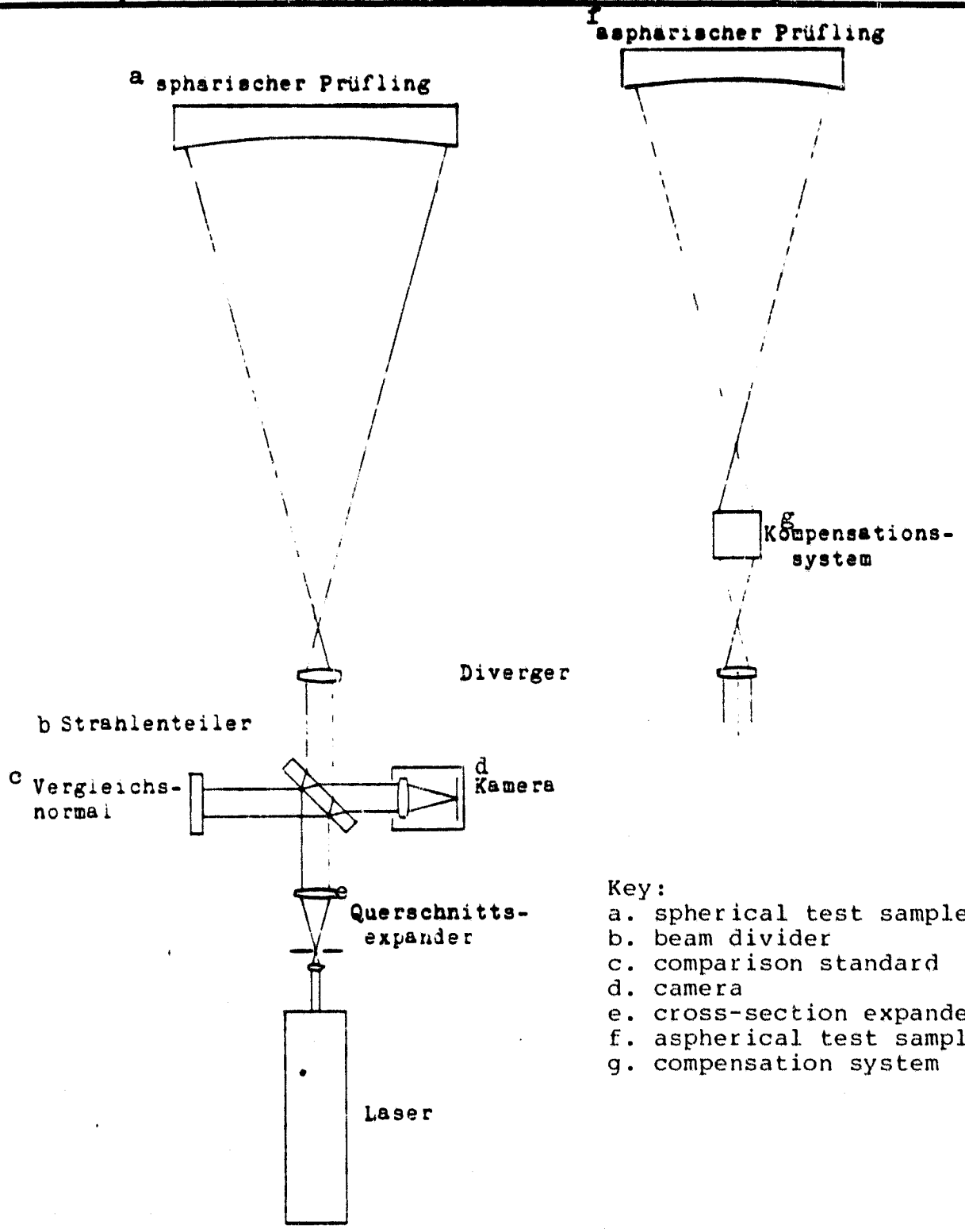

Key:
a. spherical test sample
b. beam divider
c. comparison standard
d. camera
e. cross-section expander
f. aspherical test sample
g. compensation system

Figure 3090/1: Principle of the interferometric concave mirror test.

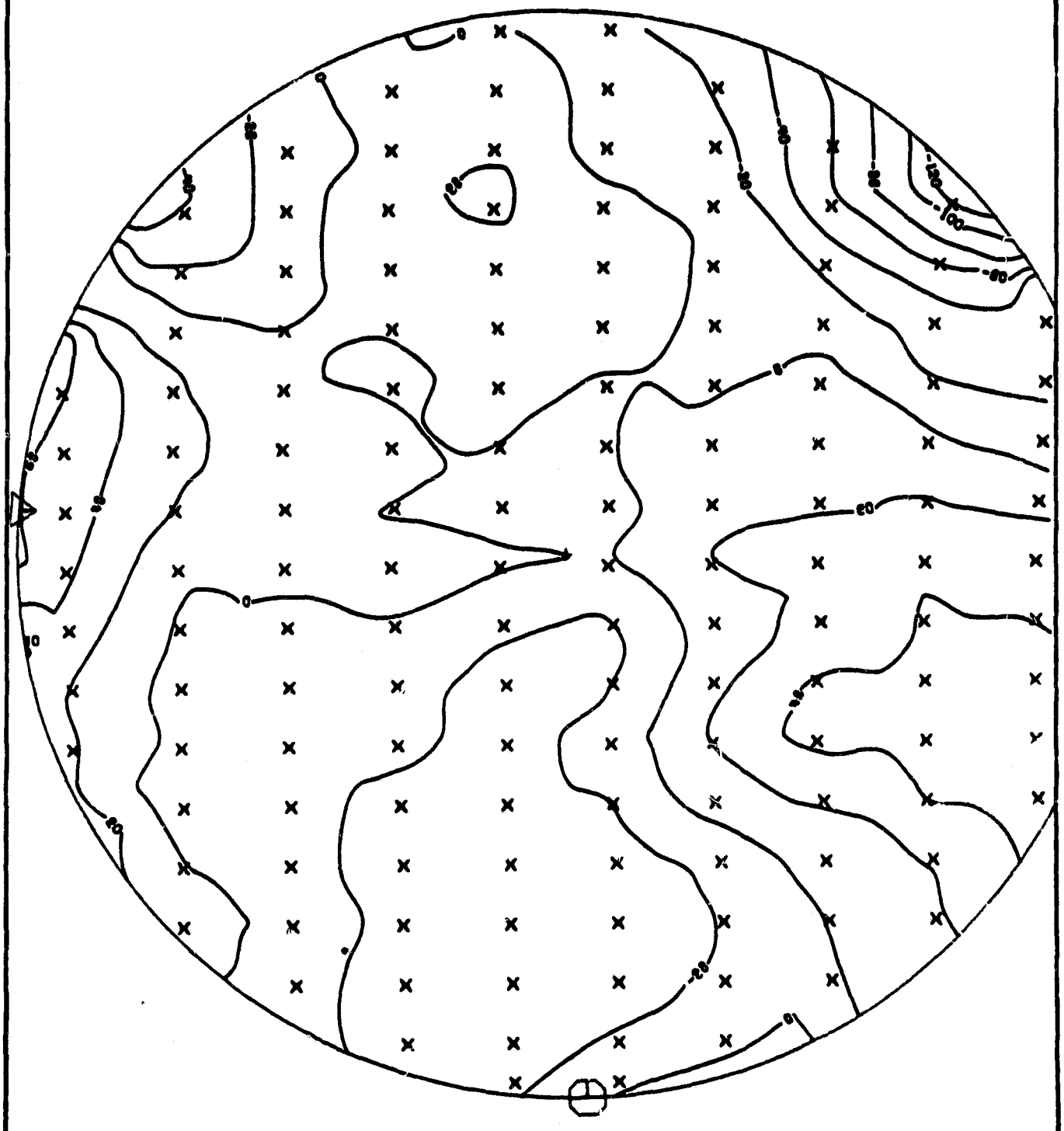

Figure 3090/2: Example of a interferogram evaluated topographically for a concave mirror test (spherical 75 cm mirror), altitude layer lines of the wave front in nm.

of it own weight by additional band suspension. The test of the unmounted mirror would then no longer be possible with simple means. Figure 3090/3 shows both possibilities of the main mirror test in the cryostat.

The absence of the measurements undertaken with the mirror samples /158 at the GHW has a very negative effect on the concept of stray light measurements with the cooled main mirror. Not only were quantitative results expected from this measurement, but also important knowledge on the measurement method. It can therefore only be hoped that the procedure presented in principle in Figure 3010/1 leads in the right direction.

One difficulty in stray light measurement in the main mirror is encountered, because the hole surface and the external surrounding of the mirror contribute in an undefined damaging way to the measurement result. The simplest possibility for preventing these portions would be the limited irradiation of the test sample with a beam diameter of less than 20 cm eccentrically in such a manner that light can fall neither into the hole nor outside of the mirror. This method, however, would have the disadvantage that it is not possible to measure the entire mirror surface at once. The test beam would therefore have to be rotated around the mirror axis in order to measure the entire surface of the test sample in several measurement steps. We therefore propose another system, presented in principle in Figure 3090/4. In order to prevent irradiation of undesired portions of the test sample, an aperture shield is suggested, located on the system L2 of the cross-section expander L1/L2. The central portion of the shield can be vaporized onto the last lens surface to avoid support bridges. The shield B2 is now projected through the lens L3, similar to a field lens, onto the main mirror in such a manner that a sufficiently large central area and the outer edge of the mirror remain free from radiation. The lens L3 is pressed away from the hole shield B4 for the effective contraction of the test beam, so that the shields B3 and B4 maintain a sufficiently large distance in order to limit the defined test beam behind the entry window of the cryostat. The decoupling system with the receiver would have to be pivoted around the vortex of the mirror just as in Figure 3010/1 so that the angle of scattering may be varied.

A further difficulty arises due to the stress on the test sample with a 1:1 projection. In the test of the wave front, this problem was removed by the compensation system in the interferometer. In the scattered light measurement, the mirror does not project the hole shield B4 stigmatically, but rather with a certain scattering circle. At an angle of 2° between the shield and its image, the diameter of this scattering circle amounts to 3 mm. The intensity in the plane of the image is therefore reduced to zero with an angle of 0.05°. /165 A scattered light measurement is only possible outside of this angle.

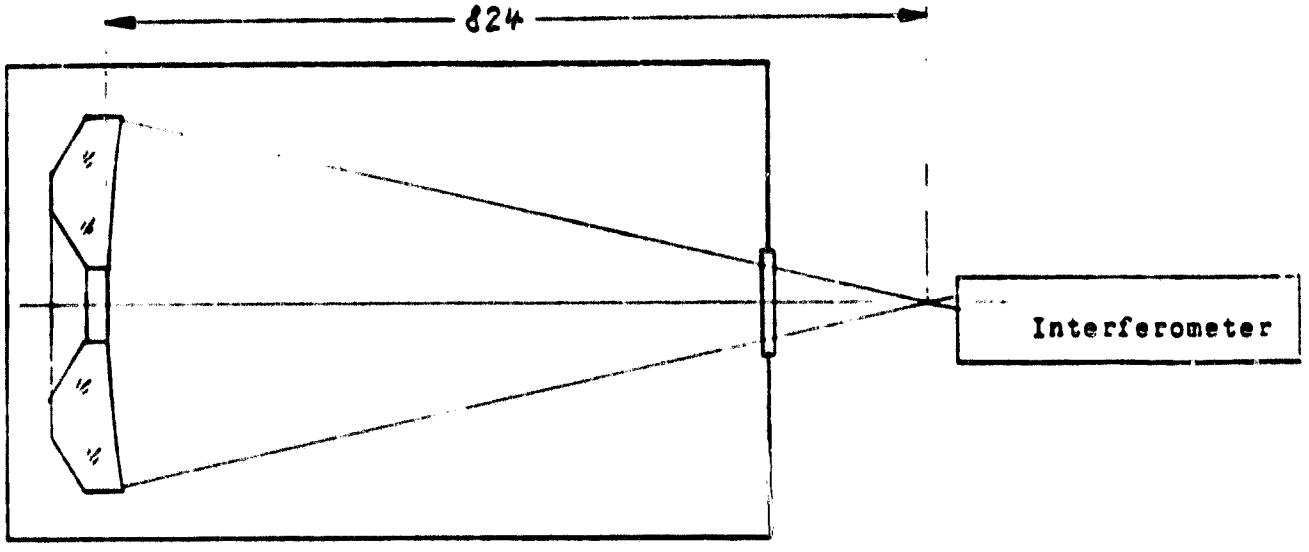

a Horizontalaufbau, Entlastung am Prüfling erforderlich

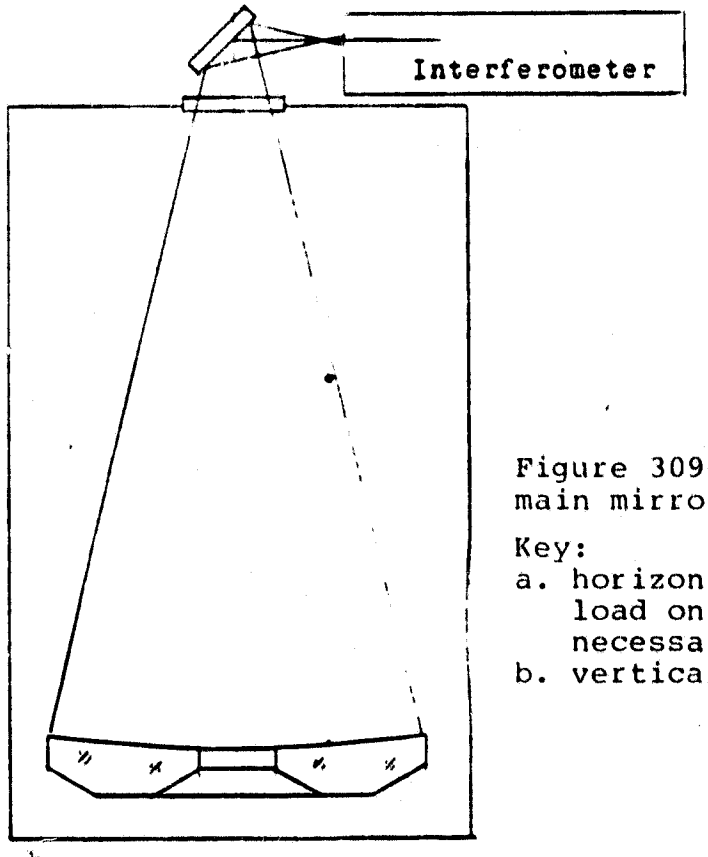

b Vertikalaufbau

Figure 3090/3: Possibilities for the main mirror test in the cryostat.

Key:
a. horizontal set up, removal of load on the test sample is necessary
b. vertical set up

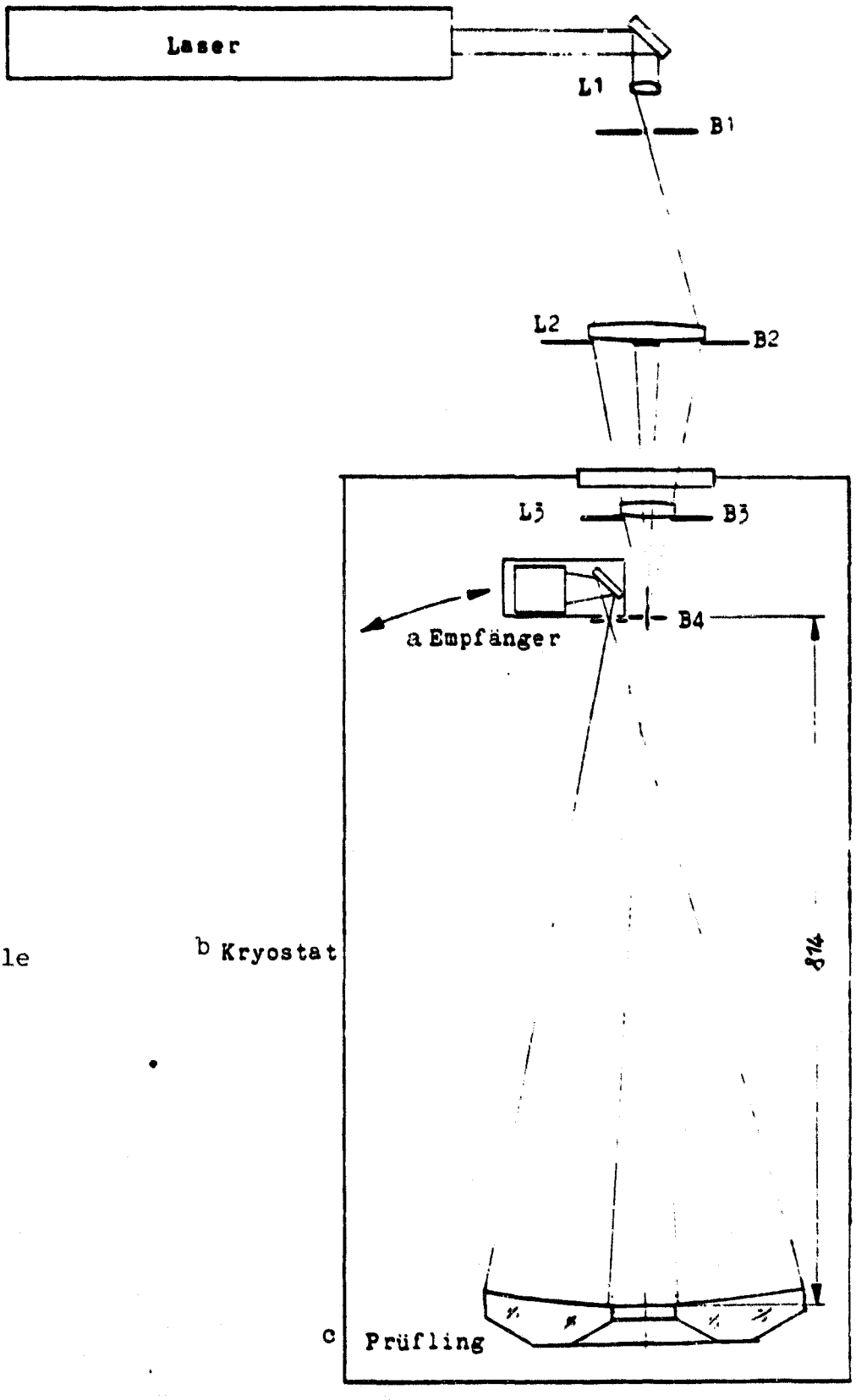

Key:
a. receiver
b. cryostat
c. test sample

Figure 3090/4: Principle of the scattered light measurement with the cooled main mirror.

a) Prüfung bei erfüllter Bedingung:
Exzentrizität = Brechungsindex

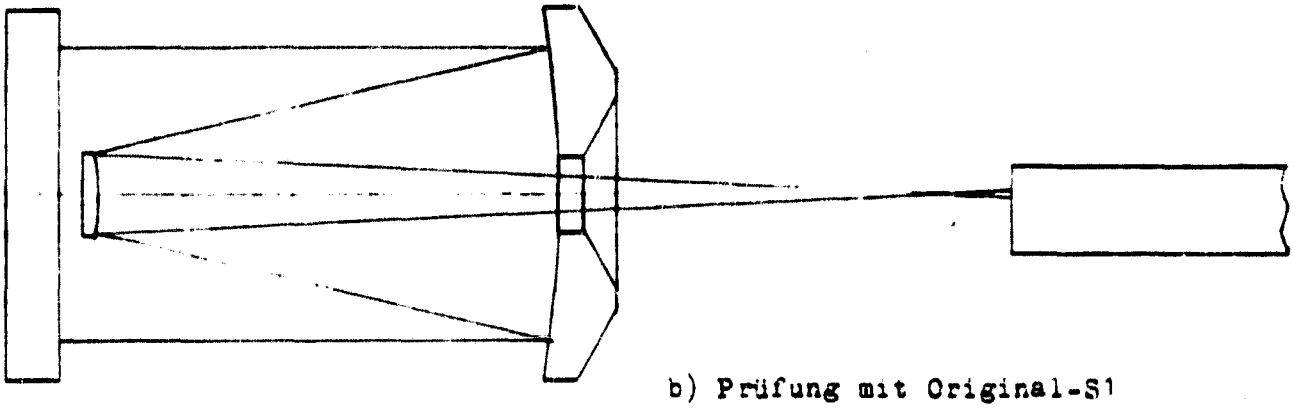

b) Prüfung mit Original-S1

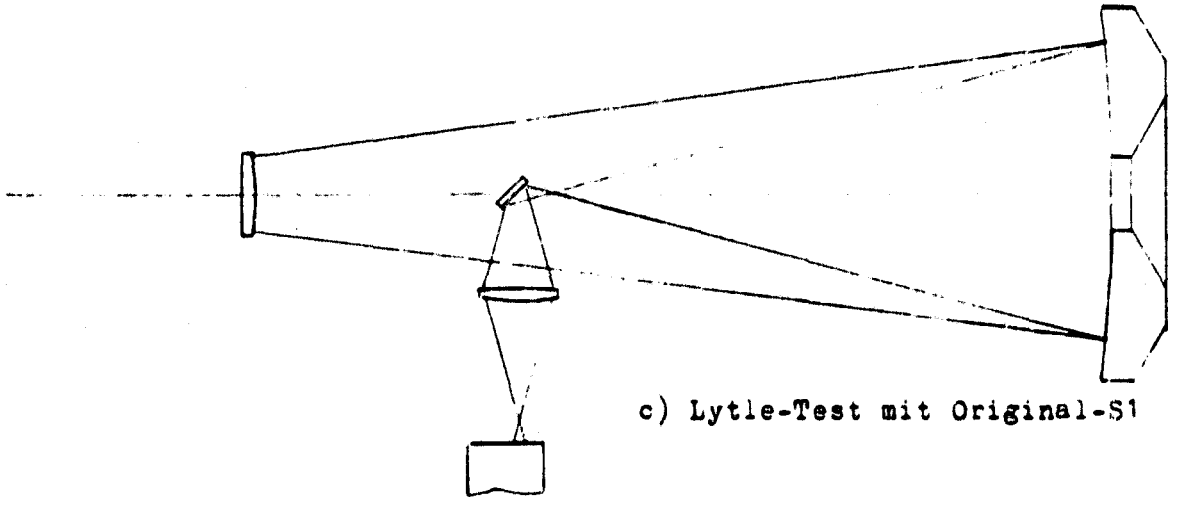

c) Lytle-Test mit Original-S1

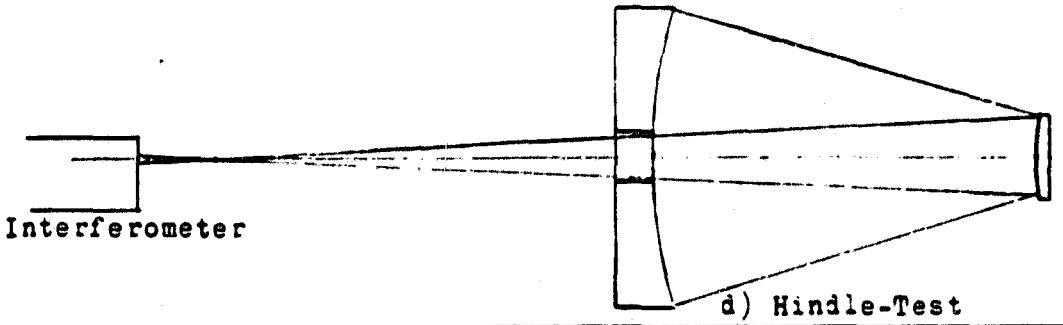

d) Hindle-Test

Figure 3090/5: Test principles for Cassegrain collection mirrors.
Key:
a. Test with fulfilled condition: eccentricity = refractive index
b. Test with original S1
c. Lytle test with original S1

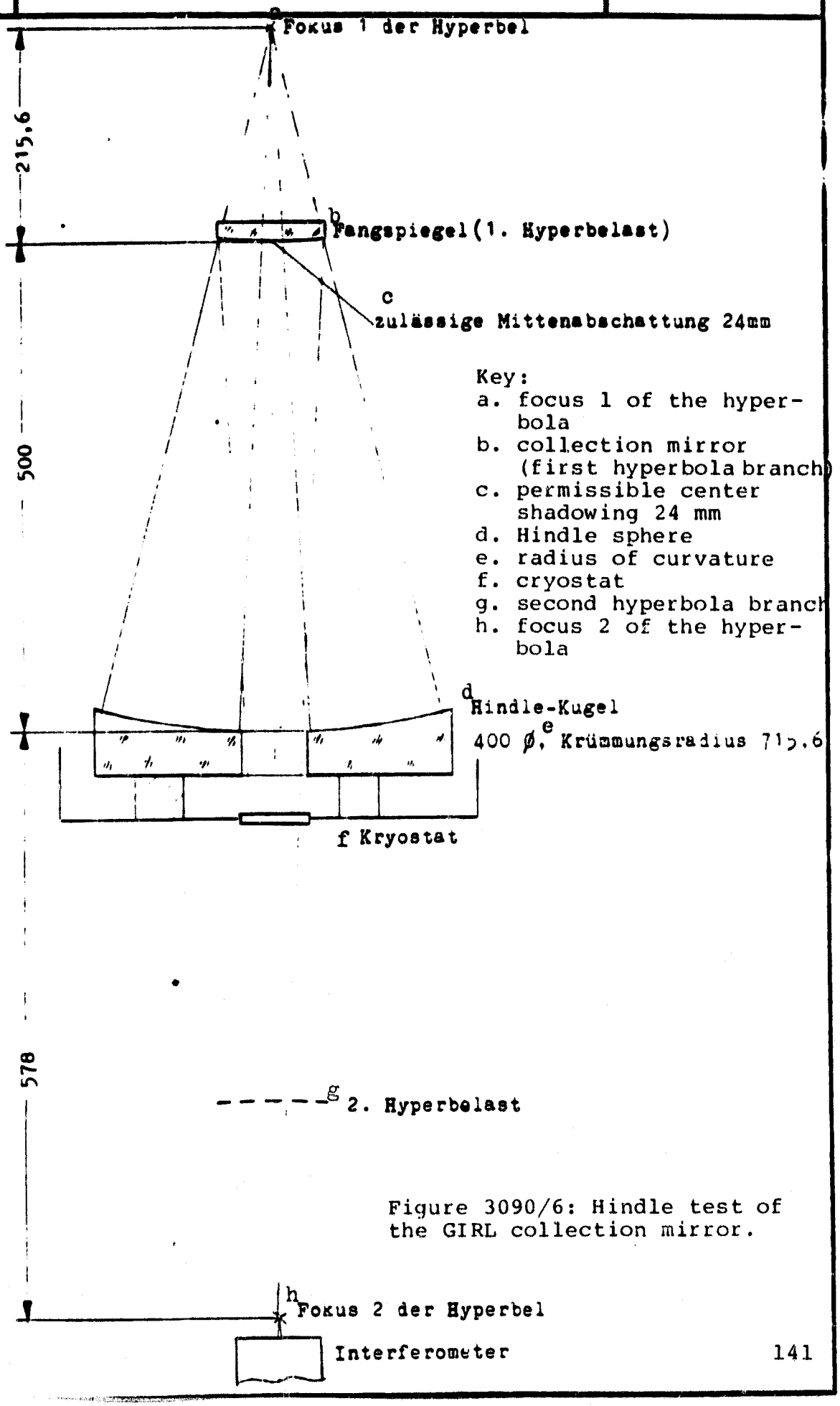

Key:
a. focus 1 of the hyperbola
b. collection mirror (first hyperbola branch)
c. permissible center shadowing 24 mm
d. Hindle sphere
e. radius of curvature
f. cryostat
g. second hyperbola branch
h. focus 2 of the hyperbola

Figure 3090/6: Hindle test of the GIRL collection mirror.

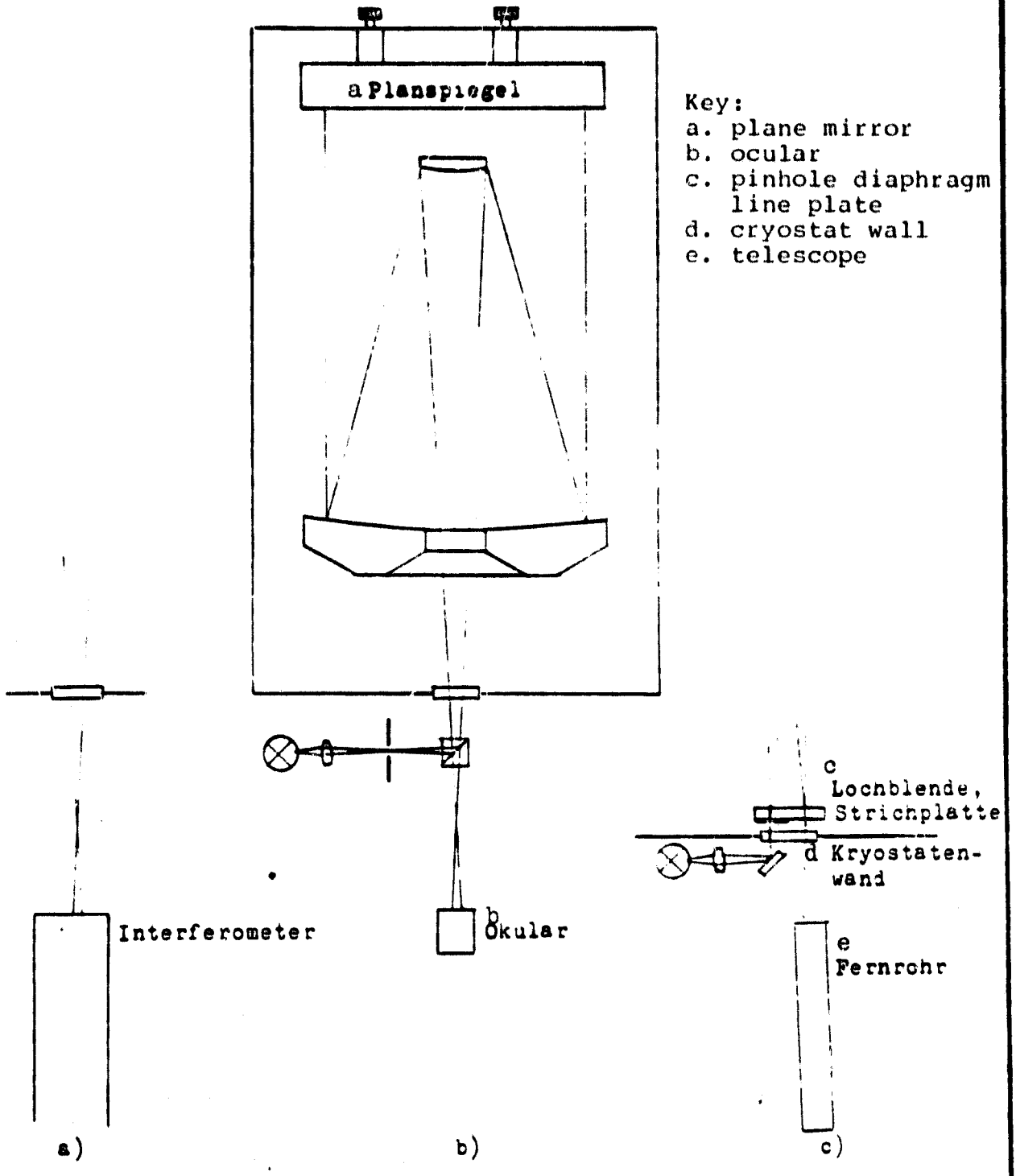

Figure 3090/7: Test of the telescope system with automatic collimation, a) quantitative wave front test, b) visual centering test, c) positioning control of the focus with cooling.

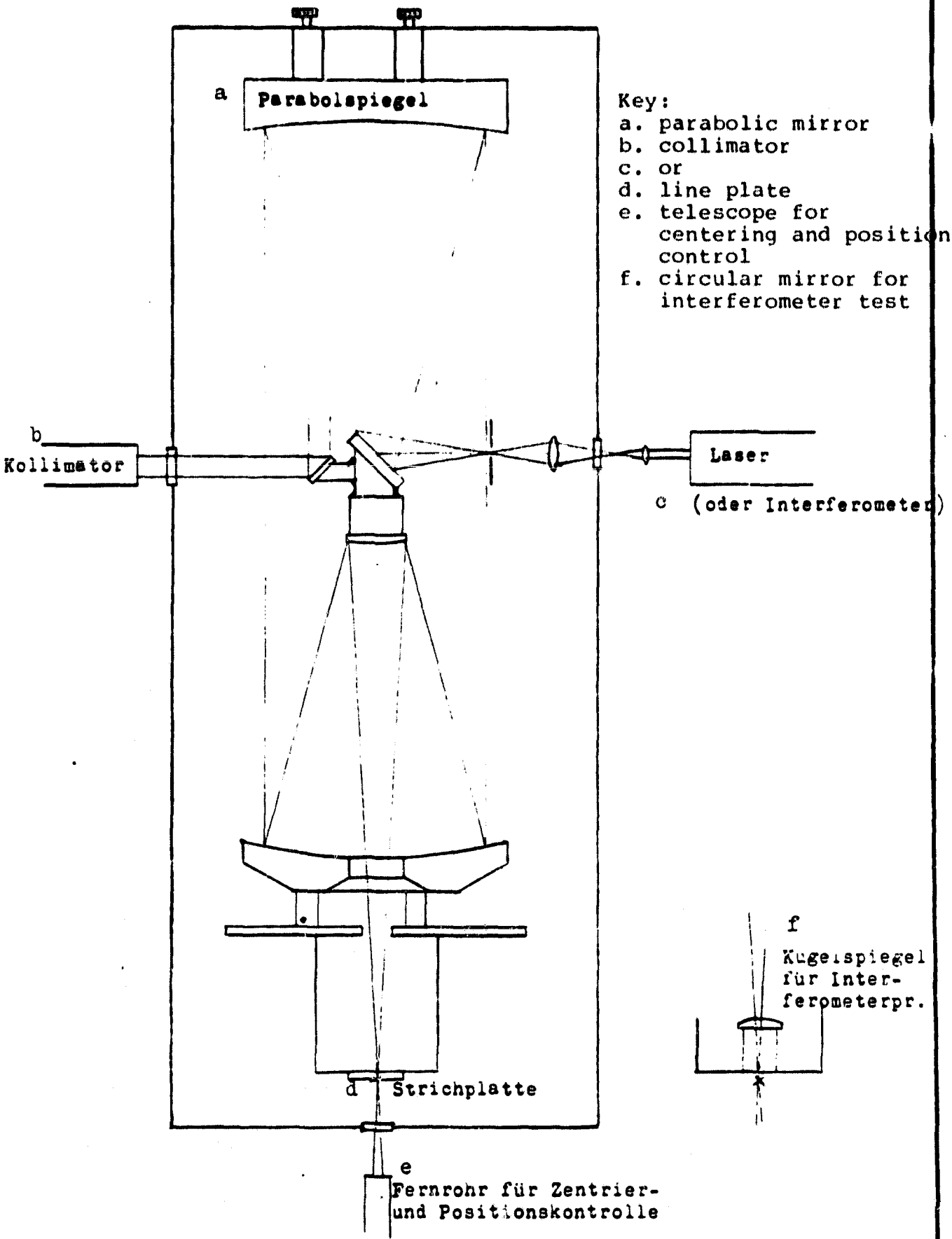

Figure 3090/8: Test of the telescope system with parabolic auxiliary mirror

a Nr.	b Testobjekt	c Testart	d Prinzip in Abb.	e Bevorz. Achslage	f Hilfsmittel (außer Kryostat u. Interferom
1	g Hauptspiegel hungefaßt	i Wellenfront jwarm	3090/1	k vertikal	l 45°-Planspiegel 100 ø
2	g Hauptspiegel m gefaßt	i Wellenfront nwarm/kalt	3090/1 3090/3	vertikal	l 45°-Planspiegel 100 ø
3	g Hauptspiegel m gefaßt	o Streulicht nwarm/kalt	3090/4	p beliebig	q IR-Laser, Empfänger, 4 Blenden, 3 Linsen
4	r Fangspiegel h ungefaßt	i Wellenfront jwarm	3090/5	s horizontal	t Hindle-Kugelspiegel 400 ø
5	r Fangspiegel h gefaßt	i Wellenfront nwarm/kalt	3090/6	p beliebig	t Hindle-Kugelspiegel 400 ø
6	r Fangspiegel n	o Streulicht warm/kalt	3090/6 komb.mit 3090/4	p beliebig	t Hindle-Kugelspiegel q IR-Laser, Empfänger 4 Blenden, 3 Linsen
7	v Teleskop komplett	i Wellenfront n warm/kalt	3090/7a	k vertikal	l Planspiegel 400 ø
8	v Teleskop komplett	w Fokuskontrolle	3090/7c (evtl. 3090/8	k vertikal	l Planspiegel 400 ø u Strichplatte, Beleuchtungseinheit, Fernrohr
9 v	Teleskop komplett	x Experimentprüfung	3090/8	k vertikal y z	Parabolspiegel 400 ø Planspiegel 160 ø 2 Linsen, 1 Blende, Laser

Table 3090/1: Compilation of the tests considered necessary and the required aids.

(Please see Key on following page.)

Key:
a. no.
b. object of the test
c. type of test
d. principle in figure
e. preferred position of the axis
f. aid (except for cryostat and interferometer)
g. main mirror
h. unmounted
i. wave front
j. warm
k. vertical
l. plane mirror
m. mounted
n. warm/cold
o. scattered light
p. arbitrary
q. IR laser, receiver, 4 diaphragms, 3 lenses
r. collection mirror
s. horizontal
t. spherical mirror
u. line plate, illumination unit, telescope
v. telescope, complete
w. focus control
x. experiment test
y. parabolic mirror
z. 2 lenses, 1 diaphragm, laser

AP 3092 Measurement of Aberration at the Second Mirror

In principle, an aberration measurement with a raised collection mirror is much more difficult than that with a concave mirror, since the raised test sample does not rejoin the divergent sample beam. Among different customary testing methods for such collection mirrors, those must be rejected from the beginning, requiring a test through the rear surface of the mirror, since the GIRL collection mirror is to be tested in the mounted state.

There is a relatively simple procedure for testing a collection mirror through the front surface, but tied to defined geometries and a defined refractive index of the glass. The method is based on knowledge, stemming from the seventeenth century and stating that beams coming from a point to a hyperbolic boundary surface under certain conditions travel parallel in the medium behind the boundary surface. Applied to the present case, this means that the collection mirror could be tested by internal reflection of the test beam at the plane polished rear surface with a point light source and such an interferometer as serves for the main mirror test. One condition is that the refractive index of the glass is identical to the eccentricity of the hyperbolic front surface of the collection mirror. Although the /166
collection mirror of GIRL exhibits the eccentricity of 1,500, appearing quite useful at first glance, the test wave length correlated to such a refractive index of cerodur would extend into the infrared

range. The method therefore cannot be applied in principle to GIRL. A further disadvantage of the method would consist in the fact that the GIRL collection mirror is provided with larger holes on the rear surface and a large amount of facets at the outer edge. For this reason, only certain portions of the front surface could be tested.

Accordingly, the test of the collection mirror must be conducted by external reflection at the mirrored front surface. For this purpose, a concave mirror is required, having a multiple of the collection mirror diameter. In order to simplify the test, the concave mirror should be set up outside of the cryostat. The possibility immediately suggesting itself is employing the original main mirror for testing the collection mirror. In this case there are again 2 possibilities for the setup. The first is that of the original telescope geometry, in which the interferometer would have to be constructed in the system focus behind the main mirror. The second possibility is the application of the so-called Lytle test, the principle of which can be seen in Figure 3090/5. Both methods have the disadvantage that the main mirror must be constantly available for the test, and can therefore not be processed simultaneously. The Lytle method has the additional disadvantage that it requires a plane divergent mirror and a lens, making adjustments difficult. Moreover, the plane mirror sometimes causes shadowing of the test sample, exceeding the original shadowing in the telescope system. The only advantage of the Lytle method is a slight angle of opening of the test beam compared to the collection mirror test in the system geometry.

Often, large spherical auxiliary mirrors are employed for the test on collection mirrors, designated as Hindle spheres. Such a sphere can be produced with greater accuracy than the main mirror of the GIRL telescope and could also be better supported with a simple cylindrical shape. The Hindle sphere utilizes the property of the hyperbola of collecting all beams, appearing to originate from one of the two focuses of the hyperboloid, in the other focus. In the present case, the Hindle sphere would have to exhibit a radius of curvature of 715.6 mm with a diameter of 400 mm. The center is to be drilled /167
so that the focus of the interferometer can be positioned at the vortex of the Hindle sphere. The test setup defined in this manner is presented to scale in principle in Figure 3090/6. In order to avoid a large window in the cryostat, the Hindle sphere is to be included in the cryostat. In this case it must be taken into consideration that the spatial requirement corresponds to approximately double the glass thickness. The spherical mirror is then to be arranged in such a way that it can be adjusted from the outside via bellows. Shaping of the mirror due to inhomogeneities of the coefficient of expansion must not be anticipated, when the mirror is manufactured of cerodur special.

Scattered light measurements at the collection mirror would be possible in accordance with the principle in Figure 3090/4, when the Hindle sphere is produced with a surface quality of high value. The contribution to the measurement results could be determined by a separate measurement and then subtracted from the total result.

AP 3093 Tests of a Complete Telescope System

In the conception of the test setup for the measurement of the wave front aberration and possible centering errors of the telescope, it must be taken into consideration that a function test of individual experiments must also be conducted, when they are illuminated with the original telescope. The test arrangement shown in Figure 3090/7 cannot be used for this latter purpose. For the test of the wave front, on the other hand, it has the advantage that it would be easier to adjust in comparison with the arrangement in Figure 3090/8 because of the lower number of necessary aids.

The test setup in accordance with Figure 3090/7 functions according to the automatic collimation principle. /168 The system is tested on the basis of the original focus by reflecting the exiting parallel beam at the plane mirror into the telescope again. All surface errors appear doubled in size in the interferogram. The adjustment is optimal when a concentric bending image of the point light source occurs only in the optical axis. In addition to the visual evaluation of the star image, the aberration can also be measured quantitatively with the laser interferometer described in AP 3091. A correlation of errors occurring to the individual components, however, can only be ascertained by rotating the components in comparison to the others. The method has the disadvantage that the focal space must be accessible for the radiation of the star source and make possible the setup of a beam divider.

In the case of the procedure shown in Figure 3090/8, the light is irradiated into the telescope aperture for the system test. A parabolic mirror serves primarily for this purpose, having the same diameter as the telescope main mirror. On the basis of the properties of the parabola, all beams originating from the focus of the parabola are reflected parallel by the mirror. The parabolic mirror should be suspended or positioned in the cryostat just as the plane mirror in the above-described procedure, so that a large window in the cryostat is avoided, possibly causing an impermissibly high heat radiation. The irradiation of the light into the parabolic axis must be carried out with the aid of a small 45° deflector mirror and one or more intermediate projections. In the last intermediate projection, there is a pinhole diaphragm of the most variable diameter possible, so that any optic in front of this pinhole diaphragm may be of lesser quality. A second intermediate projection, situated in the plane of the window, would be advantageous for attaining a minimum window diameter. The 45° deflector mirror could be mounted on the rear side of the telescope collection mirror support (chopper). Fine adjustments could then be limited to the parabolic mirror with adjustment screws guided through the cryostat. While the visual evaluation of the star image outside of the cryostat with the aid of the telescope causes no problems, the interferometric would have to be modified in comparison with the above-explained method. /169 There are two possibilities for this, the more advantageous of which is already plotted in Figure 3090/8. It permits the application of the interferometer according to Figure 3090/1 and merely requires a

raised, very small spherical mirror, to be set up concentric to the system focus of the telescope. The second possibility consists in rotating the beam divider in Figure 3090/1 by 90° and replacing the cross-section expander with a second main mirror.

A position control of the system focus could also be carried out with the parabolic mirror method. In the plane of focus, a glass plate parallel to the plane would have to be mounted with an illuminated line grid. For practical purposes, this should be carried out at the original structure of experiment E1. Only in this manner could the thermal invariance of the focusing condition of the telescope be tested. The prerequisite for this, however, is that the test beam radiated from the parabolic mirror remains parallel during cooling. This would be ensured by a control collimator located outside of the cryostat, as shown in Figure 3090/8. In the case of deviations from parallelity, the paraboloid could be raised or lowered with the adjustment screws. Measured by this additional criterium, the automatic collimation method would again be more advantageous for focus control. In this case, the pinhole diaphragm for the star generation and the line grid for the control of the star image position could be applied to the same glass plate. Irradiation and image generation would then be carried out outside of the axis, but at only a small distance with tolerable image errors. If a deviation in focus position occurs during cooling, it is measurable in both cases by the refocusing of the observation telescope. Lateral focus migration could be determined either by a grid on the line plate or by lateral, measurable shift in the observation telescope according to amount and direction.

A measurement of scattered light is very problematical in the complete telescope. An auxiliary mirror would also have to be introduced for the measurement with a scattered light portion also entering into the result. This would have to be accordingly small, requiring a high qualification of the mirror. Another possibility would be the separate measurement of the scattered light portion of the auxiliary mirror, possibly permitting an elimination of this portion from the total result. Whether the scattering of individual measurement results permits such a procedure is questionable until first results /170
are available. On the other hand, subtracting the portion of the auxiliary mirror from the total scattered light is just as problematical as the addition of both portions of the main mirror and collection mirror of the telescope, also to be measured separately. Under this aspect, the procedure of least cost would consist in adding the scattered light portion of the main mirror, as explained in AP 3091, to the scattered light portion of the collection mirror, to be determined with a high-quality Hindle sphere. The scattered light portion of the Hindle sphere would be substantially easier to determine than that of a plane mirror, which would have to be treated in testing the complete system.

AP 3100
Clean Handling /171

General Information

The US Federal Standard 209a, replaced on April 24, 1973, by the US Federal Standard 209b, is usually also employed in Europe for classifying low-dust spaces. These are supplemented in Germany by the guidelines of the working committee for clean rooms in Stuttgart and in Switzerland by the guidelines of the Swiss Society for Clean Room Technology (SRRT). The following standardized classes are included in these systems:

Designation of Class US-Standard	Europe Standard	Number of particles of 0.5 µm per spatial unit
100	1	100/Kubikfuß[a] = 3,5/l
10000	2	10000/ " = 350/l
100000	3	100000/ " = 3500/l

Key:
a. cubic foot

The number of larger particles can be seen from the distribution function in Figure 3100/1. This corresponds to the upper limit of the filter transmission curve. Smaller particles with decreasing size are held increasingly, because the collision with the filter increases due to the increase in molecular motion. In order to demonstrate the degrees of purity, some particle numbers are mentioned here, released by an operating person per minute:

Resting person without activity:	100,000 particles/minute
Person with slight manual or head motion:	500,000 particles/minute
Person sitting on a chair:	2,500,000 particles/minute
Person walking in a room:	5,000,000 particles/minute

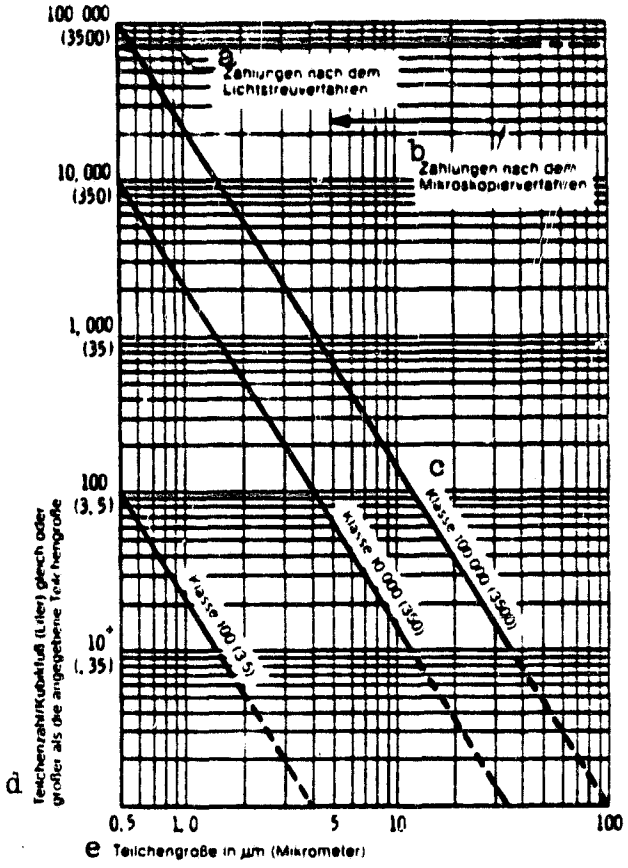

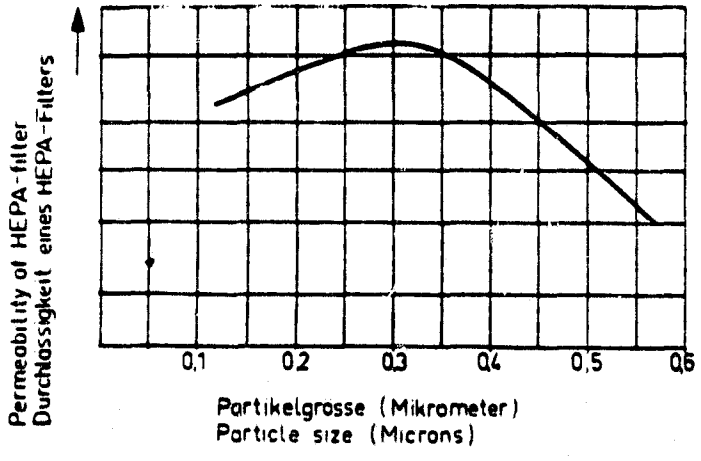

Figure 3100/1: Definition of the purity classes, filter transmission.
Key:
a. numbers according to the light scattering method
b. numbers according to the microscopic method
c. class
d. particle number/cubic foot (liter) equal to or larger than the indicated particle size
e. particle size in µm

The presently preferred pure room technology for work with /173
minute particles is the application of flow boxes, in which a constant, turbulence free air flow from the top to the bottom or from one side to the other prevents dust particles from entering the box because of a slight over pressure. The air flowing into the box passes through one or more filters, the one chosen most often is the HEPA filter (High Efficiency Particulate Air Filter). The operating person is outside of the box. Inside the box, however, there are frequent purification devices, removing the final dust particles from the pre-cleaned work pieces introduced and binding them in a liquid.

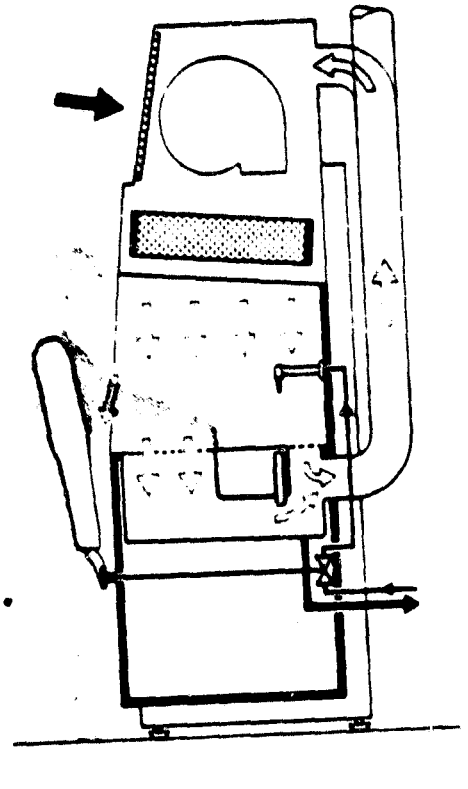

Application to the Telescope /174

It is not at all sufficient in the assembly and integration of the flight model to provide the telescope merely with clean mirrors. Instead, the entire telescope must be free of dust and delivered for integration free of dust. It must be protected with a special covering during transport for this purpose. The class 100 is desirable for all parts.

The vaporization equipment for both telescope mirrors must already be in a dust-free displacement-precipitation flow. The

precipitation flow device can be temporarily installed and covered with plastic foil. It must include purification equipment corresponding to the size of the main mirror. The main mirror and the collection mirror are brought into this clean room with heat conductors already soldered in a precleaned condition and then subsequently cleaned by moist means. Then vaporization is carried out. After ventilating the recipient with dust-free air (always to be understood in the sense of class 100), the mirror is enclosed in a transport container[1] free of dust and brought to the assembly box.

The assembly box is a laminated box of a size, permitting accommodation of the entire telescope while standing. It serves for assembling the mirror in its mountings and connecting the mountings by means of the tripod. All mechanical parts, brought into the assembly box, must be previously purified. Parts with pockets having difficult access are subsequently cleaned in a multiple-stage ultrasound bath, others are washed manually. Special problems must be anticipated in the case of dull black parts, insofar as the paint tends to give off dust. The mirrors, brought into the transport containers[1] in the assembly box, require special care. The transport containers must, of course, also be cleaned before bringing in the equipment. It must be ensured upon opening that the resulting under pressure does not blow any particles from joints or corners onto the mirror. An artificial over pressure would solve this problem.

After completed assembly, the entire telescope must be enclosed in a transport container.[1] It is brought to the test chamber or to the integration room in this container. Naturally, it is expected from /175 the test chamber with all the internal devices, that it is also free of dust. To what degree this can be achieved cannot be evaluated here due to lack of detailed knowledge.

In various stages of the project, coating the mirror surfaces with a dust-protective and cleaning varnish was considered. First, this method would be applicable only with great difficulties in the case of the large main mirror diameter and secondly, it would not make the work of clean-handling of the entire mechanics superfluous. The cleanest mirror does not remain clean when the surroundings can give off dust.

The aids required for clean handling when the above-described procedure is applied are summarized again here.

Precipitation flow device for clean-handling of a 50 cm vaporization instrument

Purification bath for dust removal of the mirror

Laminated assembly box, inner dimensions 100 x 150 x 70 cm with purification baths

---

[1]All transport containers are to be filled with protective gas.

Transport container for the main mirror

Transport container for collection mirror

Transport container for the complete telescope.

Appendix 1 /176

Remarks on the Error Budget

Contrary to the recommendation of the Dornier system, we suggest to use the main mirror as reference system for the consideration of errors. It would be provided with an attachable center cross, engraved in a transparent plane glass plate, for this purpose. The cross can be centered by rotation and freed from wobble errors. It could also be aimed at from the experiment focus with an alignment telescope with automatic collemation accessory.

The main mirror mounting should be so rigid that the remainder shaping after starting amounts to less than 2 µm. This is certainly the case when the stresses of all critical structural elements do not exceed the fourth part of the 0.2% stress limit and all connections are fixed.

The critical parts of the main mirror mounting consist of invar. Invar has a 0.2% expansion limit $\delta_{0,2}$ = 119 kp/mm^2 at 5 K. When the length of the structural elements is not too great, the cross-section q in the case of a load F (kp/mm^2) must be accordingly greater than

$$q = 0{,}034\ F\ /mm^2/$$

For the membranes and springs of the main mirror mounting, applied in pairs, for example, a limit cross-section of 2.8 mm^2 results. This was taken into consideration during construction. The welded seams, however, require special attention. Further stress tests after repairing the shake model will provide information on their behavior. If they should prove insufficient and not capable of improvement, they must be replaced by other connections.

Since the main mirror mounting is situated in the shadow of the /177
mirror, thermal shaping can only be introduced over the interface to the instrument platform. Calculations produce the result that a temperature difference of 1 K between the compensators causes a transverse off-set of the mirror axis of approx. 1 µm. Axial thermal effects are completely insignificant.

The axial component of a collection mirror motion acts according to

$$dg = -(m^2 - 1)\, de$$

(nomenclature according to K. Bahner) with a multiple of 24 of the amount in the Cassegrain focus. An adjustment error in the collection mirror in the lateral direction is intensified in the focus by a factor of 4. Errors in the collection mirror and chopper are therefore especially serious.

The attempt was made in Table A1 to list the possible errors in a table in three categories. The type of error A encompasses such errors, no longer removable under the action of gravity with the realizable adjustment devices; the type of error B encompasses those errors, arising additionally due to cooling and the removal of gravity; and the type of error C arises due to heating as a result of radiation in orbit.

Since the main mirror is to be the reference system, its errors can be set at zero in category A. Its errors in the categories B and C may also be assumed at zero in a first approximation. A slight deformation in the aluminum base may occur during cooling, but this can be determined only by testing. B_η of B_ζ may then assume the amount of a few arc seconds.

All translations given in Table A1 are defined in Cassegrain focus, all angles are image jumps in the heavens. In the assumed tilting of the tripod, it was assumed that half of the tipping angle is effective as lateral off-set and the other half of tipping. If one of the three supports is altered in length, the center of the correction mirror is thereby shifted laterally by a multiple of 3.2 in length. For example, if a support is heated from 10 K to 15 K, /180 the alteration in length is 0.4 μm (invar), the off-set of the collection mirror 1.3 μm, the image off-set 5.2 μm.

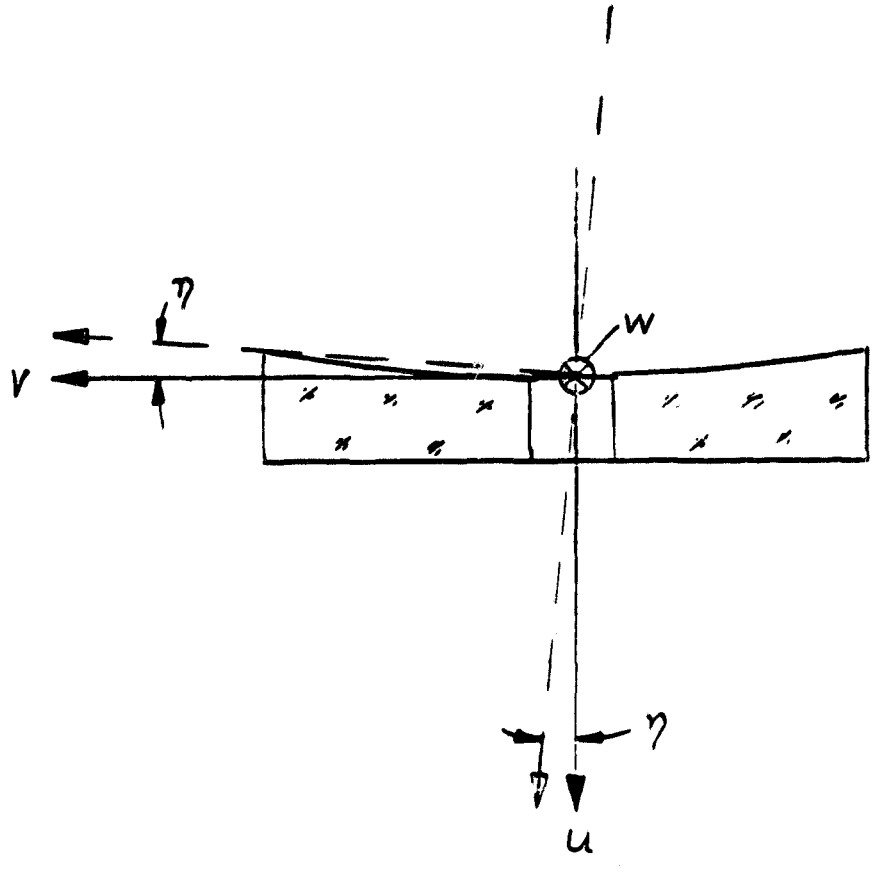

a Drehung um die w-Achse: η
b Drehung um die u-Achse: ε
c Drehung um die v-Achse: ζ
d w-Achse = Chopperachse des Fangspiegels

Figure A1: Coordinate system for the error budget of optics.

Key:
a. rotation around the w axis
b. rotation around the u axis
c. rotation around the v axis
d. w axis = chopper axis of the collection mirror

a Fehlerart	A b Restfehler nach Justierung im Warmen bei 1 g und vertikaler Aufstellung	B c Fehler, zusätzlich durch Abkühlung und Übergang auf Og und O bar hervorgerufen	C d Fehler durch Einstrahlung im Orbit und Chopperbetrieb
e Hauptspiegel	0	f 0 (Kippung?)	0
g Fangspiegel + Dreibein h (Fehler im Fokus gemessen)	$A_{u1} = \pm 0{,}12$ mm $A_{v1} = A_{w1} = \pm 0{,}1$ mm $A_{\xi 1} = A_{\eta 1} = \pm 10''$	$B_{u1} = \pm 0{,}12$ mm $B_{v1} = B_{w1} = \pm 0{,}1$ mm $B_{\xi 1} = B_{\eta 1} = \pm 5''$	$C_{u1} = \pm 0{,}015$ mm ($T = \pm 6$ K bei T=15 K $C_{v1} = C_{w1} = \pm 0{,}008$ mm $C_{\xi 1} = C_{\eta 1} = \pm 0{,}5''$
Chopper h (Fehler im Fokus gemessen)	$A_{u2} = \pm 0{,}25$ mm $A_{v2} = A_{w2} = \pm 0{,}1$ mm $A_{\varepsilon 2} = \pm 120''$ (i Chopperachse) $A_{\xi 2} = \pm 130''$ $A_{\eta 2} = \pm 70''$	$B_{u2} = \pm 0{,}2$ mm $B_{v2} = B_{w2} = \pm 0{,}02$ mm $B_{\varepsilon 2} = \pm 30''$ $B_{\xi 2} = \pm 60''$ $B_{\eta 2} = \pm 120''$	$C_{u2} = \pm 0{,}05$ mm $C_{v2} = 0$ $C_{w2} = \pm 0{,}06$ mm $C_{\varepsilon 2} = 0$ $C_{\xi 2} = \pm 1''$ $C_{\eta 2} = \pm 12''$ } j bei Extremlage

Table A1: Error budget (focus shifts generated by angle errors are not contained in u, v and w.

(See Key on following page.)

Key:
a. type of error
b. remainder error after adjustment when heated in the case of 1 g and vertical positioning
c. error, additionally caused by cooling and transition to 0 g and 0 bar
d. error due to radiation in orbit and chopper operations
e. main mirror
f. tipping
g. collection mirror + tripod
h. error measured in focus
i. chopper axis
j. in the case of extreme position

In addition to the data on collection mirror and main mirror, that of the chopper is listed separately with the index 2 in the table. These originate from communications of the MPI for Astronomy in Heidelberg, bearing the remark "we assume no responsibility". The values contained herein were presented slightly modified and simplified. The considerable errors in angle of the chopper in category B are almost impossible to reproduce. It must be the aim of chopper construction to reduce these values drastically.

Appendix 2 /181

Thermal calculations with a heat conductor contact
Thermal Calculations with a Heat Conductor Contact

Supplementing AP 3042, refined calculations were carried out with a local partial model of the main mirror in order to obtain more precise information on the origin of the impermissibly high stresses in cerodur occurring at the contact point of the heat conductor. A concentric nodal model around the axis of heat conductors was selected according to Figure A2. This takes into consideration the exact geometry of the conductor with the exception of the soft solder layer between the conductor and cerodur.

The cool-down calculation produced a total time of 30.6 hours until achieving the balance temperature of 3 K. This value is situated by approx. 10% higher than that of the entire mirror from earlier calculations. The cool-down curves are presented in the same manner as in AP 3042 in Figure A3. Only the ordinate scale of the thermal coefficient of expansion of cerodur is plotted in half the scale compared to Figure 3040/14.

Calculation of tensions was limited to the time at 24 hours after beginning cool-down, where the maximum stresses occur according to experience from AP 3042 due to the maximum expansion number of the cerodur. The maximum value occurs in the model of Figure A2 within the cerodur in element no. 22, i.e. directly at the contact point of copper and cerodur. Within the metal parts (see Table A2) the stresses attain even substantially higher values, but which are not dangerous there.

The calculated maximum stress of 2.9 kp/mm^2 would lead to the breaking off of a glass shell. Since this is not confirmed, however, by the results of the model tests, it can be concluded that the solder layer between cerodur and metal acts as a compensator to a great degree with respect to these contact stresses. Further calculations were added to the computation proof within the framework of available means. The element no. 26 was eliminated in the model Figure A2, so that air space may be assumed in its place. The direct contact of copper and cerodur is avoided by this means, corresponding approximately to an invar nipple with sack hole. In Figure A2, the results of this calculation are compared to those with the complete copper conductor. The results are startling. The stresses in element no. 22 have dropped to 1/8; instead, the maximum stresses now occur in element no. 23. The maximum value of 0.52 kp/mm^2 is situated on the boundary of the permissible value. This is also certainly reduced by the tin layer in practical situations. /185

Consequences for the Thermal Model of the Mirror

Thermal calculations show on the whole that there is no danger of fracture for the cerodur for the thermal model, taking into consideration the test results with heat contacts, when the predetermined cool-down curve of the base plate is maintained. According to Table 3040/5, the stresses do not exceed any critical values. The experimentally determined stability in the case of the model tests carried out by Linde contradict a danger due to the high stresses in Table A2. The model elements, not in direct contact with the conductor, are subjected to still permissible stresses. Two additional thermometers with increased accuracy are recommended for the control of the cooling curve on the front surface of the TM main mirror. The maximum permissible temperature difference is prescribed as a function of temperature (separate communication to MBB).

Summary of This Final Report /186

AP 3010 Optical Studies with Polished Cerodur Samples /187

Four mirror samples were produced with aluminum layer thicknesses between 50 and 400 nm. In order to simplify the measurement procedure, an exchange revolver was designed and constructed for these 4 samples. The measurement procedure was agreed upon upon the occasion of inspecting the equipment at the GHW in Wuppertal.

Due to lack of personnel and apparatus, the measurements could no longer be undertaken in Wuppertal within the time of the study. The samples showed a clear increase in scattering intensity with increasing aluminum layer thickness when inspected visually. In the cooling tests, the cemented heat conductors and measurement sensors had separated.

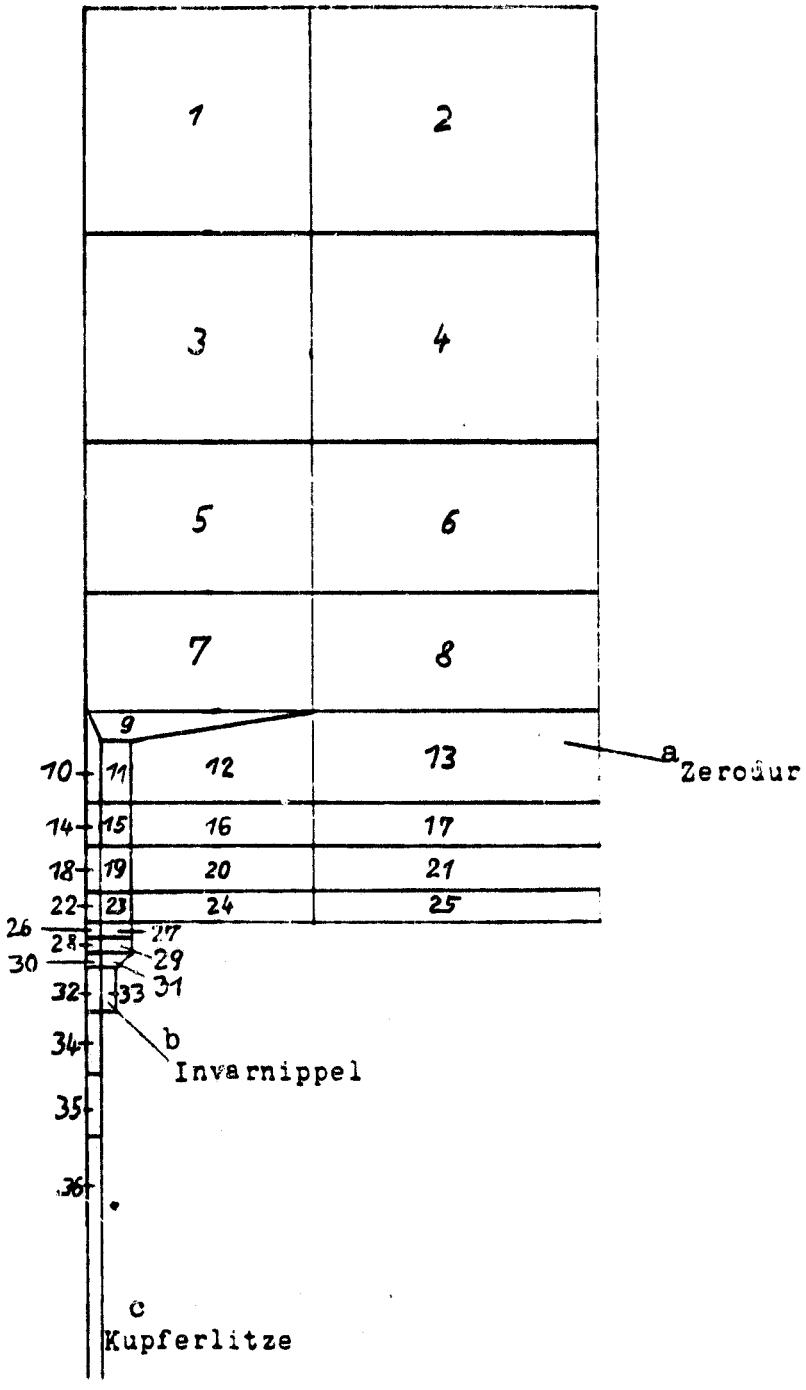

Figure A2: Nodal model for thermal calculations with individual heat conductor contact (scale 2:1)

Key:
a. cerodur
b. invar nipple
c. copper litz wire

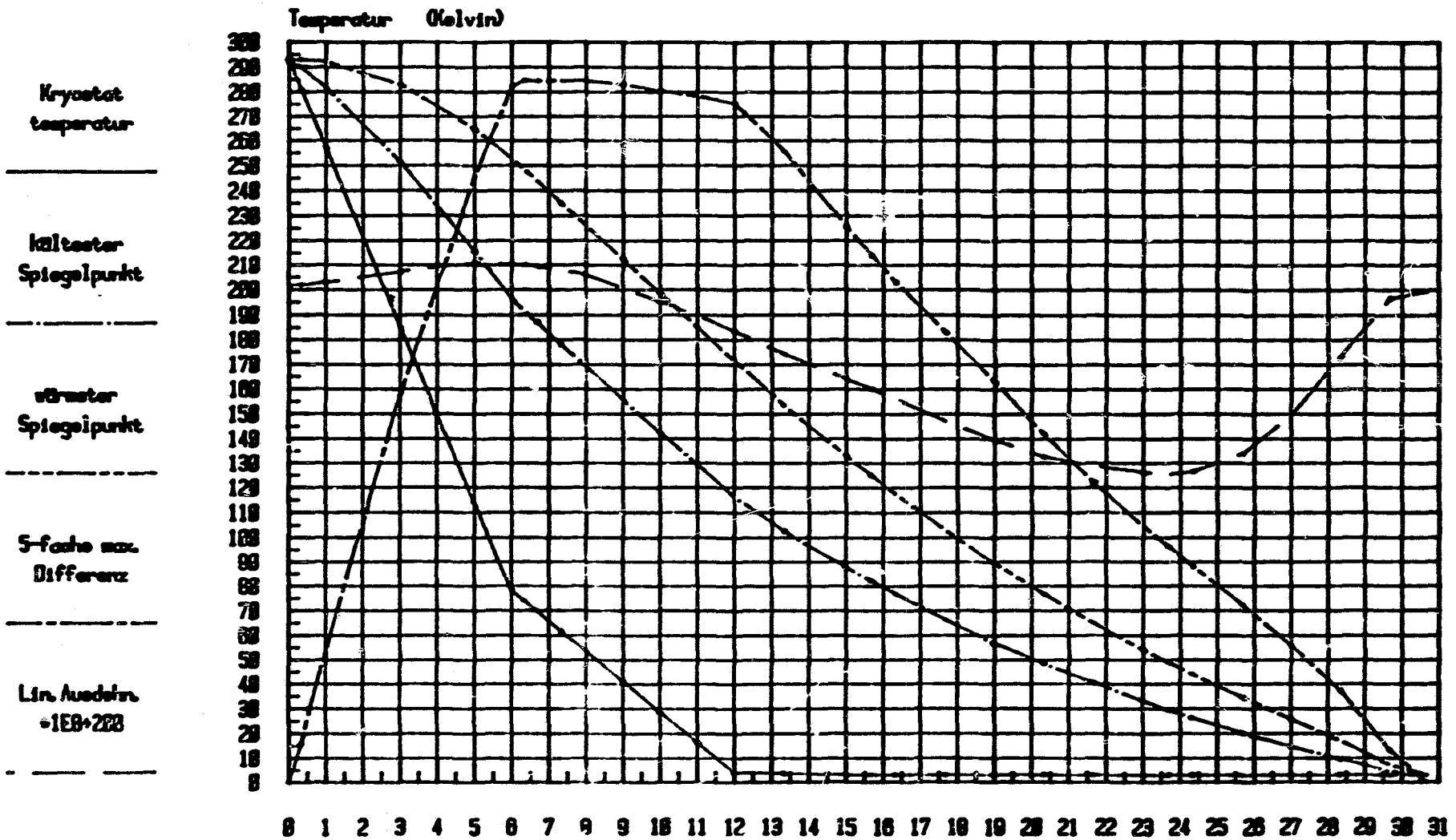

Figure A3: Cool-down course at the heat conductor contact according to model figure A2 (explanation see page 68).

ZEISS
CIRL
193

a Element-Nr.	b Spannungen: Element 26 c aus Kupfer	Element 26 d aus Luft
14	0,063 kp/mm^2	0,095 kp/mm^2
18	0,399 kp/mm^2	0,239 kp/mm^2
19	0,338 kp/mm^2	0,195 kp/mm^2
20	0,109 kp/mm^2	0,076 kp/mm^2
21	0,063 kp/mm^2	0,060 kp/mm^2
22	2,904 kp/mm^2	0,349 kp/mm^2
23	1,192 kp/mm^2	0,522 kp/mm^2
24	0,449 kp/mm^2	0,302 kp/mm^2
25	0,077 kp/mm^2	0,081 kp/mm^2
26	8,168 kp/mm^2	---
27	7,697 kp/mm^2	5,421 kp/mm^2
28	8,277 kp/mm^2	7,426 kp/mm^2
29	8,679 kp/mm^2	7,062 kp/mm^2
30	5,787 kp/mm^2	5,494 kp/mm^2
31	9,547 kp/mm^2	8,202 kp/mm^2
32	8,523 kp/mm^2	7,871 kp/mm^2
33	5,201 kp/mm^2	5,263 kp/mm^2
34	1,014 kp/mm^2	1,042 kp/mm^2

Table A2: Maximum stresses near the contact of the heat conductor.

Key:
a. element no.
b. stresses
c. of copper
d. of air

AP 3020 Geometry, Support Rings and Preparation of the Main Mirror

Manual calculations with a simplified model of the main mirror produced an optimal support ring radius of 166.3 mm. A refined calculation model of a realistically designed mirror body produced an optimal support ring radius of 165.8 mm according to computer calculations with finite elements. In the case of a three point support optimized in this manner, the aximuthal bending along the concentric rings around the mirror axis produced the maximum value of 80 nm at the outer edge of the mirror. The RMS value of deformation of the entire mirror surface amounts to 20 nm on the basis of this result and is therefore still permissible.

Cutting tests for determining possible surface alterations were undertaken with the mirror model reduced by a scale of 2 to 1 with a polished surface of high quality. A surface deformation of 0.4 wave lengths was only shown in cutting the large facet at the hole edge. This could be completely removed by etching the cut surface. The intended production technology of the mirror can therefore be carried out.

AP 3030 Construction and Tests of the Main Mirror Mount

Four different mount drafts were examined as to thermal and elastomechanical properties. The models were considered comparatively and two of them, the so-called tension-rod mount and the membrane mount were included in the final selection. The final decision in favor of the membrane mount finally had to be undertaken on the basis of very slight advantages. The desirable further examination of both concepts had to be disregarded because of cost. /188

The material for the expansion compensator necessary for the membrane model was selected in favor of Voltalef 300. The properties of the material were examined. The subsequent construction work produced a compensator which can be altered in effective length without effecting the mirror support and which does not exert any supporting function.

The surroundings of the mounting location in the mirror body was studied with a finite element model. The stresses occurring in the case of a starting load of 20 g are situated below 0.25 kp/mm^2. (The experience value of fracture resistance of cerodur at room temperature is 2 kp/mm^2.) In another stress calculation with the total mirror, a maximum stress of 0.08 kp/mm^2 was produced with the same size load in the case of forces acting in an axial direction.

The weights of main mirror and mounting amount to:

mirror body	25.0 kp
mounting groups	3 x 1.4 kp
mounting body (estimated value)	7.8 kp
total weight	37 kp

Shake tests were conducted with the main mirror provided with original mounting groups, merely etched after cutting. In the case of axial sine excitation, the resonant frequency amounted to 160 and 540 Hz. After each measurement series, increasing shifts of the mirror compared to the base plate were measured with a collimator. These were triggered by the step-wise increasing defect of a flat spring, finally requiring disruption of the test. This spring was apparently too small in size and must be altered before future measurements are taken.

In a later stage of the study, the vibration measurements were supplemented in the thermal model. The following resonant frequencies were measured with very careful excitation:

Transversal, perpendicular to a flat spring:	48 Hz	/189
Transversal, parallel to a flat spring :	77 Hz	
Axial :	125 Hz	
Torsion :	78 Hz	

AP 3040 Thermal Behavior of the Main Mirror

The calculations on the stationary temperature distribution in orbit were first begun with two concentric rings of heat conductors at the rear surface of the mirror. In order to simplify the procedure, they were designed in the beginning as homogeneous conductor cylinders. The calculation model contained 99 nodes in a radial half section of the mirror body. Later, the division of the conductor cylinder into individual litz wires was also considered. In addition to the cases of homogeneous radiation, asymmetrical radiation in the form of a cosine distribution along the mirror circumference was also introduced. The entirety of the calculation results is compiled in Table Z1.

The cool-down time of the main mirror was calculated under the following boundary condition in the slightly expanded nodal model:

Cool-down of the instrument platform from 293 K to 78 K in 6 hours
Cool-down time of the instrument platform from 78 K to 4 K in a further 6 hours
Cool-down time of the instrument platform from 4 K to 3 K in a further 3 hours

After these 15 hours, however, the mirror was only cooled down to 103 K. The thermal balance (3 K) is not achieved until after 26 hours. The corresponding calculations of stress produce the result that a maximum stress within the mirror body occurs after 22 hours and amounts to 0.12 kp/mm^2. In the case of this data, the transition triangles between the conductors and the mirror body have not been considered. They were the subject of a separate subsequent calculation with a local calculation model concentrically around the heat conductor axis.

a Radien und Querschnitt der Wärmeleitringe	b Art der Leiter	c Art der Einstrahlung	d Temp. am Fußpunkt	e Oberflächentemperaturen innerhalb 400 Ø max	min
150 mm, 180 mm² 206 mm, 360 mm²	f Zylinder, g gelötet	j homogen k (λ von Zerodur 10-fach überhöht)	1,6 K	2,160 K	2,051 K
150 mm, 180 mm² 206 mm, 360 mm²	f Zylinder, g gelötet	l asymmetrisch k (λ von Zerodur 10-fach überhöht)	1,6 K	2,077 K	1,645 K
81 mm, 126 mm² 199 mm, 252 mm²	f Zylinder, g gelötet	j homogen	1,6 K	3,52	3,00
81 mm, 60 mm² 150 mm, 100 mm² 199 mm, 120 mm²	f Zylinder, g gelötet	j homogen	3 K	3,715	3,59
81 mm, 30 mm² 150 mm, 50 mm² 199 mm, 60 mm²	f Zylinder, g gelötet	j homogen	3 K	3,92	3,78
81 mm, 18 mm² 150 mm, 30 mm² 199 mm, 36 mm²	f Zylinder, g gelötet	j homogen	3 K	3,915	3,853
81 mm, 18 mm² 150 mm, 30 mm² 199 mm, 36 mm²	f Zylinder, g gelötet	l asymmetrisch	3 K	3,809	3,093
81 mm, 18 mm² 150 mm, 30 mm² 199 mm, 36 mm²	h Litzen, g gelötet	j homogen	3 K	3,916	3,853
81 mm, 18 mm² 150 mm, 30 mm² 199 mm, 36 mm²	f Zylinder, i geklebt	j homogen	3 K	5,055	5,001
81 mm, 18 mm² 150 mm, 30 mm² 199 mm, 36 mm²	f Zylinder, i geklebt	l asymmetrisch	3 K	4,333	3,691
81 mm, 18 mm² 150 mm, 30 mm² 199 mm, 36 mm²	h Litzen, i geklebt	j homogen	3 K	5,056	5,000

Table Z1: Result of the thermal calculations in the main mirror for the stationary case of radiation.

(Please see following page for Key.)

Key:
a. radii and cross-section of the heat conductor rings
b. type of conductor
c. type of radiation
d. temperature at the base point
e. surface temperature within a diameter of 400
f. cylinder
g. soldered
h. litz wires
i. cemented
j. homogeneous
k. (λ of cerodur multiplied by 10)
l. asymmetrical

Heat Transition Measurements /191

The determination of the heat transition resistance and the tensile strength of metal and cerodur combinations at low temperatures assumed a large portion of the study. On the basis of a successful preliminary test, soft solder connections between cerodur and invar were favored. Three heat conductors soldered and cemented on baking silver were measured at the Linde Company at 2 low temperatures. The measurements also produced values of conductivity for cerodur unknown up to now. They are situated for 2 K at 10^{-4} W/cm K and for 5 K at 2.4 W/cm K. The contact resistances of the cerodur metal transitions amount to 2700 K/W or 1000 K/W at the same temperatures. The cemented contact had values approximately five times higher.

The measured tensile strength of the contacts was subjected to extreme variations. Several contacts already separated upon manipulation, while the maximum value of the strength was more than 20 kp.

AP 3050 Collection Mirror and Support /192

Building on data of the MPIA on the laboratory model of the chopper, three drafts for the collection mirror mounting were prepared. They all have an intermediate plate in common, on which, on the one hand, three flat springs positioned in a tangent to the support rings connect these with the collection mirror and, on the other hand, two universal spring joints serve for holding this plate. A decision on the type of mounting for the flat springs could not yet be made, since the appropriate strength tests could not be carried out in the present study.

In the case of a collection mirror diameter of 113 mm, a weight of the mirror body of 285 g resulted and a total weight of the moving parts of 562 g. With a weight of the vibrating counter mass of the same size, an estimated weight of chopper and collection mirror group of a total of 2,270 g is obtained.

Studies on heat dissipation were undertaken with the power losses obtained by MPIA for the individual structural elements of the chopper.

The required heat conductors for the instrument platform can be easily accommodated in the three hollow cross-sections of the tripod. The measurement results of the Linde Company and the Dornier system on the contact resistances of metallic combinations were included in the considerations. Six soldering points are provided at the mirror body itself, permitting dissipation through copper strips of the radiation heat and the heat during cooling. The total temperature drop over the heat conductor chain between the chopper and instrument platform was estimated at 1.7 K; that between mirror and instrument platform had to be supplemented by an additional 4 K because of the high contact resistance of the metal glass connections.

For calculating cool-down time and internal stresses in the collection mirror, a model of finite elements was selected as in the case of the main mirror. The arbitrarily assumed base point temperature of the heat conductors of 4 K was achieved after precisely 12 hours by all points of the mirror body. The greatest stresses occur after 2.8 hours and reach 0.24 kp/mm^2.

Due to the simplicity of the calculation model, no stresses could /193 be stated for the collection mirror in the direct vicinity of the contact points.

The inherent frequency of the collection mirror is determined by the universal spring joint of the mounting. These produce an axial inherent frequency of approx. 370 Hz, a transversal frequency of approx. 420 Hz and a torsion frequency of approx. 200 Hz. All frequencies determined with the rigidity of the 3 flat springs, are situated above 1500 Hz.

The deformation of the mirror surface during chopping was first calculated for a mirror of insufficient thickness. Increasing the thickness to 15 mm finally produced a wave front aberration of 24 nm RMS.

In the case of constructive considerations on the correction mirror support, the automatic compensation of a focus extension as well as the lowest possible torsion guide of the heat conductor strips was already taken into consideration. Open problems are listed.

AP 3060 Three-Legged Tubular Construction

With the recently suggested triangular cross-section of the mounting supports, inherent frequency calculations were carried out for the entire system. They also used a finite element model, making possible the graphic representation of the vibration images of tripod and collection mirror. An edge length of the cross-section triangle of 30 mm resulted in inherent frequencies which were too low. The increase to 40 mm at the foot of the supports produced 77 Hz as the lowest inherent frequency.

Constructive possibilities at the foot of the tripod were utilized for focusing between the main and collection mirrors.

Adjustment screws are located there, making possible both tipping as well as a parallel off-set of the collection mirror.

Focusing /194

An attempt was made to avoid active focusing, because this would introduce additional cryomechanisms, weight increases and sources of error. It was possible to prove by an alteration in the support material from titanium to invar and the introduction of additional synthetic material compensators in the chopper housing, that at least from the point of view of thermal values, a passive focusing, i.e. automatic, is possible in the case of temperature alterations. The effects of possible variations in material and alterations in temperature on the focusing state was studied and found not to be critical.

AP 3070 Preparation of the Thermal Model

The thermal model consists in an etched mirror body, mounted with the constructed original mounting structural group. The supporting structure was reduced to a simple aluminum plate. A total of 42 copper litz wires are soldered onto the rear surface of the mirror body, but unfortunately the durability of these connections leave something to be desired. Furthermore, 11 thermometers are systematically distributed on the front and rear sides of the mirror body, serving for checking the thermal calculations. They had to be installed in titanium housings, since the original aluminum housings separated during cooling on the basis of preliminary cementing tests.

Collection mirror group and tripod of the thermal model were simulated by three heat resistances, connected with copper strips to the instrument platform.

AP 3090 Optical Testing of the Telescope and Its Components /195

Suitable measurement procedures were tested and explained for testing the telescope and the individual mirrors under hot and cold conditions. They serve for testing the surface form as well as the scattered light quality and the image position of the mirror. The individual procedures and the necessary aids are compiled in Table Z2.

AP 3100 Clean Handling

The class 100 of the US Federal Standards 209b is recommended for the clean handling for the telescope and its component parts. The final assembly of the individual groups and of the telescope as well as vaporizing the mirror must be carried out in suitable laminated boxes, in which the parts concerned are to be enclosed in transport containers, to be filled with a protective gas. On the whole, the following devices are required:

Precipitation flow device for clean handling of a 50 cm vaporization instrument

Purification bath for dust removal of the mirrors

Laminated assembly box, inside dimensions 100 x 150 x 70 cm with purification baths

Transport container for main mirror

Transport container for collection mirror

Transport container for the complete telescope.

Error Budget

With the aid of data of the MPIA on the accuracy of the chopper, the table on the expected remainder inaccuracies of the telescope adjustment was prepared. The influence of cooling and transition to a state of weightlessness, on the one hand, as well as the effect of asymmetrical heat radiation, on the other hand, were taken into consideration separately. These are estimated values, corresponding to the incompleted state of the construction.

Supplementary Thermal Stress Calculations /197

The course of cool-down and maximum stresses were determined again with a finite element model in the concentric model of an individual heat conductor contact. The time up to reaching thermal balance amounts to approx. 30 hours, the maximum stress, arising directly at the contact of copper and cerodur amounts to approx. 3 kp/mm^2 in the 24th hour. The contacting copper element with a thickness of 1 mm was removed from the model in a further calculation step. Therefore, the stresses at this point were reduced to 0.35 kp/mm^2.

Nr.	Testobjekt	Testart	Prinzip in Abb.	Bevorz. Achslage	Hilfsmittel (außer Kryostat u. Interferom.)
1	Hauptspiegel ungefaßt	Wellenfront warm	3090/1	vertikal	45°-Planspiegel 100 Ø
2	Hauptspiegel gefaßt	Wellenfront warm/kalt	3090/1 3090/3	vertikal	45°-Planspiegel 100 Ø
3	Hauptspiegel gefaßt	Streulicht warm/kalt	3090/4	beliebig	IR-Laser, Empfänger, 4 Blenden, 3 Linsen
4	Fangspiegel ungefaßt	Wellenfront warm	3090/5	horizontal	Hindle-Kugelspiegel 400 Ø
5	Fangspiegel gefaßt	Wellenfront warm/kalt	3090/6	beliebig	Hindle-Kugelspiegel 400 Ø
6	Fangspiegel	Streulicht warm/kalt	3090/6 komb.mit 3090/4	beliebig	Hindle-Kugelspiegel IR-Laser, Empfänger 4 Blenden, 3 Linsen
7	Teleskop komplett	Wellenfront warm/kalt	3090/7a	vertikal	Planspiegel 400 Ø
8	Teleskop komplett	Fokuskontrolle	3090/7c (evtl. 3090/8	vertikal	Planspiegel 400 Ø Strichplatte, Beleuchtungseinheit, Fernrohr
9	Teleskop komplett	Experimentprüfung	3090/8	vertikal	Parabolspiegel 400 Ø Planspiegel 160 Ø 2 Linsen, 1 Blende, Laser

Table Z2: Compilation of the tests considered necessary and the necessary aids.

(Please see page 145 for Key.)